

Altered Contractile Mechanics and Ca^{2+} Handling Contribute to Cardiomyopathy Pathogenesis

A Thesis Submitted for the Degree of Doctor of Philosophy

Trinity Term, 2015

Cameron Turtle

St John's College

Department of Cardiovascular Medicine

University of Oxford

Supervisors:

Professor Charles Redwood and Professor Hugh Watkins

Altered Contractile Mechanics and Ca^{2+} Handling Contribute to Cardiomyopathy Pathogenesis

Cameron Turtle, St John's College, University of Oxford

A thesis submitted for the degree of Doctor of Philosophy, Trinity 2015

Abstract

Mutations in genes encoding sarcomeric proteins are the most common cause of inherited cardiomyopathies. However, cardiac disease caused by mutations in non-sarcomeric proteins exhibit remarkably similar phenotypes, suggesting that common modes of pathogenesis might exist. It is of particular interest whether non-sarcomeric mutations result in impaired contractile function akin to sarcomeric diseases. Accordingly, this thesis describes the effect of cardiomyopathy-causing mutations to an energy sensing protein (AMPK γ2) and a small heat shock protein (αB-crystallin) on cardiac myofilament biomechanics and Ca^{2+} handling.

Mutations in the regulatory γ2 subunit of AMP-activated kinase (AMPK), encoded by the *PRKAG2* gene, cause a cardiomyopathy characterized by ventricular hypertrophy, electrophysiological abnormalities, and glycogen accumulation. Data from animal models in which the mutant transgene is overexpressed suggest that the electrophysiological aspects might be caused by excess glycogen, but that this is insufficient to account for all facets of the phenotype. A novel knock-in mouse expressing R299Q AMPK γ2 (homologous to the human R302Q mutation) was generated to model PRKAG2 cardiomyopathy more accurately. Assessment of the cardiac phenotype at two months to determine the early events in disease pathogenesis revealed systolic and diastolic dysfunction in mutant animals, with no excess glycogen detected. Analysis of acetyl-CoA carboxylase phosphorylation at S79 suggested increased basal AMPK activity in mutant animals. Increased sarcomeric Ca^{2+} sensitivity of contractile activation was observed in demembranated cardiac trabeculae from mutant animals, associated with decreased phosphorylation of cardiac troponin I at S23/S24 and increased phosphorylation at S150. Treatment with protein kinase A normalized this difference in Ca^{2+} sensitivity, suggesting that reduced PKA phosphorylation is the primary abnormality in mutant tissue. Cardiomyocytes from mutant animals exhibited slowed contractile and Ca^{2+} reuptake rates, associated with reduced phosphorylation of phospholamban and myosin binding protein C, as well as an increased response to isoproterenol. The lack of glycogen accumulation in these animals, combined with abnormal contractile and Ca^{2+} handling properties, reveals a more nuanced interpretation of the mechanism of PRKAG2 cardiomyopathy development. Further, the newly identified interaction between energy- (AMPK) and stress- (PKA) signalling networks may be of importance in numerous additional disease pathways.

This thesis clarifies the role of αB-crystallin, and its cardiomyopathy-causing mutant (R157H), in regulating cardiac muscle stiffness. Specifically, mass spectrometry data revealed that αB-crystallin forms large oligomers and binds to titin Ig domains. Nuclear magnetic resonance confirmed this binding and suggested that αB-crystallin's C-terminal is responsible for titin binding. A viscoelastic model was developed to match stress relaxation in cardiac muscle fibres. Measurements using this model indicated that αB-crystallin significantly increases myocardial stiffness and that the R157H mutation weakens this effect. Further, a 9-AA peptide from αB-crystallin's C-terminus was shown to bind titin and increase overall muscle stiffness. These results reveal a novel method of cardiac muscle stiffness regulation that might contribute to the pathogenesis of cardiomyopathy.

Declaration of own work and attribution

Except where directly indicated, this DPhil thesis is entirely my own work. No portion of the document has been submitted for another degree at this University, or for a degree at any other institution. Also, as clearly attributed in the text and figure legends, the following were performed by collaborators:

Chapter 3: The targeting vector used to create the R299Q AMPK γ2 knock-in mice was designed by Dr Katalin Pinter with assistance by GenOway (Lyon). Backcrossed C57BL/6 R299Q AMPK γ2 knock-in mice were generated by Dr Arash Yavari. *In vivo* cine-MRI imaging was performed by Miss Hannah Barnes and Dr Arash Yavari. Invasive haemodynamic surgery and ex vivo cardiac perfusion was conducted by Dr Mohamed Bellahcene. Histological staining and AMPK activity assays were performed by Dr Arash Yavari.

Chapter 6: Collaborators in Dr Justin Benesch's group in the Department of Theoretical and Physical Chemistry performed structural studies of the αB-crystallin:titin interaction. Experiments were conducted by Mr Georg Hochberg, Miss Miranda Collier, and Mr Henrik Muller with supervisory assistance from Dr Andrew Baldwin and Dr Justin Benesch.

Cameron Turtle

April 2015

Acknowledgements

The work presented in this thesis could not have been completed without the help of many others. First and foremost, I am grateful to my supervisors, Prof Charles Redwood and Prof Hugh Watkins, for providing access to an outstanding research environment. Their patient mentorship and high standard of academic rigour greatly facilitated the development of this work. Further, the intellectual contribution made by this thesis is built upon the work of innumerable scientists, of whom only a limited number are directly credited in this document.

I am also heavily indebted to my friends and colleagues within Prof Watkins' research group. Of particular importance are Dr Paul Robinson and Dr Katalin Pinter, who taught me a range of laboratory techniques and principles, guided my daily experiments, and actively discussed research directions. I am also grateful to Dr Arash Yavari for experimental and intellectual support with the AMPK knock-in mice, to Dr Mohamed Bellahcene, Dr Matt Kelly, and Miss Sahar Ghaffari for assistance with research animals, to Mr Phil Townsend for tireless support of all my research needs, to Dr Henrik Isackson for introducing multiple *ex vivo* assessments of murine cardiac function, to Dr Katja Gehmlich for biochemical troubleshooting, and to Mr Suketu Patel, Dr Charlotte Hooper, Dr Matt Kelly, and Dr Carin de Villiers for day-to-day discussions and assistance.

Outside the Watkins group, a number of individuals also contributed to the completion of this thesis and my scientific development. Special thanks go to Prof Barbara Casadei, Prof Manuela Zaccolo, Dr Gil Bub, and Dr Mark Crabtree for their assessments of progress and suggestions for future work during my Transfer and Confirmation of Status examinations. I would also like to thank Dr Matt Daniels for enlightening and constructive conversations. I am grateful to Dr Jillian Simon for expert advice and guidance regarding 2D gel electrophoresis techniques. My departmental and collegiate advisors, Prof Martin Farrall and Prof Andrew Parker, also deserve thanks for pastoral care.

I am grateful to the Rhodes Trust for funding my studies and to the broader Rhodes and St John's College communities for providing outstanding opportunities for learning, engagement, and friendship. Further, my laboratory research and conference travel would not have been possible without funding from the British Heart Foundation, St John's College, the Amgen Foundation, and IonOptix.

Finally, I wish to dedicate this work to my parents and older brother, for immeasurable contributions to my educational development, and to my wife, Sarah, for her unwavering, selfless support throughout my doctoral research.

Acronyms and abbreviations

AC	Adenylate cyclase
ACC	Acetyl CoA carboxylase
ACh	Acetylcholine
ADP	Adenosine 5'-diphosphate
AICAR	5-aminoimidazole-4-carboxamide riboside
AID	Autoinhibitory domain
AMP	Adenosine 5'-monophosphate
AMPK	AMP-activated protein kinase
ANOVA	Analysis of variance
ATP	Adenosine 5'-triphosphate
BDM	2,3-Butanedione monoxime
BSA	Bovine serum albumin
CaMK	Calcium/calmodulin-dependent protein kinase
CaMKKβ	Ca^{2+}/calmodulin-dependent protein kinase kinase-β
cAMP	Cyclic adenosine monophosphate
CHAPS	3-[(3-cholamidopropyl)dimethylammonio]-1-propanesulfonate
CID	Collision-induced dispersion
Cine-MRI	Cine-magnetic resonance imaging
CrP	Creatine phosphate
cTnI	Cardiac troponin I
cTnT	Cardiac troponin T
DAPI	4',6-diamidino-2-phenylindole
dATP	2-deoxy-ATP
DCM	Dilated cardiomyopathy
DTT	Dithiothreitol
ECM	Extracellular matrix
EDPVR	End-diastolic pressure volume relationship
EDV	End-diastolic volume
EF	Ejection fraction
EGTA	Ethylene glycol tetraacetic acid
ELC	Essential light chain
ESPVR	End-systolic pressure volume relationship
ESV	End-systolic volume
FFA	Free fatty acid
FKBP12.6	FK-506-binding protein 12.6
FRET	Förster Resonance Energy Transfer
FRT	Flp recombinase recognition target
FURA-2-AM	FURA-2-acetoxymethyl ester
H&E	Haematoxylin and eosin
HCM	Hypertrophic cardiomyopathy
HDTA	1,6-Diaminohexane-N,N,N',N'-Tetraacetic acid
HEPES	4-(2-hydroxyethyl)-1-piperazineethanesulfonic acid
Het	Heterozygous
Homo	Homozygous
ICD	Implantable cardioverter-defibrillator
IEF	Isoelectric focusing
IPG	Immobilized pH gradient

IR	Inhibitory region
JNK	c-Jun N-terminal kinase
k_{tr}	Rate of tension redevelopment
LA	Left atrium
LDA	Length dependent activation
LKB1	Liver kinase B1
LTCC	L-type Ca^{2+} channel
LV	Left ventricle
MAPK	Mitogen-activated protein kinase
MOPS	3-(N-morpholino)propansulfonic acid
MS	Mass spectrometry
mTOR	Mammalian target of rapamycin
MyBPC	Myosin binding protein C
NCX	Sodium-calcium exchanger
NFAT	Nuclear factor of activated T-cells
NMR	Nuclear magnetic resonance
PAGE	Polyacrylamide gel electrophoresis
PAK3	p21-activated kinase 3
PBS	Phosphate buffered saline
pI	Isoelectric point
PKA	Protein kinase A
PKC	Protein kinase C
PKG	cGMP-dependent protein kinase
PLN	Phospholamban
RA	Right atrium
RLC	Regulatory light chain
RV	Right ventricle
RyR	Ryanodine receptor
PKA RII	PKA type II regulatory subunit
SAN	Sinoatrial node
SDS	Sodium dodecyl sulphate
SEM	Standard error of the mean
SERCA	Sarco/endoplasmic reticulum Ca^{2+}-ATPase
SL	Sarcomere length
SLN	Sarcolipin
SLS	Standard linear solid
SR	Sarcoplasmic reticulum
SV	Stroke volume
SW	Stroke work
TBST	Tris-buffered saline + Tween 20
Tm	Tropomyosin
Tn	Troponin
TnC	Troponin C
TnI	Troponin I
TnT	Troponin T
UTC	Urea-thiourea-CHAPS
WT	Wild type
β-AR	β-adrenergic receptor

Table of Contents

Abstract i

Declaration of own work and attribution ii

Acknowledgements iii

Acronyms and abbreviations iv

Chapter 1 – Introduction

1.1 Cardiac function and dysfunction ***1***

1.1.1 Macroscopic physiology 1

1.1.2 Electrical coordination of contraction 3

1.1.3 Autonomic regulation of cardiac function 4

1.1.4 The heart as a muscular pump 6

1.1.5 Failure of the muscular pump 10

1.1.6 Inherited cardiomyopathy 12

1.2 Mechanisms of ventricular muscle function ***17***

1.2.1 Microscopic physiology of ventricular muscle 17

1.2.2 Action potential generation and propagation 18

1.3 Ca^{2+} handling in ventricular cardiomyocytes ***20***

1.3.1 L-type Ca^{2+} channel (LTCC) 21

1.3.2 Ryanodine receptor (RyR) 23

1.3.3 Sarco/endoplasmic reticulum Ca^{2+}-ATPase (SERCA) 25

1.3.4 Phospholamban (PLN) 26

1.3.5 Sodium-calcium exchanger (NCX) 28

1.4 Regulation of contraction in cardiac muscle ***29***

1.5 Thin filament ***30***

1.5.1 Actin 31

1.5.2 Tropomyosin (Tm) 33

1.5.3 Troponin (Tn) 35

1.6 Thick filament ***43***

1.6.1 Myosin II heavy chains 43

1.6.2 Myosin regulatory (RLC) and essential (ELC) light chains 47

1.6.3 Myosin binding protein C (MyBPC) 49

1.7 Non-filamentous proteins 51
1.7.1 Titin 51
1.7.2 Collagen 53
1.8 β-adrenergic regulation of contractile activity 53
1.9 Diseases of the sarcomere 54
1.9.1 Hypertrophic cardiomyopathy (HCM) and energy deficiency 54
1.9.2 AMP-activated protein kinase (AMPK) and PRKAG2 cardiomyopathy 56
1.9.3 αB-crystallin and dilated cardiomyopathy 61
1.10 Hypotheses and specific aims 63
1.10.1 Hypotheses 63
1.10.2 Specific aims 63

Chapter 2 – Methods

2.1 Demembranated trabeculae 65
2.1.1 Dissection 65
2.1.2 Apparatus 65
2.1.3 Experimentation 66
2.1.4 Demembranated trabeculae treatments 68
2.1.5 Data analysis 69
2.2 Intact cardiomyocytes 71
2.2.1 Isolation 71
2.2.2 Apparatus and experimentation 73
2.2.3 Analysis 74
2.2.4 Intact Cardiomyocyte Treatment 75
2.3 Biochemical analyses 77
2.3.1 Sample preparation 77
2.3.2 Protein concentration analysis 77
2.3.3 One dimensional SDS-PAGE 78
2.3.4 Western blotting 78
2.3.5 Two dimensional gel electrophoresis 79
2.3.6 Weighted average calculation 82
2.5 Statistical analyses 83
2.6 Solutions 86

Chapter 3 – Characterisation of AMPK R299Q γ2 cardiac contractile mechanics in demembranated trabeculae

3.1 A novel mouse model of PRKAG2 cardiomyopathy 86

3.2 Specific Aims 93

3.3 Baseline characterization 94

3.4 Effect of PKA treatment 101

3.5 Discussion 108

3.5.1 Fundamental effect of R299Q γ2 mutation on AMPK activity 109

3.5.2 Consequences of increased myofilament Ca^{2+} sensitivity 112

3.5.3 Cause of increased myofilament Ca^{2+} sensitivity 113

3.5.4 Implications of a heightened response to PKA 113

3.5.5 Altered sarcomere length dependence 116

3.5.6 Conclusions 118

Chapter 4 – Characterisation of AMPK R299Q γ2 cardiac contractility and Ca^{2+} handling in intact cardiomyocytes

4.1 Specific Aims 119

4.2 Baseline characterization 120

4.3 Response to β-adrenergic stimulation 128

4.4 Effect of AICAR treatment 129

4.5 Discussion 136

4.5.1 Slowed Ca^{2+} handling and contractility 137

4.5.2 Increased isoproterenol response 140

4.5.3 Dramatic effect of AICAR treatment in WT cells 141

4.5.4 Reduced effect of AICAR treatment on mutant cardiomyocytes 144

Chapter 5 – Biochemical alterations underlying cardiac contractile abnormalities in AMPK R299Q γ2 mice

5.1 Introduction 146

5.2 Alterations to sarcomeric regulatory proteins 148

5.3 Alterations to Ca^{2+} handling proteins 156

5.4 Alteration of the PKA signalling pathway 158

5.5 Discussion 160

5.5.1 Altered phosphorylation of sarcomeric proteins underlies myofilament dysfunction 160

5.5.2 Reduced phosphorylation of Ca^{2+} handling proteins underlies Ca^{2+} transient dysfunction 162

5.5.3 Contribution of altered contractile function to the pathogenesis of PRKAG2 cardiomyopathy 163

Chapter 6 – Dilated cardiomyopathy-associated mutations in αB-crystallin alter its regulation of cardiac muscle passive stiffness

6.1 Introduction 168

6.2 Characterization of titin:αB-crystallin interaction 169

6.3 Specific aims 173

6.4 Development of a measure of cardiac stiffness 174

6.5 Effect of WT and DCM-associated αB-crystallin mutant on cardiac muscle stiffness 183

6.6 Effect of 9-AA peptide on cardiac muscle stiffness 190

6.7 Discussion 193

6.7.1 Novel insight into the αB-crystallin:titin interaction 193

6.7.2 Regulation of cardiac muscle stiffness by αB-crystallin 197

6.7.3 Conclusions 200

Chapter 7 – Discussion

7.1	***Altered contractile mechanics contribute to the pathogenesis of non-sarcomeric cardiomyopathies***	***201***
7.1.1	Contractile abnormalities underlie PRKAG2 cardiomyopathy pathogenesis	201
7.1.2	Biomechanical abnormalities due to DCM-associated αB-crystallin mutation	202
7.2	***Implications of novel pathogenesis mechanisms in broader disease***	***203***
7.2.1	Shared consequences of contractile and Ca^{2+} handling dysfunction in PRKAG2 cardiomyopathy and HCM	204
7.2.2	Altered ventricular stiffness can lead to DCM	211
7.3	***Therapeutic implications***	***213***
7.3.1	Novel treatment opportunities in hypertrophic cardiomyopathy	213
7.3.2	Novel treatment opportunities in dilated cardiomyopathy	217
7.4	***Future directions***	***219***
7.4.1	Hypertrophic cardiomyopathy, energy compromise, and PRKAG2 cardiomyopathy	219
7.4.2	Regulation of cardiac stiffness by αB-crystallin	221
7.5	***Concluding remarks***	***222***

References **224**

Chapter 1 – Introduction

1.1 Cardiac function and dysfunction

Circulation of blood throughout the body is essential to supply oxygen and nutrients, remove waste, and facilitate communication between tissues. The pumping force required to propel this circulation is generated by the muscular tissues of the heart, which undergoes a rhythmic cycle of contraction (systole) and relaxation (diastole) approximately once per second in humans. Over the course of an average lifetime, this activity results in 2.5 billion contractions and the expulsion of over 200 million litres of blood [Avraham, 2000].

Although the core utility of heart muscle is simple and well-understood, the detailed mechanisms of cardiac contractile function are far more complex and not yet fully elucidated. As these contractile mechanisms can be perturbed by various disease states and contribute to overall cardiac failure, an intimate understanding of the processes involved could lead to novel therapeutic pathways.

1.1.1 Macroscopic physiology

The heart is composed of four contractile chambers isolated by unidirectional valves (Figure 1-1) [Opie, 2003]. Deoxygenated blood from the peripheral circulation returns to the heart via the superior vena cava and inferior vena cava. This blood initially enters the right atrium (RA) and passes into right ventricle (RV) through the tricuspid valve, which remains open during diastole. During systole, as the ventricular muscle contracts and the pressure within the chamber rises, the tricuspid valve is forced shut and the pulmonary valve opens. This reciprocal valve opening and closing prevents reverse movement of blood during chamber contraction. Blood

from the RV is forced out the pulmonary valve and into the pulmonary circulation. In the capillaries of the pulmonary circulation, gas exchange between the alveoli and the blood causes CO_2 to diffuse out of the blood while O_2 simultaneously enters. This oxygenated blood continues through the pulmonary circulation until it re-enters the heart in the left atrium (LA).

Oxygenated blood in the LA then passes into the left ventricle (LV) via the mitral, or bicuspid valve. Analogously with valves of the right side of the heart, the mitral valve remains open during diastole but closes during systole as the aortic valve opens. Blood passing through the aorta travels throughout the circulation, providing oxygenated blood to all tissues of the body. In the capillaries, the thin separation between the circulation and surrounding tissues allows the exchange of gas, nutrients, and signalling molecules. Depleted blood then returns to the heart via the venous system and re-enters the RA, completing the circulation.

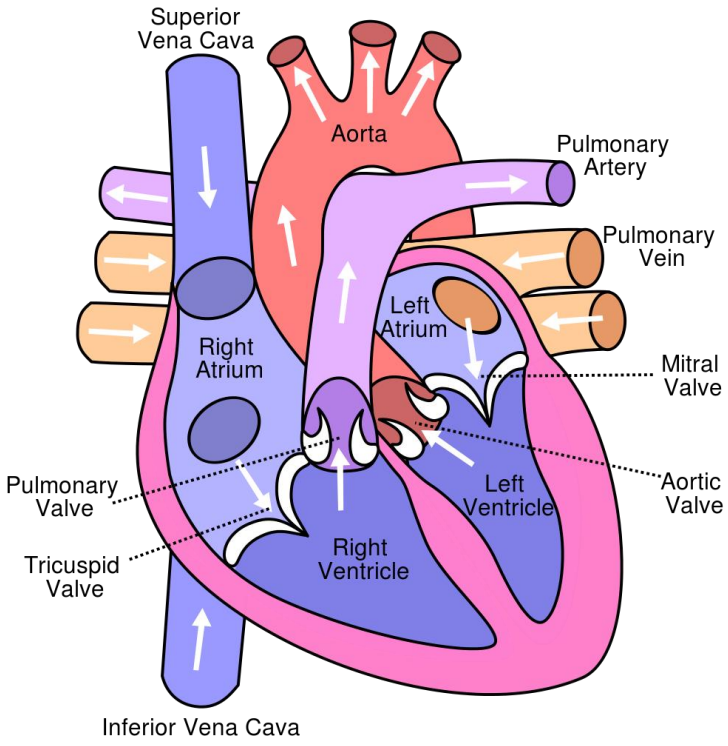


Figure 1-1 - The chambers of the heart. Retrieved from Wikimedia Commons on Feb 2, 2015.

1.1.2 Electrical coordination of contraction

The coordination of cardiac contraction is accomplished by a wave of electrical activity that passes between cardiac cells via tight attachments called gap junctions. However, to achieve the precise timings of chamber filling and ejection required for proper cardiac function, conduction between adjacent cells is insufficient. Instead, a system of specialized cells is employed to generate and propagate the electrical signal throughout the heart (Figure 1-2). Initiation of the stimulatory signal arises spontaneously from a group of cells in the RA, termed the sinoatrial node. The electrical signal propagates from the sinoatrial node throughout the atria and is recollected at a second node, the atrioventricular node. As the action potential progresses from the top of the atria towards the ventricles, this initial stimulation is responsible for ejecting the contents of the atria into the ventricles.

The electrical signal is then decelerated and condensed within the atrioventricular node before accelerating down the His bundle and into the left and right bundles branches. From these branches and the Perkinje fibres innervating the apex of the heart the electrical impulse spreads throughout the ventricular muscle. Therefore, contraction begins at the bottom of the ventricles and proceeds upwards towards the pulmonary and aortic valves, allowing maximum ejection of blood into the circulation.

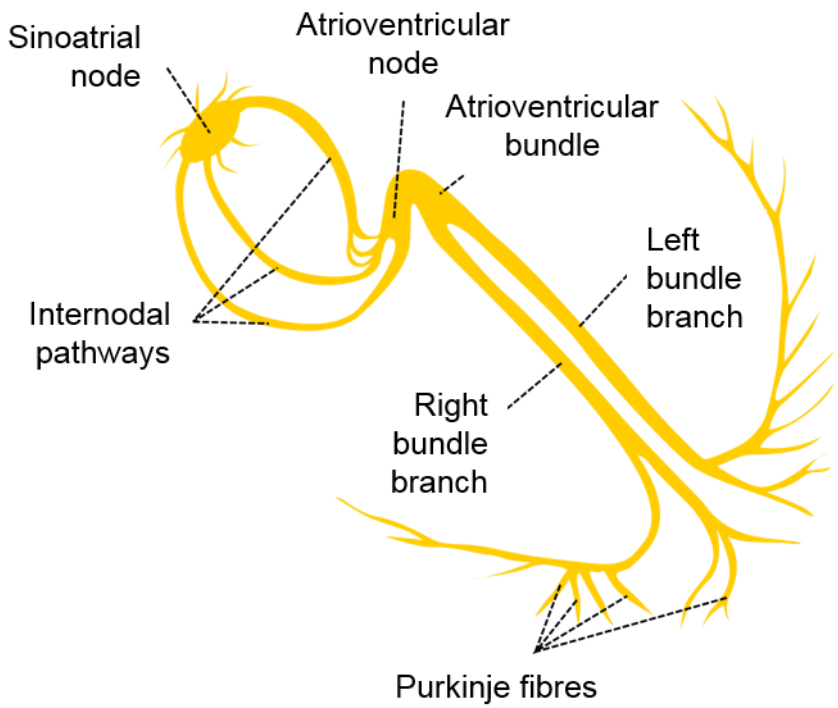


Figure 1-2 - Simplified electrical conduction system of the heart. Adapted from Wikimedia Commons, retrieved on Feb 2, 2015.

1.1.3 Autonomic regulation of cardiac function

Broad regulation of cardiac function is accomplished via two divisions of the autonomic nervous system, the sympathetic and parasympathetic. Activation of the sympathetic nervous system (Figure 1-3) by stress or exercise results in release of the excitatory messengers, epinephrine and norepinephrine, from the right and left stellate ganglion as well as the adrenal medulla. These messengers stimulate cardiac β-adrenergic receptors, leading to increased heart rate, electrical conductance, and contractility.

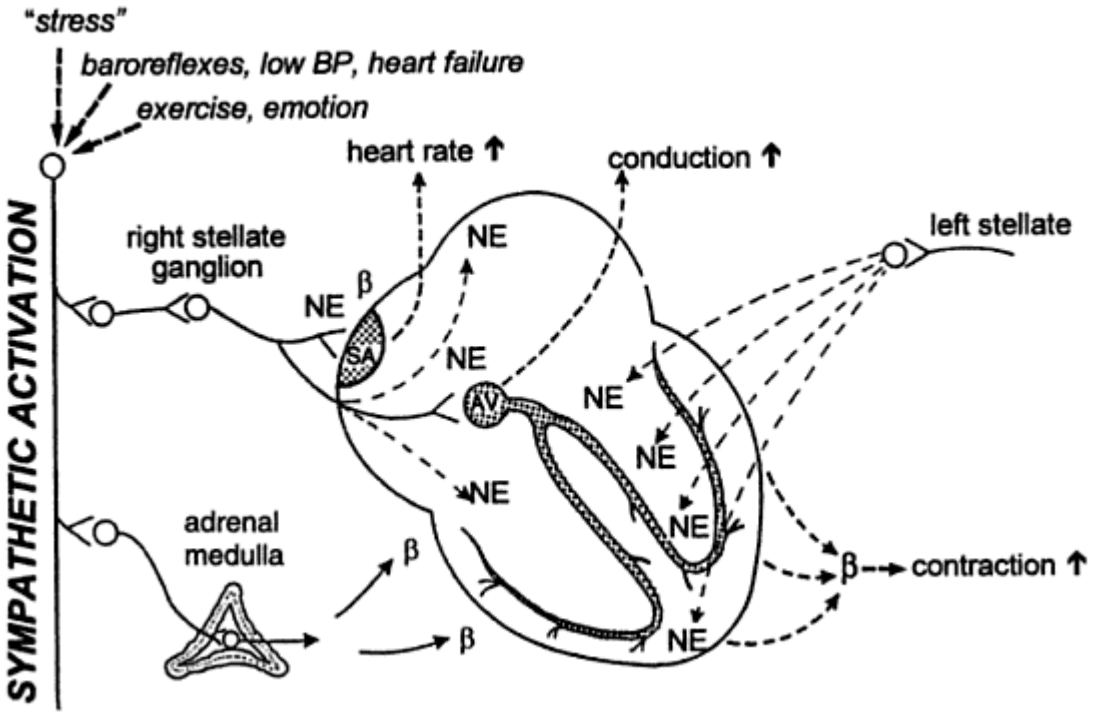


Figure 1-3 - Mechanisms of sympathetic regulation of cardiac function. Adapted from [Opie, 2003] Figure 2-1. NE = norepinephrine, β = β-adrenergic activity.

The opposing effect on cardiac output is accomplished via parasympathetic activation. The parasympathetic system is chronically active at a low level. Its activity increases during sleep, rest, or in trained athletes. The function of parasympathetic regulation occurs via release of acetylcholine (ACh) from the vagal nerve. ACh is recognized by muscarinic receptors throughout the heart. The effect of this stimulation is a reduction of heart rate as well as a minor reduction in cardiac contractility.

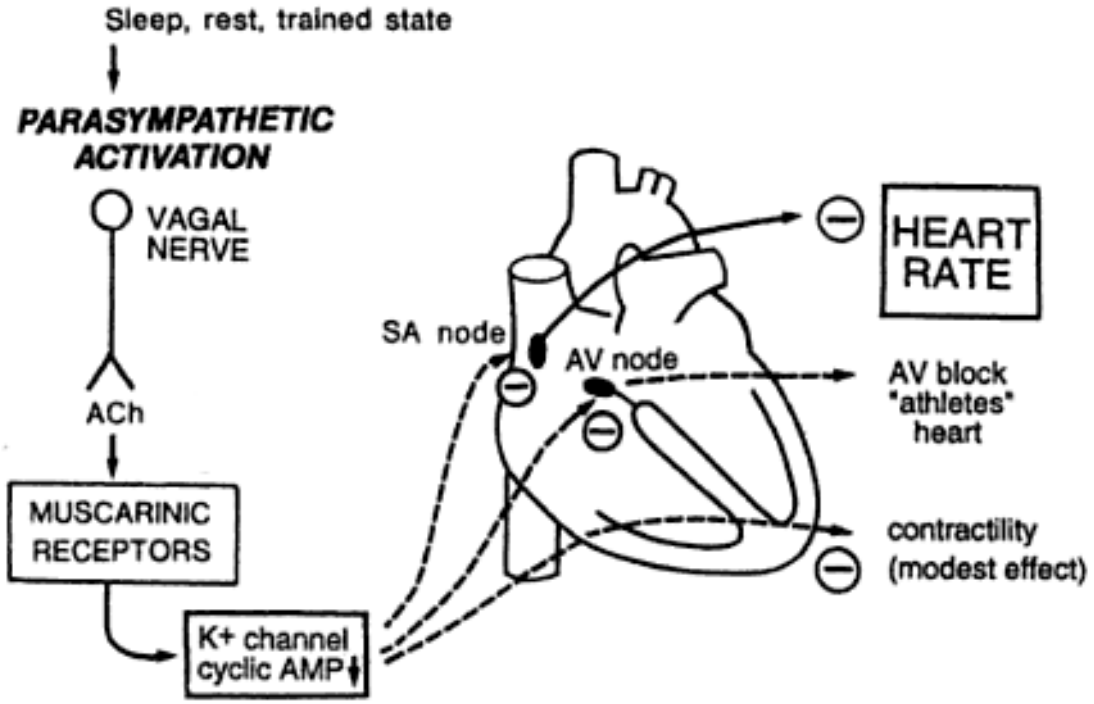


Figure 1-4 - Mechanisms of parasympathetic regulation of cardiac output. Figure adapted from [Opie, 2003] Figure 2-2. ACh = acetylcholine.

1.1.4 The heart as a muscular pump

The essential function of the heart is to consistently propel its contents of blood throughout the circulation. This activity is accomplished by the muscular ventricles, which undergo a series of phases collectively referred to as the ventricular cycle. This cycle can be represented as a continuous relationship between the volume of the ventricular chamber and its internal pressure (Figure 1-5). In the LV, filling begins just after the mitral valve opens as LV pressure decreases to less than that of the LA. During this early phase of filling, the volume of the LV increases considerably while its internal pressure increases slightly. Upon atrial contraction, additional blood is pumped into the ventricle.

The ventricle then begins contraction, increasing internal pressure within the chamber and causing closure of the mitral valve. As both the mitral and aortic valves remain closed, and blood is largely incompressible, increasing contraction of the LV muscle causes an increase in pressure without any change in LV volume (isovolumetric contraction). Once pressure within the LV exceeds that in the aorta (diastolic blood pressure), the aortic valve opens and rapid ejection of blood occurs. The LV muscle continues to contract during ejection, maintaining a nearly constant pressure within the chamber slightly above that in the aorta. As contraction in the LV decreases, blood flow decelerates but transiently continues due to inertia [Quinones *et al.*, 1976] before the aortic valve closes. Thereafter, with both the aortic and mitral valves closed, the LV undergoes isovolumetric relaxation to complete the cycle.

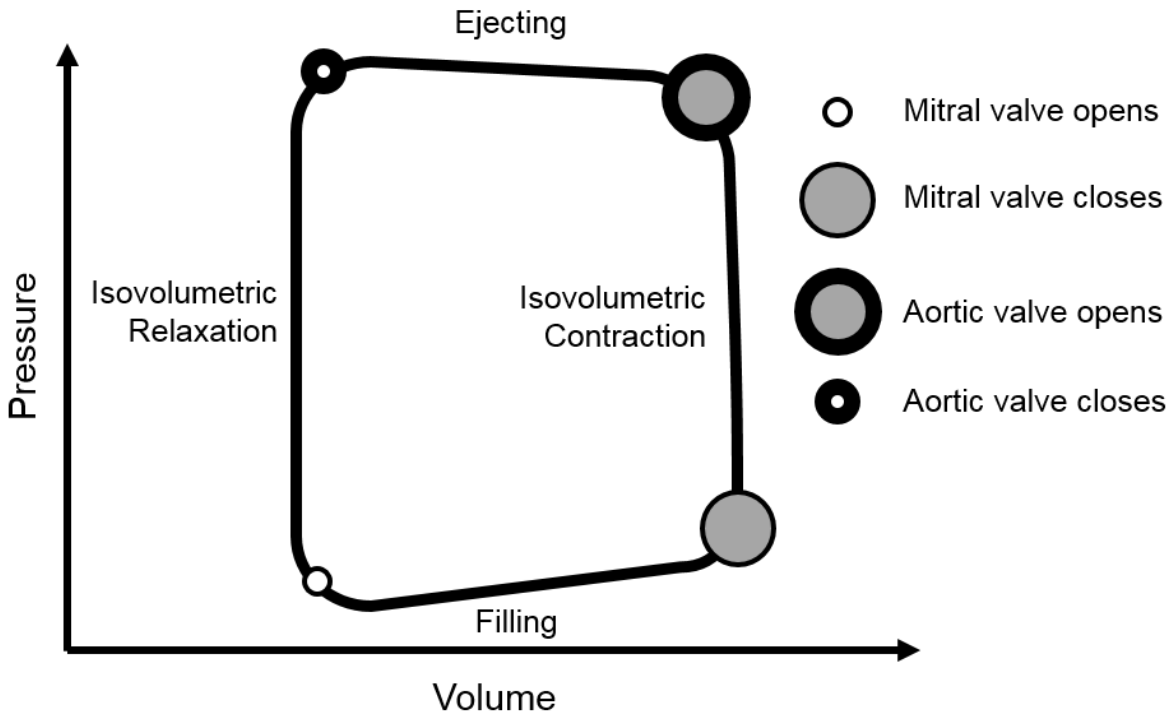


Figure 1-5 - Idealized left ventricular pressure-volume relationship.

The pressure-volume relationship is also a useful tool to describe cardiac output (Figure 1-6). The stroke volume (SV), or amount of blood ejected during each contractile cycle, is calculated as the difference between the end-diastolic volume (EDV) and the end-systolic volume (ESV). Cardiac output, defined as the amount of blood ejected over a given interval, is calculated as the product of SV and heart rate. The amount of work exerted upon the blood during each cycle is the stroke work (SW), given by the area enclosed by the pressure-volume loop. SW is approximately equal to the product of SV and developed pressure. Finally, ejection fraction (EF) measures the proportion of ventricular blood ejected during each contraction and is therefore the quotient of SV and EDV.

All of the previous parameters are measured clinically to evaluate cardiac function. However, they are also dependent on two forms of cardiac load, preload and afterload. Preload describes the stretching of the myocardium prior to contraction and is therefore dependent on the level of venous return. Afterload describes the pressure against which the heart must eject blood and is therefore directly related to blood pressure. An important relationship between ventricular preload and cardiac output is titled the Frank-Starling Law of the Heart. This law states that, all other conditions equal, stroke volume increases with preload [Konhilas *et al.*, 2002]. This increase in force is accounted for by so-called Frank-Starling mechanisms whereby the contractility of ventricular muscle increases as it is stretched [de Tombe *et al.*, 2010]. These mechanisms allow the heart to compensate during periods of increased blood return such as exercise or stress.

To avoid the dependence on cardiac load inherent with most measures of single-cycle output, it is often useful to evaluate the relationship between pressure and volume at the completion of systole and diastole over many cycles (Figure 1-6).

Both of these measurements are largely independent of preload and afterload. The end-diastolic pressure volume relationship (EDPVR) describes the filling of the ventricle, in which passive stiffness of the myocardium limits ventricular stretching. This limit is essential because the amount of force required to generate ventricular pressure is proportional to the ventricle's radius according to the Law of Laplace:

$$Pressure = \frac{Force}{Radius}$$

Given that the pressure required to eject blood is set by arterial pressure, and the force production capacity of the ventricular muscle is limited, the radius of the ventricle during filling must also be limited to prevent failure. At the opposite end of the cycle, the end-systolic pressure volume relationship (ESPVR) describes the maximum pressure that can be developed at any given volume. As the pressure developed in the ventricle is directly related to force production by the myocardium, ESPVR is a useful indicator of myocardial contractility.

The efficiency of cardiac function can also be estimated using ESPVR and EDPVR. As calculated previously, the area enclosed by the pressure-volume loop (SW) is equal to the amount of work done on the blood that is ejected. However, the heart must also do work to maintain the contractile cycle at the given potential energy. Therefore, the total amount of work done by the heart can be calculated as the sum of the stroke work and potential energy. The efficiency of this work is the quotient of stroke work over total work. The overall efficiency of stroke work ranges from 15 - 40 % depending on experimental conditions [Wendt and Gibbs, 1974].

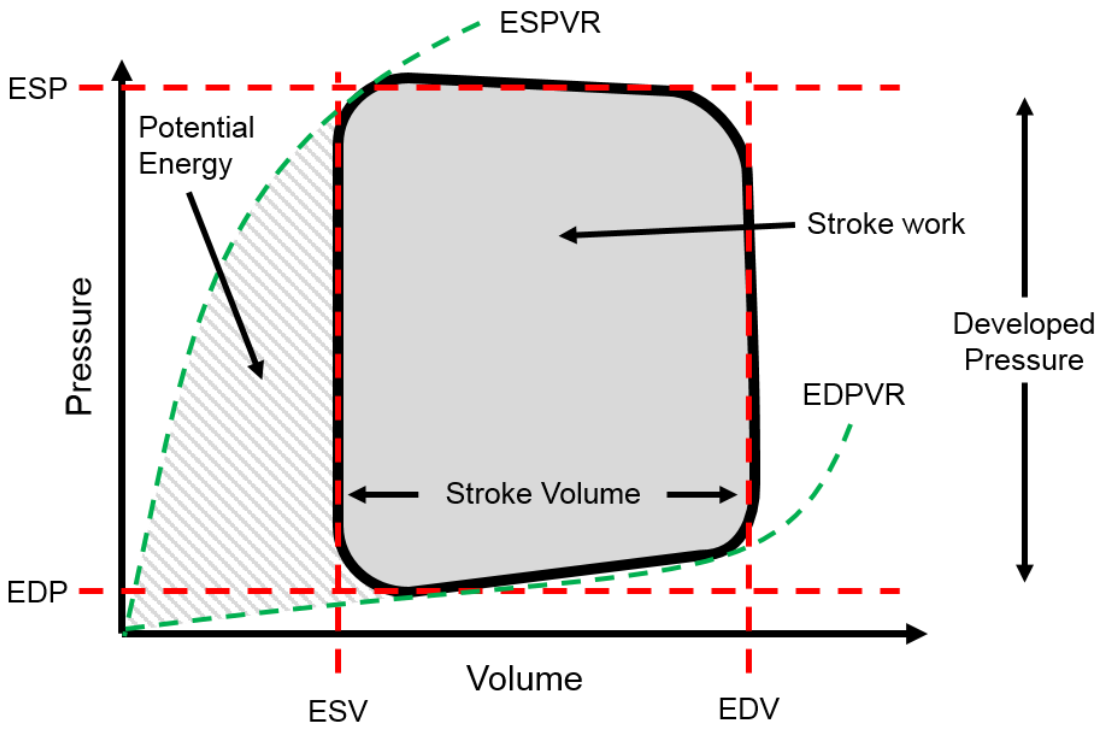


Figure 1-6 - Illustration of cardiac output using pressure-volume relationship.

1.1.5 Failure of the muscular pump

Though a complex range of regulatory mechanisms exist to tune cardiac function to physiological needs, in states of disease these pathways can be insufficient to re-establish proper activity. If the mechanisms of pathogenesis are not ameliorated, heart failure can result. The fundamental definition of heart failure is the inability of the heart to supply sufficient blood to the body [McMurray *et al.*, 2012]. This phenotype is common and costly in high-income countries. In 2011, heart failure and associated disease in the United States cost $116.3 billion in direct medical expenses and an additional $99.3 billion in loss of productivity [Mozaffarian *et al.*, 2015]. Further, increasing morbidity and mortality due to heart failure has also made prevention a key priority in low-income countries [WHO, 2014]. The proximate causes of heart failure are diverse. Abnormalities of the cardiac valves, electrical conductance, or heart rhythm can all lead to disease [McMurray *et al.*, 2012].

However, the most common classes of failure can be broadly categorized as systolic or diastolic dysfunction.

Systolic failure generally results from weakened cardiac muscle that is unable to eject ventricular contents, resulting in reduced EF. This weakening can be due to myocardial disease or as a result of acute damage. In contrast, diastolic failure is caused by impaired ventricular filling, often due to changes in ventricular stiffness. Increased myocardial stiffness can cause decreased ventricular filling, leading to reduced total cardiac output via the Frank-Starling mechanism. In the opposite manner, decreased cardiac stiffness can cause excessive ventricular filling, which cannot be compensated for by increased contractile force as required by the Law of Laplace [Opie, 2003]. In the example of severe heart failure illustrated in Figure 1-7, systolic and diastolic failures combine to reduce SV and SW. Further, the ratio of SW to potential energy decreases significantly, indicating a reduction in efficiency of contraction. The outcome of these changes is a heart that continues to utilize energy at a high rate, yet does not adequately supply blood to the body. The expected immediate symptoms of such heart failure would be fatigue, breathlessness, and fluid accumulation in the extremities. If not effectively treated, progression of the phenotype leads to additional complications and poor patient prognosis [McMurray *et al.*, 2012].

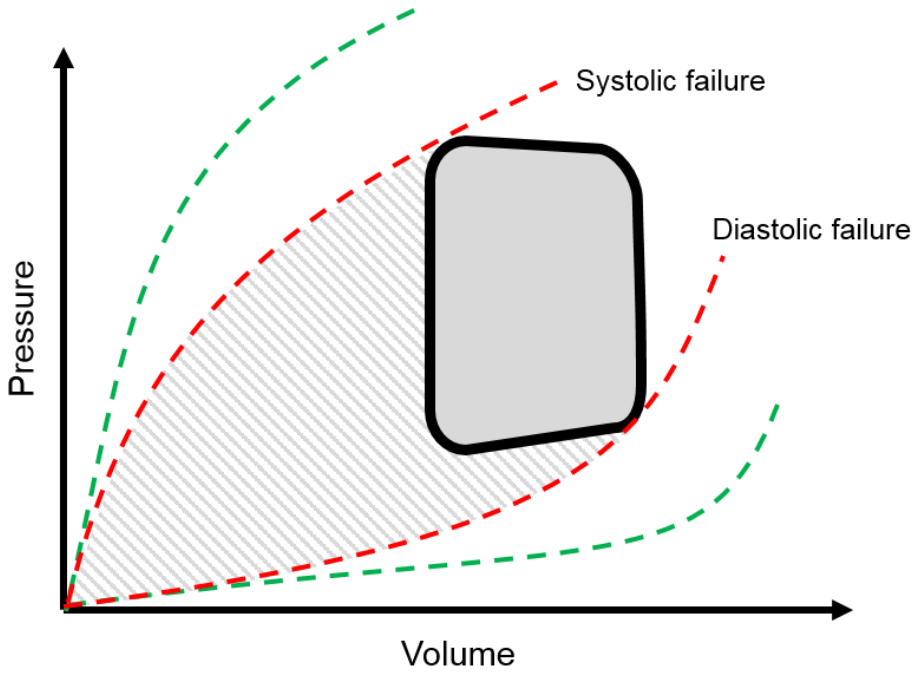


Figure 1-7 - Idealized left ventricular pressure-volume relationship during severe heart failure.

Though the ultimate heart failure phenotype may be common for a variety of patients, effective prevention and treatment of the disease requires an understanding of the mechanism leading to pathology.

1.1.6 Inherited cardiomyopathy

One fundamental cause leading toward heart failure is cardiomyopathy, which can be inherited or acquired [Watkins *et al.*, 2011]. The two most common types of cardiomyopathy are hypertrophic cardiomyopathy (HCM) and dilated cardiomyopathy (DCM), though a number of additional overlapping diseases also exist (Figure 1-8). Classification of these diseases is generally accomplished according to functional and morphologic features; however, molecular genetics can provide finer diagnostic resolution in some instances [Elliott *et al.*, 2008]. Difficulty in classification arises from considerable heterogeneity within disease categories as well as distinct phenotypic responses to mutations at differing locations of the same gene [Kamisago *et al.*, 2000].

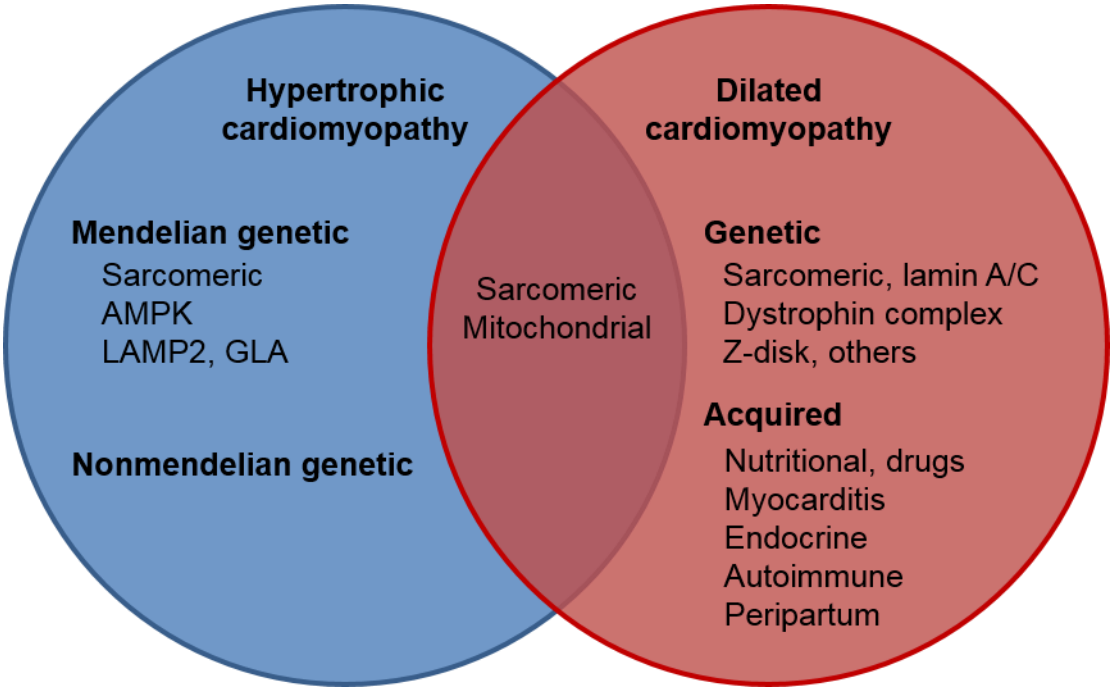


Figure 1-8 - Overlapping categories of hypertrophic and dilated cardiomyopathy. Adapted from [Watkins *et al.*, 2011] Figure 1.

HCM is the most common inherited cardiomyopathy with an estimated prevalence of 1 in 500 [Maron *et al.*, 1995]. It is also the most common cause of sudden cardiac death among young people and has gained particular attention due to its role in the deaths or early retirements of prominent athletes [Maron *et al.*, 1996]. HCM is highly heterogeneous, with symptomatic presentation possible at any age from infancy to >80 years of age [Maron, 2002]. The hallmark feature of the disease is unexplained muscular thickening (hypertrophy), predominantly of the left ventricle but often also the interventricular septum and sometimes right ventricle [Watkins *et al.*, 2011]. Additional characteristic features are disorganization of the ventricular cellular architecture, development of interstitial fibrosis, and disruption of electrical conductance pathways. Clinical diagnosis of HCM begins with a positive family history, abnormal electrocardiogram, or apparent heart murmur. Confirmation of the diagnosis is accomplished more readily by detecting a hypertrophied ventricular

chamber without apparent cause via 2-dimensional echocardiography [Elliott *et al.*, 2014].

The prognosis of HCM patients varies considerably. Patients can live asymptomatically their entire lives, or suffer sudden death in childhood. Intermediate presentations of the disease include heart failure, causing fatigue and breathlessness, or sustained arrhythmias such as atrial fibrillation. Sudden death is most prevalent in children and young adults, though it can occur at any age. Further, though sudden death is most common during rest or mild exercise, it also occurs frequently during vigorous physical activity [Maron, 1996]. The overall annual mortality rate for HCM is only about 1 %; however, subsets of the cohort may be at much higher risk (>5 % annually) [Maron, 2002]. Risk stratification of the HCM population remains a significant challenge. In general, a direct correlation between maximum LV thickness and sudden death propensity exists [Spirito *et al.*, 2000]. Further, the genetic background of a patient, particularly the specific disease-causing mutation, has also been found to play a significant role in sudden death risk. For example, certain mutations in the β-myosin heavy chain and troponin T proteins result in a higher likelihood of sudden death compared to mutations in myosin binding protein C or α-tropomyosin [Moolman *et al.*, 1997; Maron, 2002]. The increased sudden death risk due to troponin T mutations is particularly interesting given the relative lack of LV hypertrophy observed in these patients.

No direct cure exists for HCM. Therefore, physicians focus on minimising complications of the disease while managing symptoms [Elliott *et al.*, 2014]. Non-invasive, chronic management of HCM is accomplished with a variety of pharmaceuticals including β-adrenergic blockers, disopryamide, and verapamil. The primary aim of these negatively inotropic drugs is to reduce symptoms, such as

chest pain or shortness of breath, by reducing the hypercontractility seen at whole heart level which tends to lead to outflow tract obstruction. They may also lessen the risk of sudden death by slowing the heart rate and inhibiting arrhythmic pathways, but such effects are not well documented. For higher-risk patients, an implantable cardioverter-defibrillator (ICD) is the most effective method of preventing sudden death [Qintar *et al.*, 2012]. If expulsion of blood from the LV becomes obstructed by hypertrophy of the septum despite medication, surgical techniques can be applied to improve function. Specifically, ventricular septal myectomy involves removal of a small amount of muscle from the ventricular septum just beyond the margin of the mitral valve [Maron, 2002]. This can also be accomplished by injecting alcohol in a septal artery to create a scar in place of the impeding septal muscle [Elliott *et al.*, 2014]. Despite success of these methods in sudden death prevention, symptom management, and improving patient quality of life, none directly treat causes of the disease and therefore cannot stop, or reverse, its progression. To create new, curative therapeutics, it is therefore essential to understand the mechanism of disease pathogenesis.

As a familial condition, the HCM disease pathway initiates with an autosomal dominant mutation, typically inherited from one parent. The first such mutations were found in the gene encoding β-myosin heavy chain in 1990 [Geisterfer-Lowrance *et al.*, 1990; Tanigawa *et al.*, 1990]. In the 25 years since, hundreds of mutations in nine genes encoding sarcomeric proteins have been convincingly shown to cause the disease, resulting in HCM being termed a “disease of the sarcomere” [Thierfelder *et al.*, 1994; Watkins *et al.*, 2011]. Approximately 60 % of HCM cases can be attributed to a known causal mutation [Elliott *et al.*, 2014]. Of those, the most common mutations occur in *MYH7*, the gene encoding β-myosin

heavy chain, and *MYBPC3*, the encoding cardiac myosin-binding protein C. Each of these genes accounts for 25-35 % of the total identifiable cases. Other established causal mutations, in genes encoding actin, myosin light chains, troponin subunits, and tropomyosin, account for less than 5 % of cases each [Richard *et al.*, 2003]. These mutations generally cause single amino acid substitutions and result a malfunctioning protein being incorporated into the sarcomere. The exceptions to this rule are *MYBPC3* mutations that cause truncated proteins and missense mutations leading to haploinsufficiency [Marston *et al.*, 2009; van Dijk *et al.*, 2009]. These mutations cause a reduced level of functional protein within the sarcomere.

Compared to HCM, the causes of DCM are complex. Approximately one third to one half of DCM cases are caused by inherited mutations, most commonly in an autosomal dominant fashion [Jefferies and Towbin, 2010]. These mutations occur in genes encoding proteins involved in the sarcomere (both contractile and structural aspects), nuclear envelope, gene transcription, and Ca^{2+} handling [Dellefave and McNally, 2010]. Non-inherited forms of DCM can occur due to infection, drug use, or autoimmune activity [Jefferies and Towbin, 2010]. The end-stage phenotype associated with the disease includes LV dilatation, systolic dysfunction, myocyte death, and myocardial fibrosis [Watkins *et al.*, 2011]. Current treatments aim to ameliorate the development and symptoms of heart failure and prevent arrhythmias. However, the complex molecular and cellular mechanisms underlying the disease have challenged the production of curative therapies [Watkins *et al.*, 2011].

To better understand the causes of HCM and DCM, and hypothesize strategies to prevent their progression, a clear understanding of the cellular mechanisms of ventricular function must be developed.

1.2 Mechanisms of ventricular muscle function

Contraction in ventricular muscle is regulated via a process called excitation-contraction coupling. This process links electric signals generated by pace-making nodal cells to force production by cardiomyocytes in the ventricles. Transduction of this signal involves the passage of electrical stimulation, generation of a secondary Ca^{2+} signalling transient, and ultimate generation of contractile force.

1.2.1 Microscopic physiology of ventricular muscle

Ventricular cardiomyocytes are composed primarily of aligned contractile fibres, called myofilaments, which are responsible for force production. Signalling structures responsible for activating the myofilaments lie near invaginations of the cellular membrane, called T-tubules, which serve to increase the surface area available for recognition of external signals. A schematic illustration of T-tubules is shown in Figure 1-9. The figure also illustrates the temporal relationship between a stimulatory cardiac action potential, intracellular Ca^{2+} transient, and contractility.

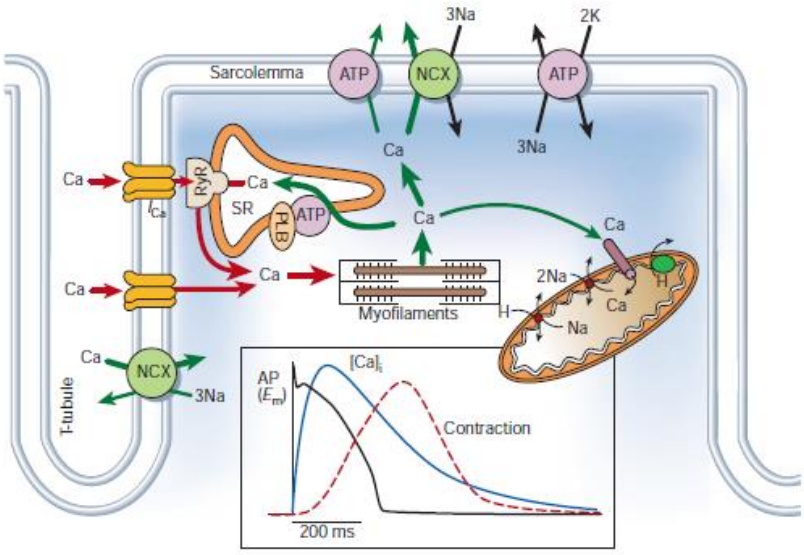


Figure 1-9 - Schematic illustration of Ca^{2+} transport mechanisms in rabbit ventricular myocytes with inset plot of membrane action potential, intracellular Ca^{2+} concentration, and cellular contraction. Adapted from [Bers, 2002] Figure 1.

1.2.2 Action potential generation and propagation

Contraction in cardiomyocytes is coordinated by the propagation of electrical action potentials. These action potentials are based on the cellular membrane potential resulting from the difference in charged ion concentrations within and outside the cell [Lote, 2012]:

Ion	Extracellular Conc. (mM)	Intracellular Conc. (mM)
Na^+	135 - 145	10
K^+	3.5 - 5	155
Cl^-	95 - 110	10 - 20
Ca^{2+}	2	10^{-4}

These concentration differences are maintained because cellular membranes are largely impermeable to charged ions. However, cardiomyocytes possess a range of membrane channels that permit passage of charged ions (primarily K^+, Ca^{2+}, Cl^-, and Na^+) across the cellular membrane. Electrical potential across the membrane can be calculated based on concentrations of charged ions as well as permeability of the membrane to each using the Goldman-Hodgkin-Katz voltage equation [Goldman, 1943]. In unstimulated cardiomyocytes, the membrane is most permeable to K^+ and largely impermeable to the other ions. Therefore, the resting potential of cardiomyocytes is dominated by the K^+ equilibrium potential (-80 mV). Taking into account the other ions, the resting potential of ventricular cardiomyocytes drops to -85 to -95 mV [Berne, 2004].

Though the membrane potential is dependent on ion channel permeability according to the voltage equation, permeability of the channels is in turn dependent on the membrane potential. The feedback loops created by this interdependence lead to rhythmic action potentials in cardiomyocytes. Specifically, upon stimulation

of ventricular cardiomyocytes (Figure 1-10, A), fast Na^+ channels open and a rapid influx of Na^+ ions increases the membrane potential. This high membrane potential inactivates fast Na^+ channels and opens K^+ and Cl^- channels. As oppositely charged ions exit the cell, little change in membrane potential occurs. The plateau phase of the action potential occurs as L-type Ca^{2+} channels open to allow Ca^{2+} ion into the cell while K^+ ions continue to leave. Subsequently, L-type Ca^{2+} channels close while additional K^+ channels open, resulting in a return of the membrane potential to its resting value. Timing of these action potentials is regulated by refractory periods – portions of time in which the membrane channels cannot be activated (or require greater stimulus). These recuperation times allow cardiomyocytes to return to resting membrane potentials between stimulations and help prevent arrhythmic beats.

In the healthy heart under normal conditions, generation of rhythmic stimuli to induce contraction occurs in a group of specialized cells in the right atrium called the sinoatrial node (SAN). Action potentials within the SAN are regulated by a similar series of events altering ion channel permeability and membrane potential. The most important difference is the increased presence of slow, inward Na^+ currents ("funny" currents) when the membrane potential is significantly negative (Figure 1-10, B). These funny currents, combined with transient inward Ca^{2+} currents through T-type Ca^{2+} channels that open at approximately -50 mV, result in spontaneous membrane depolarization. Further, as fast Na^+ channels do not exist in SAN cells, the remainder of the action potential is controlled by Ca^{2+} and K^+ flux. The rate of spontaneous depolarization within the SAN is approximately 60-100 beats per minute. However, this rate is externally controlled by the parasympathetic and sympathetic nervous system. Persistent parasympathetic stimulation

decreases the resting pacing rate whereas intermittent sympathetic stimulation is applied to increase the pacing rate to meet demand.

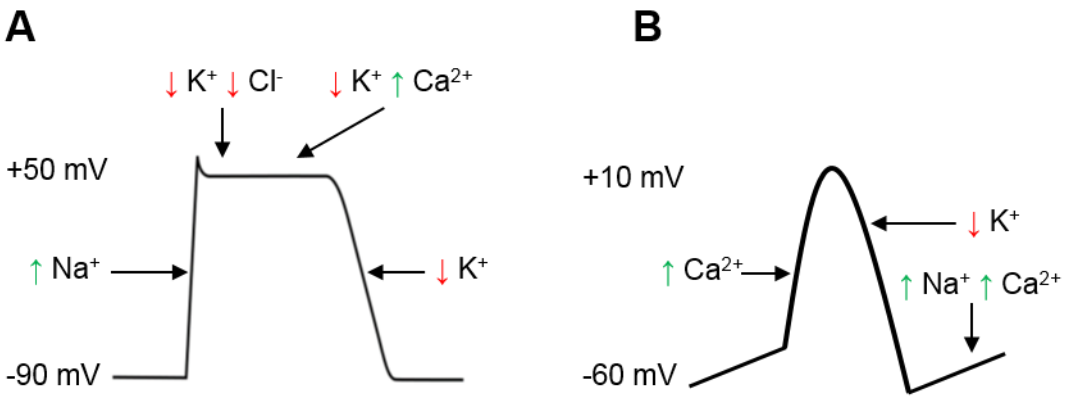


Figure 1-10 - Classical models of ventricular (A) and sinoatrial node (B) action potentials.

1.3 Ca^{2+} handling in ventricular cardiomyocytes

Beyond their role in regulating action potential generation and propagation, Ca^{2+} ions are also responsible for excitation-contraction coupling within the ventricular cardiomyocyte. This essential role requires that initiation, propagation, and termination of each Ca^{2+} transient are tightly controlled. To accomplish this regulation, a number of channels and regulators are involved. Initially, Ca^{2+} ions enter the cardiomyocyte via L-type Ca^{2+} channel, initiating calcium-induced calcium release from the sarcoplasmic reticulum (SR) via the ryanodine receptor (RyR). To reduce cytosolic Ca^{2+} concentrations during diastole, Ca^{2+} ions are pumped back into the SR by the sarco/endoplasmic reticulum Ca^{2+}-ATPase (SERCA), which is essentially regulated by phospholamban (PLN). In addition, Ca^{2+} ions are pumped out of the cell by the sodium-calcium exchanger (NCX). The approximate contributions of these channels and pumps to the overall Ca^{2+} transient, including timing and magnitude, is indicated in Figure 1-11. The structure, function, and regulation of each protein is discussed in greater detail in the following sections.

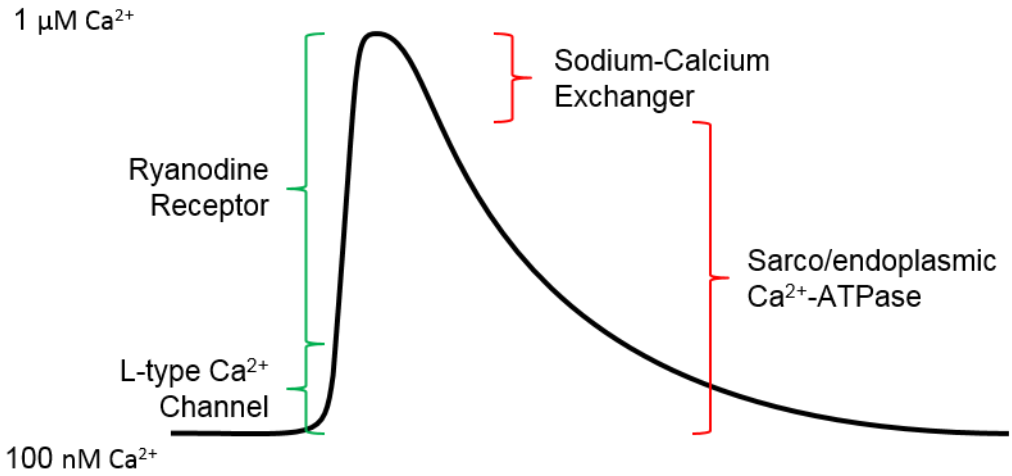


Figure 1-11 - Schematic illustration of a Ca^{2+} transient in a ventricular cardiomyocyte. Approximate contributions by essential Ca^{2+} pumps and channels to calcium intake/release (green) and reuptake/extrusion (red) are also indicated.

1.3.1 L-type Ca^{2+} channel (LTCC)

The predominant Ca^{2+} channel involved in the cardiac action potential and Ca^{2+} transient is the "L-type" Ca^{2+} channel [Reuter, 1983]. This naming convention was established following the discovery of the three primary Ca^{2+} channel in chick sensory neurons. The channels were named based on the period of increased channel conductance following strong membrane depolarization – long-lasting ("L-type"), transient ("T-type"), or unitary ("N-type") [Fox *et al.*, 1987; Fox *et al.*, 1987]. The initial purification of the LTCC was conducted in skeletal muscle, taking advantage of the high-affinity binding of dihydropyridine antagonists to the channels as well as a high density of LTCCs within the transverse T-tubules of the muscle [Curtis and Catterall, 1984]. This high affinity to dihydropyridines has resulted in the LTCC also being termed the dihydropyridine receptor [Rios and Brum, 1987].

The LTCC is made up of α1 (175 kDa), α2 (143 kDa), β (54 kDa), γ (30 kDa), and δ (27 kDa) subunits [Tanabe *et al.*, 1987; Ellis *et al.*, 1988; Ruth *et al.*, 1989; Jay *et al.*, 1990].The α1 subunit is composed of four homologous membrane-spanning domains and is predicted to form the majority of the channel structure [Yamakage

and Namiki, 2002]. Each membrane-spanning domain contains a single transmembrane segment distinguished by a series of positively-charged amino acids. This region serves as a voltage sensor, inhibiting passage of non-Ca^{2+} ions [Ghosh and Greenberg, 1995]. The α2 subunit contains multiple transmembrane segments as well as a significant extracellular domain which is heavily glycosylated [Ellis *et al.*, 1988]. The β subunits are hydrophilic and not glycosylated, so likely intracellular [Takahashi *et al.*, 1987]. The γ subunits are primarily transmembrane whereas the δ subunits have transmembrane and extracellular domains [Catterall, 1995]. The expression of the α1 subunit is sufficient to produce a functional Ca^{2+} channel regulated by dihydropyridines [Mikami *et al.*, 1989]; however, addition of the secondary subunits significantly alters conductance of the channel under various stimuli. Further, these secondary subunits are the target of many drugs, kinases, and phosphatases that influence behaviour of the channel [Catterall, 1995]. Of particular importance is phosphorylation of the α and β subunits by protein kinase A (PKA), which increases the open probability and conductance of the channel [Curtis and Catterall, 1985].

Activation of the LTCC channel occurs over the range of membrane potentials between -20 and + 20 mV whereby conformational shifts allow the influx of Ca^{2+} ions into the cell [Fox *et al.*, 1987]. This activity decays exponentially with a time constant of approximately 500 ms. This influx of Ca^{2+}, combined with mechanical interaction between the L-type Ca^{2+} channel and the RyR on the SR, initiates a process called calcium-induced calcium release to amplify the Ca^{2+} signal and drive contraction within the cardiomyocyte [Fabiato, 1983].

1.3.2 Ryanodine receptor (RyR)

The mechanism of calcium-induced calcium release relies on the RyR channel protein on the SR surface. This theory suggests that the Ca^{2+} influx from the L-type Ca^{2+} channels does not directly activate contraction but instead triggers a more significant release of Ca^{2+} from the SR [Fabiato, 1983]. Evidence for this theory includes findings that no amount of extracellular Ca^{2+} could initiate contraction without initiating Ca^{2+} release from the SR [Fabiato and Fabiato, 1977; Fabiato and Fabiato, 1979], that the SR is the only Ca^{2+} storage site capable of initiating contraction [Fabiato and Fabiato, 1975; Fabiato and Fabiato, 1978], and that the rate of extracellular Ca^{2+} influx alone could not match experimental measurements [Fabiato, 1982]. Subsequent experiments demonstrated that Ca^{2+} ions entering the cell activate RyR receptors on the surface of the SR and cause SR Ca^{2+} release.

The RyR was discovered as the SR Ca^{2+} channel [Inui *et al.*, 1987] and named as such due to its specific binding of the poisonous plant alkaloid ryanodine. RyRs exist in three isoforms (RyR1, RyR2, and RyR3) with RyR2 being the predominant form in cardiac muscle. Each isoform is approximately 5000 amino acids and forms a homotetrameric channel with a quarterfoil shape [Wagenknecht *et al.*, 1989]. The centre of the quaternary structure includes a 1-2 nm pore, most likely representing the Ca^{2+} channel. On the cytoplasmic end of the structure, a “plug” of the channel impedes its permeability at rest [Zucchi and Ronca-Testoni, 1997]. Activation of the RyR receptor is accomplished by the combination of at least two mechanisms. First, the proximate L-type Ca^{2+} channel undergoes a conformational shift upon sarcolemmal depolarization and activates the RyR mechanically [Rios and Pizarro, 1991]. Second, and presumed to be the dominant effect in cardiac muscle, Ca^{2+} influx increases local Ca^{2+} concentrations, directly activating the RyR [Nabauer *et*

al., 1989]. Upon activation, the channel "plug" shifts and the RyR mediates efflux of Ca^{2+} from the SR. RyRs span the SR membrane and preferentially locate near the sarcolemmal T-tubules and associated L-type Ca^{2+} channels (Figure 1-9) [Fleischer *et al.*, 1985].

Activity of the RyRs can be modulated by a number of endogenous agents. *In vivo*, RyR2 exists as a macromolecular complex containing cAMP-dependent protein kinase (PKA), FKBP12.6 (FK-506-binding protein 12.6), phosphatases (PP1 and PP2a), calmodulin, calmodulin-dependent protein kinase II (CaMKII), phosphodiesterase 4D, triadin and junctin [Bers, 2006]. In addition, RyR has been shown to be a substrate of cGMP-dependent protein kinase (PKG) and protein kinase C (PKC) [Zucchi and Ronca-Testoni, 1997]. Phosphorylation of RyR by PKA, PKG, or PKC at Ser-2808 has been shown to increase its open probability and Ca^{2+} sensitivity [Takasago *et al.*, 1991]. However, other recent reports have suggested that phosphorylation at Ser-2030 is instead the dominant cause of the PKA response [Xiao *et al.*, 2006]. Determination of RyR's regulatory pathways is of keen interest to the field because the open probability and Ca^{2+} sensitivity of RyR2 has been linked to human arrhythmias [Jiang *et al.*, 2005].

The most-studied exogenous modulator of RyR activity is caffeine. At low concentrations (0.5 to 2 mM), caffeine caused increased Ca^{2+} sensitivity of RyR activation. At higher concentrations of caffeine (5 to 10 mM), RyR could be activated by picomolar Ca^{2+} concentrations. Caffeine treatment also increased the lifetime of the open channel [Lai *et al.*, 1988; Rousseau *et al.*, 1988]. Caffeine treatment of intact cardiomyocytes is expected to cause a complete, or nearly complete, release of Ca^{2+} from the SR [Bassani, 1995].

The activation of a RyR via calcium-induced calcium release results in a rapid efflux of Ca^{2+} ions from the SR into the cytosol, termed a Ca^{2+} spark [Cheng *et al.*, 1993]. The spatial and temporal summation of thousands of such sparks raises the average cytosolic Ca^{2+} concentration from ~100 nM to 1 μM [Cannell *et al.*, 1994]. Thus, the small amount of Ca^{2+} entering the cell via the L-type Ca^{2+} channels is amplified by Ca^{2+} release from the SR to yield a signal of sufficient magnitude to activate the contractile apparatus.

1.3.3 Sarco/endoplasmic reticulum Ca^{2+}-ATPase (SERCA)

The cytosolic Ca^{2+} concentration must be reduced following each contraction to allow muscle relaxation and replenishment of Ca^{2+} stores. For this reason, other than the small regions proximate to T-tubules specialized for Ca^{2+} release, the majority of the cardiac SR is dedicated for Ca^{2+} reuptake. The primary protein channel in these areas is appropriately the Ca^{2+} ATPase SERCA [Stewart and MacLennan, 1974; Periasamy and Huke, 2001], which removes >70 % of cytosolic Ca^{2+} after each beat [MacLennan and Kranias, 2003].

The SERCA family of protein pumps is encoded by three highly homologous genes (*SERCA1*, *SERCA2*, and *SERCA3*) [Arai *et al.*, 1994]. In cardiac muscle, the predominant form is a splice isoform of *SERCA2*, called SERCA2a [Zarain-Herzberg *et al.*, 1990]. SERCA is a 110 kDa protein whose crystal structure was solved by Toyoshima et al. [Toyoshima *et al.*, 2000]. The transmembrane region of the pump comprises 10 α-helices (M1-M10) with varying length and inclination to the membrane. Ca^{2+} ion binding occurs in two sites: one between M5, M6, and M8 and the other proximate to M4. The cytoplasmic region of the enzyme encompasses three domains which are the sites of regulatory phosphorylation and ATP hydrolysis.

The function of SERCA is characteristic of P-type ATPases and can be described in four stages [MacLennan *et al.*, 1997]. First, two Ca^{2+} ions bind to the enzyme. SERCA is then phosphorylated by ATP to SERCA-P, causing a conformational shift that prevents re-exchange of Ca^{2+} ions into the cytosol. Third, and the rate-limiting step of the reaction, is release of two captured Ca^{2+} ions into the SR in exchange for two protons. Finally, hydrolysis of SERCA-P restores accessibility of the high-affinity Ca^{2+} binding pockets to the cytosol.

The importance of SERCA in reducing cytosolic Ca^{2+} concentrations and restoring SR Ca^{2+} content is highlighted by its relevance to pathophysiology and therapeutic development. Dysfunction in SR Ca^{2+} reuptake has been identified in animal models of heart disease as well as end-stage human heart failure [Arai *et al.*, 1993; Arai *et al.*, 1994]. This impaired activity results in increased basal cytosolic Ca^{2+} concentrations and reduced SR Ca^{2+} stores, both of which can contribute further to dysfunction [Beuckelmann *et al.*, 1992]. Associated with this dysfunction were decreases in SERCA2a expression at both mRNA and protein levels [Arai *et al.*, 1993; Hasenfuss *et al.*, 1994]. Therapeutically, gene transfer of SERCA to isolated cardiomyocytes from failing human hearts was shown to improve contractile function [del Monte *et al.*, 1999]. This improvement could also be demonstrated using SERCA2a overexpression in aortic-banded rats [Miyamoto *et al.*, 2000]. These early successes have led to multiple clinical trials of SERCA2a gene therapy in humans [Periasamy and Kalyanasundaram, 2008].

1.3.4 Phospholamban (PLN)

Regulation of SERCA's activity is accomplished most significantly by PLN, which is a 52-AA, reversibly phosphorylated protein located in the SR membrane [MacLennan and Kranias, 2003]. The cytosolic domains of the protein (amino acids

1-30) contain two phosphorylation sites (S16 and T17) which are essential to the protein's regulatory function. The interaction between PLN and SERCA occurs in PLN's transmembrane domain (amino acids 31-52).

Binding of PLN to SERCA inhibits the pump's activity by decreasing its Ca^{2+} affinity by 50-70 % [Tada *et al.*, 1975] and reducing the energetic efficiency of Ca^{2+} transport [Frank *et al.*, 2000]. At physiological Ca^{2+} concentrations, these effects reduce Ca^{2+} transport from 90 to 30 μM/s [Bers, 2001]. The binding of PLN to SERCA is relieved by phosphorylation of PLN by PKA at S16 or by Ca^{2+}/CaM-dependent protein kinases at T17 during β-adrenergic stimulation [Kranias and Solaro, 1982; Wegener *et al.*, 1989]. Removing inhibition of SERCA activity is presumed to be the primary determinant of the positive inotropic and lusitropic effect of β-adrenergic stimulation [MacLennan and Kranias, 2003]. Studies using phosphorylation-site-specific PLN mutants suggested that S16 phosphorylation alone may be sufficient to yield the complete β-adrenergic response [Luo *et al.*, 1998; Chu *et al.*, 2000] whereas T17 phosphorylation may be more important during direct cardiac stress such as ischaemic insult [Vittone *et al.*, 2002]. These phosphorylations cause a conformation change in PLN that reduces its affinity for SERCA while increasing its affinity for other PLN monomers. Phosphorylated PLN detaches from SERCA and forms homopentameric complexes, serving as temporary stores of the inhibitory proteins [Kimura *et al.*, 1997].

As described above, impaired SR Ca^{2+} reuptake and diminished SR Ca^{2+} stores are associated with reduced SERCA levels in human heart failure. In contrast, levels of PLN in these disease states appear unaffected [Movsesian *et al.*, 1994; Schwinger *et al.*, 1995]. This discrepancy results in a decreased SERCA/PLN ratio, leading to greater inhibition of the remaining SERCA pumps. Phosphorylation of PLN at S16

and T17 is also reduced in examples of heart failure [Meyer *et al.*, 1995; Schwinger *et al.*, 1995; Schwinger *et al.*, 1999], further increasing SERCA inhibition and exacerbating Ca^{2+} reuptake dysfunction.

A homolog of PLN is sarcolipin (SLN), which possesses highly similar structure and may also regulate SERCA activity [Odermatt *et al.*, 1997; Odermatt *et al.*, 1998].

1.3.5 Sodium-calcium exchanger (NCX)

Though the majority of cytosolic Ca^{2+} is taken back into the SR during diastole, the NCX also transports 7 - 30 % (species dependent) of cytosolic Ca^{2+} ions outside the cardiomyocyte [Bers, 2000; DiPolo and Beauge, 2006]. Under normal conditions, the NCX utilizes energy stored in the electrochemical gradient of Na+ ions to transport one Ca^{2+} ion out of the cell in exchange for three Na+ ions. This activity begins the reduction of intracellular Ca^{2+} transient while simultaneously counterbalancing the Ca^{2+} ions that entered the cell via the L-type Ca^{2+} channels.

The NCX was initially hypothesized based on experiments in giant squid axons that demonstrated Ca^{2+} efflux from neurons could be altered by modulating Na^{+} concentration in the external media [Reuter and Seitz, 1968]. The NCX family is composed of three isoforms – NCX1, NCX2, and NCX3, with NCX1 being the cardiac isoform found abundantly in the sarcolemma [Nicoll *et al.*, 1990]. NCX1 is a 110 kDa protein with ten transmembrane regions and one large cytoplasmic domain [Nicoll *et al.*, 1999; Ren and Philipson, 2013]. At present, a complete understanding of the ion-binding sites and ion transport pathway has yet to be developed.

The NCX is a high-capacity transporter (maximum turnover of 5000/s [Niggli and Lederer, 1991]) relative to SERCA (100 /s to 150 /s at physiological conditions [MacLennan, 1970]). However, NCX has very low Ca^{2+} affinity, so operates at a

much lower activity at physiological Ca^{2+} concentration. In disease states, however, when SERCA levels are reduced and cytosolic Ca^{2+} concentrations increased, NCX activity accounts for a greater share of Ca^{2+} removal from the cytosol [Bers, 2000]. Regulation of NCX activity is accomplished by a number of extracellular and intracellular agents [Shigekawa and Iwamoto, 2001]. Of particular interest is that phosphorylation by PKC causes a 30 – 40 % increase in NCX activity [Iwamoto *et al.*, 1996].

In addition to its function in exporting Ca^{2+} ions at high systolic Ca^{2+} concentrations, depolarization of the cellular membrane can reverse the exchanger's direction, resulting in Ca^{2+} influx and Na^{+} export. For example, during the cardiac action potential, the large influx of Na^{+} ions depolarizes the membrane and increases intracellular Na^{+} concentrations. Under normal conditions, this reversal switches back upon the influx of Ca^{2+} through the L-type Ca^{2+} channel later in the action potential [Bers, 2002]. However, if internal Na^{+} concentration is increased or action potential durations are prolonged, the reversed NCX activity may persist.

1.4 Regulation of contraction in cardiac muscle

The intracellular Ca^{2+} transient regulated by the aforementioned proteins and channels is the primary signal to the force production apparatus of cardiac muscle: the sarcomere. The sarcomere is the fundamental unit of contraction in striated muscle and is composed of interlocking thin and thick filaments protruding from the structural Z-disk and M-line [Gordon *et al.*, 2000] (Figure 1-12). The thin filament is primarily made up of the filamentous protein actin, which offers binding sites for the contractile motor protein myosin that makes up the thick filament. The interactions between actin and myosin, called actomyosin cross-bridges, produce force and shorten the sarcomere. To regulate the number of active cross-bridges, and

therefore the level of force production, a variety of regulatory pathways act on both thick and thin filaments.

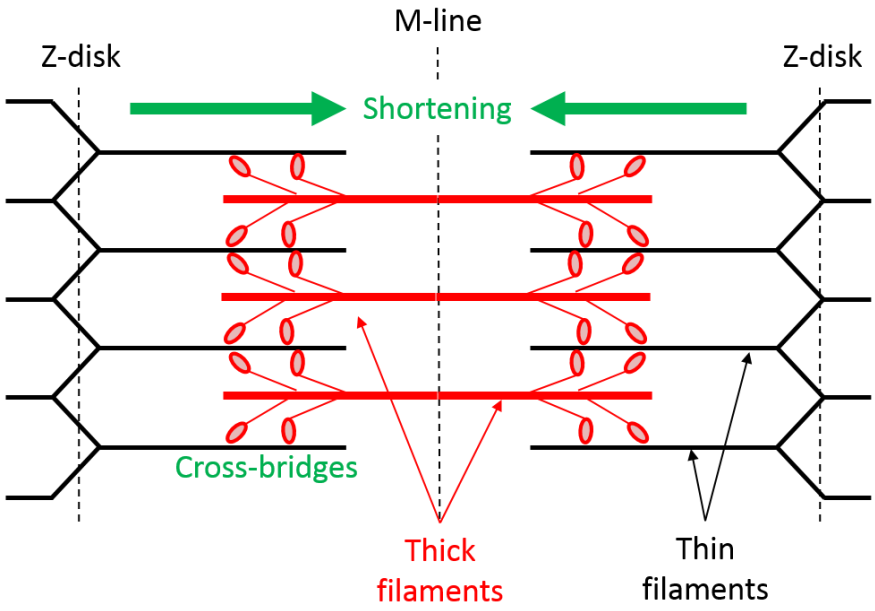


Figure 1-12 - Schematic illustration of the sarcomere. Thin actin filaments are represented in black. Thick myosin filaments are shown in red.

1.5 Thin filament

The thin filament is composed of actin, tropomyosin (Tm), and the troponin (Tn) complex (including TnC, TnI, and TnT subunits) in a 7:1:1 ratio. Together, these proteins form a scaffold to which myosin heads may bind and initiate contraction. During relaxation, myosin binding sites are obstructed by the helical protein Tm, which is held in place by interactions with the Tn protein complex. Upon Ca^{2+} binding to Tn, its restraining action on Tm is relieved, allowing Tm to shift away from myosin binding sites on actin. As myosin heads bind and form strong attachments to the thin filament, Tm shifts further, opening adjacent myosin binding sites. This transduction pathway from initial Ca^{2+} binding to cooperative myosin attachment yields a highly sensitive mechanism for muscular contraction. The structure,

function, and regulation of each of these thin filament proteins are discussed in greater detail in the following sections.

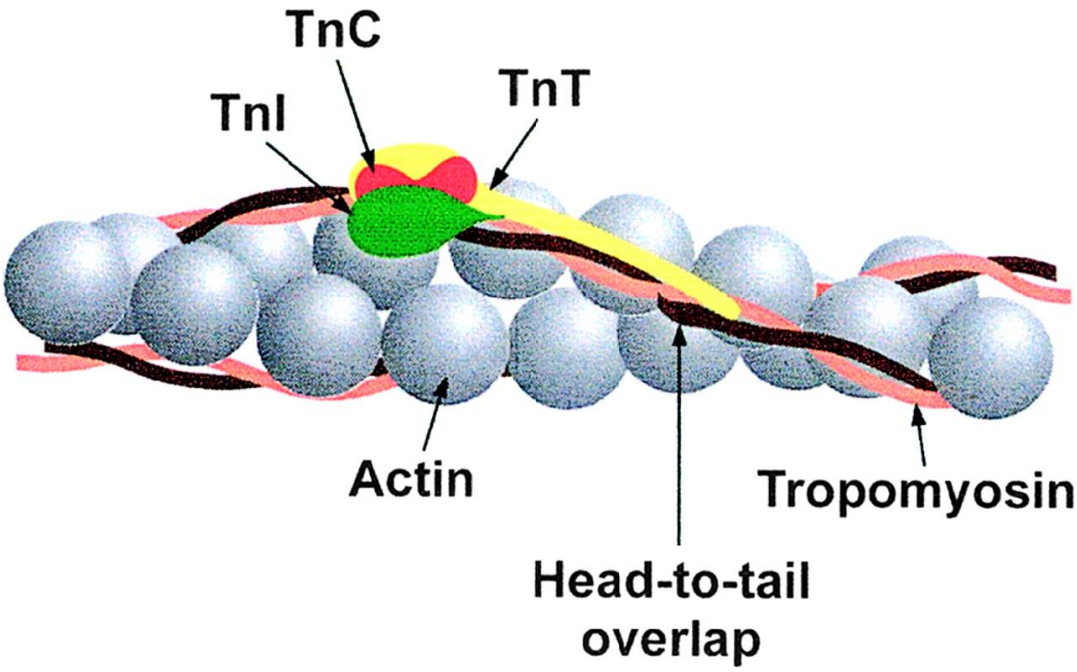


Figure 1-13 - Schematic illustration of thin filament structure. From [Gordon *et al.*, 2000]

1.5.1 Actin

Actin is globular protein that spontaneously forms helical microfilaments in physiological conditions [Reisler, 1993]. These filaments are involved in a large number of cellular processes besides muscle contraction, including cell division and motility, vesicle and organelle movement, and cell signalling. Actin was initially discovered in 1887 as a “ferment which brings about the coagulation of myosin” by W.D. Halliburton [Halliburton, 1887] though was more thoroughly described by Straub in 1942 [Straub, 1942]. Actin is expressed at high levels across cell types; in muscle, it makes up approximately 20 % of total protein mass [Tobacman, 1996]. Further, the structure of actin is highly conserved across species with approximately 95 % primary protein structure homology between *homo sapiens* and *saccharomyces cerevisiae*. *In vivo*, actin exists in a dynamic equilibrium between

its globular G-actin and filamentous F-actin form [Oda *et al.*, 2009]. The crystal structure of G-actin was first solved in 1990 [Kabsch *et al.*, 1990], followed immediately by an accepted model of F-actin structure [Holmes *et al.*, 1990].

Each actin molecule is composed of four subdomains [Gordon *et al.*, 2000]. The smaller subdomains 1 and 2 are located at the periphery of the filament and are involved in myosin binding. The larger subdomains 3 and 4 are axially located within the filament and surround a binding cleft. This cleft includes a pocket for a nucleotide (ATP/ADP) and a divalent ion (Mg^{2+} or Ca^{2+}). Incorporation of an actin molecule into a filament activates the actin ATPase [Pollard, 2007], hydrolysing ATP, ejecting inorganic phosphate, and causing a conformational shift leading to polymerization [Otterbein *et al.*, 2001]. The maintenance of proper actin filament length is regulated by a process called treadmilling, in which polymerization at one end of the filament occurs simultaneously with depolymerisation at the other end [Wegner, 1976].

The structure of F-actin was developed based on X-ray fibre diffraction data. By constructing a model using the solved G-actin crystal structure and comparing the expected and observed diffraction pattern, the F-actin structure is sequentially improved [Oda *et al.*, 2009]. In general, the filament forms a two-stranded long-pitch helical structure. Each actin molecule interacts with two adjacent molecules on the same strand as well as two molecules on the opposite strand (Figure 1-14).

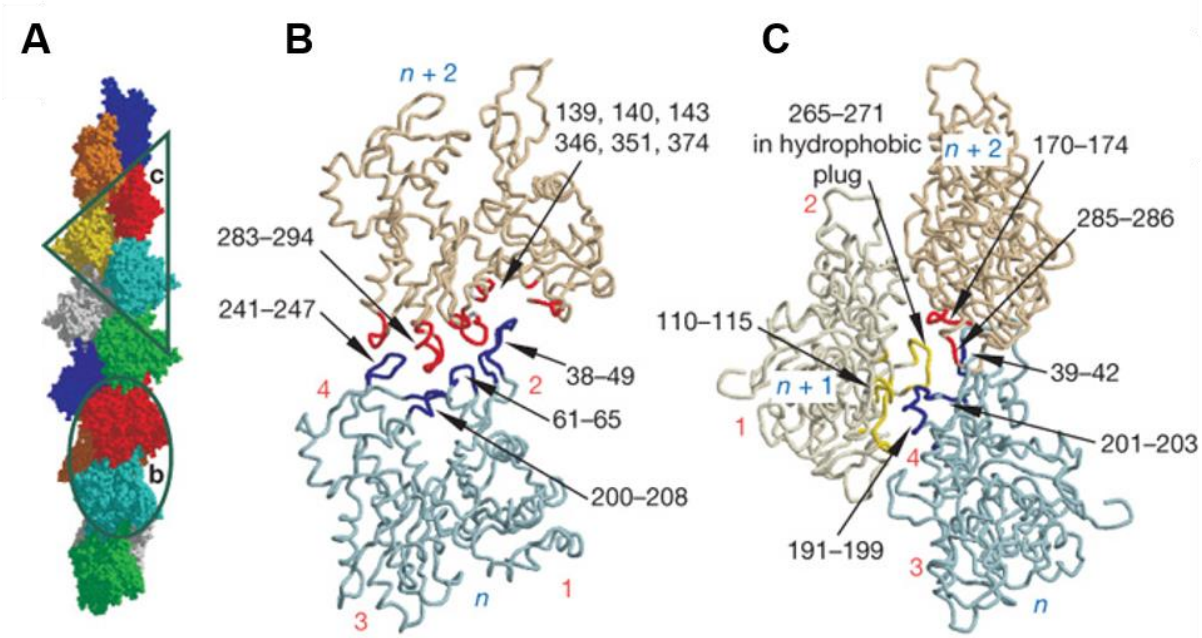


Figure 1-14 - Model of F-actin structure including 13 subunits (A). Interactions between two adjacent subunits is shown in (B). Intra-strand interactions are shown in (C). Adapted from [Oda *et al.*, 2009] Figure 3.

In cardiac muscle, actin filaments serve as the scaffold to which myosin heads bind and exert contractile force. The availability of binding sites on the filament is regulated by the protein Tm, which lays on the actin filament and impedes actomyosin interactions.

1.5.2 Tropomyosin (Tm)

Tm is encoded by four genes, yielding α and β isoforms with varying levels of expression [Tobacman, 1996]. Each gene is capable of differential splicing, yielding even greater mRNA diversity. These isoforms form homodimers or heterodimers depending on the species and muscle type. In cardiac muscle from large mammals, α-α homodimers predominate. The quarternary structure of these dimers is a highly extended coiled coil of α-helices with a length of approximately 42 nm. The stability of this structure is conferred by hydrophobic interactions between side chains on each coil. These structures bind to the actin filament and each spans seven adjacent actin monomers. Electrostatic interactions between charged side chains of Tm and

the periphery of F-actin stabilize this binding. Further, adjoining Tm coils overlap in a head-to-tail fashion, strengthening the filament binding and resulting in a periodicity of 38.5 nm along the thin filament [Gordon *et al.*, 2000].

The length and flexibility of Tm molecules, combined with their relatively weak electrostatic interactions with actin, allow significant motion on the filament surface. This constant, regulated stochastic movement is responsible for the filament's level of activation. Three positions of tropomyosin are associated with increasing levels of activation – blocked, closed, and open (Figure 1-15) [McKillop and Geeves, 1993]. In the absence of Ca^{2+}, the Tn complex restrains Tm in a position blocking myosin binding sites on the actin filament. Specifically, TnI is bound to two actin monomers while the TnT subunit binds to Tm at the Tm-Tm overlap region [Gordon *et al.*, 2001]. Upon Ca^{2+} binding to TnC, TnC interacts with TnI and causes it to detach from actin [Solaro and Rarick, 1998], allowing Tm to move on the filament surface [Xu *et al.*, 1999]. This motion exposes primarily weak, but also some strong, binding sites for myosin heads on the actin filament. At saturating Ca^{2+} concentrations, Tm molecules are positioned such that 80 % of the filament is in the closed state, while 20 % is in the open state [McKillop and Geeves, 1993]. Upon strong myosin binding to actin sites, the Tm molecule is further shifted and confined to the open position.

The head-to-tail interactions of adjacent Tm molecules also allow transduction of the activation signal along the filament. Upon strong cross-bridge binding, the thin filament is activated in the surrounding 12-14 actin monomers [Maytum *et al.*, 1999], greater than a single tropomyosin regulatory section. This suggests that shifting of a single Tm molecule contributes to the motion of adjacent molecules. This transmission leads to cooperativity in the system, reducing the amount of Ca^{2+}

signal required to activate the filament and yield high levels of contraction. As Ca^{2+} intake/extrusion is an energy-intensive process, this cooperativity is essential to reduce muscular energetic expenditure. In addition, the cooperative nature of thin filament activation contributes to coordination of muscle contraction [Gordon *et al.*, 2001].

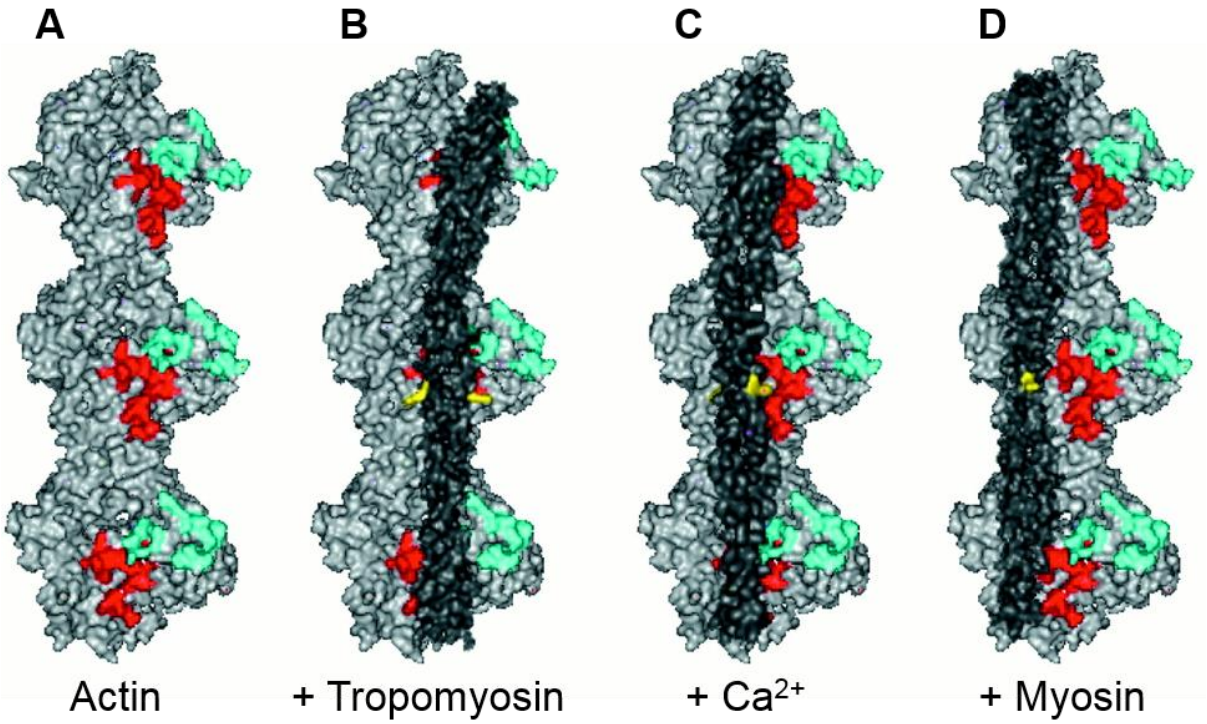


Figure 1-15 - Restriction of myosin binding availability by tropomyosin at various levels of thin filament activation. Actin residues interacting with myosin are highlighted (green = weak interaction, red = strong interaction). Three adjacent actin molecules within one strand of the filament are shown in A. At rest, the Tm helix is shown to block both weak and strong interaction residues (B,"blocked"). Activation of the filament by Ca^{2+} (C, "closed") is shown to shift Tm, exposing weakly interacting actin residues. Upon myosin binding (D, "open"), Tm is further shifted to expose strongly interacting actin residues. Figure adapted from [Gordon *et al.*, 2001] Figure 2.

1.5.3 Troponin (Tn)

Though tropomyosin fundamentally regulates the availability of myosin binding sites on the actin filament, its motion and flexibility is heavily controlled by interactions with the Tn complex. The three subunits of the Tn complex are named according to their primary function: troponin C (TnC) binds Ca^{2+} ions, troponin I (TnI) inhibits

myosin attachment via interactions with Tm, and troponin T (TnT) structurally links the Tn complex with Tm. A schematic illustration of the interactions between Tn subunits and the thin filament is shown in Figure 1-16.

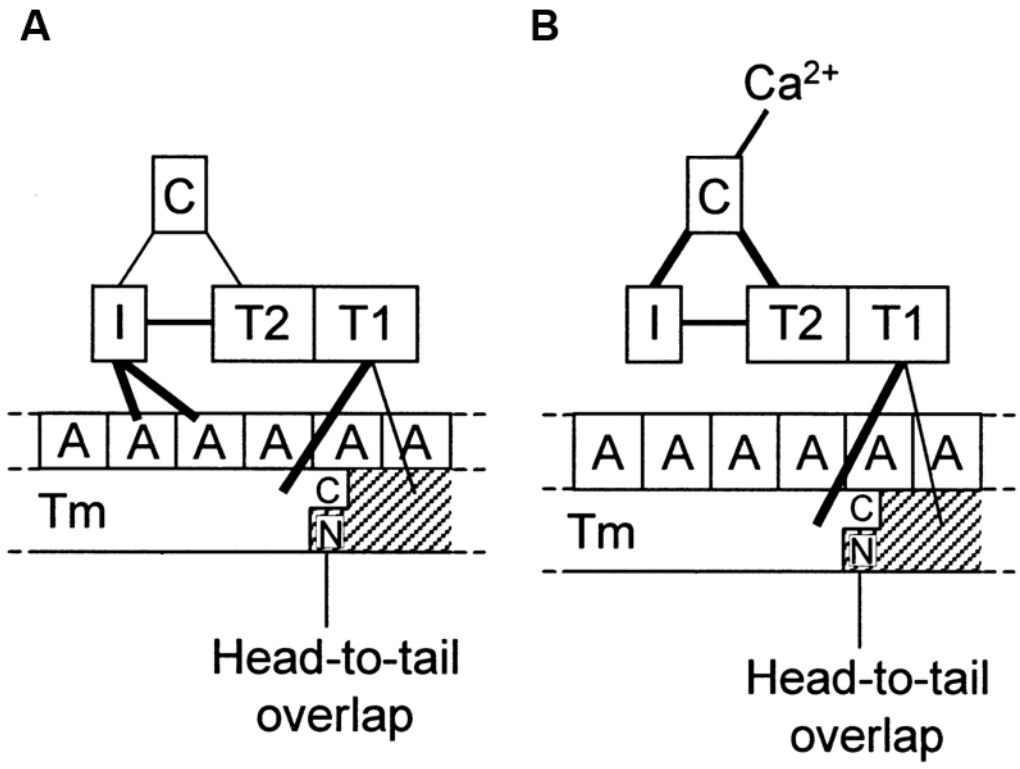


Figure 1-16 - Illustration of troponin subunit interactions. Actin monomers are represented by A blocks, TnI by I, TnC by C, the N-terminal (resides 1-158) of TnT by T1, the C-terminal (159-259) of TnT by T2, and tropomyosin (including head-to-tail overlap section) by Tm. In the absence of Ca^{2+} (A), TnI binds to actin monomers to stabilise the blocked conformation of Tm. In the presence of Ca^{2+} (B), the TnC-TnI and TnC-TnT interactions are strengthened, releasing the binding of TnI to actin and allow the motion of Tm. Figure adapted from [Gordon *et al.*, 2000] Figure 3.

TnC is the fundamental Ca^{2+} sensor within both cardiac and skeletal muscle and its crystal structure has been solved in a variety of conditions [Sundaralingam *et al.*, 1985; Houdusse *et al.*, 1997; Spyracopoulos *et al.*, 1997]. The general shape of the protein is a dumbbell in which the N- and C-terminal domains are separated by a long central α helix. Each terminal domain contains two metal-binding EF-hand motifs. Under physiological conditions, the C-terminal sites (III and IV) are occupied

by Mg^{2+} ions that strengthen the TnC-TnI interaction [Zot and Potter, 1982]. These sites are therefore “structural” and do not play a major role in the activation of the thin filament. In contrast, the N-terminal EF-hand motifs (I and II) have a high selectivity for Ca^{2+} over Mg^{2+} and are therefore primary sensors for intracellular Ca^{2+} concentration within muscular tissues [Potter and Gergely, 1974]. In cardiac muscle, however, site I contains three amino acid substitutions that prevent the coordination of Ca^{2+} ions [van Eerd and Takahshi, 1976]. In addition, it has been shown that removal of site II inhibits Ca^{2+} activation in the myofilament and that titration with the domain restores this functionality [Moss *et al.*, 1985; Pan and Solaro, 1987]. Therefore, cardiac TnC possesses only a single regulatory Ca^{2+} binding domain.

Upon Ca^{2+} binding to the N-terminal EF-hand domains, TnC undergoes a conformational shift that exposes hydrophobic amino acids proximate to TnI. This shift precipitates a hydrophobic interaction between the two proteins leading to detachment of TnI from the actin filament. The extent of the conformational shift may be smaller in cardiac muscle than in skeletal muscle, requiring TnI binding to force open the hydrophobic domain on TnC [Lakowicz *et al.*, 1988]. In addition, the kinetics of cardiac TnC activation by Ca^{2+} are considerably slower than in skeletal muscle. Finally, even in systolic Ca^{2+} concentrations, not all cardiac TnC is activated [Wang and Cheung, 1986]. Together, the weakening of the Ca^{2+} activation pathway in cardiac muscle is suspected to increase the requirement of cooperative activation pathway involving myosin binding [Gordon *et al.*, 2000].

Cardiac TnI (cTnI) is a 23.8 kDa protein responsible for restricting movement of Tm on the actin filament. The cardiac isoform structure is highly homologous to the skeletal isoform, but contains a 27-33 amino acid N-terminal extension. cTnI consists of a flexible central inhibitory region (IR, residues 137-148) surrounded by

four rigid α-helices (residues 43-79 (H1), 90-135 (H2), 150-159 (H3), 164-188 (H4)) [Takeda *et al.*, 2003]. Helices H1 and H2 flank and are stabilized by TnT. Helices H3, H4, and the C-terminal domain lie near the filament at rest. In the presence of Ca^{2+}, H1 also binds to the C-terminal of TnC. Helix H3 is the Ca^{2+}-dependent switch region that dissociates from actin and binds to TnC [Sykes, 2003] upon Ca^{2+} activation. This movement and re-binding of H3 likely drags H4 and the C-terminal region away from actin interactions as well, a motion initially hypothesized based on biochemical studies [Tripet *et al.*, 1997].

The function of cTnI is a Ca^{2+}-dependent brake on tropomyosin motion and muscle activity. The inhibitory effect of the protein was demonstrated by reconstituting filaments with either full-length TnI or the positively charged domain from residues 96-116 (rabbit skeletal TnI, equivalent to IR) and observing a partial inhibition of the myosin ATPase rate [Schaub *et al.*, 1972; Farah *et al.*, 1994]. Complete inhibition of the myosin ATPase required addition of a larger TnI fragment extending into the C-terminus [Farah and Reinach, 1995], equivalent to the H3 and H4 regions.

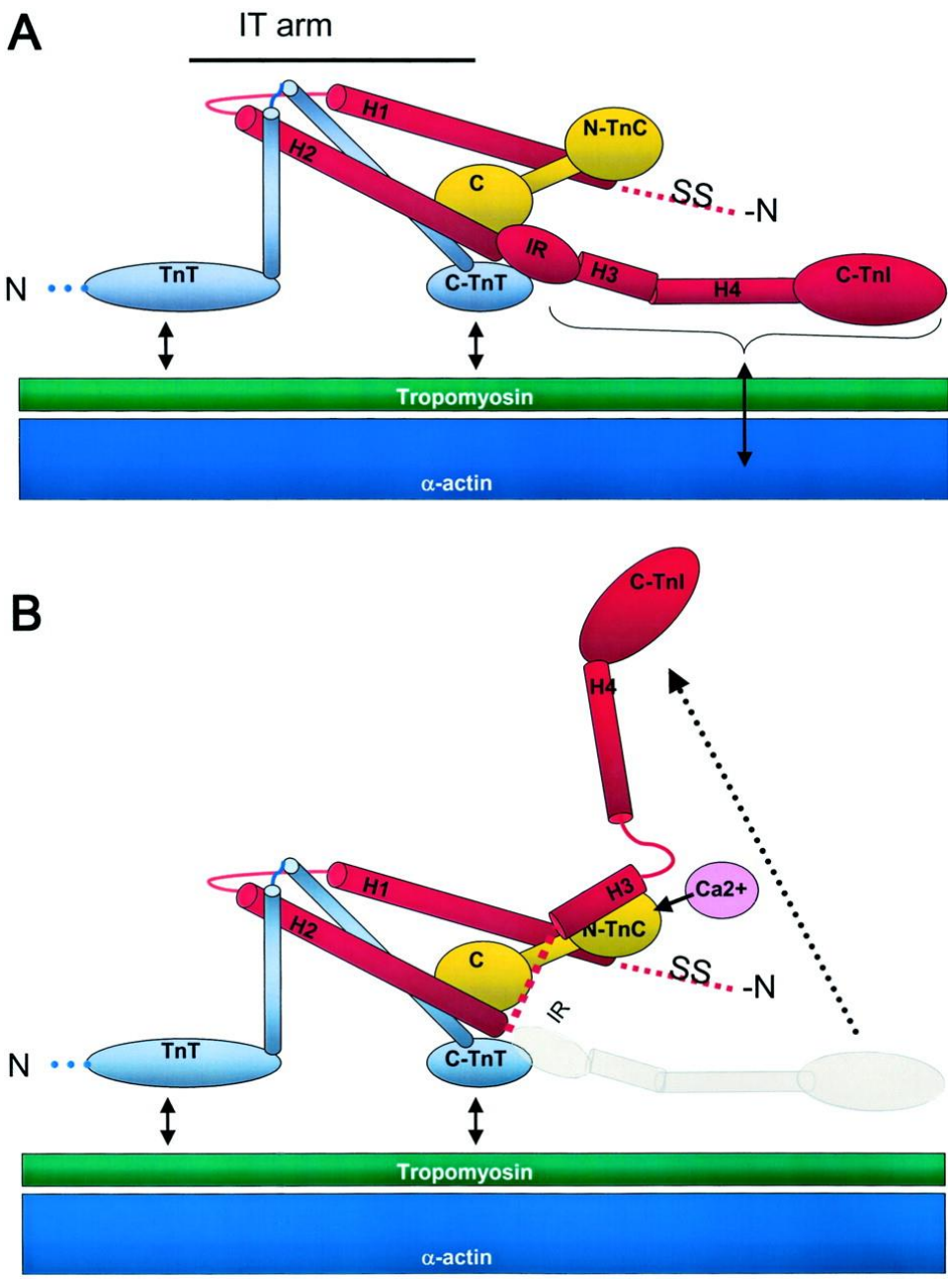


Figure 1-17 - Illustration of calcium-dependent alterations to the troponin core structure. In the absence of Ca^{2+} (A), strong interactions exist between TnI, TnT, actin, and tropomyosin. Upon the addition of Ca^{2+}, TnC-TnI interactions are strengthened and TnI-actin binding is relieved. Helices resolved by Takeda et al [Takeda *et al.*, 2003] are numbered accordingly whereas unsolved domains are represented as ellipses. Figure from [Metzger and Westfall, 2004] Figure 2.

cTnI is also a major target of regulatory kinase activity [Layland *et al.*, 2005] (Figure 1-18). Of foremost importance is phosphorylation of serine residues 23 and 24, located in the N-terminal cardiac extension, by PKA (predominantly), PKG, or PKC. This phosphorylation reduces the strength of the cTnC-cTnI interaction [Metzger and Westfall, 2004] and also increases the speed of Ca^{2+} release from cTnC

[Robertson *et al.*, 1982]. Both of these effects inhibit Ca^{2+}-dependent activation of the thin filament. In some experiments, cTnI S23/S24 phosphorylation increased myosin cross-bridge cycling speeds [Kentish *et al.*, 2001], though the mechanism of this effect is less well-defined. In general, phosphorylations at S23/S24 cause decreased sarcomeric Ca^{2+} sensitivity and increased relaxation speeds.

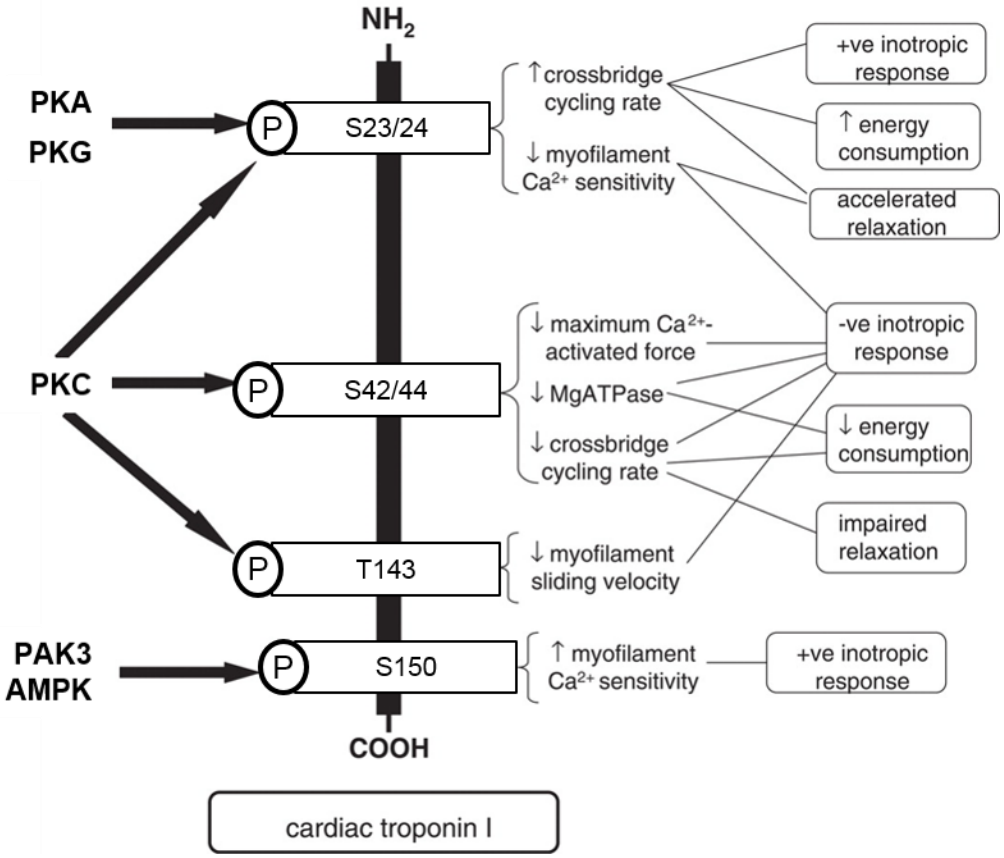


Figure 1-18 - Schematic illustration of the regulation of cardiac function by cTnI phosphorylation. Adapted from [Layland *et al.*, 2005] figure 1 with human amino acid numbering.

cTnI is also phosphorylated at S42/S44 and T143 by PKC. Interestingly, these phosphorylations have opposing effects compared to S23/S24 phosphorylation. In reconstituted filaments or in vitro motility assays, phosphorylation at S42/S44 caused slowed myosin cross-bridge cycling and phosphorylation at T143 caused slowed filament sliding [Burkart *et al.*, 2003]. Further, twitch rates were slowed in

cardiomyocytes treated with PKC but this effect could be abolished by replacing PKC phosphorylation residues with non-phosphorylatable alanine residues [Pi *et al.*, 2002]. As phosphorylation at the S23/S24 sites is known to increase twitch speeds, the slowing effect is likely due to the S42/S44 and T143 sites [Layland *et al.*, 2005].

Finally, more recent studies reveal an additional regulatory phosphorylation site at S150, which is targeted by p21-activated kinase 3 (PAK3) [Buscemi *et al.*, 2002] and 5' AMP-activated protein kinase (AMPK) [Sancho Solis *et al.*, 2011; Oliveira *et al.*, 2012]. Though phosphorylation at this site is relatively rare *in vivo* with basal levels of approximately 2 % [Sancho Solis *et al.*, 2011], the location is directly adjacent to the IR and therefore likely to have a significant effect. The functional impact of this modification was investigated via Förster Resonance Energy Transfer (FRET) experiments with cTnI and cTnC labelled with fluorescent probes. These studies indicated that cTnI S150 phosphorylation increases cTnI-cTnC interaction strength, particularly in the presence of Ca^{2+} (Figure 1-19) [Ouyang *et al.*, 2010]. As the hydrophobic cTnI-cTnC interaction is an essential transduction element linking Ca^{2+} binding to cTnC and force generation, this increased interaction strength would increase Ca^{2+} sensitivity of activation. This expectation was verified by measuring the Ca^{2+} sensitivity of activation in demembranated fibres containing pseudo-phosphorylated cTnI S150D [Nixon *et al.*, 2012; Oliveira *et al.*, 2012].

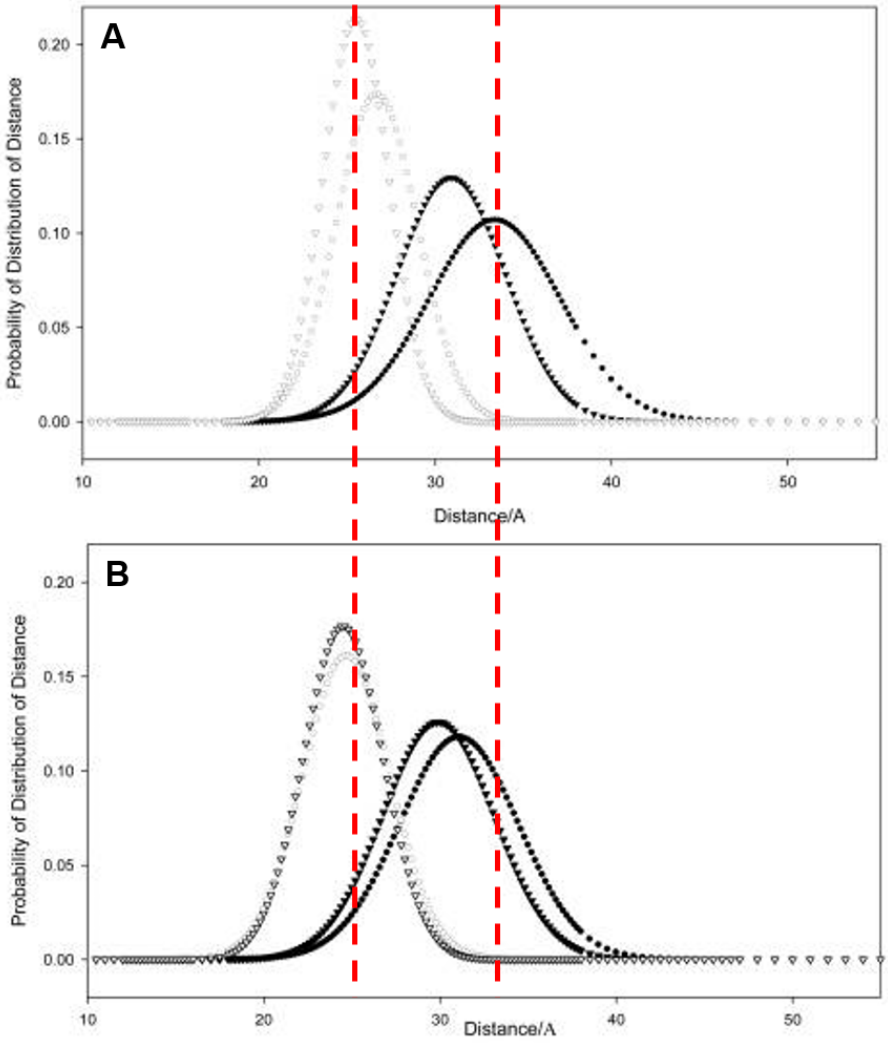


Figure 1-19 - Distance between Cys160 of cTnI and Cys89 of cTnI without (A) and with (B) pseudo-phosphorylated cTnI S150 using steady-state, time-resolved Förster Resonance Energy Transfer (FRET). Pseudo-phosphorylation of cTnI S150 resulted in smaller cTnI-cTnC separations, indicating stronger interactions. Light symbols represent distances in the absence of Ca^{2+}, dark symbols represent distances in the presence of Ca^{2+}. Circles represent distances in the absence of strongly bound cross-bridges, triangles represent distances in the presence of strongly bound cross-bridges. Adapted from [Ouyang *et al.*, 2010] Figure 2.

In general, phosphorylation of cTnI profoundly affects its essential function in regulating the development of force within the sarcomere. In physiological conditions, these modifications are utilized to tune cardiac function to match demand. In a pathological state, altered phosphorylation of cTnI may contribute considerably to impaired cardiac function.

TnT is a primarily structural protein that anchors the TnC Ca^{2+} sensor and TnI inhibitory switch to actin and Tm [Perry, 1998]. It has a large number of isoforms

and splice variants but generally exists as a highly asymmetric 31-36 kDa protein. Cardiac TnT (cTnT) is approximately 20 nm long [Cabral-Lilly *et al.*, 1997], with a globular C-terminal head and extended N-terminal tail. The globular head interacts with TnC, TnI, and Tm while the tail lies along the Tm molecule in its C-terminal and overlap regions [White *et al.*, 1987]. This position allows TnT to regulate the flexibility and motion of Tm while simultaneously influencing TnC-TnI interactions. Specifically, TnC-TnI binding requires TnT's C-terminus [Pearlstone and Smillie, 1983], and cooperative transmission of Tm motion via the overlap region requires TnT's N-terminus [Schaertl *et al.*, 1995]. Thus, TnT is the essential "glue" that binds the Tn complex to the thin filament and permits transmission of its essential activities [Tobacman, 1996].

1.6 Thick filament

Whereas actin, Tm, and Tn regulate the availability of cross-bridge binding sites on the thin filament, the proteins of the thick filament are responsible for forming these force-producing cross-bridges and regulating their activity. The most essential component of the thick filament is therefore myosin II and its two heavy motor chains. The four regulatory myosin light chains and the myosin binding protein C (MyBPC) also contribute by tuning the rate of motor cycling.

1.6.1 Myosin II heavy chains

The myosin family of proteins share the basic properties of actin-binding, ATP hydrolysis, and force production and are responsible for a range of motility activities within eukaryotic cells [Cheney *et al.*, 1993]. In cardiac muscle, myosin II is responsible for producing contractile force. It is composed of two heavy chains, each approximately 2000 amino acids in length, which make up the catalytic head domains and coiled-coil tail (Figure 1-20). The protein also contains four light chains,

two “essential” and two “regulatory,” that are discussed in more detail in the following section. The tails of the heavy chains make up the sarcomeric thick filament and stabilise the heads within this structure. The head domain, also called the S1, form acto-myosin cross-bridges and are therefore of particular interest.

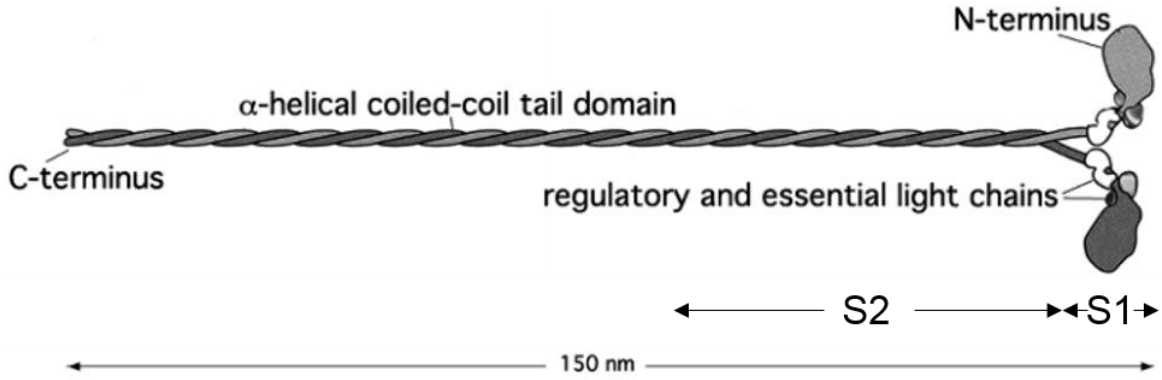


Figure 1-20 - Illustrative structure of myosin II and its component fragments. Figure adapted from [Holmes, 2008] Figure 2.1.

The S1 motor domain contains the sites of actin and ATP binding and hydrolysis. The structure of this domain was first solved in chicken skeletal myosin in the post-cross-bridge state [Rayment *et al.*, 1993] (Figure 1-21). The head consists of numerous α-helices surrounding a 7-stranded β-sheet. The actin binding region is a deep cleft between α-helices that closes upon binding. ATP is bound to a P-loop motif comparable to those found in G-proteins [Smith and Rayment, 1996]. Adjacent to the catalytic core of the S1 head are the converter and lever arm regions, which are the domains that undergo the conformational shifts that drive the myosin “power stroke” and muscle contraction.

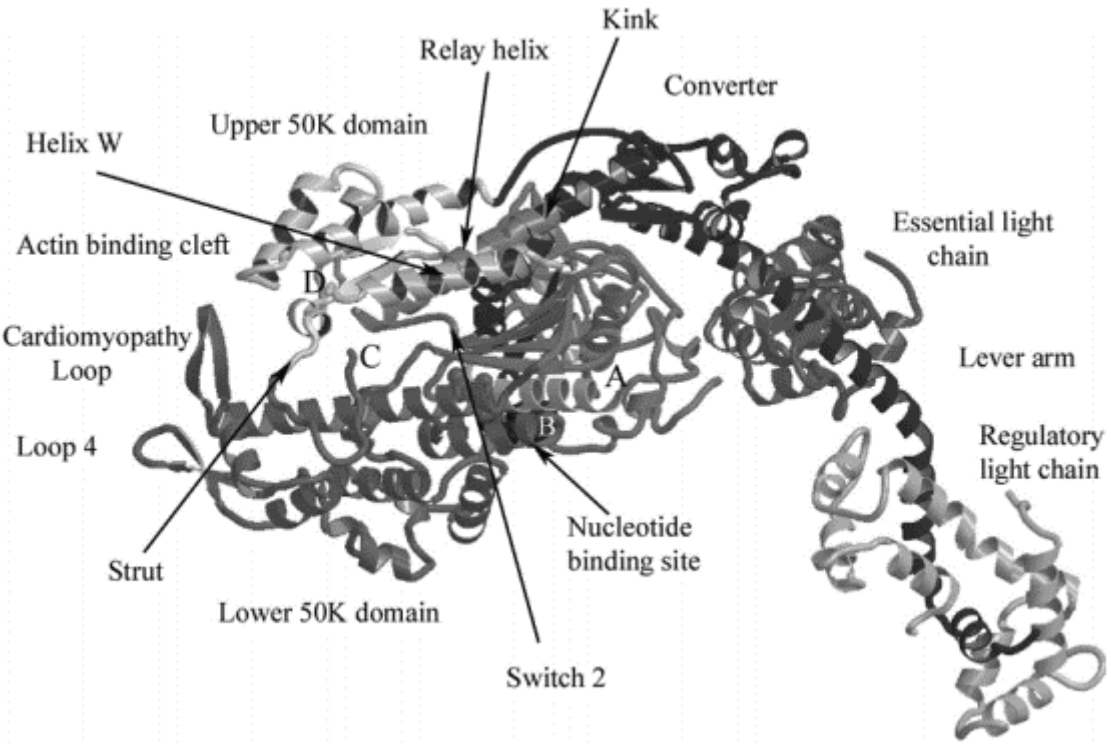


Figure 1-21 - Ribbon structure of myosin S1 fragment including labelled actin and nucleotide binding sites, converter and lever regions, and light chains. Figure adapted from [Geeves and Holmes, 2005].

The myosin power stroke is the force-generating step of the cross-bridge cycle, which describes the cyclic binding, force production, release, and rejuvenation of the S1 myosin heads. This cycle can be described using many-state models that closely match experimental results [Cooke, 1997]. However, a four-state cycle that was first proposed by Lymn and Taylor in 1971 [Lymn and Taylor, 1971] is still considered a reasonable first approximation (Figure 1-22). The Lymn-Taylor cycle proceeds as follows:

1. Following its power stroke, the myosin head is bound to the actin filament (AM)
2. ATP binding to myosin causes detachment from actin (M●ATP)
3. Myosin hydrolyses ATP, restoring its “cocked” power stroke state (M’●ADP●P_i)
4. Myosin binds to actin, releases the ATP hydrolysis products, and undergoes a power stroke (AM)

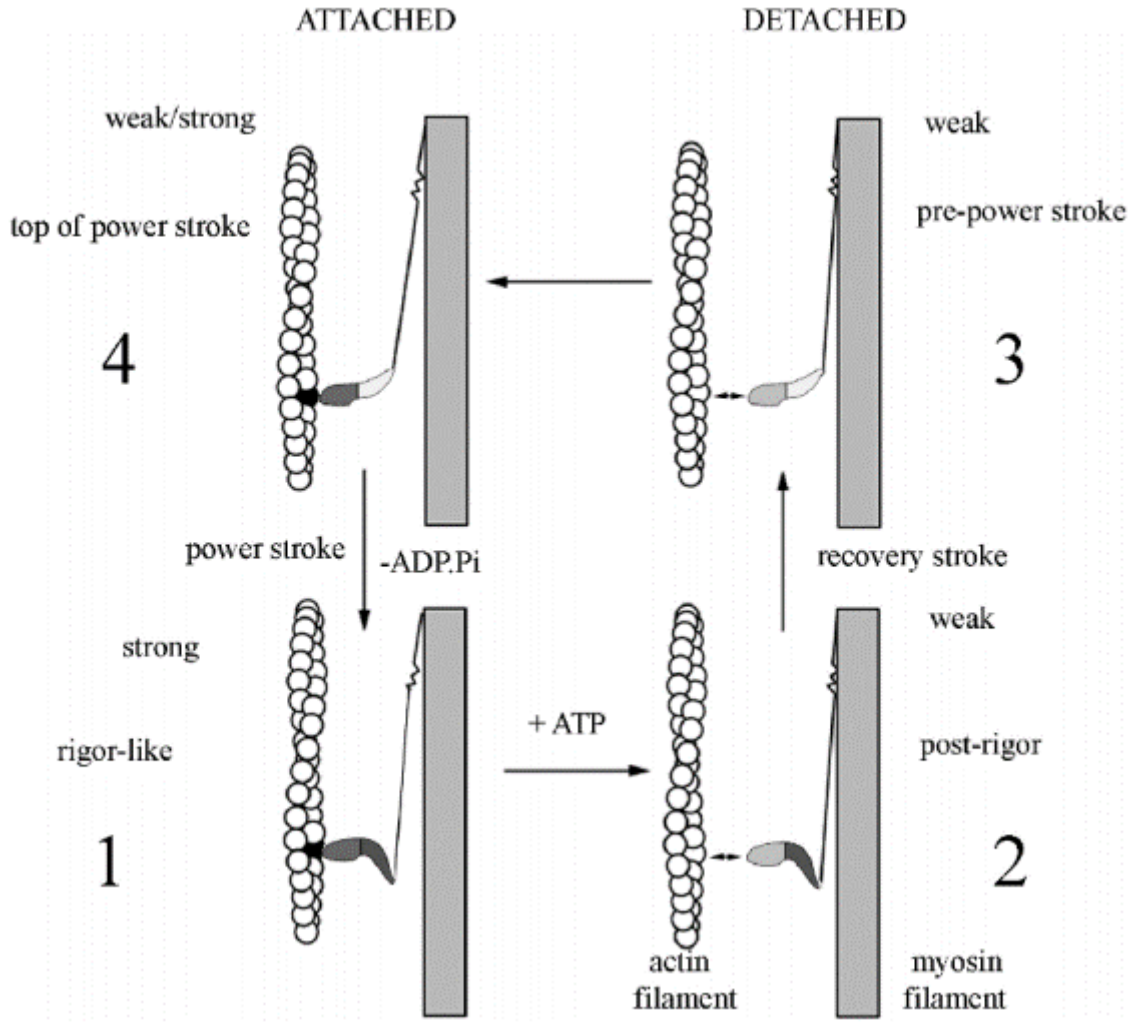


Figure 1-22 - The four-state Lymn-Taylor cross-bridge cycle. Figure from [Holmes, 2008] Figure 2.2.

The rate at which this cycle operates, as well as the force generated per cycle, determines the level of force production within the sarcomere. Consequently, significant effort has been made to characterize the speed of each transition within the cycle (e.g. ATP binding or ADP release). In myosin alone, the rate-limiting reaction is the release of P_i at 0.5 s^{-1} at 20 °C [Malik and Martonosi, 1971]. ATP hydrolysis product release is predicted to be rate-limiting *in vivo* as well. However, thin filament regulation by Tm and the Tn complex also significantly affect the rates of myosin binding, transition through the power stroke, and release [Gordon *et al.*, 2000].

The power stroke itself, being the shortening and force-producing step of the cycle, has been separately well-characterized. Initially, the motion of cross-bridges was described as a rotation or rolling of the S1 head along the filament [Huxley and Simmons, 1971; Lymn and Taylor, 1971]. However, spectroscopic studies indicated that the majority of the myosin molecule is stationary during the power stroke [Cooke, 1986] and crystal structures of the myosin S1 head [Rayment *et al.*, 1993] and actin filament [Holmes *et al.*, 1990] allowed the development of an actin-myosin structure [Rayment *et al.*, 1993] that was inconsistent with the hypothesized rolling motion. Instead, a theory of motion has been developed in which the S1 head binds to actin and only the lever arm undergoes significant movement (the "swinging lever arm") [Holmes, 1996]. This novel hypothesis is strongly supported by evidence from *in vitro* motility assays in which the speed of cross-bridge cycling was directly proportional to the length of the genetically engineered myosin lever arm [Uyeda *et al.*, 1996].

1.6.2 Myosin regulatory (RLC) and essential (ELC) light chains

In the thick filament, regulation of myosin cross-bridge activity begins with the myosin light chains [Szczesna *et al.*, 2002]. Each myosin II molecule contains two regulatory and two essential light chains (RLC and ELC), one of each for the two heavy chains. The RLC and ELC are considerably smaller than the heavy chains, with molecular weights of 20 and 17 kDa, respectively. These chains bind to the myosin lever arm, ideally locating them to regulate motion of the motor [Rayment *et al.*, 1993]. Though myosin is functional without these chains, the velocity of sliding filaments lacking RLC and ELC *in vitro* motility assays was shown to decrease from 8.8 μm/s to 0.8 μm/s without a significant reduction in ATP usage [Lowey *et al.*,

1993]. These data suggest that the light chains optimize myosin function and allow force development to match physiological needs. The importance of RLC and ELC in regulating cardiac muscle function is highlighted by the fact that mutations in the proteins are common causes of familial cardiomyopathies [Hernandez *et al.*, 2007].

Both RLC and ELC belong to the EF-hand family of Ca^{2+} binding proteins and bind to, and stabilize, the lever arm of the myosin heavy chain (Figure 1-21). Partial or complete extraction of RLC alone reduces the myosin ATPase rate [Margossian, 1985] and disorders myosin head structure [Levine *et al.*, 1998]. In smooth muscle, phosphorylation of RLC is required for contraction [Trybus, 1994]. Though this is not the case in cardiac muscle, it is still known to be a potent regulator of myosin activity. Basal phosphorylation of RLC's only identified phosphorylation site, S13, is 40-50 % and maintained by slow rates of phosphorylation and dephosphorylation [Silver *et al.*, 1986]. The upstream kinases responsible for RLC phosphorylation are likely cardiac-specific Ca^{2+}/calmodulin-activated myosin light chain kinase and zipper-interacting protein kinase [Ding *et al.*, 2010]. This phosphorylation increases the myosin ATPase rate [Griffith *et al.*, 1987] and enhances force development and cross-bridge cycling rates at low Ca^{2+} concentrations [Sweeney *et al.*, 1994]. The structural effect of this phosphorylation is a neutralization of positively charged N-terminal amino acids in RLC, resulting in a shift of the heads towards the thin filament [Levine *et al.*, 1996]. The spatial gradient of RLC phosphorylation throughout the heart (from high in the epicardium to low in the endocardium) may also contribute to the torsional contractions required for proper ventricular ejection [Davis *et al.*, 2001].

The ELC is also essential for optimal force development – selective removal of ELC from chicken skeletal myosin resulted in a ~50 % reduction in force production in

motility assays [VanBuren *et al.*, 1994]. Two major variants of the ELC exist [Muthu *et al.*, 2011]. The dominant form in ventricular muscle is the longer isoform that contains a 43-AA N-terminal extension. This N-terminal extension can interact with actin and alter myosin binding dynamics [Timson, 2003]. Specifically, myosin containing the long ELC exhibits higher affinity for actin and slower cross-bridge turnover [Lowey *et al.*, 1993], likely resulting in increased force production per cross-bridge. The functional effect of ELC phosphorylation, as well as the responsible kinases, are not fully known [Hernandez *et al.*, 2007]. However, alteration to ELC phosphorylation may be involved in the mechanism of cardioprotection via pharmacological preconditioning [Arrell *et al.*, 2001] or during heart failure [Moretti *et al.*, 2002].

1.6.3 Myosin binding protein C (MyBPC)

Further regulation of myosin activity, and potentially maintenance of thick filament structure, is accomplished by MyBPC [Flashman *et al.*, 2004]. MyBPC variants are expressed from three genes, of which *MYBPC3* is the cardiac-specific isoform [Pfuhl and Gautel, 2012]. MyBPC consists of eight Ig-like domains and three fibronectin-like domains. Importantly, MyBPC also contains a unique ~100 AA domain containing key regulatory phosphorylation sites. The interactions of MyBPC's C-terminus are relatively well understood – it binds to both the myosin rod and titin [Okagaki *et al.*, 1993; Freiburg and Gautel, 1996]. These interactions are thought to primarily control the location of MyBPC and may not be essential for thick filament organization – *MYBPC3* knock-out animals did not exhibit altered sarcomeres [Harris *et al.*, 2002].

The N-terminal interactions of MyBPC are more controversial. Different research groups have suggested interactions with the S2 fragment of myosin heavy chains

[Gruen and Gautel, 1999], F-actin [Squire *et al.*, 2003; Razumova *et al.*, 2006], tropomyosin [Whitten *et al.*, 2008], or other sarcomeric proteins such as creatine kinase [Uys *et al.*, 2011]. The N-terminal interactions of MyBPC likely drive its functional effect. Recent interaction models predict steric clashes of MyBPC with tropomyosin on the actin filament, particularly in conditions of low Ca^{2+}, and potentially displacing tropomyosin from its blocked conformation [Whitten *et al.*, 2008]. This finding neatly explains observations of increased force development at low Ca^{2+} [Herron *et al.*, 2006] and the increased Ca^{2+} sensitivity of cross-bridge cycling in the presence of MyBPC [Harris *et al.*, 2004].

Regulation of MyBPC structure and function is accomplished by phosphorylation at S273, S282, S302 by PKA and phosphorylation at S273 and S302 by PKC [Sadayappan *et al.*, 2005]. These sites are located near the N-terminus of the protein, particularly close to the location which binds the S2 domain of myosin [Gruen and Gautel, 1999]. These phosphorylations are predicted to cause movement of myosin heads towards the thin filament, promoting the formation of cross-bridges [Weisberg and Winegrad, 1996]. However, these phosphorylations have not been seen to cause changes in Ca^{2+} sensitivity of myosin ATPase activity, force-Ca^{2+} sensitivity, or sarcomere length dependence. In contrast, replacement of native MyBPC with a non-phosphorylatable mutant was shown to adversely affect cardiac haemodynamics [Sadayappan *et al.*, 2005]. Recently, phosphorylation of MyBPC at S282 by ribosomal S6 kinase has been shown to independently reduce myofilament Ca^{2+} sensitivity [Cuello *et al.*, 2011]. Further, in end-stage heart failure, MyBPC phosphorylation levels modulate changes in Ca^{2+} sensitivity due to PKA-phosphorylation of cTnI [Kooij *et al.*, 2010].

1.7 Non-filamentous proteins

1.7.1 Titin

Another key regulator of cardiac mechanical function is the giant elastic protein titin, the largest human protein at approximately 3-3.3 MDa and the third most abundant protein within cardiac muscle [Trinick *et al.*, 1984]. Of the many existing isoforms of titin, the N2B (shorter, 2.97 MDa) and N2BA (longer, 3.3 MDa) are the most common in cardiac muscle [Guo *et al.*, 2010]. Both isoforms are highly elongated, flexible molecules that stretch from the Z-disk (N-terminal) to M-line (C-terminal) of the sarcomere (Figure 1-23). Interactions between titin and numerous sarcomeric proteins have been identified. Most importantly, titin binds to both thick and thin filaments and anchors them to the orthogonal M-lines and Z-Disks [Linke, 2008]. This functionality is essential – knocking out titin results in defective sarcomere assembly [van der Ven *et al.*, 2000].

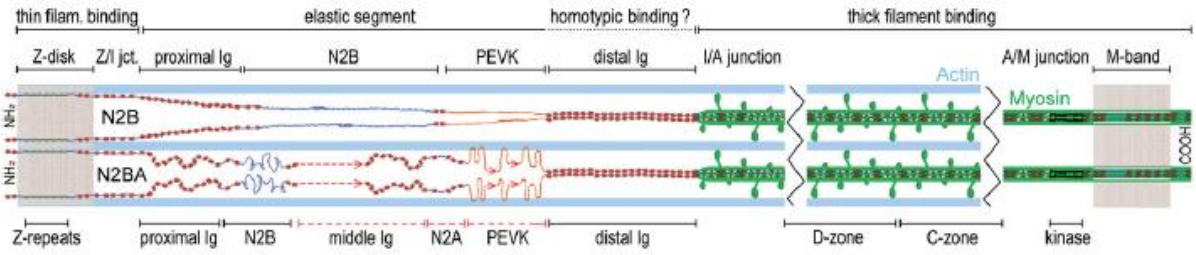


Figure 1-23 – Schematic illustration of titin N2B and N2Ba structures. From [Linke, 2008] Figure 1.

Beyond organizing sarcomeric structure, titin also plays a key role in cardiac stiffness. The elastic region of the molecule proximate to the Z-disk contains three extensible sections: a PEVK segment, a series of spring-like Ig domains, and a unique sequence in the N2B region (Figure 1-23) [Labeit and Kolmerer, 1995]. During cardiac filling, these regions extend and begin producing force, making titin a three-element molecular spring [Wu *et al.*, 2000]. This force limits the extent of

cardiac filling during diastole and also contributes to contractile force developed in early systole. The specific stiffness of cardiac muscle is tuned by the ratio of N2B/N2BA titin (more of the shorter N2B form causes stiffer muscle) as well as post-translational modifications of the protein [Wu *et al.*, 2000]. Further, at the end of systole, the extensible regions are over compressed, creating a restoring force that aids in developing “suction” to refill the heart during early diastole.

Recent results suggest that titin also contributes to stretch-sensing within cardiac muscle [Linke, 2008]. By necessity, this stretch sensing is a bi-directional mechanism (Figure 1-24). External forces, such as the hemodynamic load filling the heart (pre-load) and resisting blood ejection (after-load), must be transmitted efficiently from the extracellular matrix (ECM) to the cardiomyocyte to tune their function. In the reverse fashion, forces generated by the sarcomeres themselves must be transmitted to the ECM to allow whole heart contraction. To accomplish this coupling, titin binds together a number of Z-disk and M-line protein structures and stabilises the thick and thin filaments.

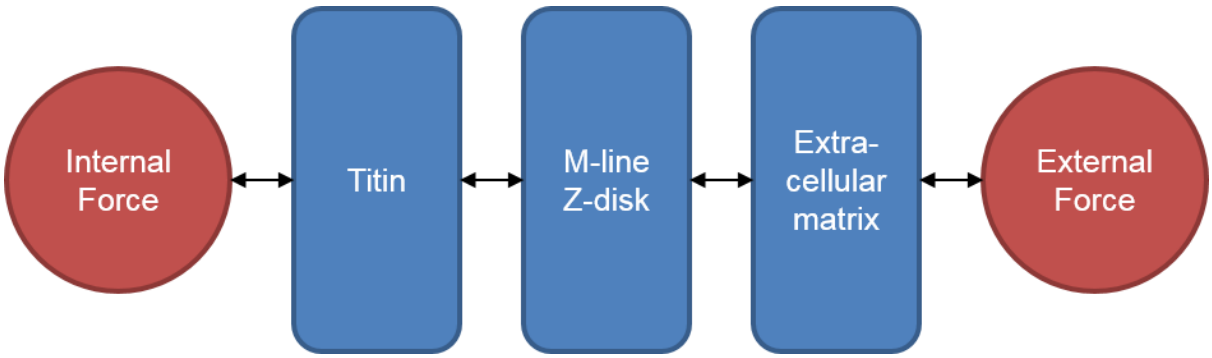


Figure 1-24 - Bi-directional cardiac force transduction pathway.

In addition to direct force transduction, titin and its associated proteins in the Z-disk and M-line may be responsible for mechanosensing and signal transduction. Of particular importance are interactions with telethonin and muscle LIM protein, which

have been associated with transcriptional signalling and pathophysiological responses [Linke, 2008]. Mutations in these proteins [Geier *et al.*, 2003], or altered levels are also associated with familial cardiomyopathies and heart failure [Zolk *et al.*, 2000]. Though the pathways associated with stress sensing have not been fully elucidated, it is clear that the giant protein titin plays a central role [Linke, 2008].

1.7.2 Collagen

Outside the cardiomyocyte, stiffness of cardiac muscle, transduction of force, and maintenance of overall architecture is accomplished by the ECM [Weber, 1989]. The principle component of this tissue is collagen, which is synthesized by cardiac fibroblasts. Collagen is made up of three polypeptide strands that coil into a right-handed super-helix. Many types of collagen have been described in various species and tissues – types I and III dominate in the cardiac ECM. Type I collagen forms large, well-defined fibres whereas type III forms a reticular network. As type III networks are far more compliant than type I strands [Medugorac, 1982], the ratio of collagen types in cardiac muscle is partially responsible for setting cardiac stiffness [Wu *et al.*, 2000]. In cardiac muscle, collagen fibres contribute little to stiffness of the muscle at short sarcomere lengths but dominate at longer lengths, suggesting that the ECM influences the maximum filling volume of the heart.

1.8 β-adrenergic regulation of contractile activity

Modulation of the Ca^{2+} handling and contractile apparatus is required to tune cardiac function to meet physiological demand. As described for the whole organ, the pathway that most dramatically alters function begins with activation of the sympathetic nervous system [Triposkiadis *et al.*, 2009]. The resulting release of epinephrine and norepinephrine results in the activation of β-adrenergic receptors. Via the second messenger cyclic AMP (cAMP), this activation leads to

phosphorylation of numerous targets to increase cardiac inotropy (Figure 1-25). The specific effect of these phosphorylations on protein function has been discussed in previous sections.

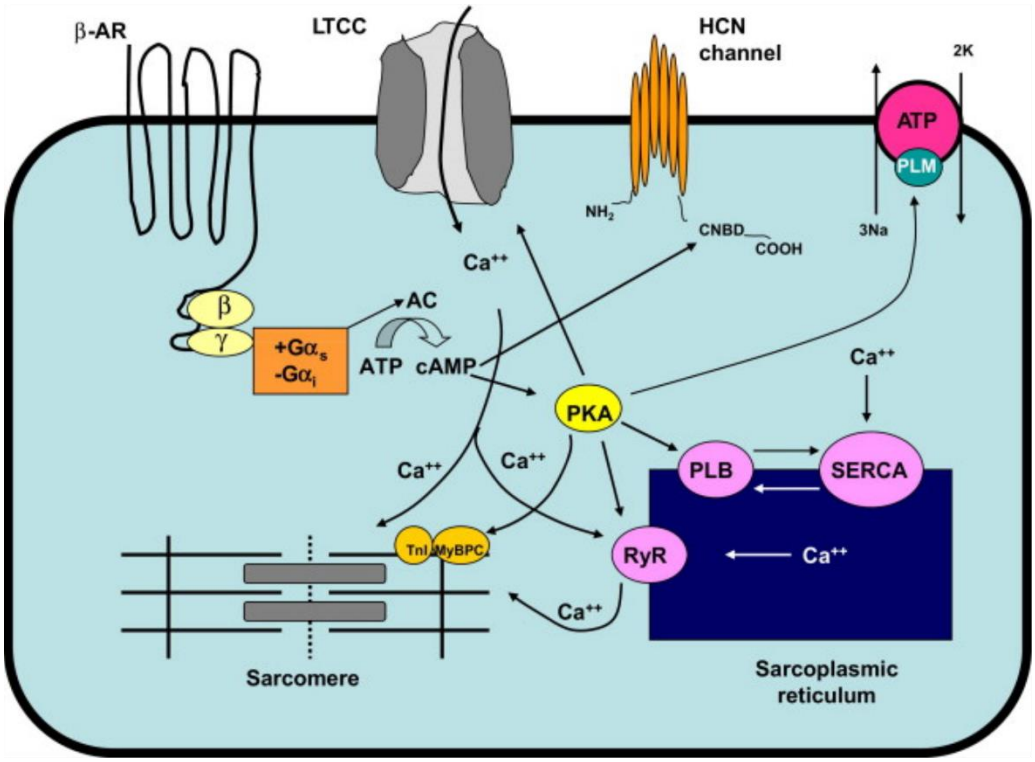


Figure 1-25 – Summary of β-adrenergic stimulation within the cardiomyocyte. Stimulation of the β-adrenergic receptor (β-AR) causes activation of the G-α subunit, leading to modulation of adenylate cyclase (AC) activity. G_s subunits active AC, while G_i subunits inhibit AC. AC utilizes ATP to produce cAMP, which in turn activates PKA. PKA phosphorylates the L-type Ca^{2+} channel (LTCC), phospholemman (PLM), phospholamban (PLN), the ryanodine receptor (RyR), troponin I (TnI), and myosin binding protein C (MyBPC). The overall effect of these mutations is increased cardiac inotropy. Figure from [Triposkiadis *et al.*, 2009] Figure 2.

1.9 Diseases of the sarcomere

1.9.1 Hypertrophic cardiomyopathy (HCM) and energy deficiency

As described in Section 1.1.6, HCM is predominately caused by mutations in genes encoding sarcomeric proteins. The immediate result of these mutations on contractile function is varied [Redwood *et al.*, 1999]. However, in general, *in vitro* studies and murine models of HCM suggest increased contractility due to heightened sensitivity of activation or increased myosin cycling speeds [Seidman

and Seidman, 2001]. In addition, experiments in isolated cardiac myofibrils suggest that HCM-causing mutations yield an increased energetic cost of force production [Belus *et al.*, 2008]. As cross-bridge cycling accounts for 70 % of cardiomyocyte energy usage at baseline, excess cross-bridge activity or inefficient force generation could negatively impact the energetic state of the cells. Further, because the healthy heart ejects the majority of its contents during each cycle, hypercontractility is unlikely to increase cardiac output [Ashrafian and Watkins, 2007]. Therefore, energetic deficiency may be a unifying mechanism of disease pathogenesis in HCM. Evidence for this theory comes from observations of compromised energetics in murine models of HCM [Spindler *et al.*, 1998] as well as early-stage human patients [Crilley *et al.*, 2003].

A mechanism leading from energy deficiency to the ultimate HCM phenotype has been hypothesized (Figure 1-26). Reduction of available ATP would be expected to decrease the activity of SERCA [Ashrafian *et al.*, 2003], resulting in lowered Ca^{2+} reuptake and increased diastolic Ca^{2+} concentrations. This reduction in SERCA activity and increased Ca^{2+} concentrations has been observed in murine models of HCM and has also been linked to the development of HCM-associated arrhythmias [Knollmann *et al.*, 2003; Schober *et al.*, 2012]. Increased diastolic Ca^{2+} concentration is also likely to promote hypertrophic signalling pathways [Bers and Guo, 2005]. Further, inefficient energy usage resulting in an impaired energetic state would increase mitochondrial demand, leading to increased production of damaging reactive oxygen species, mitochondrial failure, and cardiomyocyte apoptosis [Ashrafian *et al.*, 2003]. This hypothesis has already yielded novel viable therapeutics. A randomized trial of perhexiline, a small molecule drug that shifts cardiac metabolism from fatty acid oxidation to more efficient glucose metabolism,

improved cardiac ATP levels, diastolic dysfunction, and exercise capacity [Abozguia *et al.*, 2010].

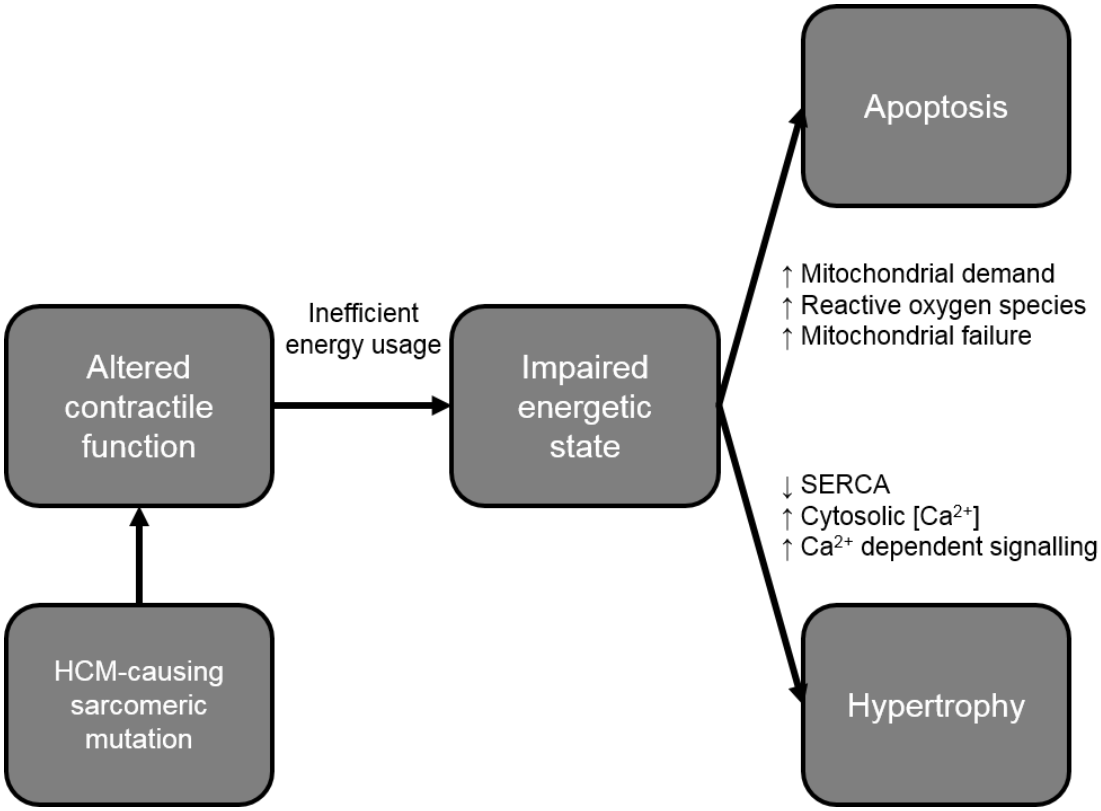


Figure 1-26 – Hypothesized mechanism linking sarcomeric mutations to the ultimate HCM phenotype via energetic compromise [Ashrafian *et al.*, 2003].

1.9.2 AMP-activated protein kinase (AMPK) and PRKAG2 cardiomyopathy

Interest in relationships between energetic compromise, ventricular hypertrophy, and cardiomyopathy intensified following the discovery that mutations in the gene *PRKAG2*, which encodes the energy-sensing protein AMP-activated protein kinase (AMPK), cause a phenocopy of HCM [Blair *et al.*, 2001]. AMPK is a highly conserved serine/threonine kinase that plays a central role in the regulation of cellular and whole-body energy balance [Hardie, 2007]. AMPK is a heterotrimeric complex consisting of a catalytic α subunit, structural/regulatory β-subunit, and regulatory γ-

subunits [Carling *et al.*, 2012]. Each subunit contains multiple isoforms (α1, α2, β1, β2, γ1, γ2, and γ3) encoded by distinct genes [Hardie *et al.*, 1998; Cheung *et al.*, 2000]. Further, several of the genes are differentially spliced or utilize alternate promoters, adding additional complexity to the system [Pinter *et al.*, 2012]. Though the complete AMPK heterotrimer structure has yet to be fully determined, a number of recent crystal structures have partially elucidated the assembly and regulation of the complex [Townley and Shapiro, 2007; Xiao *et al.*, 2011].

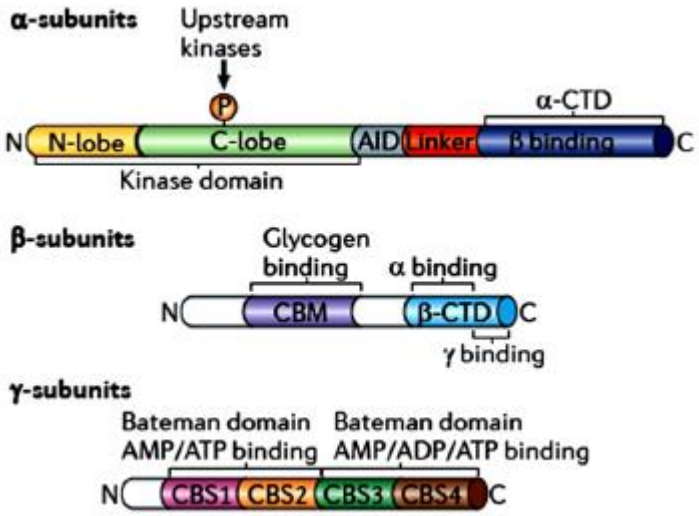


Figure 1-27 – Primary structure of AMPK subunits and identified functions. From [Hardie *et al.*, 2012] Figure 2.

The α-subunit contains a conventional serine/threonine kinase domain in its N-terminus flanked by an autoinhibitory domain (AID). Adjacent to the AID is a linker domain which wraps around the γ-subunit, followed by a C-terminal domain that binds to the β-subunit. The β-subunit is the core of the complex, binding the C-terminal of α-subunit and the N-terminal of γ-subunit within its C-terminus [Amodeo *et al.*, 2007]. The β-subunit also contains a glycogen-binding domain, which is thought to aid in the localization of AMPK [Hardie, 2011] and might also lead to glycogen-based regulation of kinase activity [Oakhill *et al.*, 2010].

The γ-subunit is considered the regulatory subunit because it possesses four conserved regulatory adenine nucleotide binding sites [Carling *et al.*, 2011]. These are termed CBS-domains because of their initial discovery in cystathionine β-synthase [Bateman, 1997], and are numbered 1-4 from the N-terminal. Recent structural studies suggest that sites 2 and 4 do not participate in energy-sensing and activity regulation – site 2 does not bind nucleotides while site 4 permanently binds AMP. In contrast, sites 1 and 3 interchangeably bind AMP/ADP/ATP and are therefore responsible for the energy-sensing ability of AMPK.

Regulation of AMPK activity is primarily accomplished via reversible phosphorylation of T172 in the α-subunit. Phosphorylation of T172 within the α-subunit kinase domain is the primary activator of the complex, resulting in an increase in activity over 100-fold [Hardie, 2011]. The kinases implicated in this phosphorylation are liver kinase B1 (LKB1) and Ca^{2+}/calmodulin-dependent protein kinase kinase-β (CaMKKβ) [Carling *et al.*, 2008]. LKB1 is regarded as the predominant upstream kinase, as AMPK in cells lacking LKB1 is not activated by established stimulators such as the nucleoside AICAR (5-aminoimidazole-4-carboxamide riboside, which is taken up by cells via adenoside transporters and converted to ZMP, an analogue of AMP [Hawley *et al.*, 2003; Hardie, 2007]). LKB1 is constitutively active in most cell types, however, so its activation of AMPK is not restricted based on cellular energetics. The discovery that AMPK can be activated in cells lacking LKB1 by increased intracellular Ca^{2+} [Carling *et al.*, 2008] subsequently led to the discovery of CaMKKβ as a second potential activator [Hawley *et al.*, 2005; Hurley *et al.*, 2005; Woods *et al.*, 2005]. CaMKKβ is activated by increased intracellular Ca^{2+}, linking the AMPK activity to Ca^{2+} signalling pathways.

Though the phosphorylation of α-subunit by upstream kinases is the primary "on-off" switch of AMPK activity, the likelihood of phosphorylation and subsequent fine-tuning of AMPK activity is regulated by adenine nucleotide binding to CBS domains of the γ subunit. AMP binding to CBS domain 1 causes allosteric activation of the catalytic α subunit (5-fold increase in activity) [Carling *et al.*, 2012]. At site 3, AMP or ADP binding inhibits α subunit dephosphorylation while ATP binding enhances α subunit dephosphorylation [Carling *et al.*, 2012]. Thus, AMPK's activity is fundamentally controlled by the relative prevalence of ATP to ADP/AMP and therefore associated with the energetic state of the cell.

Interest in AMPK's role in the heart grew upon finding that dominant mutations in the gene encoding the γ2 subunit (*PRKAG2*) cause a heterogeneous cardiac pathology characterized by left ventricular hypertrophy, systolic and/or diastolic impairment, cardiac glycogen accumulation, ventricular pre-excitation and other electrophysiological disorders, and sudden death [Blair *et al.*, 2001; Gollob *et al.*, 2001]. Clinical findings and phenotypes of overexpressing transgenic murine models have led to the disease being described as a glycogen storage disorder [Arad *et al.*, 2002; Arad *et al.*, 2003]; however, although excess glycogen appears to underlie the electrophysiological facets of the phenotype, it does not fully account for cardiac hypertrophy [Arad *et al.*, 2003; Davies *et al.*, 2006; Watkins *et al.*, 2011]. Specifically, although transgenic mouse models overexpressing mutant γ2 subunits exhibit significant hypertrophy and pronounced glycogen accumulation, in absolute terms the glycogen only accounts for a small fraction of the total hypertrophy [Arad *et al.*, 2003; Davies *et al.*, 2006; Watkins *et al.*, 2011]. In addition, mutant mice exhibit significant up-regulation of hypertrophy-associated genes [Davies *et al.*, 2006; Banerjee *et al.*, 2010], suggesting cardiomyocyte growth is due to an increase

in protein content. Further, multiple clinical reports demonstrate the existence of symptomatic, genotype-positive PRKAG2 cardiomyopathy patients without any glycogen accumulation [Tan *et al.*, 2008; Kelly *et al.*, 2009]. Thus, though altered AMPK activity is logically associated with dysfunction of glycogen metabolism, accumulation of glycogen seems to be insufficient to explain the complete phenotype. Therefore, a more nuanced view of the disease is required to explain cardiac hypertrophy and dysfunction. As the most common cause of inherited cardiac hypertrophy and dysfunction are sarcomeric mutations leading to hypertrophic cardiomyopathy [Frey *et al.*, 2012], we hypothesized that PRKAG2 mutations may directly affect sarcomeric function in a similar manner.

A potential pathway by which altered AMPK activity could directly affect sarcomeric function was recently reported by our group [Oliveira *et al.*, 2012]. Specifically, it was found that AMPK phosphorylates cTnI at S150. This phosphorylation strengthens cTnI's interaction with cardiac troponin C during Ca^{2+}-dependent activation and leads to an increased Ca^{2+} sensitivity of force production in demembranated muscle [Sancho Solis *et al.*, 2011]. As mutant AMPK γ2 subunits are thought to cause initially increased basal AMPK activity [Arad *et al.*, 2003; Patel *et al.*, 2003; Banerjee *et al.*, 2007], *PRKAG2* mutations would be predicted to cause increased Ca^{2+} sensitivity of activation akin to the change observed in sarcomeric HCM. We therefore hypothesized that *PRKAG2* mutations directly affect cardiac contractile function and that this contributes to cardiac dysfunction in PRKAG2 cardiomyopathy.

1.9.3 αB-crystallin and dilated cardiomyopathy

The α-crystallins are ~20 kDa small heat shock proteins that highly abundant in the vertebrate lens, making up 30-40 % of total protein content [Horwitz, 2000; Jaenicke and Slingsby, 2001]. The two most common α-crystallins are αA-and αB-crystallin, highly homologous proteins encoded by distinct genes (*CRYAA* and *CRYAB*, respectively) [Van Der Ouderaa *et al.*, 1974; van den Heuvel *et al.*, 1985]. *In vivo* and *in situ* these chaperones form large multimeric complexes (> 1000 kDa) that bind partially unfolded proteins and prevent aggregation. In the lens, this activity preserves transparency [Horwitz, 1992]. αB-crystallin is also prevalent in non-ocular tissues, notably striated skeletal and cardiac muscle, where it makes up 3-5 % of total soluble protein content [Bhat and Nagineni, 1989]. However, despite its significant prevalence, the specific role of αB-crystallin in cardiac muscle has not yet been fully elucidated.

αB-crystallin predominantly resides in the cardiac cytosol, though may translocate to the myofibrils upon stress [van de Klundert *et al.*, 1998]. In particular, during or following ischemia, αB-crystallin is thought to enter the myofibrils and prevent structural damage [Martin *et al.*, 1997]. Using immunoelectron microscopy, αB-crystallin was shown to translocate specifically to the I-band region of the myofilament [Golenhofen *et al.*, 2002]. Further, αB-crystallin was suggested to bind to titin using selective extraction of actin and co-purification of αB-crystallin with titin [Golenhofen *et al.*, 2002]. The specific binding location was investigated by stretching cardiac myofibrils and noting the location of αB-crystallin antibodies compared to known regions of titin [Bullard *et al.*, 2004]. These studies suggested that αB-crystallin binds to the elastic N2B region of titin. Further, atomic force microscopy measurements demonstrated that greater forces were required to

unfold binding domains in the presence of αB-crystallin [Bullard *et al.*, 2004]. Presumably, this function is accomplished by stabilization of the domains by αB-crystallin multimer binding. Thus, αB-crystallin appears to translocate to titin elastic domains and increase their stiffness during stress.

The importance of αB-crystallin in regulating contractile function is also supported by the association of αB-crystallin mutations with skeletal and cardiac myopathies [Vicart *et al.*, 1998; Selcen and Engel, 2003]. In addition, cardiomyopathy-causing mutations in the cardiac-specific titin N2B region [Itoh-Satoh *et al.*, 2002; Tskhovrebova and Trinick, 2003] led to the discovery of a novel *CRYAB* mutation (R157H) in a family with DCM [Inagaki *et al.*, 2006]. This mutation was shown to decrease the binding affinity of αB-crystallin to the titin N2B domain without affecting the cellular distribution of αB-crystallin. As dilated cardiomyopathy is often associated with alterations to ventricular stiffness [Makarenko *et al.*, 2004; Nagueh *et al.*, 2004], impairment of αB-crystallin stiffening of the titin N2B domain due to the R157H mutation may underlie disease pathogenesis.

1.10 Hypotheses and specific aims

Mutations in genes encoding sarcomeric proteins are the most common cause of inherited cardiomyopathies. These mutations directly affect contractile function in ventricular muscle and therefore the mechanisms leading from the initial mutation to ultimate disease phenotype are more easily described. However, mutations in non-sarcomeric proteins, such as AMPK γ2 or αB-crystallin, are also associated with familial cardiomyopathies. The relationships between these proteins and contractile function of the heart are poorly understood, challenging the determination of pathogenesis.

1.10.1 Hypotheses

Given that AMPK has a direct sarcomeric phosphorylation target, and comparable HCM phenotypes are fundamentally caused by sarcomeric dysfunction, I hypothesize that *PRKAG2* mutations directly affect cardiac contractile function and that this contributes to the development of cardiomyopathy. To test this theory, a mouse model possessing the PRKAG2 cardiomyopathy-causing R299Q (homologous to human R302Q) AMPK γ2 mutation was utilized. The component hypotheses were that the R299Q AMPK γ2 mutation causes:

I. altered sarcomeric function;

II. altered Ca^{2+} handling and cardiomyocyte contractility;

III. altered kinase regulation of cardiac function

As αB-crystallin binds to titin and increases the force required to unfold the protein, I hypothesize that mutations to αB-crystallin alter this activity and therefore overall cardiac muscle stiffness.

1.10.2 Specific aims

In accordance with these hypotheses, this thesis aims to characterize the contractile mechanics and underlying regulatory pathways of the R299Q AMPK γ2 mouse. In addition, this thesis will investigate the effect of αB-crystallin on cardiac muscle stiffness. The specific aims of this work are therefore:

Aim 1 – To evaluate force production, stiffness, Ca^{2+} sensitivity of activation, Frank-Starling dependence of activation, cross-bridge cycling mechanics, and the response to PKA stimulation in demembranated cardiac fibres from mutant and WT animals (Chapter 3).

Aim 2 – To characterize baseline sarcomere lengths and Ca^{2+} concentrations, magnitudes of cardiomyocyte shortening and Ca^{2+} release, rates of contraction, relaxation, Ca^{2+} release, and Ca^{2+} reuptake; response to caffeine stimulation, β-adrenergic stimulation, and energetic stress in cardiomyocytes isolated from mutant and WT animals (Chapter 4).

Aim 3 – To assess levels and post-translational modification status of essential cardiac regulatory proteins TnI, MyBPC, RLC, ELC, PLN, SERCA, and RyR (Chapter 5).

Aim 4 – To determine the interaction between αB-crystallin and titin, measure the effect of αB-crystallin on overall cardiac muscle stiffness, and establish the effect of the R157H mutation on αB-crystallin function (Chapter 6).

Chapter 2 – Methods

Note: Recipes for all solutions are included as an appendix.

2.1 Demembranated trabeculae

2.1.1 Dissection

Mice were dispatched via cervical dislocation in accordance with Schedule 1 of A(SP)A 1986. The chest was opened immediately at the sternum and ribs were cut away using two vertical, lateral incisions. Hearts were rapidly excised, submerged in ice cold Tyrode solution, and cleared of blood. Hearts were then transferred to dissecting solution and trabeculae were cut from the left ventricular wall. Ideal trabeculae were aligned, non-branching fibres of width 80-250 µm and length 1.0-3.0 mm. Dissected trabeculae were transferred to a 0.6 mL microcentrifuge tube containing skinning solution and left overnight on a rotator at 4 °C. Remaining heart tissue was snap frozen in liquid nitrogen and stored at -80 °C. After overnight skinning, trabeculae were transferred to glycerinated relaxing solution and clipped between aluminium T-clips (Kem-Mil Co, unit number 277906). Trabeculae were stored in glycerinated relaxing solution at -20 °C for up to 5 days prior to experimentation.

2.1.2 Apparatus

Mechanical measurements on trabeculae were conducted using an Aurora Scientific Permeabilized Fibre Test System (Figure 2-1). Skinned trabeculae were connected via aluminium T-clips to pin hooks on a force transducer and motor. Sarcomere length was monitored via laser diffraction and experiments were conducted at 15°C.

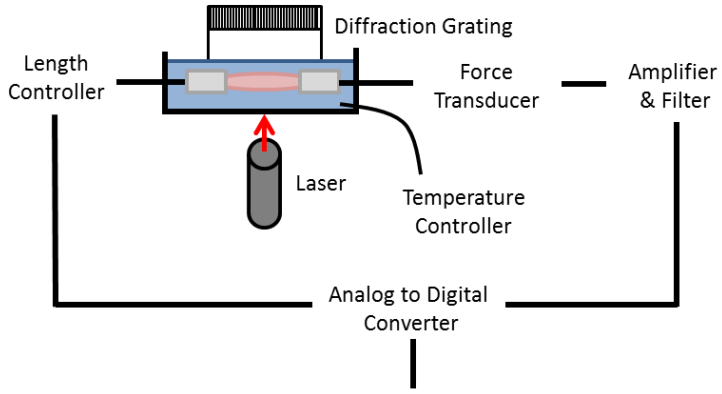


Figure 2-1 – Schematic illustration of demembranated trabeculae force-fibre test system. Fibres were held between a length controller and force transducer using aluminium T-clips. A laser and diffraction grating were used to measure sarcomere length. A temperature controller and liquid cooling system was used to maintain solution temperature.

2.1.3 Experimentation

Pre-conditioning – Trabeculae were maintained in glycerinated relaxing solution on ice prior to experimentation. All muscles were first equilibrated in force fibre solution pCa 9.0 (relaxing solution) and stretched to a specified sarcomere length (either 2.0 or 2.3 µm). Trabeculae were transferred to pre-activating solution (equivalent to pCa 9.0 except lacking ethylene glycol tetraacetic acid (EGTA), limiting the carryover of Ca^{2+}-chelating EGTA to activating solutions) for 30 seconds. Fibres were then transferred to maximally activating pCa 4.0 and allowed to reach full force development. Slight adjustments in fibre position and orientation were commonly observed during activation.

The muscles were then relaxed in pCa 9.0 and sarcomere length was again measured. Adjustment of muscle length was often required following initial activation due to changes in trabeculae position. After sarcomere length was confirmed, the length and width of the fibre were measured using an ocular reticule.

The cross-sectional area of the fibre was calculated for subsequent normalization assuming an elliptical cross-section:

$$Cross\ sectional\ area = (\pi)\left(\frac{Diameter}{2}\right)\left(\frac{Diameter}{4}\right) = (\pi)\left(\frac{Diameter^2}{8}\right)$$

Following these pre-conditioning steps, force-Ca^{2+} sensitivity and tension redevelopment rate and/or stress relaxation was measured.

Force-Ca^{2+} relationship and tension redevelopment rate – The force-Ca^{2+} relationship was measured by submerging the fibre in pCa solutions according to the following schedule: 9.0, pre-Activating, 4.0, 9.0, pre-Activating, 6.6, 6.4, 6.2, 6.0, 5.8, 5.6, 5.4, 4.0, 9.0 (Figure 2-2). In each solution, the force production of the fibre was monitored until it reached a stable equilibrium. The fibre was then shortened to 85 % of its original length (0.85*L_0), held for 50 ms, re-stretched to 1.05*L_0, and returned to L_0.

In some experiments, sarcomere length sensitivity was investigated by repeating force-Ca^{2+} sensitivity and tension redevelopment rate measurements at SL = 2.3 and 2.0 µm.

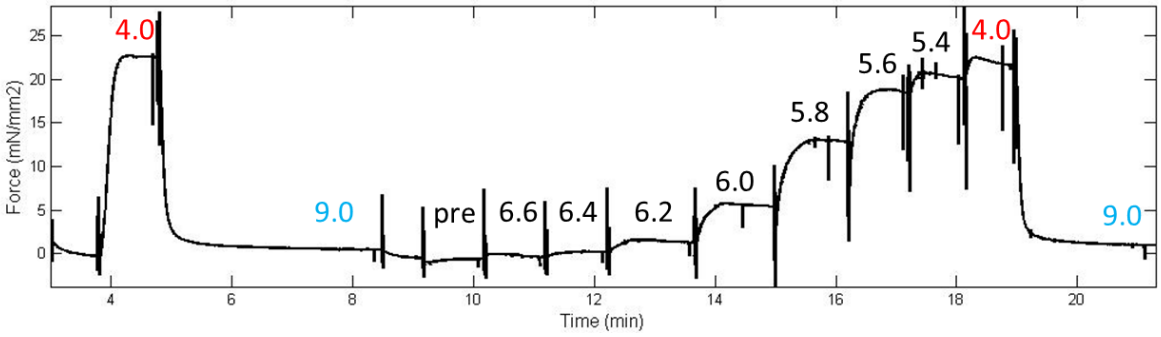


Figure 2-2 – Example force-Ca^{2+} relationship raw data trace. Fibres were sequentially submerged in increasing Ca^{2+} concentrations and resulting force development was recorded.

Passive stiffness and stress relaxation – Passive stiffness measurements were conducted in low-Ca^{2+} (pCa 9.0) solution and initial fibre length was set to SL = 2.0 µm. Fibres were then stretched to 1.05*L_0 over 15 seconds and maintained at that length for 180 seconds. The stretch-and-hold procedure was repeatedly applied to produce lengths 1.05*L_0, 1.10*L_0, 1.15*L_0, 1.20*L_0, 1.25*L_0, and 1.30*L_0 (Figure 2-3). SL was measured after each stretch; fibres were excluded from analysis if SL at 1.30*L_0 was not within 5 % of 2.6 µm.

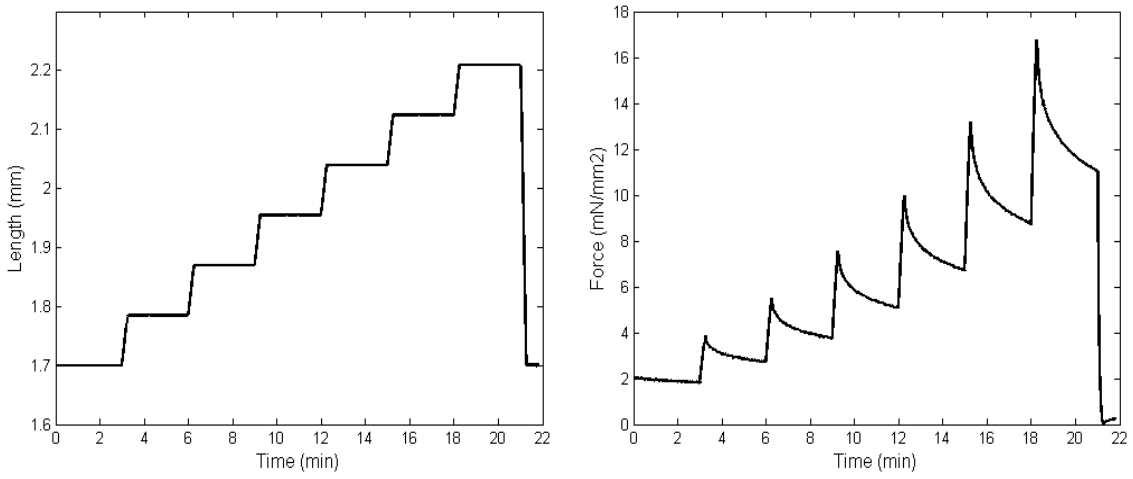


Figure 2-3 - Characteristic stress relaxation curves of cardiac muscle fibres stretched from sarcomere length 2.0 µm to 2.6 µm by increments of 0.1 µm.

After experiments were completed, fibres dried briefly before being stored at -20 °C.

2.1.4 Demembranated trabeculae treatments

PKA – In some experiments, fibres were treated with 100 units of protein kinase A (PKA) catalytic subunit from bovine heart (Sigma) between mechanical measurements. This treatment was performed in 200 µL of force fibre solution pCa 9.0 for 45 minutes at 22 °C while the fibre remained attached to the apparatus.

αB-crystallin – To test the effect of αB-crystallin on cardiac muscle stiffness, fibres were incubated in pCa 9.0 containing the protein (at varied concentrations) for 1

hour at room temperature on a roller. The incubation solution was transferred to the Permeabilized Fibre Test System and the fibre was maintained in this solution for stress-relaxation measurements.

2.1.5 Data analysis

Force-Ca^{2+} sensitivity and tension redevelopment rate – Custom software, including a front-end user interface, was developed in Matlab to analyse force-Ca^{2+} sensitivity and k_{tr} (Figure 2-4).

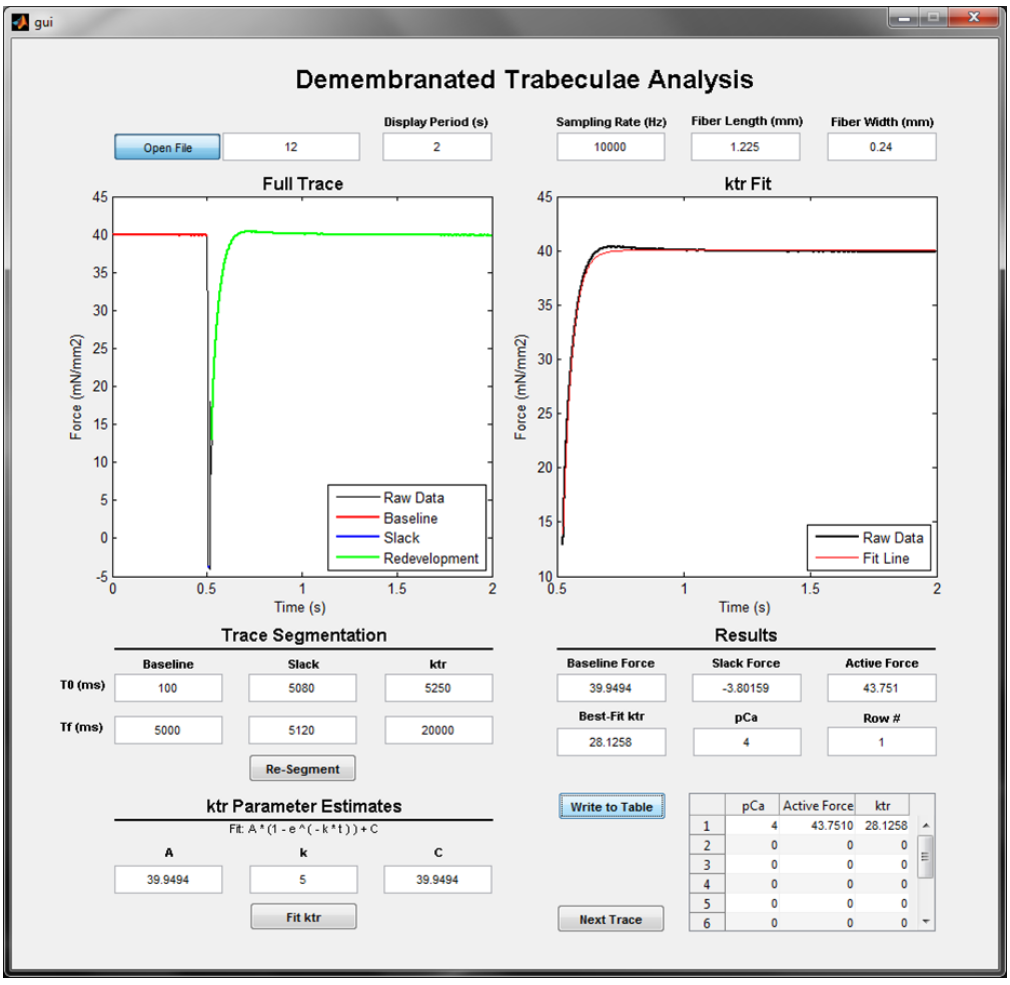


Figure 2-4 - Screenshot of custom-built application for analysis of force-[Ca^{2+}] sensitivity and k_{tr}. Custom-built software isolates relevant sections of the data trace and calculates isometric force and force redevelopment values. The software utilizes a small amount of user input to prevent gross systematic errors.

Isometric force at each pCa was calculated by subtracting the force measured at 0.85*L_0 (slack force) from the baseline force. The rate of tension redevelopment (k_{tr}) was measured by fitting a single exponential equation to the force redevelopment plot following return of the fibre to L_0:

$$Force = F_{Max} * (1 - e^{k_{tr}*t}) + F_{Res}$$

where F_{Max} is maximum tension, k_{tr} is rate of tension redevelopment, t is time after re-stretch, and F_{Res} is residual tension present immediately after the re-stretch.

Maximum isometric force (pCa 4.0) was measured at the beginning and end of the experimental protocol to allow for calculation of tension "rundown" (percentage of force lost during experiment). Fibres with >10 % rundown were excluded from analysis. Force was measured at pCa 9.0 at the beginning and end of the experimental protocol to determine passive stiffness. This passive stiffness was subtracted from the force measured in each pCa solution to yield the Ca^{2+}-dependent force.

Ca^{2+}-dependent force was plotted against pCa and the force-pCa relationship was characterized by fitting a modified Hill equation to the data points:

$$F = \frac{F_{Max}}{1 + 10^{\eta_H(pCa - pCa_{50})}}$$

where F_{Max} is the active force at pCa 4.0, η_H is the Hill coefficient (governs steepness of the curve), and pCa_{50} is the [Ca^{2+}] at which 50 % of maximal force is reached. EC_{50} values for each fibre were calculated as follows:

$$EC_{50}(\mu M) = 10^{-pCa_{50}} * 10^6$$

Passive stiffness and stress relaxation – A method for assessing the stiffness and relaxation properties of cardiac muscle was adapted from a number of texts [Mirsky, 1976; Fung, 1993; Roylance, 2001]. Development of this method is presented in Chapter 6. Briefly, force decay following rapid fibre lengthening was fit with a double-exponential equation:

$$\sigma(t) = k_1 + k_2 e^{\frac{-t}{\tau_2}} + k_3 e^{\frac{-t}{\tau_3}}$$

where the fit variables represent physiological parameters detailed in the table below:

Table 2-1 - Physiological significance of viscoelastic fit terms.

Fit term	Significance
k_1	Residual stiffness
k_2	Rapidly decaying stiffness
k_3	Slowly decaying stiffness
τ_2	Rate of rapid stiffness decay
τ_3	Rate of slow stiffness decay

These parameters were calculated for each fibre at each sarcomere length and various comparisons made between groups.

2.2 Intact cardiomyocytes

2.2.1 Isolation

Mice were dispatched via cervical dislocation in accordance with Schedule 1 of the A(SP)A 1986. The chest was opened immediately at the sternum and ribs were cut away using two vertical, lateral incisions. The pericardium was removed along with all tissues obstructing the aorta. Suture was fed under the aorta and tied loosely. The aorta was cut 1-2 mm above the atria and the cannula was inserted into the

aorta's lumen. The depth of cannula insertion allowed the aorta to be tied off but did not cause the cannula to enter the ventricle. The suture was tightened and a second knot was added to hold the cannula in place. The heart was removed from the chest and immediately perfused with 1 mL of Tyrode solution from a 1 mL syringe.

The heart was rapidly transferred to a Langendorff apparatus and was perfused with Tyrode solution for 3 minutes. The perfusion was then switched to a Tyrode solution containing 0.16 % (w/v) bovine serum albumin (BSA), 0.1 % (w/v) collagenase type II 250 units/mg (Worthington Biochemical Corporation), and 0.005 % (w/v) protease from Streptomyces (Sigma) for 9 minutes. Constant pressure was maintained during perfusion by pumping the solutions to a fixed height (1 m) and allowing gravitational pressure to feed solutions through the heart. Solutions were kept at 37 °C using water-jacketing and were oxygenated in their reservoirs.

Following perfusion, the heart was removed from the Langendorff system and placed in a sterile petri dish. The ventricles were cut away, mechanically agitated, and placed into Tyrode solution containing 0.16 % (w/v) BSA, 0.016 % (w/v) collagenase type II 250 units/mg, and 75 μM $CaCl_2$ which was previously oxygenated. Ventricles were shaken in the solution for 5 minutes in a water bath at 37 °C. After shaking, the solution was poured through a sterile nylon filter to separate isolated cardiomyocytes from the undigested tissue. 10 mL of a Tyrode solution containing 1 % BSA and 1 mM $CaCl_2$ was added to the isolated cardiomyocytes to prevent excess enzymatic degradation.

Bulk tissue remaining in the filter was removed and shaken for an additional 5 minutes in a Tyrode solution containing 1 % BSA and 1 mM $CaCl_2$. This solution was then passed through the nylon filter once more and added to the initial fraction.

The combined cardiomyocyte solution was centrifuged in a sterile 50 mL falcon tube at 500 RPM for 2 minutes, the supernatant was discarded, and the pelleted cells were suspended in 5 mL of storage solution. Variability in cardiomyocyte yield was greater within, rather than between, genotype groups across all experiments. Cells were stored for <6 hours prior to experimentation.

Measurement of intracellular [Ca^{2+}] was possible due to incubation with FURA-2-acetoxymethyl ester (FURA-2-AM) (Life Technologies F1201) prior to experimentation. Cells were suspended in 250 μM $CaCl_2$ perfusion solution containing 1 mM FURA-2-AM and 2 μM Pluronic (to improve FURA-2-AM uptake). After letting cells settle for 5 minutes, the supernatant was discarded and pelleted cells were re-suspended in 500 μM $CaCl_2$ perfusion solution for 10 minutes. The supernatant was once again discarded and the cells suspended in 500 μM $CaCl_2$ perfusion solution for storage until experimentation.

2.2.2 Apparatus and experimentation

Intact cardiomyocytes were examined using an IonOptix-μStep Myocyte Contractility System (Figure 2-5). Cells were dispensed into the perfusion chamber and left to settle for 4 minutes on unused cover glass slides. 37 °C perfusion solution was introduced at approximately 1 mL/minute using peristaltic pumps. Electrical field stimulation (20 V square wave, varying frequency) was applied using a function generator. Excitation of the FURA-2-AM dye was accomplished using the μStep filter device.

Cells were selected for experimentation based on their appearance (rectangular shape with regular striations) and contractile profile (consistent visible contractions at 1 Hz stimulation, no spontaneous contractions). Sampling bias was minimized by

recording every cell on the field that met these characteristics. Baseline measurements involved recording of 20+ contractions at each stimulation frequency, which was increased from 1 Hz to 3 Hz to 6 Hz. Many cardiomyocytes that met selection criteria at 1 Hz stimulation were not able to maintain consistent contractility at 6 Hz stimulation and were therefore excluded from those analyses.

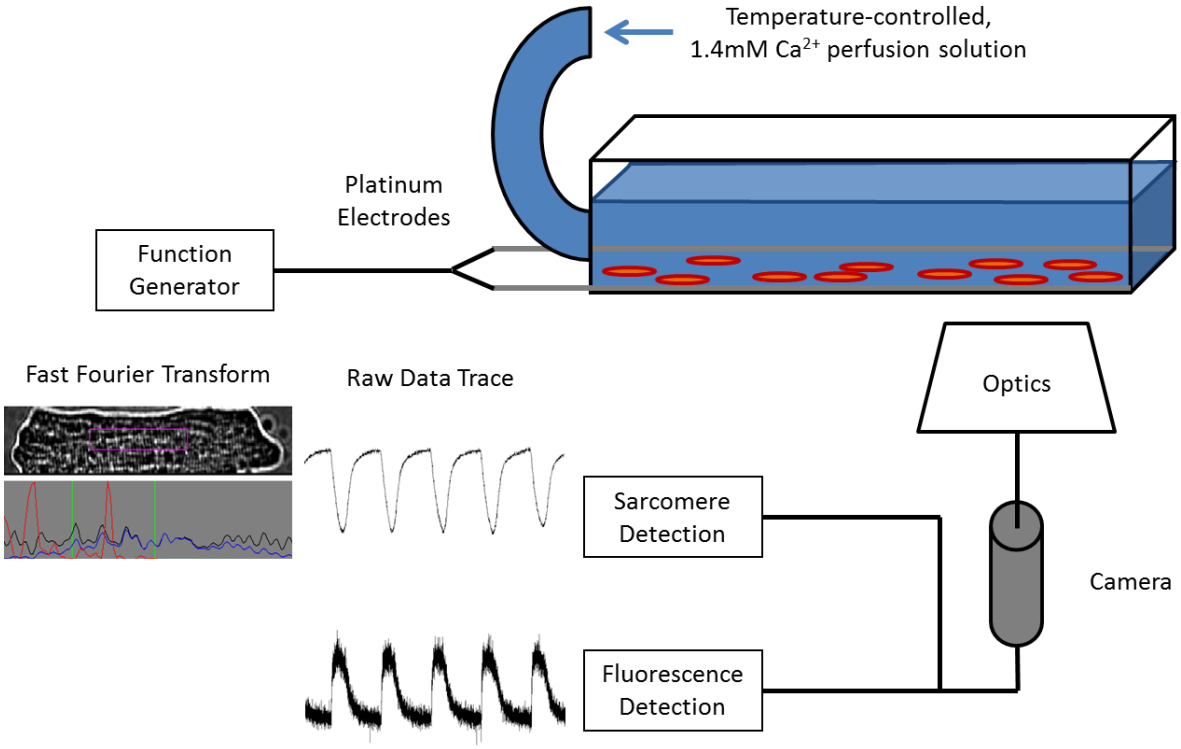


Figure 2-5 - Schematic illustration of IonOptix-μStep Myocyte Contractility System. Cardiomyocytes were dispensed into a perfusion chamber and left to settle. Temperature controlled perfusion was applied using peristaltic pumps. Electrical field stimulation at various frequencies was produced using a function generator. Detection of sarcomeres and fluorescence was accomplished optically and traces were produced using built-in IonOptix software.

2.2.3 Analysis

Analysis of cardiomyocyte contractility and Ca^{2+} handling was performed using IonWizard 6.3.4.69 (IonOptix). Sarcomere length and Ca^{2+} transient traces for each cell and stimulation frequency were averaged over all contractions. A fit to the averaged shortening and Ca^{2+} transient traces was generated. The following

parameters were collected from each shortening and Ca^{2+} fitted average trace: baseline, peak, peak height (peak – baseline), normalized peak height ((peak – baseline)/baseline), time to 50 % peak, and time to 50 % baseline. The mean traces for each group were calculated by averaging the aggregate trace for each cell.

2.2.4 Intact Cardiomyocyte Treatment

Caffeine – In some experiments, after measurements at each stimulation frequency were completed, stimulation was paused briefly and a spritz of caffeine treatment solution was applied directly to the cell using a pre-positioned syringe (Figure 2-6).

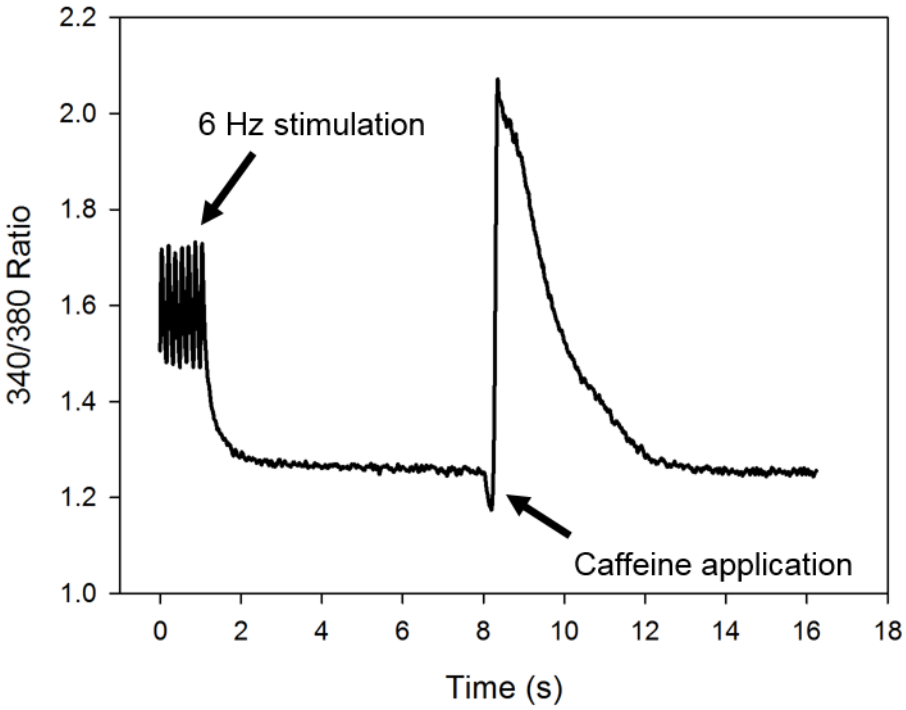


Figure 2-6 - Example caffeine application trace.

Cells that responded to the stimulus but were not displaced were analysed by measuring the Ca^{2+} transient height and decay rate. As caffeine binding to the ryanodine receptor results in a nearly complete release of Ca^{2+} from the sarcoplasmic reticulum [Bassani, 1995], the height of the caffeine transient was

taken to be the total sarcoplasmic reticulum load. Further, as sustained exposure to caffeine results in inhibition of SR Ca^{2+} re-uptake [Bassani, 1995], the rate of Ca^{2+} transient decay following caffeine spritz was determined by the activity of the NCX and other slow mechanisms. During normal pacing conditions, NCX, the slow mechanisms, and SERCA contribute to the reduction in intracellular Ca^{2+} during diastole. Therefore, the SERCA activity at each stimulation frequency was calculated by subtracting NCX activity from the total Ca^{2+} transient decay rate as follows [Puglisi *et al.*, 2014]:

$$\frac{1}{\tau_{pacing}} = K_{SERCA} + K_{NCX} + K_{slow}$$

$$\frac{1}{\tau_{Caffeine}} = K_{NCX} + K_{slow}$$

$$K_{SERCA} = \frac{1}{\tau_{pacing}} - \frac{1}{\tau_{Caffeine}}$$

Isoproterenol – In some experiments, paired measurements of individual cells were conducted with and without 10 nM isoproterenol in the perfusion solution. Cells were first measured in cardiomyocyte perfusion solution. After a minimum of 20 contractions were recorded, 10 nM isoproterenol perfusion solution was introduced. The response of the cell was observed until homogenous contractions were achieved (<5 minutes) and a minimum of 20 additional contractions were recorded.

AICAR – In some experiments, cells were treated with 2 mM AICAR for 15 minutes prior to examination. This treatment was conducted in cardiomyocyte storage solution and the cells were agitated every 5 minutes. Control cells were subjected to the same incubation in storage solution without added AICAR. AICAR-treated

cells were examined and analysed using the same protocol as control cells except 2 mM AICAR was included in the perfusion solution.

2.3 Biochemical analyses

2.3.1 Sample preparation

Demembranated trabeculae were prepared for one-dimensional sodium dodecyl sulphate polyacrylamide gel electrophoresis (1D SDS-PAGE) by dissolving the fibres in mammalian tissue lysis buffer (Sigma C3228) and 5x SDS loading buffer. Samples were then sonicated for 2 minutes in a water bath and held at 95 °C for 5 minutes.

Cardiomyocyte pellets were dissolved for phospholamban analysis via 1D SDS PAGE in 50 µL of 5x SDS loading buffer and water. Pellets were agitated using a syringe but were not boiled or sonicated.

Cardiomyocyte pellets were dissolved for 2D gel electrophoresis in 160 µL of Urea-thiourea- 3-[(3-cholamidopropyl)dimethylammonio]-1-propanesulfonate (CHAPS) buffer (UTC buffer). Pellets were sonicated for 10 minutes, vortexed for 30 minutes, and again sonicated for 10 minutes. The sample was then centrifuged at 17,000 xg for 10 minutes and the pellet was discarded.

2.3.2 Protein concentration analysis

Protein concentration was determined using the Bradford protein assay. Briefly, standards were prepared using bovine serum albumin. Standards and samples were combined with the Bradford reagent (Sigma) and measured in triplicate using a FLUOstar Omega plate reader. A calibration curve was created using Microsoft

Excel to relate absorbance measurements with protein concentration. This calibration curve was used to assess protein concentration in the unknown samples.

2.3.3 One dimensional SDS-PAGE

Both pre-cast commercial gels and self-made SDS-PAGE gels were used. Self-made gels contained varying acrylamide concentrations depending on the protein of interest. Gels for TnI were 10 % acrylamide and gels for Phospholamban were 15 % acrylamide. For PhosTag gels, 100 µM PhosTag and 200 µM $MnCl_2$ was added to the resolving gel.

Pre-cast Mini-PROTEAN TGX Stain-free gels (4-15 % gradient) were used for some experiments to allow measurement of total protein loading in the same gel as subsequent Western blots.

Gels were run using a standard tris-glycine SDS-PAGE running buffer at 100 V at room temperature until the dye front reached the resolving gel. Then, voltage was increased to 180 V until the dye reached the bottom of the gel.

2.3.4 Western blotting

Transfer of protein from SDS-PAGE gels to nitrocellulose membranes was accomplished using a BioRad Wet/Tank Blotting System. Transfer time was varied from 1 hour to overnight based on protein size. All blots were run at 300 mA and 4 °C using a 48 mM Tris base, 390 mM Glycine, 20 % methanol, 0.1 % SDS buffer. Membranes were transferred to 50 mL Falcon tubes and continuously rotated during blocking and incubation. In general, blocking was conducted with 5 % dry milk in TBST for 1 hour at room temperature. Primary antibodies were incubated overnight at 4 °C in 5 % dry milk in TBST while secondary antibodies were incubated 1 hour

at room temperature. Troubleshooting blots was accomplished by varying the blocking agent (using GE Healthcare membrane blocking agent) and/or concentrations of blocking agent and antibodies. The membrane was washed with tris-buffered saline + Tween 20 (TBST, 50 mM Tris HCl, 150 mM NaCl, 0.05 % Tween 20) for 3 x 5 minutes after primary antibody incubation and 5 x 5 minutes following secondary antibody incubation. Membranes were developed using GE Healthcare Amersham ECL Select/Prime Western Blotting Detection Reagent and imaged using a BioRad ChemiDoc XRS system. Gel densitometry was conducted using ImageJ or BioRad's ImageLab software.

In some experiments, sequential antibodies were applied to a single nitrocellulose membrane. Following imaging with the first set of primary and secondary antibodies, membranes were washed with TBST for 5 minutes. Membranes were then treated with Restore ® Western Blot Stripping Buffer (Thermo) for 8 minutes at room temperature before another 5 minute TBST wash. Membranes were then blocked and probed with another primary + secondary antibody combination. Effective stripping was assessed for each antibody pair by re-imaging the membrane following the stripping procedure before application of the next antibody.

2.3.5 Two dimensional gel electrophoresis

Samples were prepared for 2D electrophoresis using GE Healthcare's 2D Gel Clean-up Kit. The kit precipitates sample proteins and washes away contaminating detergents, salts, lipids, phenolics, and nucleic acids. Following clean-up, the protein was re-suspended in UTC buffer, sonicated for 10 minutes, and vortexed for 30 minutes.

Isoelectric focusing (IEF) - 40 μg of protein was dissolved in 160 μL (total) of sample solution and IEF rehydration buffer. The solution was dispensed in a continuous, bubble-free bead between positive and negative electrodes in one well of a BioRad PROTEAN IEF Cell. An 11 cm, nonlinear immobilized pH (3-11) gradient (IPG) strip (GE Healthcare) was lowered onto the solution. 1-2 mL of mineral oil was added to cover the strips and prevent dehydration. Focusing consisted of a five-part protocol:

Table 2-2 - Isoelectric focusing protocol.

Stage	Voltage	Ramp Speed	Time
Rehydration	Passive	N/A	>3 hours
1	250	Rapid	30 minutes
2	6000 V	Slow	1 hour
3	8000 V	Rapid	30,000 V-hr
Hold	500 V	N/A	< 2 hours

If the hold stage was longer than 2 hours, a 1 hour 8000 V refocusing step was applied. After focusing, strips were removed from the IEF cell, excess mineral oil was removed, and the strips were frozen at -80 °C.

2nd dimension electrophoresis – Strips were removed from -80 °C and left to equilibrate at room temperature. The strips were then incubated with 2.5 mL of IEF equilibration buffer + 1 % (w/v) dithiothreitol (DTT) on a rotator (~50 RPM) for 10 minutes. Next, strips were incubated with 2.5 mL of IEF equilibration buffer + 2.5 % (w/v) iodoacetamide. Strips were then rinsed briefly in SDS-PAGE running buffer before being placed onto a 4-15 % Criterion™ TGX™ IPG+1 Gel (BioRad). A full-range rainbow marker (Amersham) was loaded in the +1 lane. Gel electrophoresis was run at 200 V until the lowest marker (12 kDa) reached the cassette bottom.

Staining and imaging – Gels were stained using SYPRO ® Ruby Protein Gel Stain (Life Technologies). Gels were fixed using two 30 minute washes with 100 mL of a 50 % methanol, 7 % acetic acid solution. Staining was accomplished using 60 mL of SYPRO ® Ruby Protein Gel Stain overnight in a darkened container. The gels were washed in 100 mL of a 10 % methanol, 7 % acetic acid solution for 30 minutes before imaging. Imaging was completed using UV illumination and low-wavelength detection on a BioRad ChemiDoc XRS system.

Image analysis – A characteristic 2D gel electrophoresis + Ruby stain result is shown in Figure 2-7. Determination of protein identities was accomplished based on published results [Dokhac *et al.*, 1986; Helper *et al.*, 1988; Sadayappan *et al.*, 2006] and laboratory expertise (Dr Jillian Simon). Confirmation of MyBPC's identity was made by applying a MyBPC antibody to a Western-blotted 2D gel.

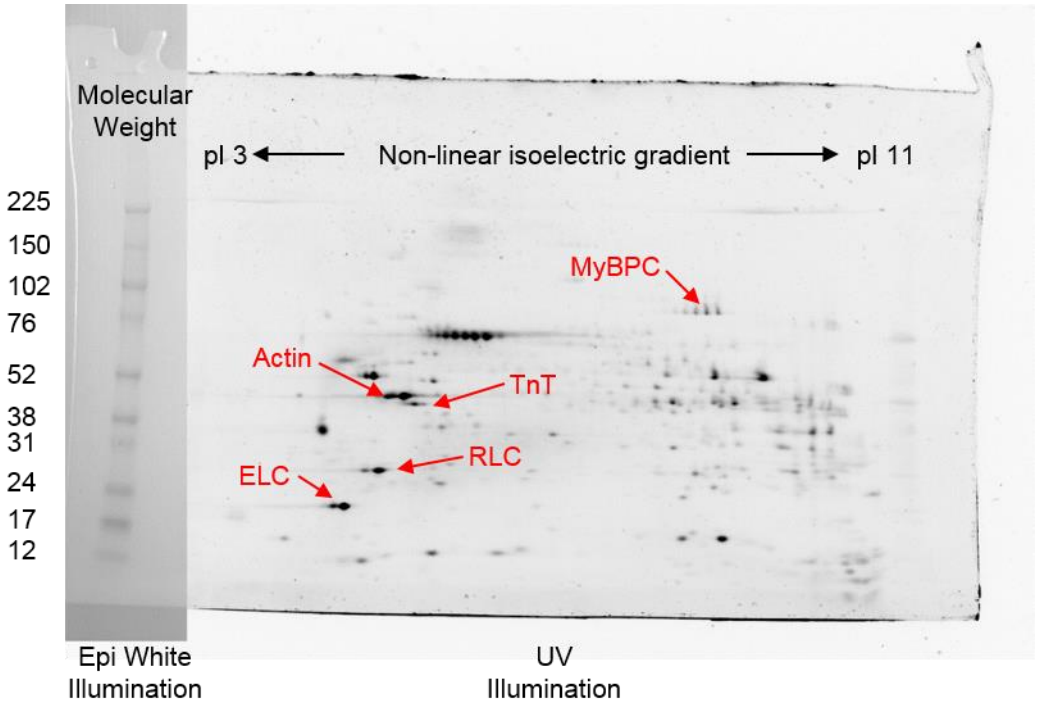


Figure 2-7 - Example 2D gel electrophoresis result. Images generated using white light (molecular weight marker) and UV (Sypro stain) illuminations are combined for convenience.

Analysis of protein isoelectric distributions was completed using ImageJ's built-in gel analysis tools (Figure 2-8). First, image brightness was matched across all results. A horizontal box surrounding all spots was drawn and image intensity (integrated vertically) was plotted against horizontal position. After subtracting background intensity, the continuous signal was split into individual peaks. The area under each curve was measured and assumed to approximate the abundance of protein located at that isoelectric position.

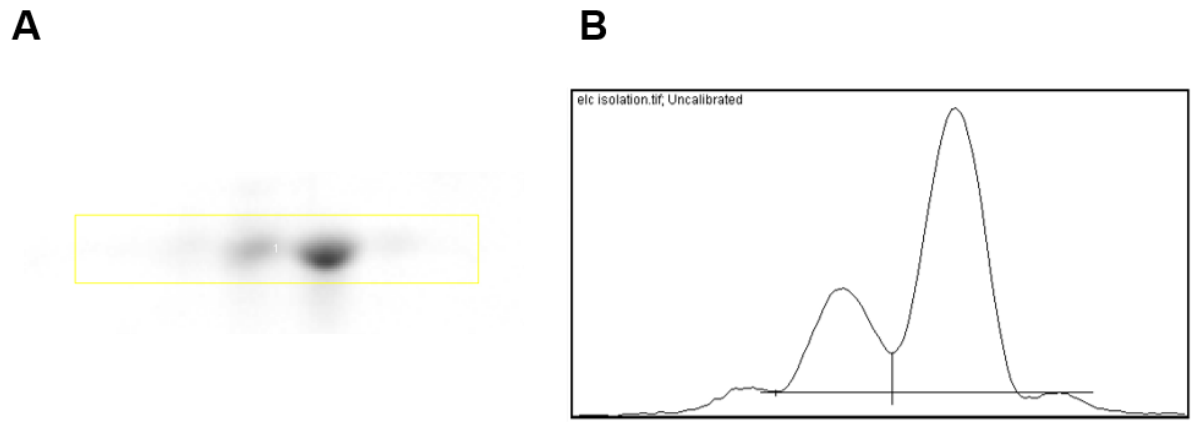


Figure 2-8 - Example analysis of 2D gel electrophoresis result. Image brightness was matched between comparison groups and individual proteins were assessed using ImageJ's built-in gel analysis tools (A & B)

2.3.6 Weighted average calculation

A weighted average calculation was used to determine the mean number of phosphorylations per molecule using PhosTag gels and average isoelectric position of proteins using 2D electrophoresis:

$$\bar{x} = \frac{\sum_{i=1}^{n} w_i x_i}{\sum_{i=1}^{n} w_i}$$

where w is the weight/proportion of the protein in state i, and x is the position of state i. For example, the mean phosphorylation state of TnI with a PhosTag

distribution of 80% bis-phosphorylated, 15 % mono-phosphorylated, and 5 % un-phosphorylated would be:

$$\bar{x} = \frac{0.80 * 2 + 0.15 * 1 + 0.05 * 0}{0.80 + 0.15 + 0.05} = 1.75$$

2.5 Statistical analyses

Statistical tests were conducted using Matlab. The type of test used for each measurement is indicated in figure legends. To summarize, determinations of significant genotype, treatment, and interaction effects were conducted via multiple linear regressions and/or 2-way analysis of variance (ANOVA) followed by post-hoc corrected tests (Tukey-Kramer and Bonferroni) using Matlab's multiple comparison tool (multcompare). Assessment of differences between control and treatment groups were conducted using paired or unpaired ANOVA. Non-parametric data were analysed by the Mann-Whitney U test or Kruskal-Wallis test for two or three unpaired groups, respectively. Significance of differences between WT and mutant groups were reported at $p < 0.05$, $p < 0.01$, and $p < 0.001$ levels with single (*), double (**), and triple asterisks (***), respectively, above the mutant group. Differences between control and treatment groups were reported between the bars. Interaction effects were determined using 2-way ANOVA, and were reported at $p < 0.05$, $p < 0.01$, and $p < 0.001$ levels using single (†), double (††), and triple daggers (†††), respectively (shown in the lower right-hand corner of plots).

2.6 Solutions

Tyrode

Component	Concentration (mM)
NaCl	130
KCl	5.6
HEPES	5
$NaH_2PO_4 \cdot 12H_2O$	0.4
$MgCl_2 \cdot 6H_2O$	3.5

Cardiomyocyte perfusion

Component	Concentration (mM)
NaCl	120
KCl	5.6
MgSO4 · 7H2O	5
HEPES	10
Na Pyruvate	5

Cardiomyocyte storage

Component	Concentration (mM)
NaCl	140
KCl	5.6
MgCl2	1.2
HEPES	5
CaCl	140

Caffeine treatment

Component	Amount
Cardiomyocyte perfusion	
Caffeine (powder)	10mM

Isoproterenol perfusion

Component	Amount
Cardiomyocyte perfusion	
Isoproterenol	10 nM

Dissecting

Component	Concentration (mM)
EGTA	10
MgCl2	5.6
KCl	100
Imidazole	20
ATP	5
CrP	10
BDM	20
Protease inhibitors	As directed

Glycerinated relaxing

Component	Concentration (mM)
EGTA	10
MgCl2	5.6
KCl	100
Imidazole	20
ATP	5
CrP	10
Glycerol	50%
Protease inhibitors	As directed

Skinning

Component	Volume
Glycerinated Relaxing	99%
Triton X-100	1%

Pre-activating

Component	Concentration (mM)
EGTA	0.1
MgCl2	1
MOPS	80
HDTA	14.9
ATP	5
KCl	Correct to ionic strength = 170 mM

PKA treatment

Component	Concentration/ Volume
Force-fibre pCa 9.0	200 µL
DTT	0.1 mM
Protein Kinase A Catalytic Subunit from bovine heart (Sigma P2645)	100 units

SDS-PAGE running buffer

Component	Concentration
Tris base	25 mM
Glycine	192 mM
SDS	0.1 %

Western transfer buffer

Component	Concentration
Tris base	48 mM
Glycine	390 mM
SDS	0.1 %
Methanol	20 %

Force-fibre

Component	Concentration
Temperature	15°C
pH	7
Ionic Strength	170 mM
pMg	3
Total EGTA	15 mM
Total MOPS	80 mM
MgATP	5 mM
Total CP	15 mM
Free K	83 mM
Free Na	52 mM
Free Ca^{2+} (pCa)	Range 4-9

UTC buffer

Component	Concentration
Urea	7 M
Thiourea	2 M
CHAPS	4 %

IEF Rehydration Buffer

Component	Concentration
Base = UTC buffer	
DTT	100 mM
Destreak (GE Healthcare)	1 %
3-11 NL IPG Buffer (GE Healthcare)	0.5 %

IEF Equilibration Buffer

Component	Concentration
Base = ddH_20	
Urea	6 M
Glycerol	30 % (v/v)
SDS	5 % (w/v)

Chapter 3 – Characterisation of AMPK R299Q γ2 cardiac contractile mechanics in demembranated trabeculae

3.1 A novel mouse model of PRKAG2 cardiomyopathy

To determine whether PRKAG2 cardiomyopathy represents a primary cardiomyopathy or purely a glycogen storage disease, an AMPK R229Q γ2 knock-in mouse model was produced. This model avoids the inherent disadvantages of an overexpressing transgenic model by maintaining the native promoter and endogenous gene expression control mechanisms. The genetic modification strategy generated R229Q γ2 knock-in mutant heterozygous (Het), homozygous (Homo), and wild type (WT) mice that were viable and fertile (Figure 3-1). Mutant mice were generated on a mixed C57BL/6/129/Ola genetic background and subsequently backcrossed for 7 generations to C57BL/6. Cardiac function of these animals was assessed to determine if the mice effectively modelled PRKAG2 cardiomyopathy. Cine-magnetic resonance imaging (Cine-MRI) and invasive haemodynamics were used to characterize systolic and diastolic function in the animals (Figure 3-2). Mutant mice exhibited reduced ejection fractions, increased end systolic volumes, and slowed diastolic relaxation compared to WT controls. AMPK R299Q γ2 homozygous mice also exhibited intrinsic sinus bradycardia and mild QRS prolongation, but no ventricular pre-excitation [Yavari, 2010].

As glycogen accumulation is assumed to underlie the pathogenesis of PRKAG2 cardiomyopathy [Arad *et al.*, 2002; Arad *et al.*, 2003], histological staining of ventricular sections was conducted to assess myocardial glycogen content. Even after 12 months, however, mutant mice exhibited no significant glycogen

accumulation (Figure 3-3). Sections of cardiac tissue stained with haematoxylin and eosin (H&E) were comparable between age-matched WT and mutant littermates. Most importantly, no glycogen vacuoles were observed in mutant tissues. Staining of collagen with Sirius red, indicative of myocardial fibrosis, revealed no differences between WT and mutant groups (Figure 3-3).

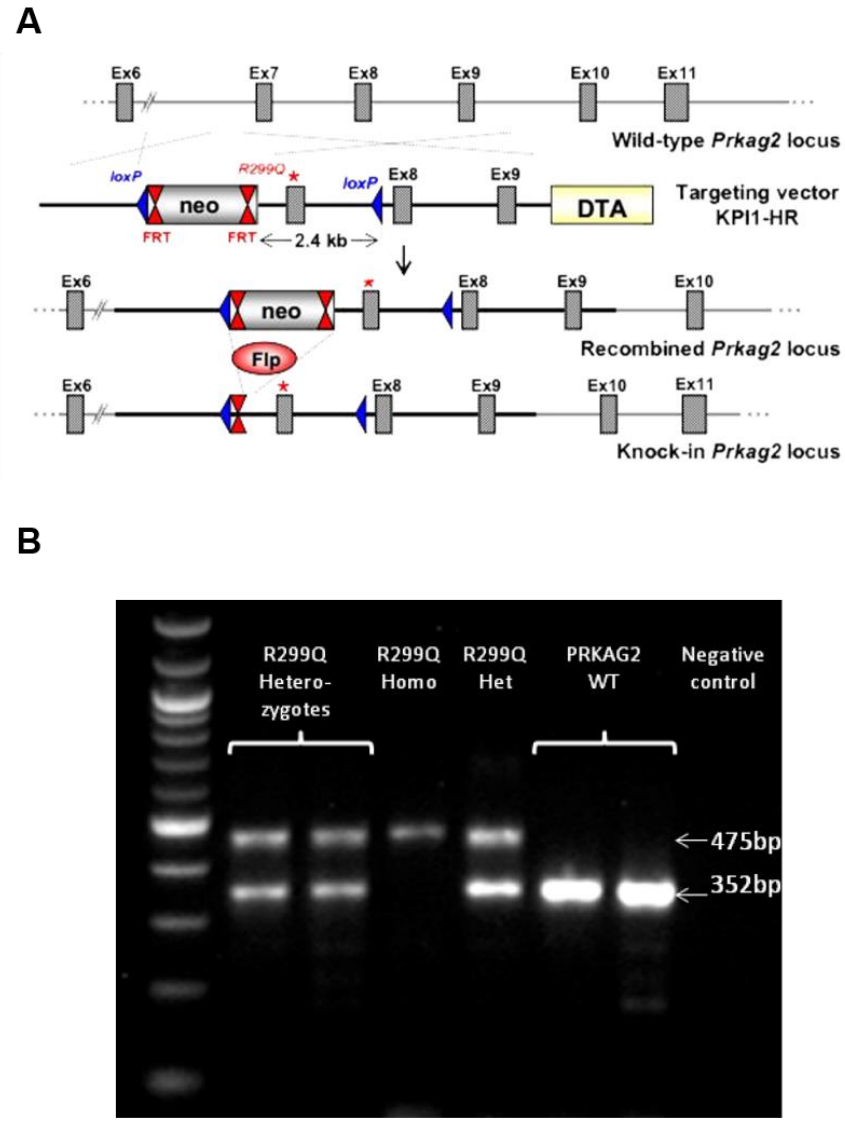


Figure 3-1 - Gene targeting strategy and validation of model. The gene targeting strategy (A) utilized a neomycin selection cassette (neo) flanked by Flp recombinase recognition target (FRT) domains and loxP sites, designed by Dr Katalin Pinter. Founder mice were bred with mice expressing Flp recombinase to remove neo and produce R299Q heterozygote floxed mice. Assistance with vector design and generation of the F1 generation was provided by GenOway (Lyon, France). PCR products from ear-notch gDNA run on a 1 % agarose gel (B) confirm presence of WT and mutant KI alleles (amplification products of 352 and 475 bp, respectively). Experiments were conducted by Dr Arash Yavari.

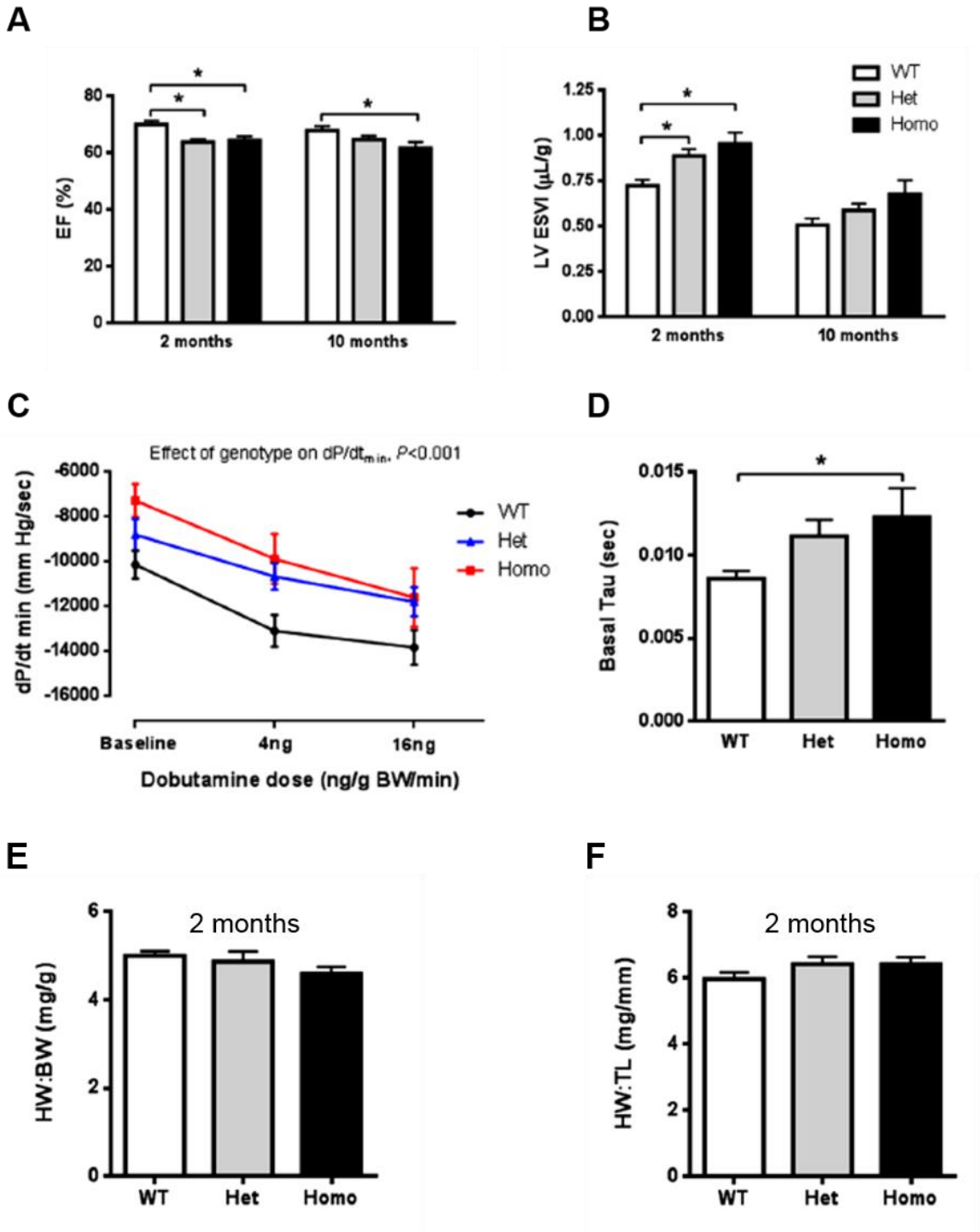


Figure 3-2 - *In vivo* assessment of cardiac function of R299Q mutant and WT littermates at 2 and 10 months of age by cine-MRI (A & B), invasive haemodynamics (C & D), and heart weight measurements (E & F). Mutant animals exhibited reduced ejection fraction and increased end-systolic volume (indexed to body weight, ESVI) compared to WT controls at both early and late time points. Mutant animals also exhibited slowed cardiac relaxation, evidenced by increased minimum relaxation times across dobutamine doses. No significant difference in heart weight, normalized to body weight or tibia length, was observed at 2 months. Experiments were conducted by Miss Hannah Barnes, Dr Arash Yavari, and Dr Mohamed Bellahcene.

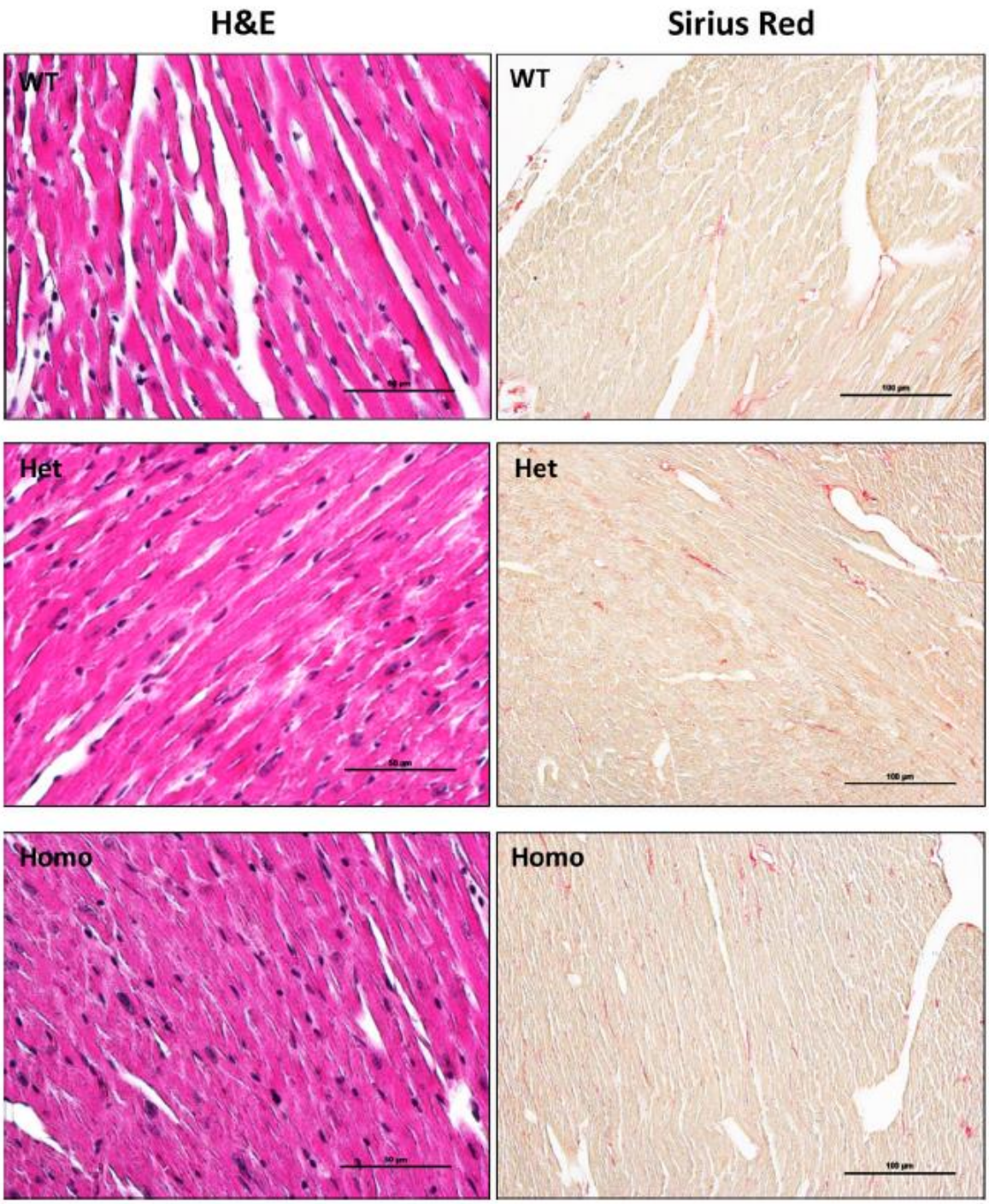


Figure 3-3 – Characteristic histological staining of cardiac tissue from R299Q mutant and WT mice at 12 months of age. Left-hand panels illustrate H&E staining (50 μm scale bar), right-hand panels illustrate Sirius red staining (100 μm scale bar). No apparent differences between mutant and WT panels were observed with either stain. Experiments were conducted by Dr Arash Yavari.

Given the observed *in vivo* dysfunction despite no significant glycogen accumulation, determination of an alternative mechanism of pathogenesis was a primary goal. Of particular initial interest was the fundamental effect of R299Q γ2 mutation on overall AMPK activity. As this mutation is located within a CBS domain involved in regulation of AMPK activity by AMP/ADP/ATP binding, we hypothesized that the mutation would alter baseline AMPK activity and/or regulation. To test this, we measured *in situ* AMPK activity. In this experiment, hearts were rapidly excised from WT and homozygous mice and immediately perfused via aortic cannulation to stabilise the cellular energetic state. The hearts were then freeze-clamped and γ2-specific AMPK activity was measured using the SAMS peptide assay, which measures the rate of incorporation of radiolabled phosphate from [γ-^{32}P]-ATP into a synthetic peptide substrate, SAMS (HMRSAMSGLHLVKRR) by AMPK [Davies *et al.*, 1989]. In the absence of AMP, γ2-specific AMPK was increased in homozygous samples compared to WT controls. The introduction of 0.2 mM AMP resulted in a 130 % increase in γ2-specific AMPK activity in WT samples, but no significant increase in γ2-specific AMPK activity in homozygous samples.

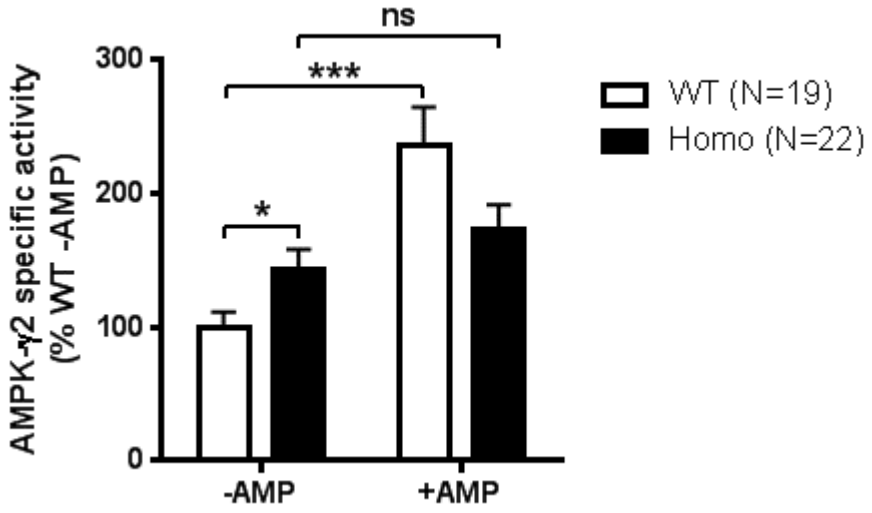


Figure 3-4 – γ2-specific AMPK activity via SAMS peptide assay from isolated, perfused hearts with or without AMP. AMPK activity was significantly increased in homozygous samples compared to WT controls in the absence of AMP. Inclusion of 0.2 mM AMP significantly increased AMPK activity in WT samples, but not in homozygous samples. Significance of differences was determined using t-tests. Experiments were conducted by Dr Arash Yavari.

Basal AMPK activity was also assessed in snap-frozen, homogenized, heart samples. Phosphorylation of AMPK's canonical target, S79 of acetyl CoA carboxylase (ACC), was assessed as this is the most reproducible measure of overall AMPK activity [Hardie, 2014]. Samples from homozygous animals exhibited significantly increased ACC S79 phosphorylation compared to samples from WT and heterozygous animals. No difference in total ACC levels was detected in any group.

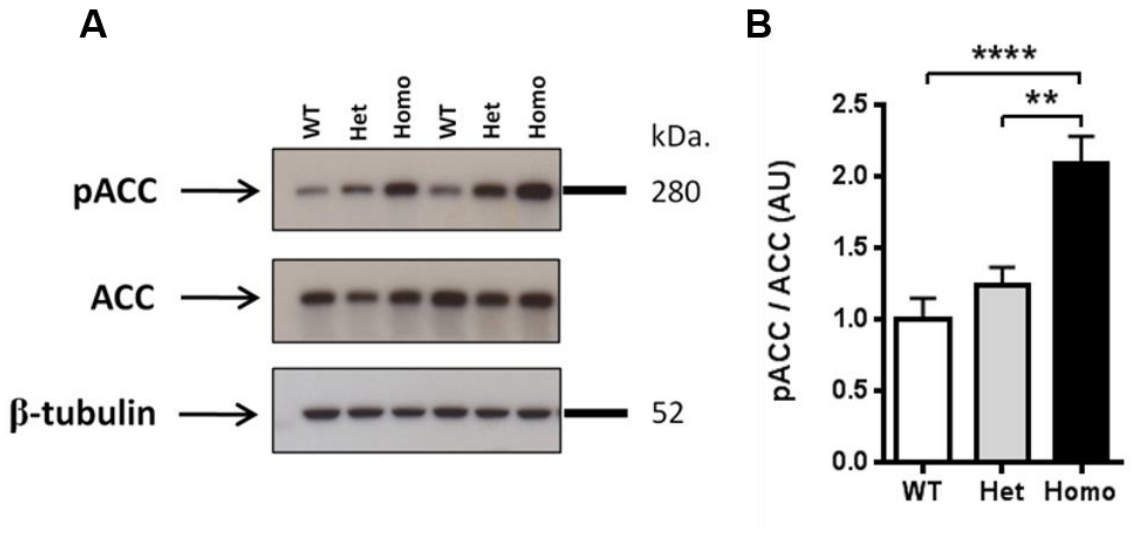


Figure 3-5 – Characteristic Western blots using phospho-ACC S79, total ACC, and β-tubulin antibodies. Samples from homozygous animals exhibited increased ACC S79 phosphorylation compared to samples from WT and heterozygous animals. No difference in total ACC levels (relative to β-tubulin) was observed in any group. Measurements were taken from snap frozen, whole heart homogenates. Significance of differences were determined by t-tests. Experiments were conducted by Dr Arash Yavari.

To test the responsiveness of the mutant AMPK compound to energetic stress, ACC S79 was assessed in isolated cardiomyocytes with or without prior incubation with the AMPK-activator AICAR. At baseline, S79 phosphorylation of ACC was increased in homozygous mutant cardiomyocytes by 50 % compared to that in WT controls. Following AICAR treatment, ACC S79 phosphorylation was significantly increased across both groups, resulting in no significant difference between genotypes.

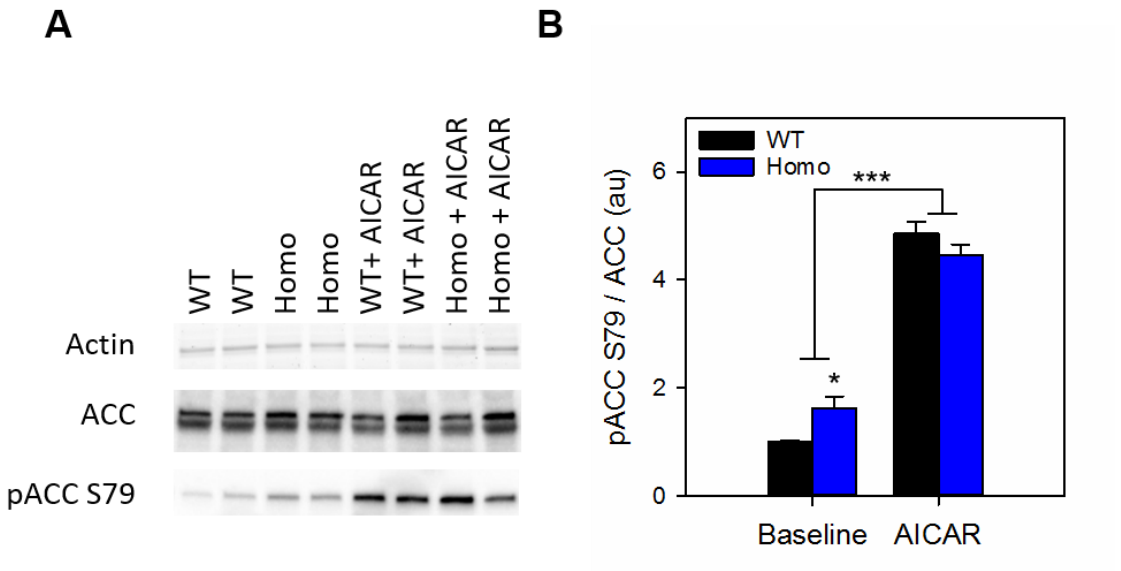


Figure 3-6 – Characteristic actin band on stain-free gel and Western blots using ACC and phospho-ACC S79 antibodies (A) and associated quantitation (B). Phosphorylation of ACC at S79 was significantly increased in cardiomyocytes from homozygous animals compared to WT controls. 15 minute incubation with AICAR significantly increased phosphorylation across both groups to an equivalent level. Measurements were taken from 8 cardiomyocyte samples per group. Significance of differences were determined using 2-way ANOVA followed by post-hoc corrected tests.

3.2 Specific Aims

The previous data demonstrate impaired cardiac function at a young age in a genetically accurate model of PRKAG2 cardiomyopathy in the absence of significant glycogen accumulation. This suggests that cardiac dysfunction in the AMPK R299Q γ2 mice is at least partially independent of glycogen accumulation. Further, the R299Q γ2 mutation was shown to increase basal AMPK activity in mutant mice. To begin examining downstream implications of this initial disturbance, biomechanical properties of isolated cardiac muscle from 6-8 week old mice were assessed. Specifically, skinned left ventricular fibres from R299Q γ2 heterozygous and homozygous mice, along with wild-type littermate controls, were examined to determine the potential role of altered myofilament mechanics in the progression of PRKAG2 cardiomyopathy. This approach isolates the cardiac sarcomere from the

excitation-contraction system and allows direct evaluation of contractile function. A variety of measurements and treatments were applied to these tissues to analyse potential changes in any of the range of behaviours exhibited by normal myocardium. Specifically, experiments in this section aimed to explore potential alterations to the following parameters:

I. Ca^{2+} sensitivity of force development
II. Cooperativity of force development
III. Maximum force production capacity
IV. Passive stiffness
V. Sarcomere length dependence of activation
VI. Cross-bridge cycling rates
VII. Responsiveness to protein kinase A stimulation

3.3 Baseline characterization

To investigate sensitivity of the myofilament to the contraction-initiating ion, Ca^{2+}, demembranated fibres from each genotype group were submerged in solutions containing varying amounts of Ca^{2+} and resulting forces produced by the muscles were measured. This procedure was repeated at both long (2.3 μm) and short (2.0 μm) sarcomere lengths. The relationship between Ca^{2+} concentration (expressed in logarithmic pCa units) and force production (normalized to maximum production for each fibre) was plotted and fit with a modified Hill equation. The averaged data and fits at each sarcomere length are shown in Figure 3-7. At both sarcomere lengths, normalized force production by mutant fibres at submaximal pCa was increased compared to that in WT controls. These changes result in a “left-shift” of the force-Ca^{2+} relationship fit, indicating increased myofilament Ca^{2+} sensitivity in mutant

animals. The difference in normalized force production between groups is most significant at physiologically relevant pCa 6.0 (1 μM Ca^{2+}), where heterozygous and homozygous fibres produced 31 % and 36 % more force than their WT counterparts (SL 2.3 μm).

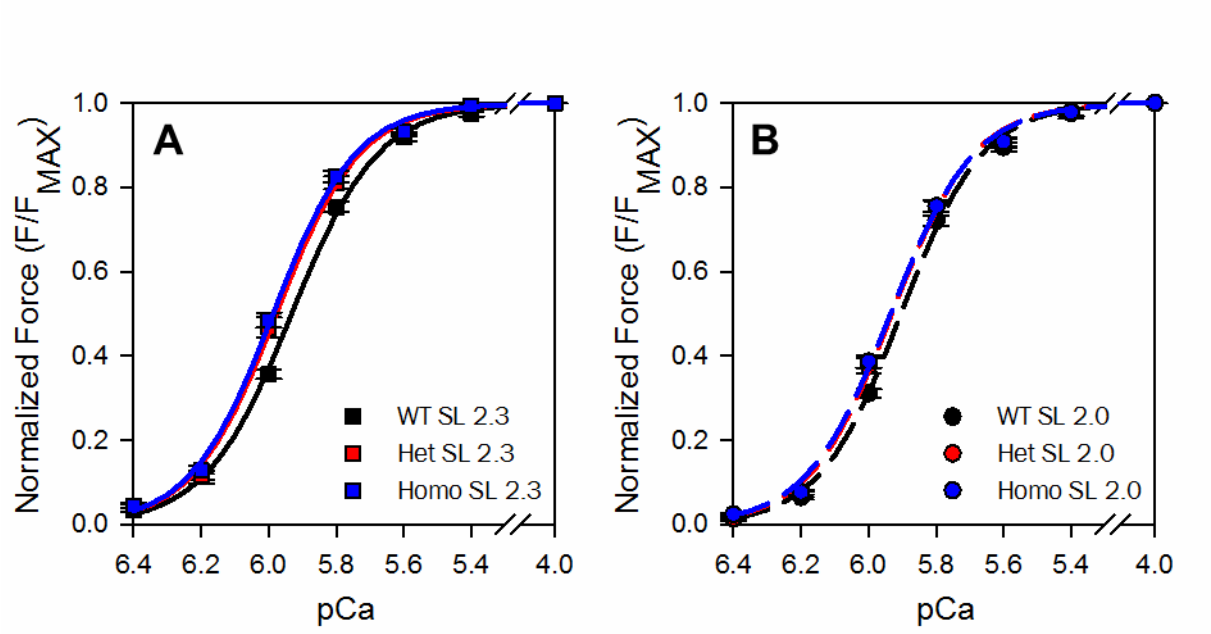


Figure 3-7 - Force-Ca^{2+} sensitivity of demembranated fibres from WT, Heterozygous, and Homozygous animals at sarcomere lengths 2.3 μm (A) and 2.0 μm (B). Fits of force-pCa data from mutant fibres were left-shifted compared to fits of WT data, indicating an increase in Ca^{2+} sensitivity. 3-5 fibres were examined from 5 mice in each group.

In order to quantify the magnitude and significance of this increased sensitivity, each fibre's force-Ca^{2+} relationship was fit using a modified Hill equation:

$$F = \frac{F_{Max}}{1 + 10^{\eta_H(pCa - pCa_{50})}}$$

pCa_{50} values was converted to EC_{50}, which represents the Ca^{2+} concentration (μM) at which the fibre produced half its maximum force. Lower EC_{50}s indicate that less Ca^{2+} was required to achieve half maximal force and imply higher Ca^{2+} sensitivity in the fibre. The second parameter, the Hill coefficient, measures steepness of the force-pCa relationship. Higher Hill coefficients indicate a sharper rise in force

production and therefore greater cooperativity of activation. Means and variations of the parameters within each genotype and sarcomere length group were compiled (Figure 3-8, Table 3-1). In accordance with the Frank-Starling-associated length dependence of Ca^{2+} sensitivity, all groups exhibited reduced EC_{50}s at SL 2.3 μm compared to SL 2.0 μm. In addition, as suggested by the left-shifted force-pCa curves, fibres from heterozygous and homozygous animals exhibited a dose-dependent reduction in EC_{50} compared to WT controls at both sarcomere lengths. At SL 2.3 μm, heterozygous and homozygous EC_{50} averages were 8.9 % and 13.1 %, respectively, lower than the WT EC_{50} average. These data confirm that the cardiac myofilament in mutant animals is sensitized to Ca^{2+}.

No differences in Hill Coefficients were detected between genotype groups at either sarcomere length.

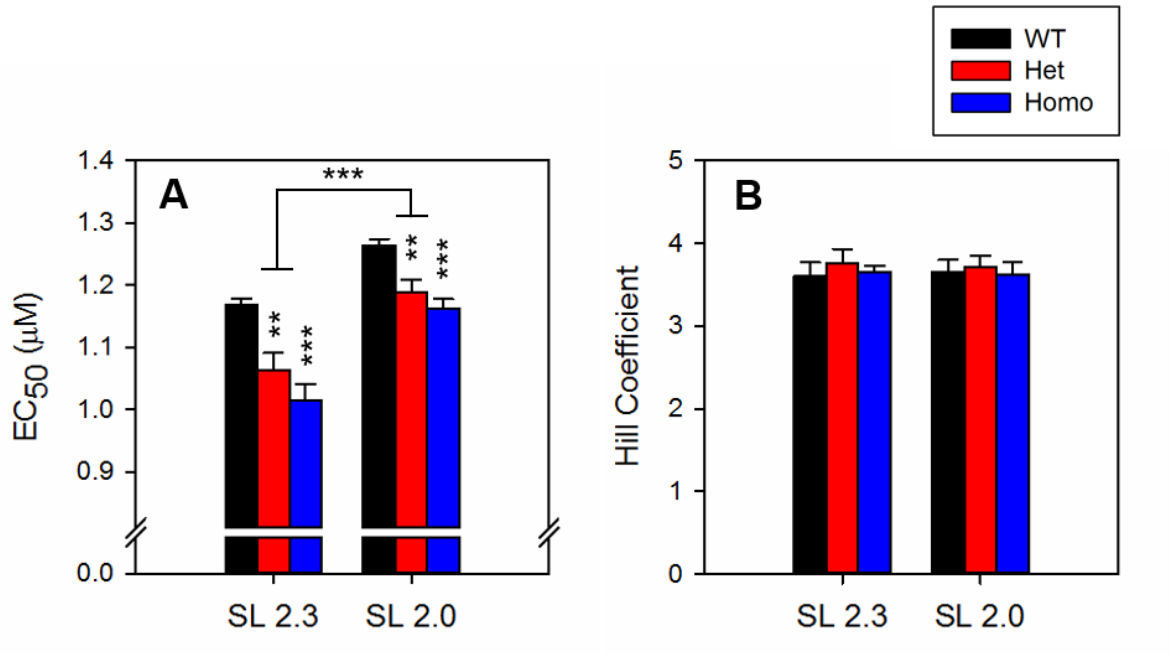


Figure 3-8 - Quantification of force-Ca^{2+} relationship by EC_{50} (Ca^{2+} sensitivity, A) and Hill Coefficient (cooperativity, B). Fibres from mutant animals exhibited a dose-dependent increase in Ca^{2+} sensitivity at both long and short sarcomere lengths but no change in cooperativity of activation. Significance of differences between groups was determined by post-hoc corrected tests following 2-way ANOVA.

In addition to Ca^{2+}-dependence of force development, the maximum force production capacity and passive stiffness of the tissues were also investigated. Maximum force was measured by submerging fibres in high Ca^{2+} (pCa 4.0), measuring the resultant force development, and normalizing production to the cross-sectional area of the fibre. Passive stiffness was measured in the same fashion at low Ca^{2+} (pCa 9.0). A summary of these measurements is given in Figure 3-9. As expected, fibres from all groups produced more force at SL 2.3 μm. However, no significant differences in maximum force production were observed between groups at either sarcomere length. Passive stiffness was higher in all genotypes at SL 2.3 μm compared to SL 2.0 μm, though no differences between genotypes were observed at either length.

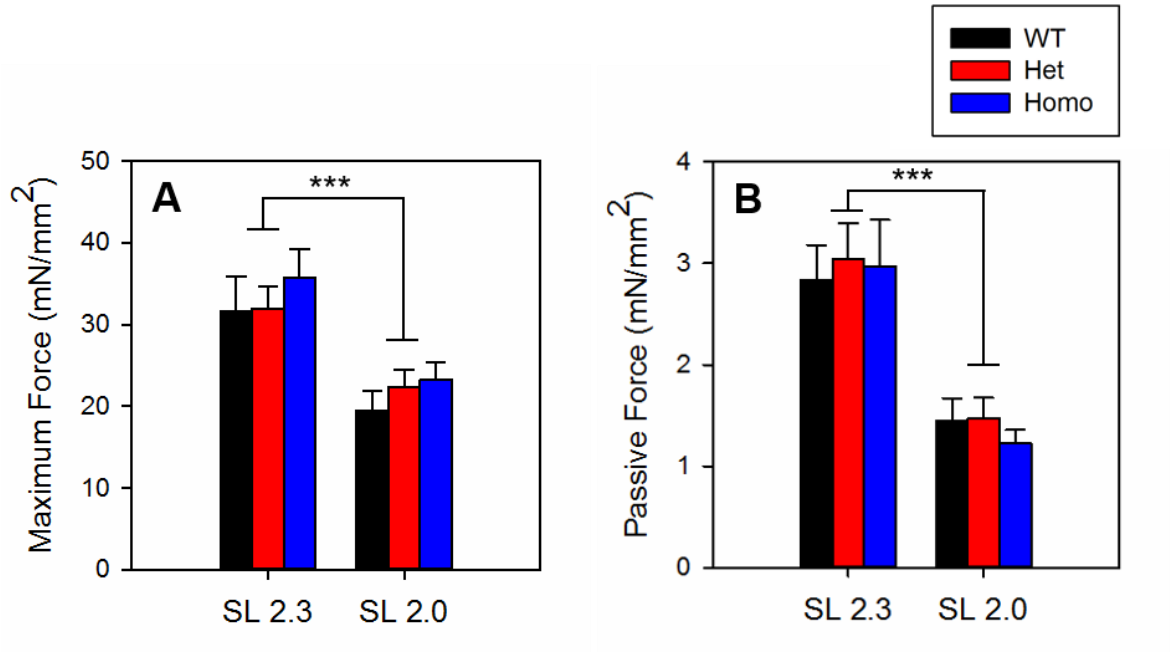


Figure 3-9 - Magnitudes of maximum active (pCa 4.0, A) and passive (pCa 9.0, B) force generated by demembranated fibres. No significant changes were observed between fibres from WT and mutant animals in either parameter. Significance of differences between groups was determined by post-hoc corrected tests following 2-way ANOVA.

Table 3-1 – Mean (± SEM) mechanical parameters of demembranated trabeculae from WT, heterozygous, and homozygous animals.

		WT	Het	Homo
	n	24	18	21
SL 2.3 µm	**EC_{50} (µM)**	1.16 ± 0.01	1.06 ± 0.03	1.01 ± 0.03
	Hill coefficient	3.60 ± 0.17	3.77 ± 0.17	3.59 ± 0.18
	Active force (mN/mm^2)	31.6 ± 4.2	31.9 ± 2.7	35.7 ± 3.5
	Passive force (mN/mm^2)	2.8 ± 0.3	3.0 ± 0.3	3.0 ± 0.5
SL 2.0 µm	**EC_{50} (µM)**	1.26 ± 0.01	1.19 ± 0.02	1.16 ± 0.02
	Hill coefficient	3.65 ± 0.15	3.72 ± 0.13	3.62 ± 0.15
	Active force (mN/mm^2)	19.5 ± 2.4	22.4 ± 2.1	23.3 ± 2.1
	Passive force (mN/mm^2)	1.5 ± 0.2	1.5 ± 0.2	1.22 ± 0.1

The Frank-Starling response in these preparations was quantified using both Ca^{2+} sensitivity and force production measurements. The difference between each fibre's EC_{50} at SL 2.3 µm and its EC_{50} at SL 2.0 µm (ΔEC_{50}) was used to measure the length dependence of Ca^{2+} sensitivity. To measure the length dependence of force production, the ratio of maximum force produced at SL 2.0 µm/SL 2.3 µm was calculated. The results of these comparisons are displayed in Figure 3-10. A significant genotype effect was detected on length dependence of Ca^{2+} sensitivity by 1-way ANOVA, though no significant difference between individual groups was determined. No significant difference in length dependence of force production was observed. Together, these data suggest the mutation has minimal effect on Frank-Starling mechanisms within the myofilament.

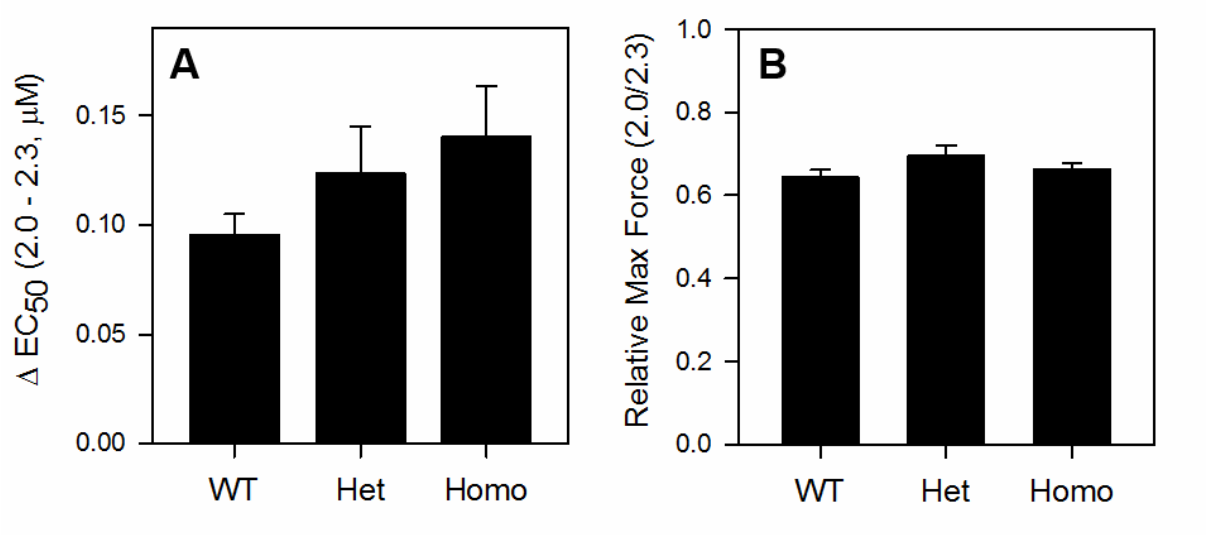


Figure 3-10 - Quantification of sarcomere length dependence of Ca^{2+} sensitivity (A) and maximum force development (B). Fibres from mutant animals exhibited a mild dose-dependent increase in sarcomere length dependence of Ca^{2+} sensitivity ($p < 0.05$ genotype effect by ANOVA) but no significant difference in relative maximum force production.

To investigate potential alterations to cross-bridge functionality, muscle fibres were rapidly shortened and re-stretched at each pCa to detach bound cross-bridges and allow measurement of the reattachment/force redevelopment rate. At high Ca^{2+} (pCa 4.0), the thin filament is fully Ca^{2+}-activated, so the rate of force development is indicative of the maximum cross-bridge cycling rate. At submaximal Ca^{2+}, only a proportion of thin filament regulatory units are active, so the rate of force development measures the speed at which cycling cross-bridges can activate the sarcomere. Thus, tension redevelopment rates at submaximal Ca^{2+} are dependent on myofilament Ca^{2+} sensitivity. The rates of tension redevelopment as a function of pCa and normalized force are shown in Figure 3-11. At pCa 6.0, a genotype dependence of k_{tr} was determined by 1-way ANOVA. However, by plotting k_{tr} vs normalized force (Figure 3-11, C & D), this increase in cross-bridge cycling speeds appears to follow the general trend. This suggests that the increased cross-bridge cycling speeds observed in fibres from mutant animals at pCa 6.0 is due to increased Ca^{2+} sensitivity and not increased cross-bridge cycling rates.

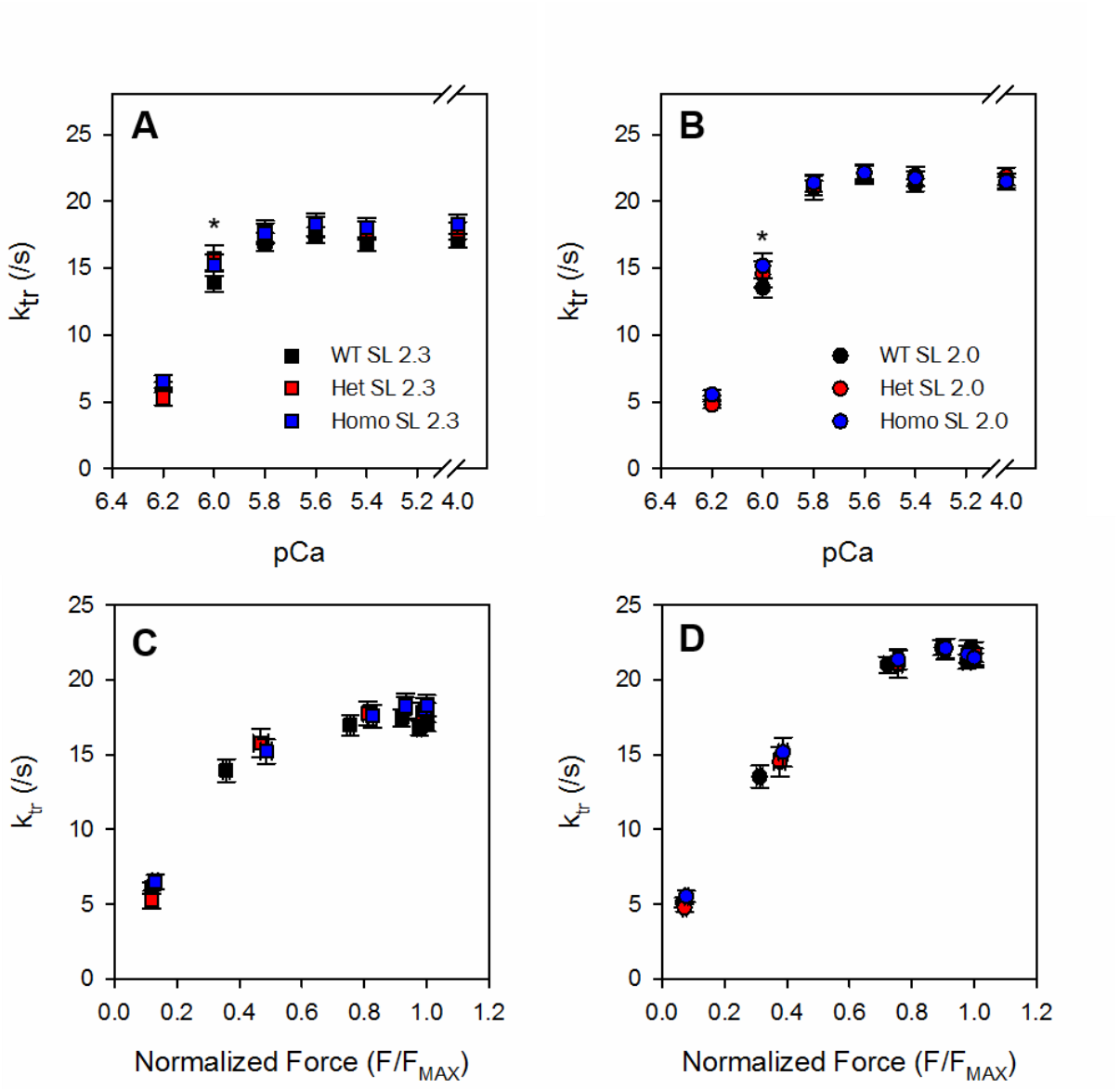


Figure 3-11 – Rates of tension redevelopment (k_{tr}) vs pCa (A, B) and normalized force (C, D) at sarcomere lengths 2.3 and 2.0 µm. Tension redevelopment in mutant fibres was mildly faster than WT controls at pCa 6.0. When plotted against normalized force, this difference is explained by the general force-k_{tr} relationship. * indicates a $p < 0.05$ genotype effect by 1-way ANOVA.

3.4 Effect of PKA treatment

To investigate the potential that alterations to baseline functionality were caused by dissimilar levels of myofilament phosphorylation by PKA, pairwise assessments of the previously described properties were conducted before and after a 1-hour incubation with the activated catalytic subunit of PKA. This treatment aimed to normalize PKA phosphorylation and probe for novel, unexplained differences between groups.

The force-pCa relationships at SL 2.3 μm before and after PKA treatment are shown in Figure 3-12. In all genotype groups, PKA treatment resulted in a right-shift of the force-pCa relation, indicating a decrease in Ca^{2+} sensitivity. However, the magnitude of this shift was significantly different between groups. Specifically, the shift in EC_{50} before and after PKA treatment in mutant groups was significantly larger than in WT controls (SL 2.3 ΔEC_{50} WT 0.06 ± 0.02, Het 0.13 ± 0.02, Homo 0.19 ± 0.01).

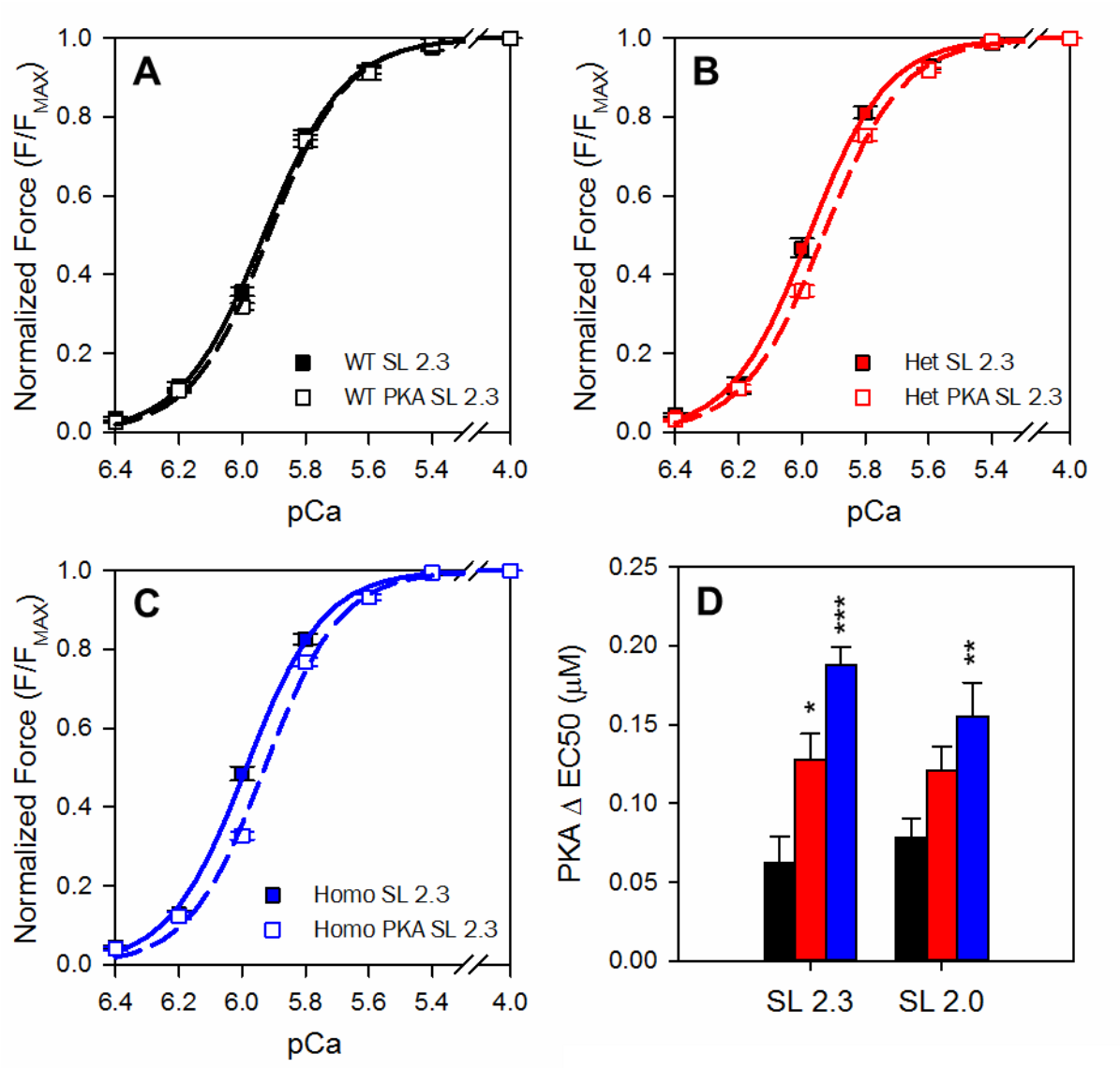


Figure 3-12 – Force-pCa relationship before and after PKA treatment of fibres from WT (A), heterozygous (B), and homozygous (C) animals. Quantification of pairwise shifts of all genotypes at both sarcomere lengths (D). Fibres from mutant animals exhibited a dose-dependent increased responsiveness to PKA treatment in terms of Ca^{2+} desensitization. 3-5 fibres were taken from 3 mice in each group, data shown are means ± SEM. Significance of differences between groups was determined by post-hoc corrected tests following 2-way ANOVA.

A comparison of force-pCa relationships after PKA treatment between genotypes is shown in Figure 3-13. These plots illustrate that the larger PKA-dependent shifts in Ca^{2+} sensitivity in mutant groups result in no significant differences between genotypes in post-PKA force-pCa relationships.

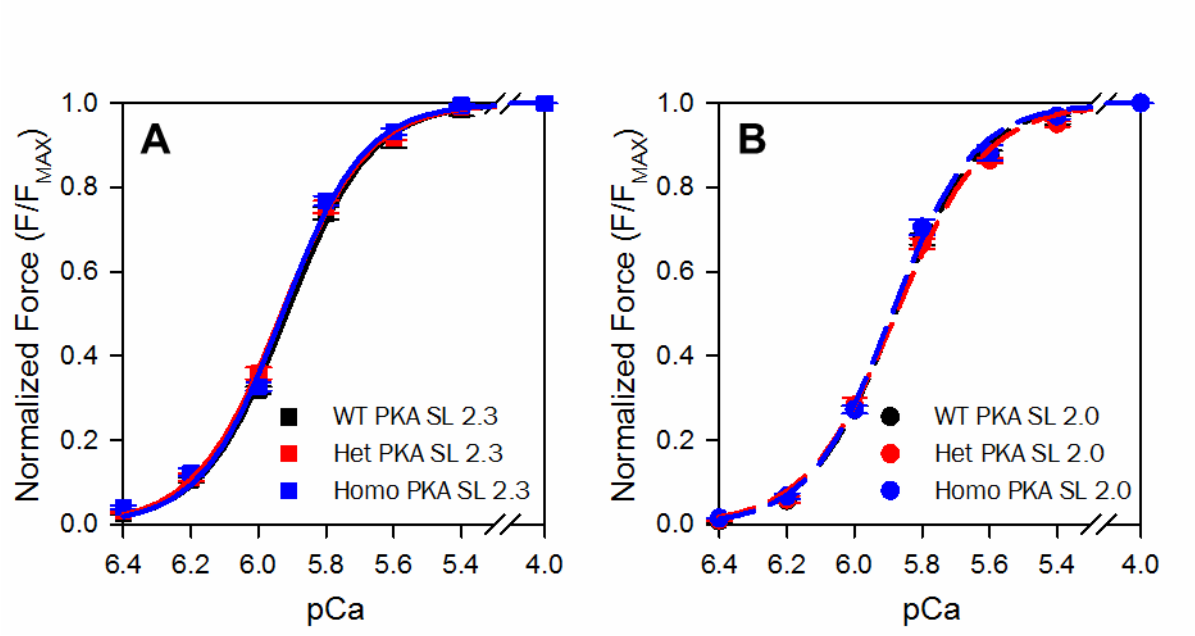


Figure 3-13 - Force-Ca^{2+} sensitivity of demembranated fibres from WT, Heterozygous, and Homozygous animals at sarcomere lengths 2.3 µm (A) and 2.0 µm (B) after treatment with PKA. Fibres from mutant animals exhibited no significant difference from WT animal fibres in their force-pCa relationship after PKA treatment.

Quantification of the post-PKA force-pCa relationships is shown in Figure 3-14. As suggested by the averaged traces, no significant difference in Ca^{2+} sensitivity between genotypes is retained at either sarcomere length following PKA treatment. However, a significant sarcomere length dependence of Ca^{2+} sensitivity does remain following treatment. No significant difference in Hill coefficients were observed between genotypes or sarcomere lengths following PKA treatment.

Treatment with PKA had little effect on maximum force development or passive stiffness levels besides expected run-down (repeated measurements resulting in reduced force development). Significant difference between sarcomere lengths remained but no significant differences between genotypes at either length was determined.

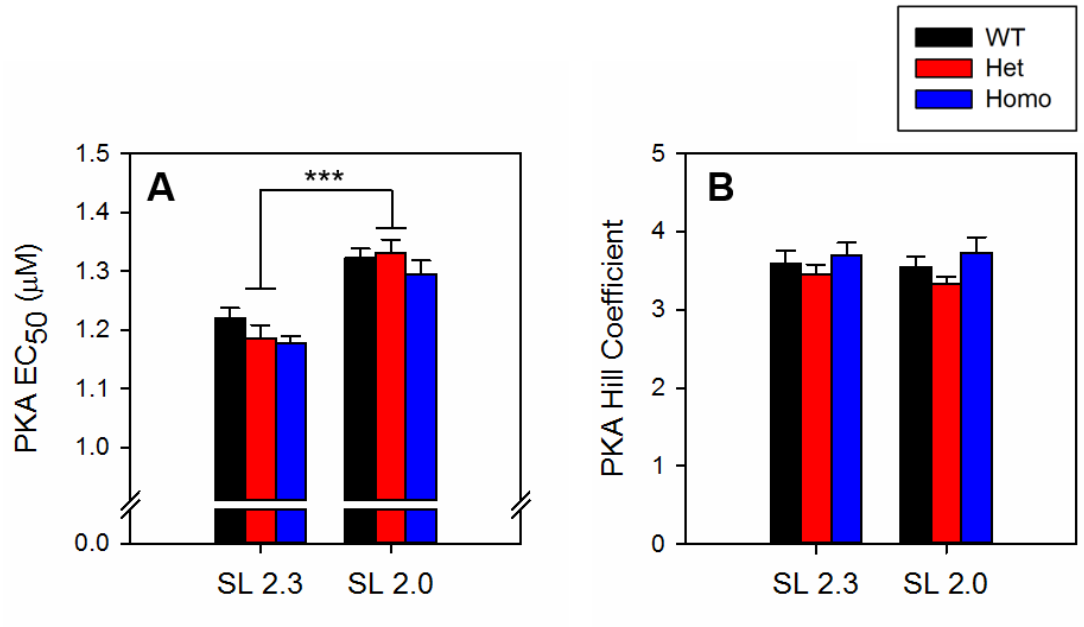


Figure 3-14 - Quantification of force-Ca^{2+} relationship by EC_{50} (Ca^{2+} sensitivity, A) and Hill Coefficient (cooperativity, B) after PKA treatment. Fibres from mutant animals exhibited no significant differences in Ca^{2+} sensitivity or cooperativity at either long or short sarcomere lengths.

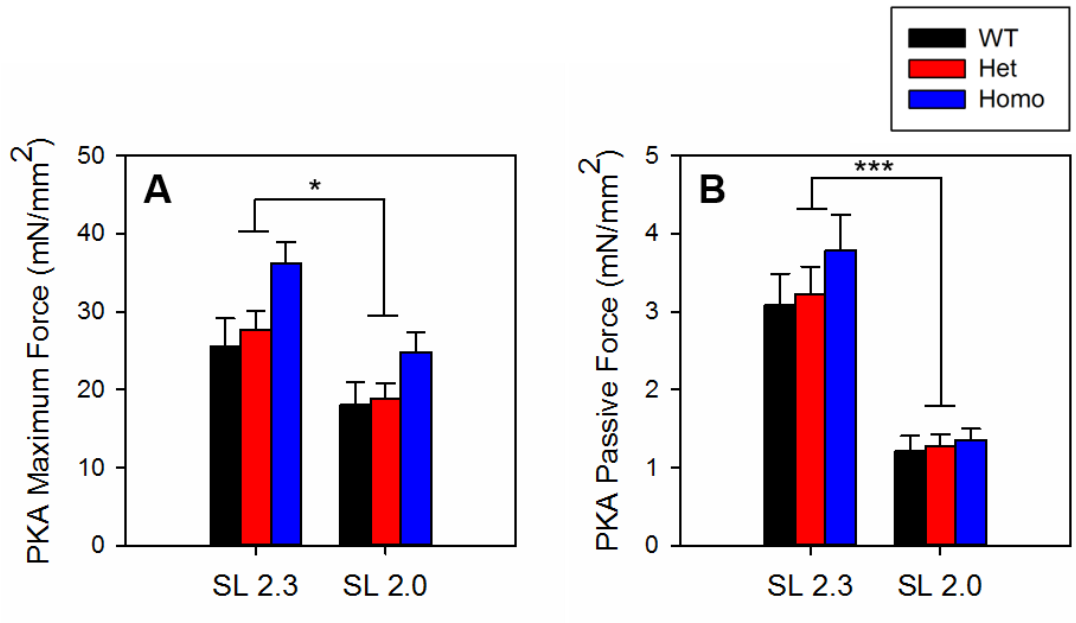


Figure 3-15 - Magnitudes of maximum active (pCa 4.0, A) and passive (pCa 9.0, B) force generated by demembranated fibres after PKA treatment. Fibres from homozygous animals exhibited increased maximum force production compared to WT fibres at sarcomere length 2.3 µm. No significant changes were observed between fibres from WT and mutant animals in passive stiffness. Significance of differences between groups was determined by post-hoc corrected tests following 2-way ANOVA.

The mild genotype effect on sarcomere length dependence of Ca^{2+} sensitivity was eliminated after treatment with PKA. PKA treatment had no effect on the length dependence of force development in any group.

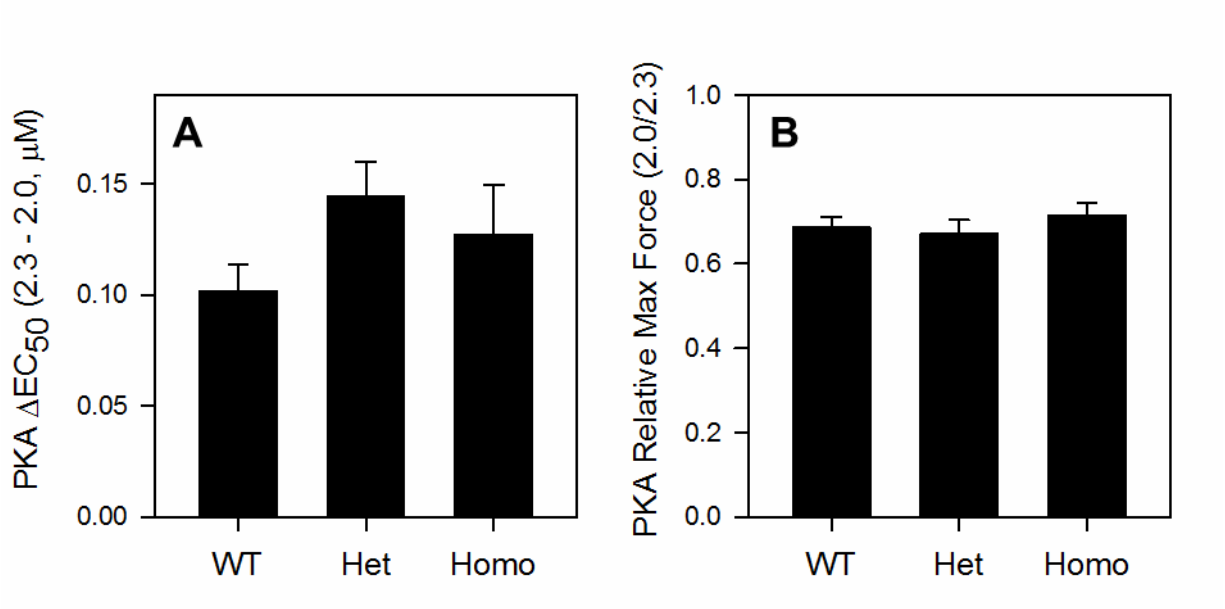


Figure 3-16 - Quantification of sarcomere length dependence of Ca^{2+} sensitivity (A) and maximum force development (B) after PKA treatment. Fibres from mutant animals exhibited no differences from WT animal fibres in either parameter.

The effect of PKA on tension redevelopment rates at each sarcomere length and pCa is shown in Figure 3-17. PKA treatment increased tension redevelopment rates by a comparable margin in all groups. In mutant groups, PKA treatment caused left-shift of the k_{tr}-force relationship.

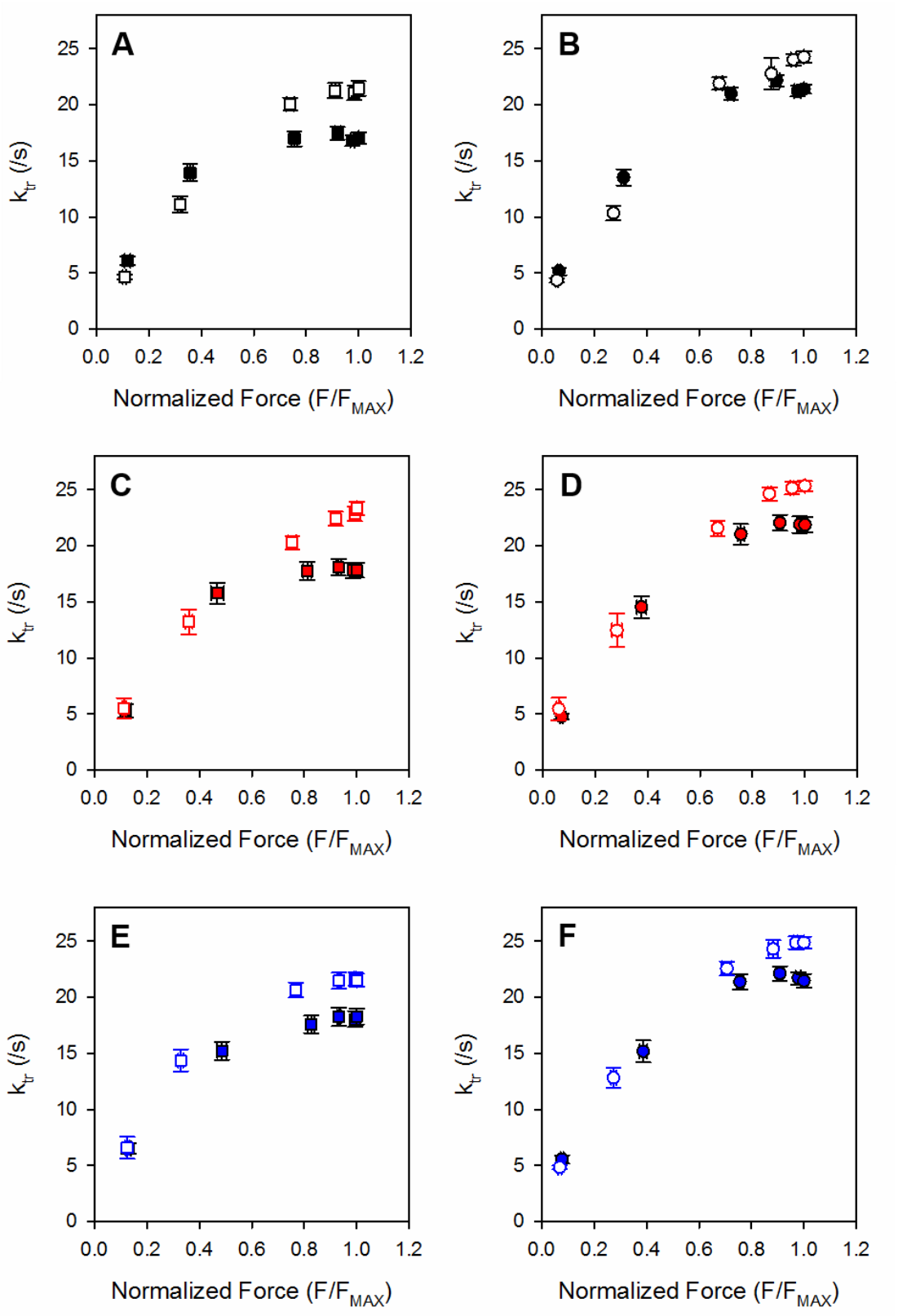


Figure 3-17 - Rates of tension redevelopment following rapid slackening and re-stretching at long (A, C, E) and short (B, D, F) sarcomere lengths before (solid) and after (open) treatment with protein kinase A. The effect of PKA was broadly similar in each genotype group, though the shift due to PKA was larger at sub-maximal Ca^{2+} in mutant groups.

A direct comparison of tension redevelopment rates between genotype groups after PKA treatment is shown in Figure 3-18. A significant genotype effect was observed at pCa 6.0 at SL 2.3 µm by 1-way ANOVA. No other significant differences were detected.

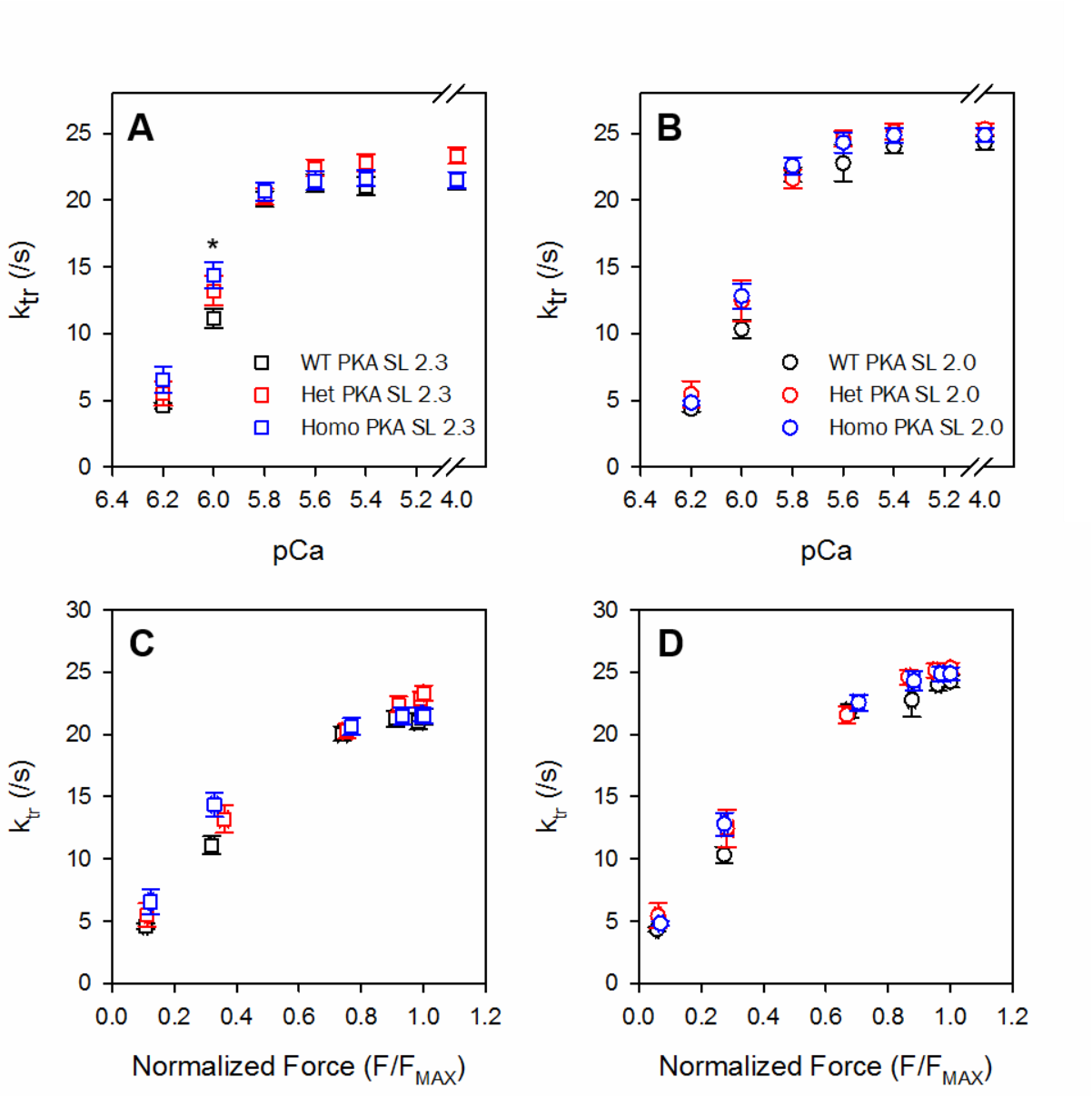


Figure 3-18 - Rates of tension redevelopment (k_{tr}) vs pCa (A, B) and normalized force (C, D) at sarcomere lengths 2.3 and 2.0 µm after PKA treatment. 1-way ANOVA indicated a significant genotype-dependent increase in k_{tr} at pCa 6.0 at sarcomere length 2.3 µm.

3.5 Discussion

In this chapter, the biomechanical function of demembranated cardiac fibres from a gene-targeted knock-in mouse model of PRKAG2 cardiomyopathy was assessed. Compared to samples from WT animals, samples from mutant animals exhibited:

i. Increased basal AMPK activity. Reduced γ2-specific responsiveness to energetic stimuli (AMP) but no difference in intact cardiomyocyte ACC S79 phosphorylation following AICAR treatment.
ii. Increased Ca^{2+} sensitivity of activation. A 10 % decrease in EC_{50} was observed at long sarcomere length in fibres from homozygous animals. The resulting 35 % increase in force production at 1 µM Ca^{2+} is highly relevant to *in vivo* function and could be a plausible explanation for impaired relaxation in the whole heart.
iii. A greater response to PKA stimulation. Following PKA treatment, no difference in Ca^{2+} sensitivity was observed between genotype groups, suggesting that the initial divergence may have been caused by altered phosphorylation of PKA target sites within the sarcomere.
iv. Mildly increased sarcomere length dependence of activation. Following PKA treatment, this genotype effect was eliminated.
v. No change in cooperativity of activation, maximum force production, or passive stiffness.
vi. Reduced maximal tension redevelopment rates and increased sub-maximal (pCa 6.0) tension redevelopment rates. PKA treatment normalized the difference in maximal rates but did not alter the difference in sub-maximal rates.

The findings of particular interest are discussed in greater detail below.

3.5.1 Fundamental effect of R299Q γ2 mutation on AMPK activity

Results presented in this chapter suggest a ~1.5-2 fold increase in basal AMPK activity in homozygous knock-in AMPK R299Q γ2 mice. As AMPK is presumed to be activated by AMP/ADP only during acute energetic stress [Coven *et al.*, 2003; Arad *et al.*, 2007], the basal increase in activity is likely to be the fundamental cause of the phenotype. These results correspond well with findings from other mouse models of PRKAG2 cardiomyopathy.

Mutations causing PRKAG2 cardiomyopathy generally occur within, or near, regions encoding the nucleotide-binding CBS domains (Figure 3-19). As these locations are responsible for AMPK's energy-sensing capacity, the mutations are suspected to alter AMPK activity. The net effect of the mutations on AMPK activity is not inherently clear, however, given that ATP-binding inhibits AMPK activity whereas AMP/ADP-binding promotes AMPK activity.

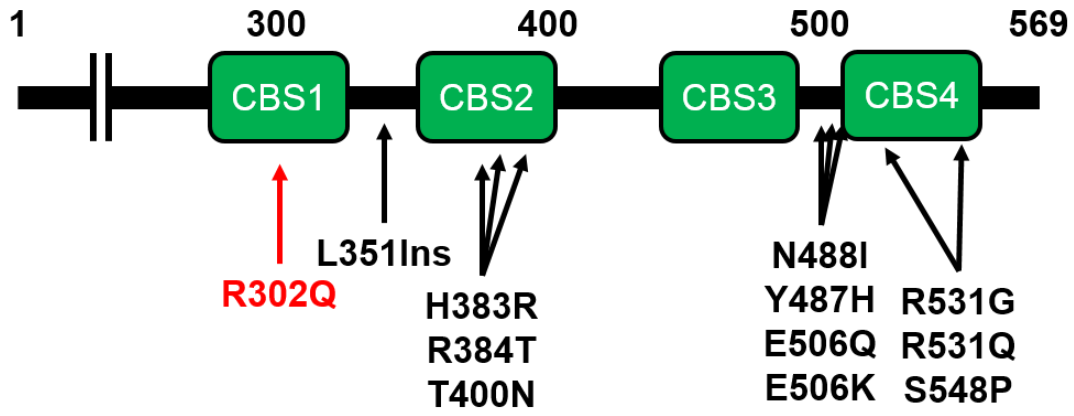


Figure 3-19 – Illustration of locations of PRKAG2 cardiomyopathy-causing mutations within the *PRKAG2* gene. Figure based on Akman, H. et al [Akman *et al.*, 2007] figure 4 with updated mutations.

In vitro analyses of these mutations on AMPK activity have been conducted by multiple groups, though studies have not yielded consistent results [Daniel and Carling, 2002; Scott *et al.*, 2004; Burwinkel *et al.*, 2005]. Using CCL13 cells, no

difference in AMPK activity was determined between WT and mutant γ2 AMPK complexes, though mutant complexes exhibited a reduced response to AMP stimulation [Daniel and Carling, 2002; Scott *et al.*, 2004]. However, in HEK293 cells, a 3.5 fold increase in AMPK activity was associated with the disease-causing R531Q mutation [Burwinkel *et al.*, 2005]. As identified by the authors of this study, the critical difference between CCL13 and HEK293 cells is that CCL13 cells lack the essential AMPK-activating kinase, LKB1. It is therefore likely that, in the presence of sufficient LKB1, PRKAG2 cardiomyopathy-causing mutations cause increased basal AMPK activity (due to impaired ATP binding) but reduced stimulated activity (due to impaired AMP/ADP binding).

Results in murine models of PRKAG2 cardiomyopathy have also not sufficiently clarified the immediate effect of mutations on AMPK activity. Overexpressing transgenic animals possessing the N488I mutation exhibited increased basal AMPK activity [Arad *et al.*, 2003], whereas animals overexpressing the R302Q [Sidhu *et al.*, 2005] and R531G [Davies *et al.*, 2006] mutations exhibited reduced AMPK activity. These seemingly disparate results may be brought into agreement by the finding of a biphasic effect on AMPK activity in a model possessing the T400N *PRKAG2* mutation [Banerjee *et al.*, 2007]. Specifically, at an early age, mutant animals exhibited increased AMPK activity compared to WT controls. At later time points, AMPK activity in mutant animals was either depressed or equivalent to controls. These animals also exhibited florid glycogen accumulation over time, and AMPK activity was shown to be inversely correlated to glycogen content (potentially via an interaction between glycogen and the AMPK β subunit). As glycogen content was markedly increased in the overexpressing R302Q and R531G models, negative regulation of AMPK activity by glycogen may explain the reduced overall activity.

Therefore, in the absence of glycogen accumulation and at early time points, it is likely that PRKAG2 cardiomyopathy-causing mutations cause increased basal AMPK activity. Further, because γ2 is a minority cardiac isoform, accounting for < 20 % of total AMPK γ subunits [Cheung *et al.*, 2000], it is unlikely that mutations causing reduced activity would be sufficient to cause severe dysfunction. This reasoning, combined with evidence from *in vitro* and *ex vivo* assessments, suggest that γ2 mutations result in an abnormal gain-of-function at baseline.

As the measurements reported in this chapter were made on cardiomyocytes isolated from animals with no significant glycogen accumulation at a young age, the increase in basal AMPK activity matches the established paradigm of PRKAG2 cardiomyopathy-causing mutations. However, the equivalent ACC S79 phosphorylation in WT and Homozygous groups following AICAR treatment is perhaps unexpected given previously observed reduced responsiveness to AMP-activation in other models of PRKAG2 cardiomyopathy. A number of plausible mechanisms could explain this finding. First, the AICAR treatment would be expected to activate AMPK complexes containing γ1 subunits, which make up ~80 % of cardiac AMPK [Cheung *et al.*, 2000]. Despite reduced activation of AMPK complexes containing γ2 subunits, the functional γ1 subunits may be sufficient to yield a complete response. This compensation is likely to be significantly altered in mouse models overexpressing AMPK γ2. Further, AICAR treatment could have partially activated γ2 subunits via the unaltered CBS domain 3. Finally, the R299Q mutation may not completely abolish AMP/ZMP binding to γ2 CBS domain 1, allowing a sufficient AICAR treatment to fully activate the complex.

3.5.2 Consequences of increased myofilament Ca^{2+} sensitivity

The direct effect of increased myofilament Ca^{2+} sensitivity is higher levels of cross-bridge binding and force production throughout the Ca^{2+} release/reuptake cycle [Gordon *et al.*, 2000]. Furthermore, there are important downstream implications of this sensitization. A variety of secondary and compensatory symptoms, some of which are exhibited in PRKAG2 cardiomyopathy, have been associated with Ca^{2+} sensitization. Foremost among these effects is an increased prevalence of arrhythmias [Arad *et al.*, 2007].

The causative mechanism between sarcomeric Ca^{2+} sensitization and arrhythmias was described recently using murine models of HCM (TnT-I79N, TnT-F110I, TnT-R278C) [Baudenbacher *et al.*, 2008; Schober *et al.*, 2012]. These works demonstrated that increased myofilament Ca^{2+} sensitivity results in higher cytosolic Ca^{2+} buffering, leading to prolonged Ca^{2+} transients. Further, after a pause, mutant cardiomyocytes released a greater amount of Ca^{2+} from the sarcomeres and triggered early afterdepolarizations and arrhythmia susceptibility. Ultimately, the Ca^{2+} sensitizing effect of various TnT mutants was shown to be directly proportional to the risk of ventricular tachycardia. This effect was recapitulated by the Ca^{2+} sensitizing molecule EMD 57033 and prevented by the Ca^{2+} desensitizing molecule blebbistatin, supporting the hypothesis that the arrhythmogenicity was driven by sarcomeric Ca^{2+} sensitivity and not an alternative effect of the TnT mutations.

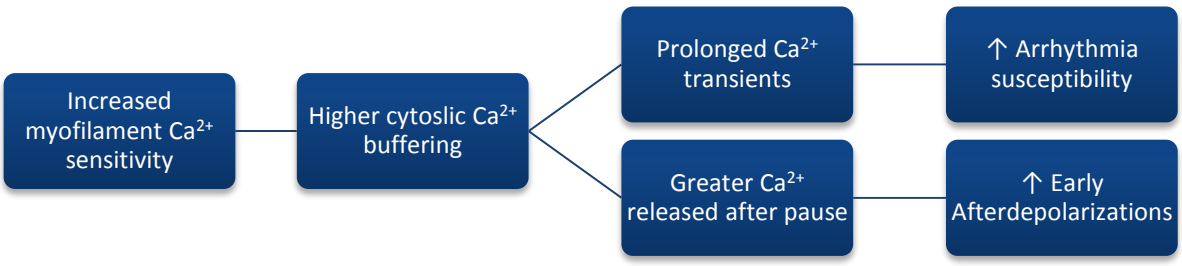


Figure 3-20 - Schematic representation of mechanism linking sarcomeric Ca^{2+} sensitization and arrhythmia propensity [Baudenbacher *et al.*, 2008; Schober *et al.*, 2012].

3.5.3 Cause of increased myofilament Ca^{2+} sensitivity

The level of Ca^{2+} sensitization observed in the R299Q mice is seen in a variety of well-studied disease states and can be caused by distinct mechanisms. For example, in end-stage heart failure, Ca^{2+} sensitivity of activation is increased due to reduced TnI phosphorylation [van der Velden *et al.*, 2003]. In inherited cardiomyopathies, mutations to regulatory proteins directly alter thin filament Ca^{2+} binding [Robinson *et al.*, 2007]. However, in this model of PRKAG2 cardiomyopathy, the mechanism leading from increased basal AMPK activity to increased sarcomeric Ca^{2+} sensitivity is not directly implied. Without a sarcomeric mutation to directly induce sensitization, the explanation must be secondary or compensatory. To elucidate this pathway, assessment of biochemical changes to the myofilament regulatory proteins was conducted. The results of these experiments are presented in Chapter 5.

3.5.4 Implications of a heightened response to PKA

Broadly, the effect of PKA treatment on myofilament function was as previously described – desensitization of the myofilament to Ca^{2+} and enhancement of maximum cross-bridge cycling rates [Stelzer *et al.*, 2007]. However, the magnitude of Ca^{2+} desensitization following PKA treatment was significantly larger in fibres from mutant animals. This result indicates that mutant fibres were either more

responsive to PKA treatment or had a lower level of basal PKA phosphorylation. Given that post-PKA Ca^{2+} sensitivity was similar across genotype groups, it is likely that basal PKA phosphorylation was lower in mutant fibres. In addition, these data suggest that AMPK-dependent phosphorylation of cTnI S150 does not contribute significantly to differing Ca^{2+} sensitivity in the mutant animals. Only the remaining small difference in Ca^{2+} sensitivity after PKA treatment could be explained by increased cTnI S150 phosphorylation in mutant fibres.

These data suggest that a reduction in PKA phosphorylation causes increased myofilament Ca^{2+} sensitivity in mutant animals. This mechanism has been implicated in other forms of heart muscle disease. In patient samples of end stage heart failure, an increased percentage of unphosphorylated cTnI was associated with increased Ca^{2+} sensitivity [van der Velden *et al.*, 2003]. The same was found in patients with dilated cardiomyopathy [Zakhary *et al.*, 1999]. In cardiomyocytes isolated from myectomy samples of patients with HCM, increased basal Ca^{2+} sensitivity compared to healthy controls was largely normalized by treating the cells with activated PKA (Figure 3-21) [Sequeira *et al.*, 2013]. Thus, the mechanism leading to increased Ca^{2+} sensitivity in this model of PRKAG2 cardiomyopathy may be shared across a variety of other conditions.

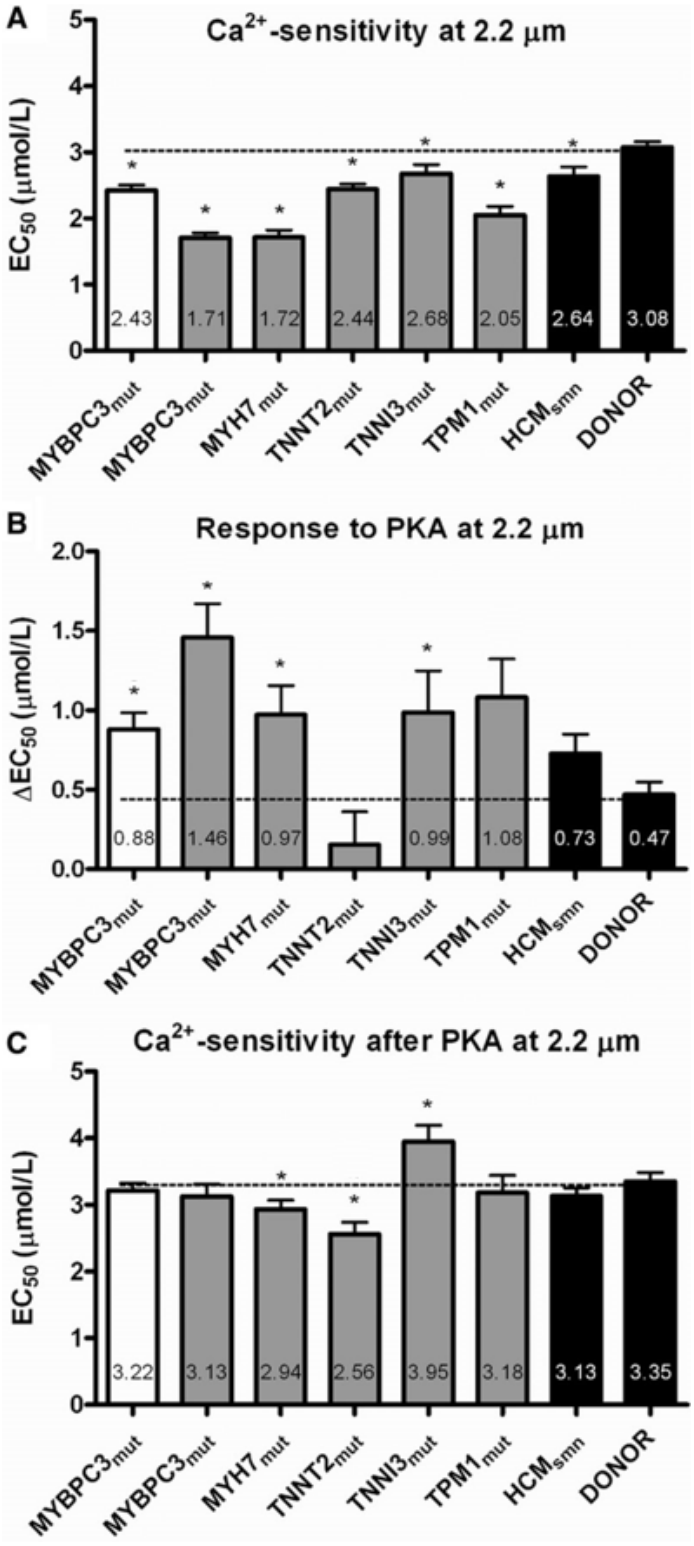


Figure 3-21 – EC_{50} values of demembranated cardiomyocytes from HCM patients and WT controls before (A) and after (C) PKA treatment. Pairwise differences in EC_{50} are also given (B). Ca^{2+} sensitivity was significantly higher in all HCM groups compared to donors before PKA treatment. PKA treatment had a significantly larger effect on Ca^{2+} sensitivity in most HCM groups. After PKA treatment, Ca^{2+} sensitivity in all but two HCM groups was equal or lower than in controls. *'s indicate $p < 0.05$ compared to donor. Adapted from Sequeira et al. Figure 1 [Sequeira *et al.*, 2013].

3.5.5 Altered sarcomere length dependence

As described in section 1.1.4, the Frank-Starling Law of the Heart describes the proportionality of ventricular preload and cardiac output partially responsible for autonomous beat-to-beat regulation of contractility. This property is at least partially due to length dependent activation (LDA) within the ventricular muscle. However, despite the essential contribution of LDA to overall cardiac function, and its relatively obvious experimental presentation, a clear understanding of the molecular mechanisms underlying the property has yet to be established.

The most commonly asserted basis for LDA within striated muscle is inter-filament spacing [Konhilas *et al.*, 2002]. Specifically, the pseudo-isovolumetric nature of cardiac myofilaments causes an inverse relationship between sarcomere length and the distance between thick and thin filaments (Figure 3-22). Closer proximity between filaments increases the probability of cross-bridge formation, resulting in greater force production at all levels of Ca^{2+}. The strongest support for this theory comes from experiments in which high-molecular-weight molecules (e.g. dextran), which cannot enter the sarcomere and instead compress the structure, were shown to increase Ca^{2+} sensitivity and force production [McDonald and Moss, 1995]. Taking this experiment further, LDA was shown to be eliminated by maintaining fibre diameter at every SL using varying concentrations of dextran [Fuchs and Smith, 2001]. These experiments suggest that inter-filament spacing is an essential determinant of LDA within striated muscle.

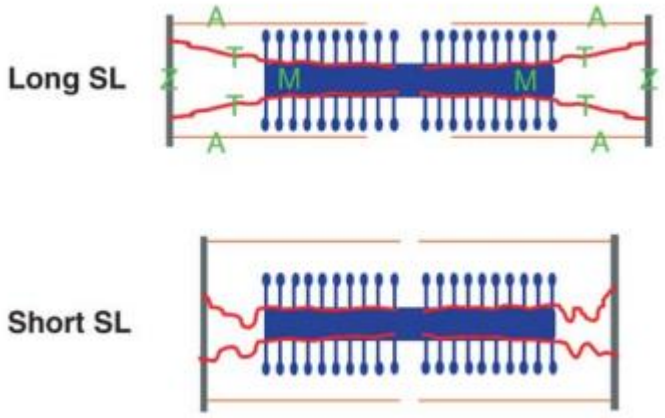


Figure 3-22 – Illustration of the variability of inter-filament spacing due to sarcomere length. At longer sarcomere lengths, the distance between thick and thin filaments is reduced, promoting cross-bridge formation. Figure from Konhilas, J. et al [Konhilas *et al.*, 2002] figure 2.

However, this proposed mechanism cannot account for the significant difference in LDA between skeletal and cardiac muscles. Specifically, despite sharing sarcomeric structure and therefore dependence on inter-filament spacing, cardiac muscle exhibits a much steeper dependence of force development and Ca^{2+} sensitivity on sarcomere length [Moss *et al.*, 2004]. It is therefore likely that regulatory proteins, of which differing isoforms are expressed in skeletal and cardiac muscle, contribute to LDA [Solaro, 2007]. This hypothesis was supported by the finding that exchanging cardiac TnI with slow skeletal TnI in demembranated cardiac muscle results in a significant reduction in LDA [Konhilas *et al.*, 2003]. Further, selective removal or altered mechanical strain of titin was shown to reduce LDA [Cazorla *et al.*, 2001]. Finally, PKA treatment was shown to increase inter-filament spacing and LDA [Konhilas *et al.*, 2003]. Thus, it is likely that interactions between sarcomeric regulatory proteins also contribute to LDA.

In this chapter, the R299Q γ2 mutation was shown to cause a mild increase in sarcomere length dependence of Ca^{2+} sensitivity. As the effect of inter-filament spacing on LDA is unlikely to be affected by the mutation, these results suggest that regulation of LDA in the R299Q γ2 mice is altered due to changes to sarcomeric regulatory proteins. However, the difference in LDA was eliminated following PKA treatment. As the overall difference in Ca^{2+} sensitivity was also negated by PKA treatment, both results suggest differing levels of PKA phosphorylation in the R299Q γ2 mice.

3.5.6 Conclusions

On the whole, myofilament function in fibres from heterozygous and homozygous mice was mildly altered compared to that in WT counterparts. Of particular interest was the finding that mutant fibres exhibited increased Ca^{2+} sensitivity at baseline, but no difference in Ca^{2+} sensitivity following PKA treatment. These results suggest that reduced phosphorylation of PKA target sites causes altered myofilament in our murine model of PRKAG2 cardiomyopathy. A simplified pathway between this Ca^{2+} sensitization and *in vivo* dysfunction has also been described. However, the reductionist experiments presented in this chapter only probed cardiac myofilament function and could ignore fundamental alterations, or compensatory changes, to Ca^{2+} handling and excitation-contraction coupling mechanisms. Therefore, to expand and clarify the mechanism behind dysfunction in the R299Q γ2 mice, it was desirable to explore functional changes in intact cardiomyocytes.

Chapter 4 – Characterisation of AMPK R299Q γ2 cardiac contractility and Ca^{2+} handling in intact cardiomyocytes

4.1 Specific Aims

To determine if the changes to sarcomeric function described in Chapter 3 affect contractility in living myocardium, and to investigate whether the AMPK R299Q γ2 mutation causes alteration in cardiac Ca^{2+} handling, intact cardiomyocytes from WT and mutant animals were studied. These cells were incubated in a fluorescent Ca^{2+} indicator to allow simultaneous measurement of intracellular Ca^{2+} concentration and cellular shortening. In addition, pharmacological treatments were applied to the cells to assess potentially altered responses to physiological challenges. Specifically, experiments in this chapter characterized the following parameters in cardiomyocytes from mutant animals and WT controls:

I. Baseline cardiomyocyte shortening and Ca^{2+} transients
II. Frequency dependence of contractility
III. Sarcoplasmic reticulum load
IV. Sodium calcium exchanger and SERCA activities
V. Responsiveness to β-adrenergic stimulation
VI. Responsiveness to energetic stress

Cardiomyocytes from all three genotype groups (WT, heterozygous, homozygous) were assessed. In general, a dose response to the R299Q γ2 mutation in functional parameters was observed. For ease of examination and comment, only the homozygous and WT cells are illustrated in the plots in this section. Statistical significance of genotype effects is only reported if the determination was positive across all three groups.

4.2 Baseline characterization

To simultaneously investigate both cardiac contractility and Ca^{2+} handling, cardiomyocytes were isolated from WT and mutant mice and incubated in a fluorescent indicator, FURA-2-AM, whose relative excitation at 340 nm vs 380 nm is proportional to intracellular Ca^{2+} concentrations [Grynkiewicz *et al.*, 1985]. Upon pacing, sarcomere length of the cells was monitored concurrently with the FURA-2-AM 340/380 ratio. The cells were paced at 1, 3, and 6 Hz and shortening and Ca^{2+} flux traces for each cell at each stimulation frequency were calculated. Comparison of these traces between WT and homozygous groups are shown in Figure 4-1. Across all frequencies, but to different extents, traces from homozygous cells were slowed compared to their WT counterparts. Changes in the magnitudes of shortening and Ca^{2+} flux were not consistently different between WT and homozygous groups across the stimulation frequencies.

Shortening and Ca^{2+} handling traces were fit and quantified to allow statistical comparison between groups. The calculated parameters were: baseline sarcomere length, diastolic Ca^{2+} concentration, fractional shortening, Ca^{2+} transient magnitude, time to 50 % contraction/relaxation, and time to 50 % Ca^{2+} release/reuptake. At 1 Hz stimulation, little difference in baseline sarcomere length was seen between groups (Figure 4-A). However, as stimulation frequency increased, baseline sarcomere length in WT cells decreased faster than that in homozygous cells. This resulted in a significantly higher basal sarcomere length in cells from homozygous animals at 6 Hz stimulation. This difference in basal sarcomere length was not associated with a difference in baseline Ca^{2+} at any stimulation frequency (Figure 4-B). The magnitudes of sarcomere shortening and Ca^{2+} release were also not significantly different across stimulation frequencies (Figure 4-, C & D).

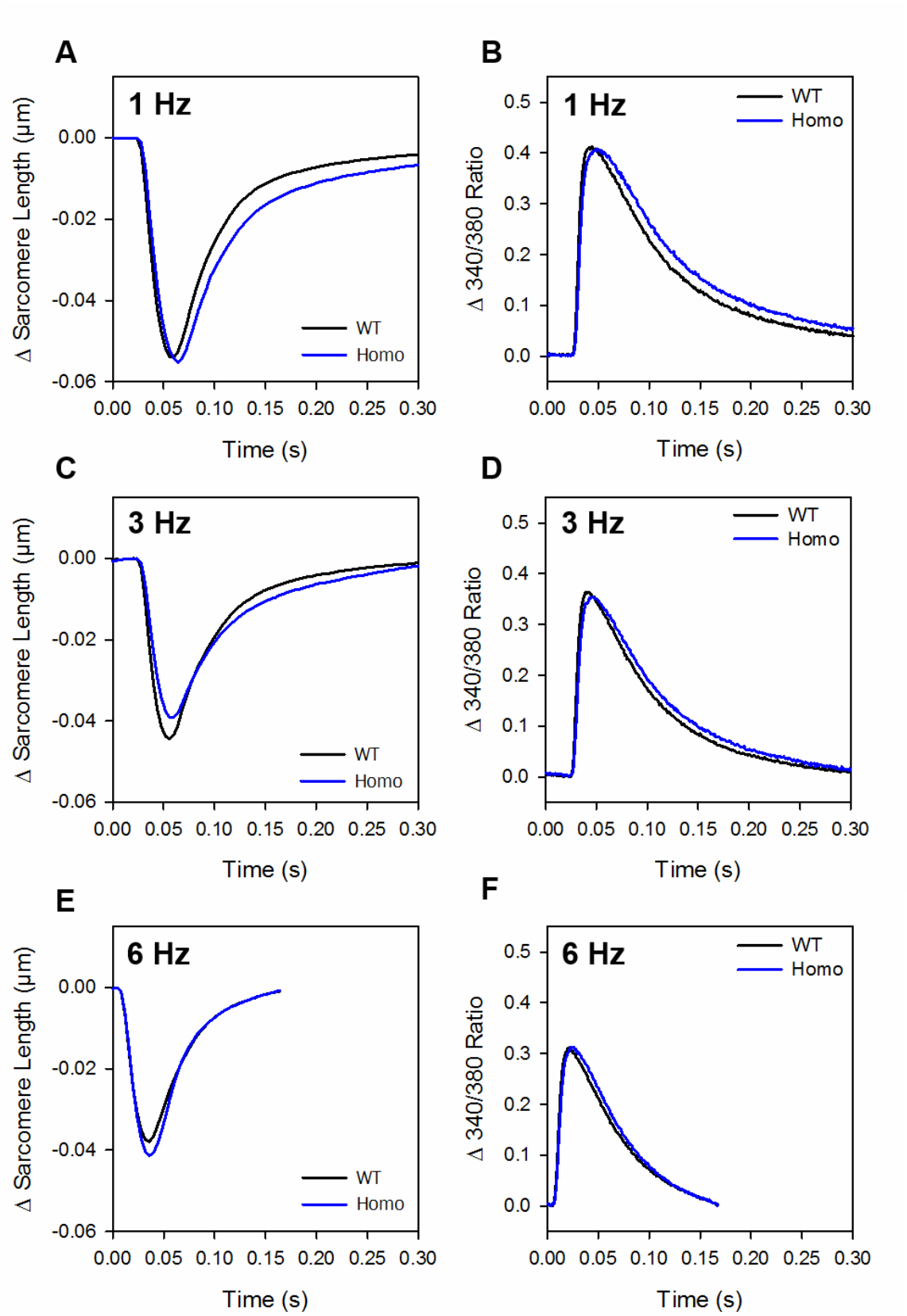


Figure 4-1 – Average normalized sarcomere length shortening and Ca^{2+} transient traces of cardiomyocytes from WT and homozygous animals at 1 Hz (A & B), 3 Hz (C & D), and 6 Hz (E & F) stimulation frequencies. 5 animals per genotype group were assessed, 15-20 cardiomyocytes per heart were measured.

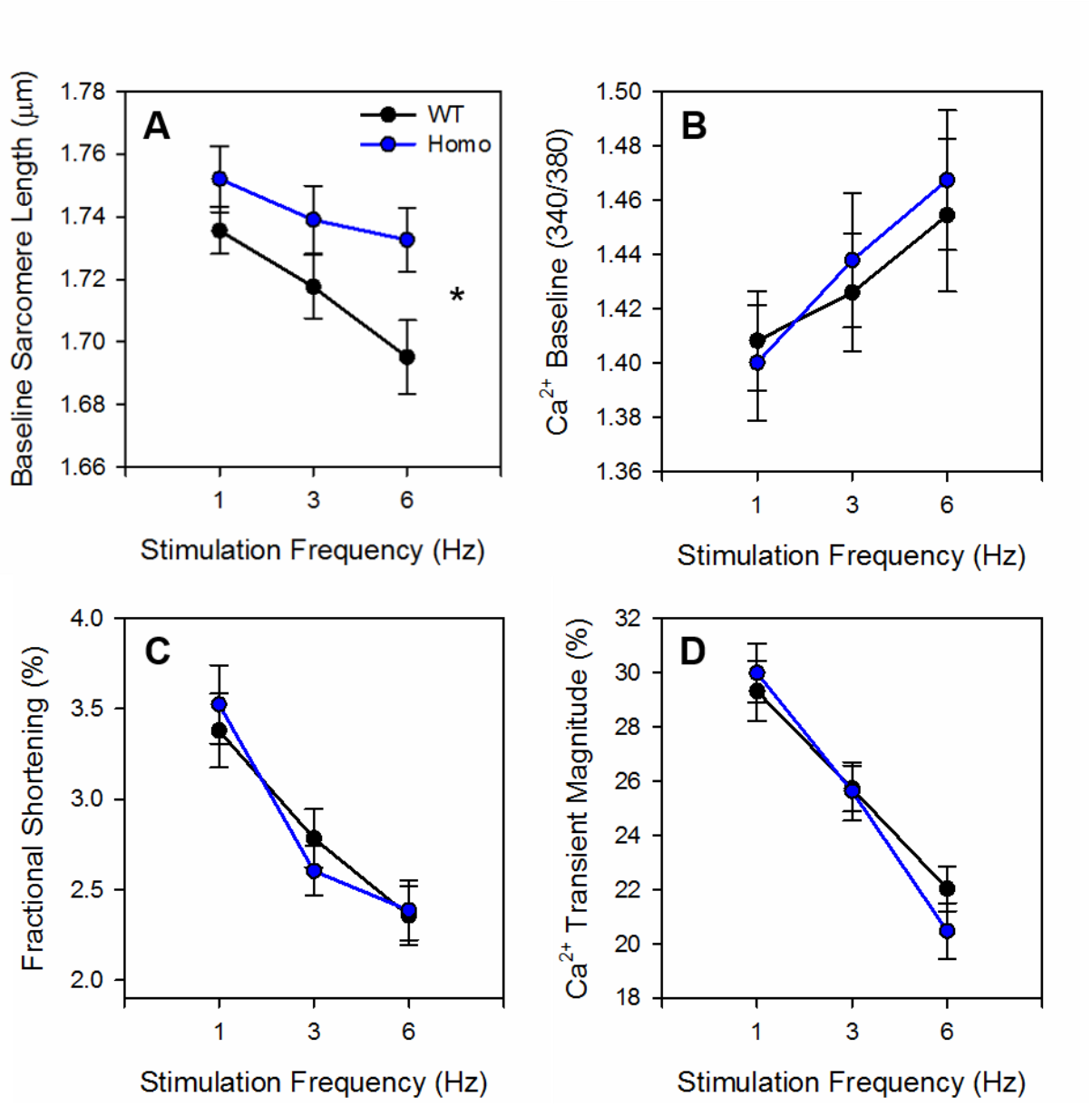


Figure 4-1 – Baseline sarcomere length (A), baseline Ca^{2+} (B), fractional shortening (C), and Ca^{2+} transient magnitude (D) of cardiomyocytes from WT and homozygous animals at all stimulation frequencies. Cells from mutant animals exhibited a mild reduction in basal sarcomere length but no significant difference in Ca^{2+} baseline. Further, no differences in the magnitudes of shortening or Ca^{2+} flux were observed. Significance of genotype effect was determined using 2-way ANOVA across all three stimulation frequencies.

Though the magnitudes of shortening and Ca^{2+} release were unchanged, the rate of these functions was significantly slower in cells from homozygous animals (Figure 4-2). Specifically, cells from homozygous mice exhibited 29 % slower contractile speeds, 16 % slower relaxation speeds, 32 % slower Ca^{2+} release speeds, and 15

% slower Ca^{2+} reuptake speeds (at 3 Hz stimulation). In most parameters, the difference between genotype groups decreased with increased stimulation frequency (Table 4-).

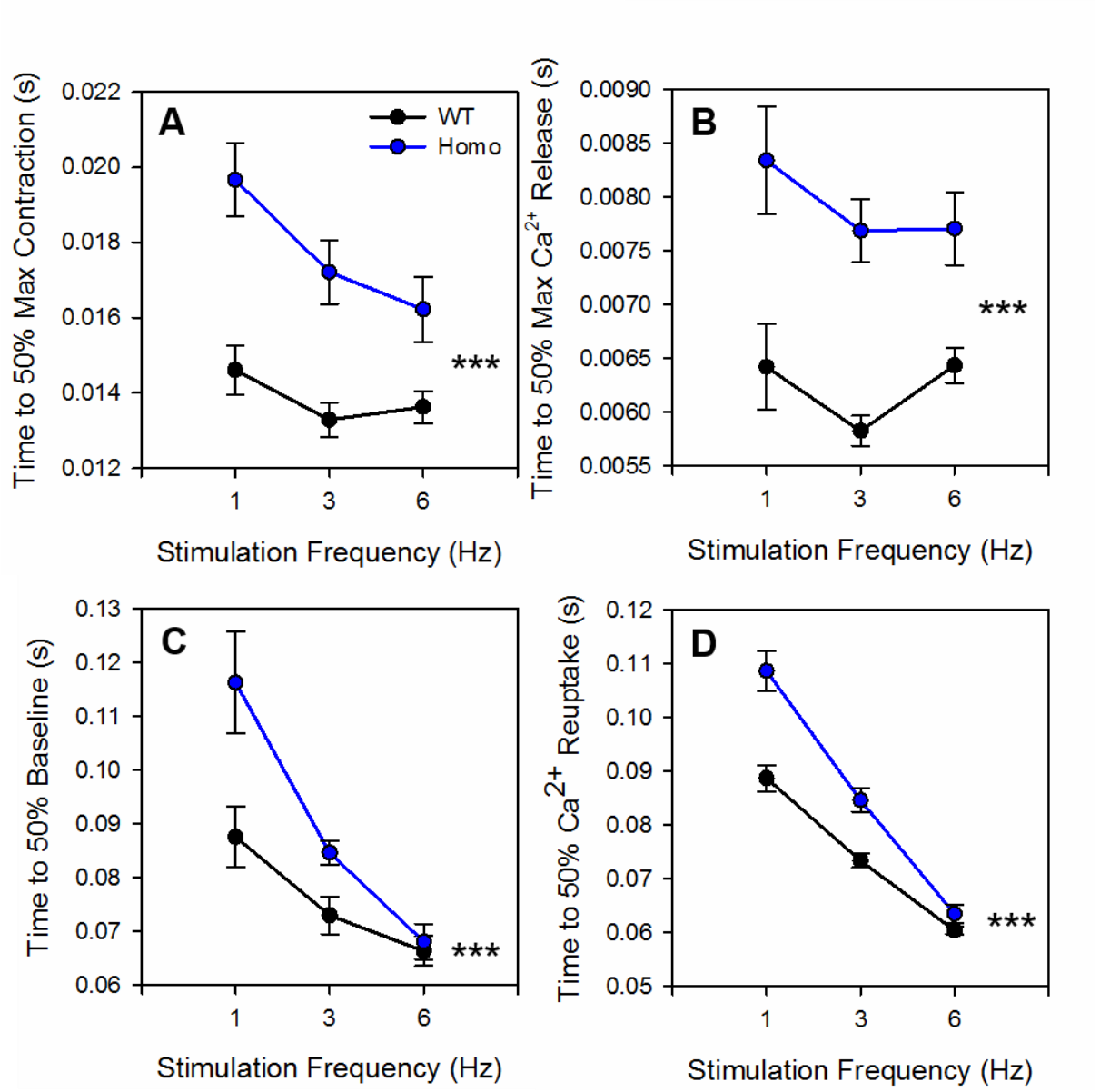


Figure 4-2 – Rates of cardiomyocyte shortening (A) and relaxation (C), and Ca^{2+} release (B) and reuptake (D) rates in cardiomyocytes from WT and homozygous animals at all stimulation frequencies. All kinetic measurements were significantly slowed in cells from mutant animals. Significance of genotype effect was determined using 2-way ANOVA across all three stimulation frequencies.

Table 4-2 – Mean (± SEM) shortening and Ca^{2+} handling kinetics of intact cardiomyocytes isolated from WT, Heterozygous, and Homozygous animals.

		WT	Het	Homo
1 Hz	n	90	82	90
	Time to 50% max contraction (s)	0.015 ± 0.001	0.017 ± 0.001	0.020 ± 0.001
	Time to 50% max [Ca^{2+}] (s)	0.088 ± 0.006	0.086 ± 0.006	0.116 ± 0.009
	Time to 50% SL relaxation (s)	0.006 ± 0.000	0.008 ± 0.001	0.008 ± 0.000
	Time to 50% baseline [Ca^{2+}] (s)	0.089 ± 0.003	0.099 ± 0.003	0.109 ± 0.004
3 Hz	n	87	83	90
	Time to 50% max contraction (s)	0.013 ± 0.000	0.014 ± 0.000	0.017 ± 0.001
	Time to 50% max [Ca^{2+}] (s)	0.073 ± 0.003	0.068 ± 0.003	0.093 ± 0.006
	Time to 50% SL relaxation (s)	0.066 ± 0.003	0.057 ± 0.002	0.064 ± 0.002
	Time to 50% baseline [Ca^{2+}] (s)	0.073 ± 0.001	0.078 ± 0.001	0.085 ± 0.002
6 Hz	n	62	65	89
	Time to 50% max contraction (s)	0.014 ± 0.000	0.014 ± 0.000	0.016 ± 0.001
	Time to 50% max [Ca^{2+}] (s)	0.066 ± 0.003	0.057 ± 0.002	0.064 ± 0.002
	Time to 50% SL relaxation (s)	0.006 ± 0.000	0.007 ± 0.000	0.008 ± 0.000
	Time to 50% baseline [Ca^{2+}] (s)	0.066 ± 0.003	0.057 ± 0.002	0.064 ± 0.002

To compare the relationship between shortening and Ca^{2+} handling, sarcomere length was plotted against FURA-2 signal over the course of one average contraction (Figure 4-3, A & B). Chronologically, these loops progress clock-wise beginning from basal sarcomere length and Ca^{2+} concentration (top-left). Increasing intracellular Ca^{2+} concentrations and sarcomeric contraction are tracked along the top of the curve, with decreasing intracellular Ca^{2+} concentrations and sarcomeric relaxation tracked along the bottom. Comparison of curve shapes is facilitated by normalizing the initiation point of these contractile loops (Figure 4-3, C & D). In these curves, chronological progression begins at the origin and proceeds counter-clockwise. In both absolute and normalized loops, a dysregulation of frequency responsiveness is apparent in cells from homozygous animals. Specifically, basal sarcomere length does not decrease correspondingly with increases in stimulation

frequency in mutant cells. Further, the magnitude of shortening in the mutant cells decreases significantly from 1 to 3 Hz, but not from 3 to 6 Hz.

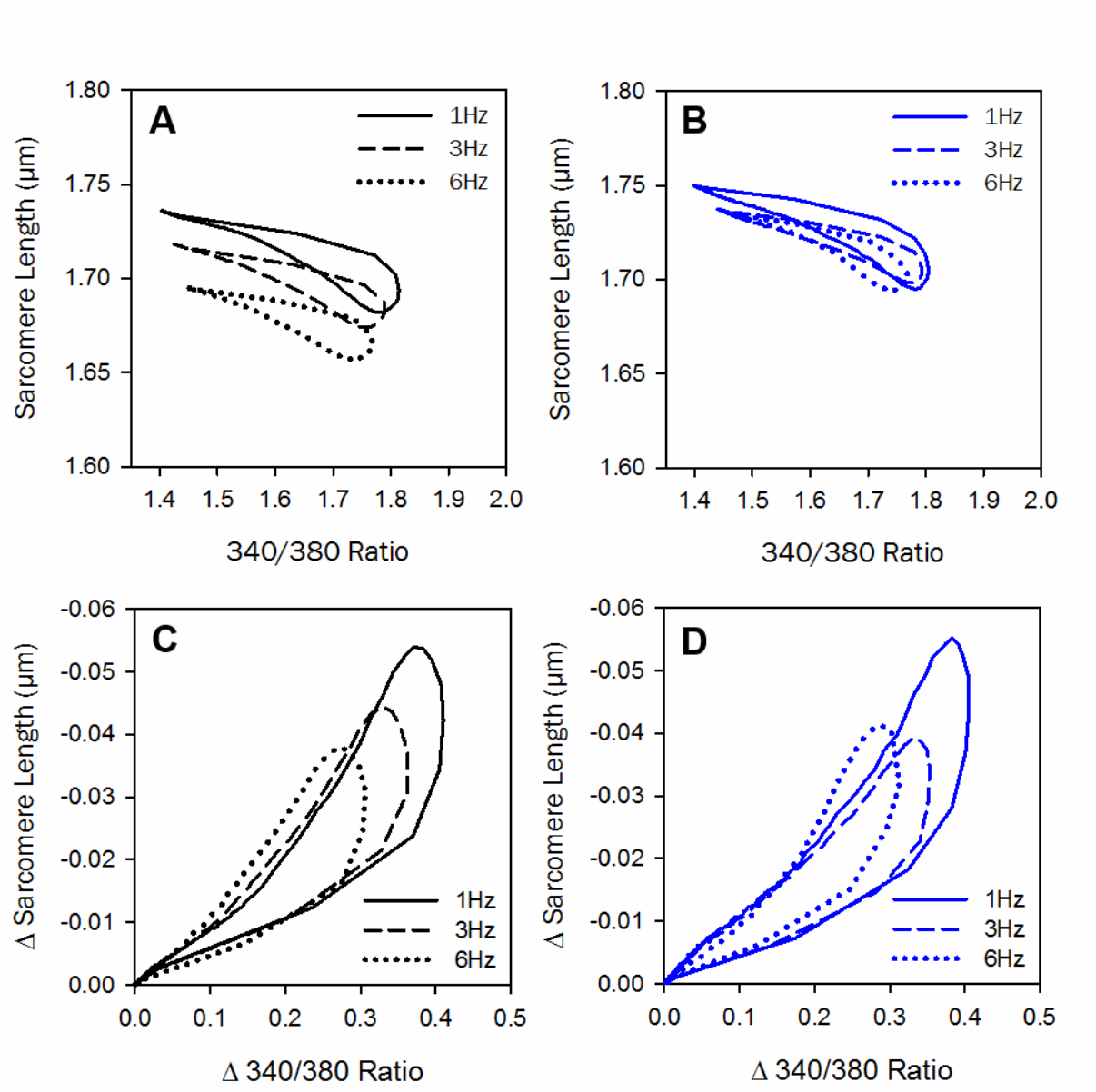


Figure 4-3 – Absolute (A & B) and normalized (C & D) shortening and Ca^{2+} transient relationships of cardiomyocytes from WT and Homozygote animals. Cells from mutant animals exhibited a smaller frequency-dependence of basal sarcomere length than cells from WT controls.

Beyond simple observation of physiological cardiomyocyte Ca^{2+} release and shortening, the isolated cells provide a platform to explore the capacity of the system under various stimuli. Of particular interest was Ca^{2+} content of the SR and activity of the essential Ca^{2+} pumps – the NCX and SERCA2. To test these parameters, cardiomyocytes were exposed to a brief spritz of perfusion solution containing 10 mM caffeine. As caffeine binds to the RyR and causes channel opening at basal intracellular [Ca^{2+}] [Rousseau *et al.*, 1988; Herrmann-Frank *et al.*, 1999], this stimulus results in the release of nearly all Ca^{2+} from the SR [Herrmann-Frank *et al.*, 1999]. Therefore, height of the FURA-2-AM signal following caffeine stimulation is proportional to the amount of Ca^{2+} in the SR (the SR load). Here, no difference in SR load was detected between cardiomyocytes from WT and mutant animals (Figure 4-4). As exposure to caffeine also results in inhibition of Ca^{2+} reuptake into the SR [Bassani, 1995], the Ca^{2+} decay rate is assumed to be due to the sum of NCX extrusion and other slow mechanisms. Again, no significant genotype-dependent difference in Ca^{2+} extrusion rate was detected. During normal pacing, the rate of Ca^{2+} re-uptake/extrusion is the sum of slow mechanisms and the activities of NCX and SERCA. Therefore, the rate of SERCA activity during normal pacing can be calculated by subtracting the rate of Ca^{2+} extrusion during caffeine stimulation [Bassani, 1995]. As total Ca^{2+} re-uptake/extrusion was slower in cells from mutant animals, and no difference in NCX + slow extrusion rates was detected, the calculated SERCA activity was found to be lower in cells from homozygous animals than from WT animals across all stimulation frequencies. The magnitude of this reduced activity was 21 % at 1 Hz, 15 % at 3 Hz, and 5 % at 6 Hz stimulation.

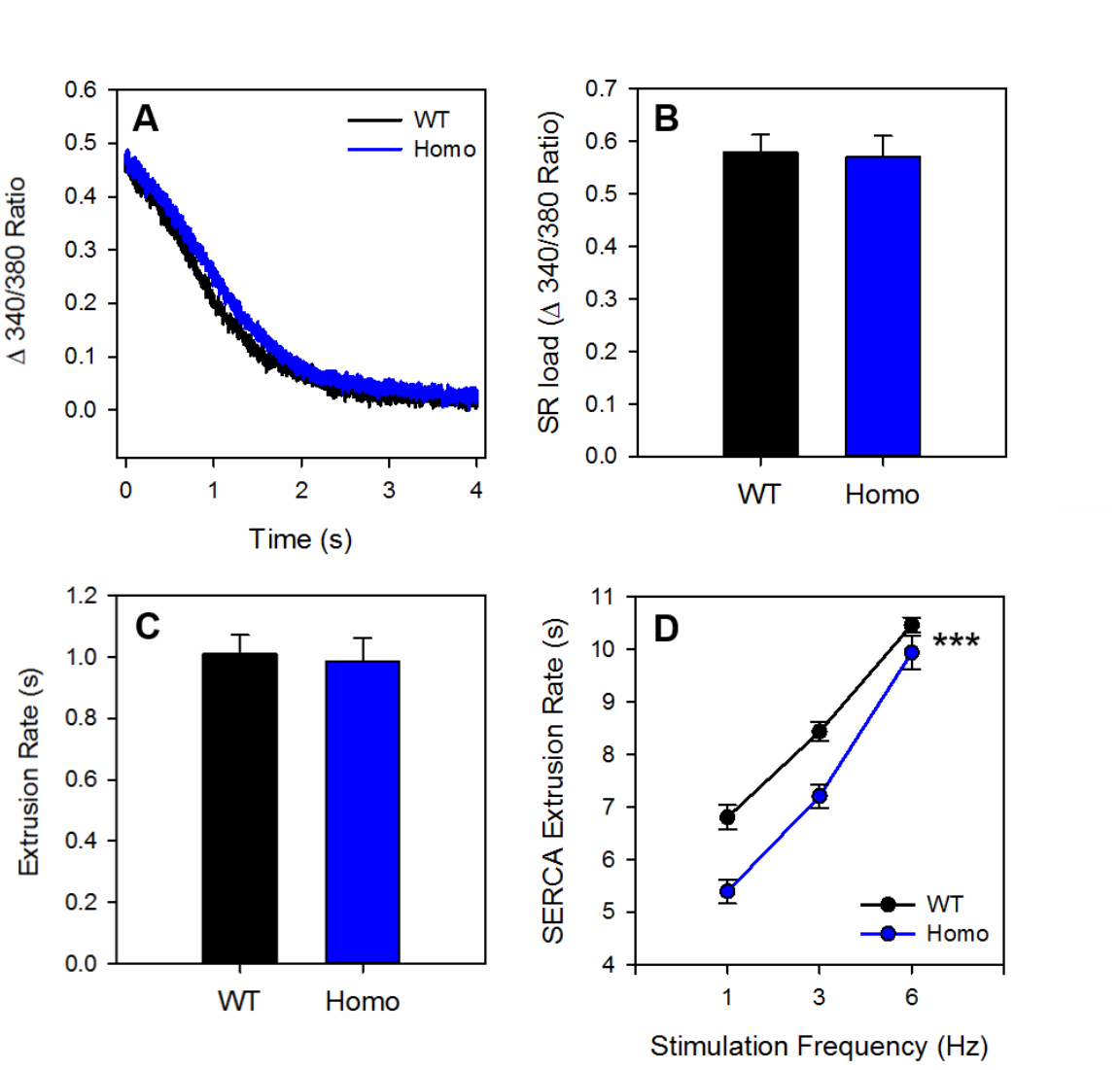


Figure 4-4 - Averaged Ca^{2+} reuptake traces following caffeine spritz (A), total sarcoplasmic reticulum load as given by the magnitude of FURA-2-AM signal rise (B), Ca^{2+} extrusion rate following caffeine spritz (C), and calculated SERCA activity at each stimulation frequency under normal pacing conditions (D) of cardiomyocytes from WT and Homozygote animals. The response to stimulation with caffeine yielded similar results in mutant and WT cells – no difference in total SR loads or extrusion rates were observed. By subtracting the total extrusion rate from total Ca^{2+} reuptake/extrusion during normal pacing conditions, a significant difference in SERCA activity was detected in mutant cells. 5 animals per group were assessed, 5-10 cells per heart were measured. Significance of genotype effect was determined using 2-way ANOVA across all three stimulation frequencies.

4.3 Response to β-adrenergic stimulation

Given the differing response to PKA treatment between genotype groups in demembranated fibres, the response to β-adrenergic stimulation was also probed in intact cardiomyocytes. Single cardiomyocytes were assessed initially in normal perfusion solution before being subjected to solution containing 10 nM isoproterenol. This methodology allowed pairwise determination of cellular response to the stimulus. In all cells, isoproterenol treatment resulted in a significant increase in the magnitude of shortening as well as rates of shortening and relaxation (Figure 4-5). However, the relative effect of treatment was not equivalent between WT and homozygous groups. Specifically, cardiomyocytes from homozygous animals exhibited approximately twice the increase in shortening (Homo: +91 %, WT: +45 %) and moderately larger reductions in relaxation time (Homo: -20 %, WT: -15 %) compared to WT cells.

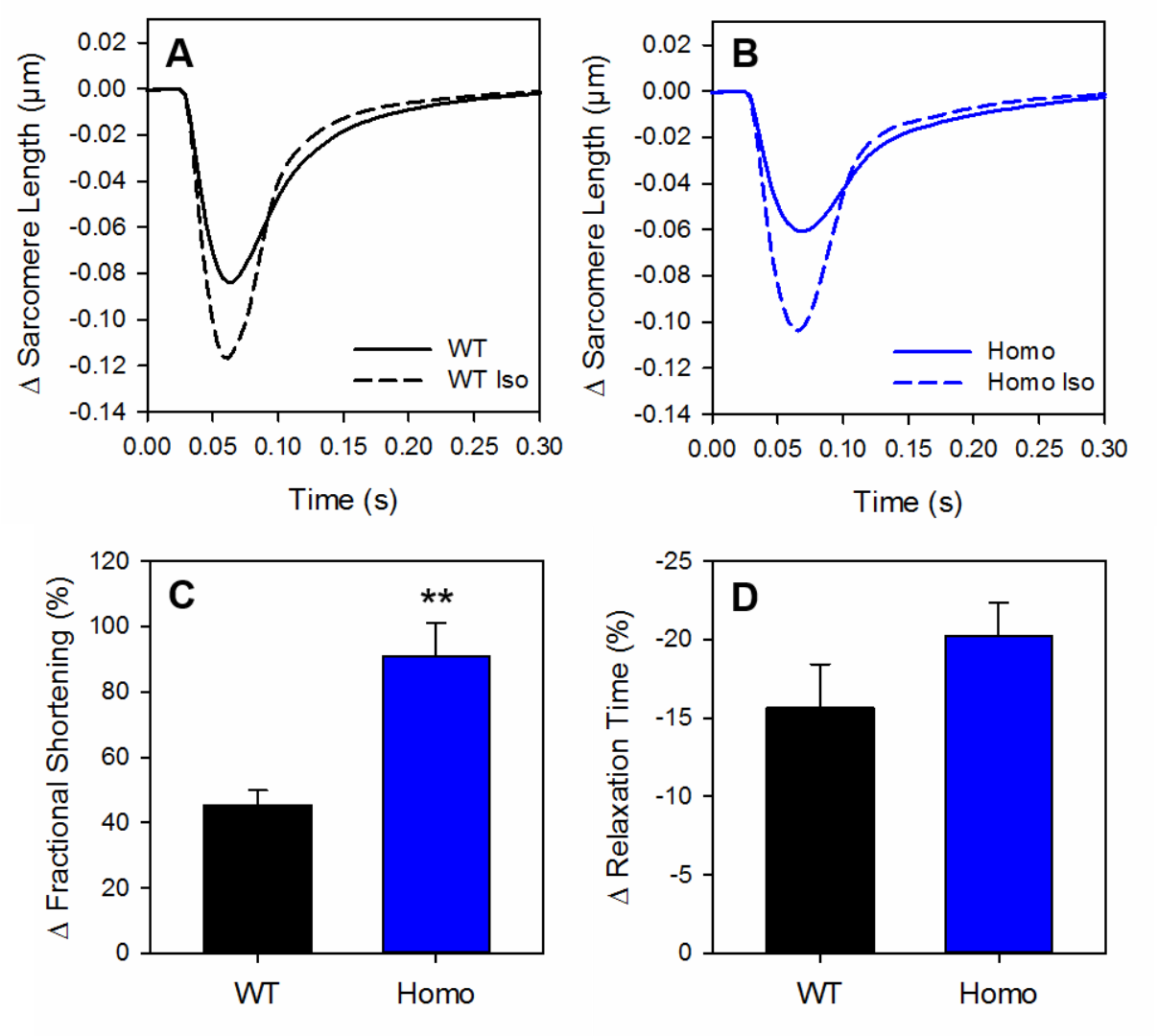


Figure 4-5 – Averaged shortening traces of cardiomyocytes from WT (A) and homozygous (B) animals before (solid) and after (dashed) treatment with 10 nM isoproterenol, percentage change in fractional shortening due to isoproterenol treatment (C), and percentage change in time to 50 % relaxation due to isoproterenol treatment (D). Cells from mutant animals exhibited an increased response to isoproterenol across most parameters, though most significantly in fractional shortening. Measurements were taken from 3 mice in each group, 10-15 cells per animal were measured. Significance of differences was determined using t-tests.

4.4 Effect of AICAR treatment

Given that the R299Q γ2 mutation being studied is located in one of the essential AMP-binding domains within the subunit, the effect of the mutation on energetic signalling was of keen interest. To investigate this, cardiomyocytes were isolated from R299Q γ2 mutant and WT animals and incubated in either normal storage

solution (control) or storage solution containing 2 mM AICAR for 15 minutes before their contractility and Ca^{2+} handling were investigated. As AICAR is metabolized to the AMP analogue ZMP upon cellular uptake, treatment with 2 mM AICAR mimics a dramatic energetic stress and is known to activate AMPK [Merrill *et al.*, 1997]. The qualitative effect of AICAR treatment was readily apparent in shortening and Ca^{2+} concentration traces (Figure 4-6). Broadly, significant impacts to fractional shortening, Ca^{2+} transient magnitude, contraction rate, and relaxation rate were observed in AICAR-treated cells. The effect of this treatment was found to be significant across all genotype groups and stimulation frequencies, though was greater in cells from WT animals.

Quantitation of the functional effect of AICAR treatment was conducted as previously described and results from WT and Homozygous cells at 3 Hz stimulation frequency are shown in Figure 4-7. AICAR treatment reduced fractional shortening (-46 % in WT, -24 % in Homo) and Ca^{2+} transient magnitudes (-46 % in WT, -48 % in Homo), while increasing times to 50 % maximal contraction (+47 % in WT, +33 % in Homo) and relaxation (+105 % in WT, +64 % in Homo). In addition, the effect of AICAR was significantly different between cells from WT and Homozygous animals (as evidenced by a significant genotype-treatment interaction effect by 2-way ANOVA) in fractional shortening, Ca^{2+} release time, and Ca^{2+} reuptake time. Specifically, cells from Homozygous animals exhibited a smaller response to AICAR treatment than WT controls in each of these three parameters.

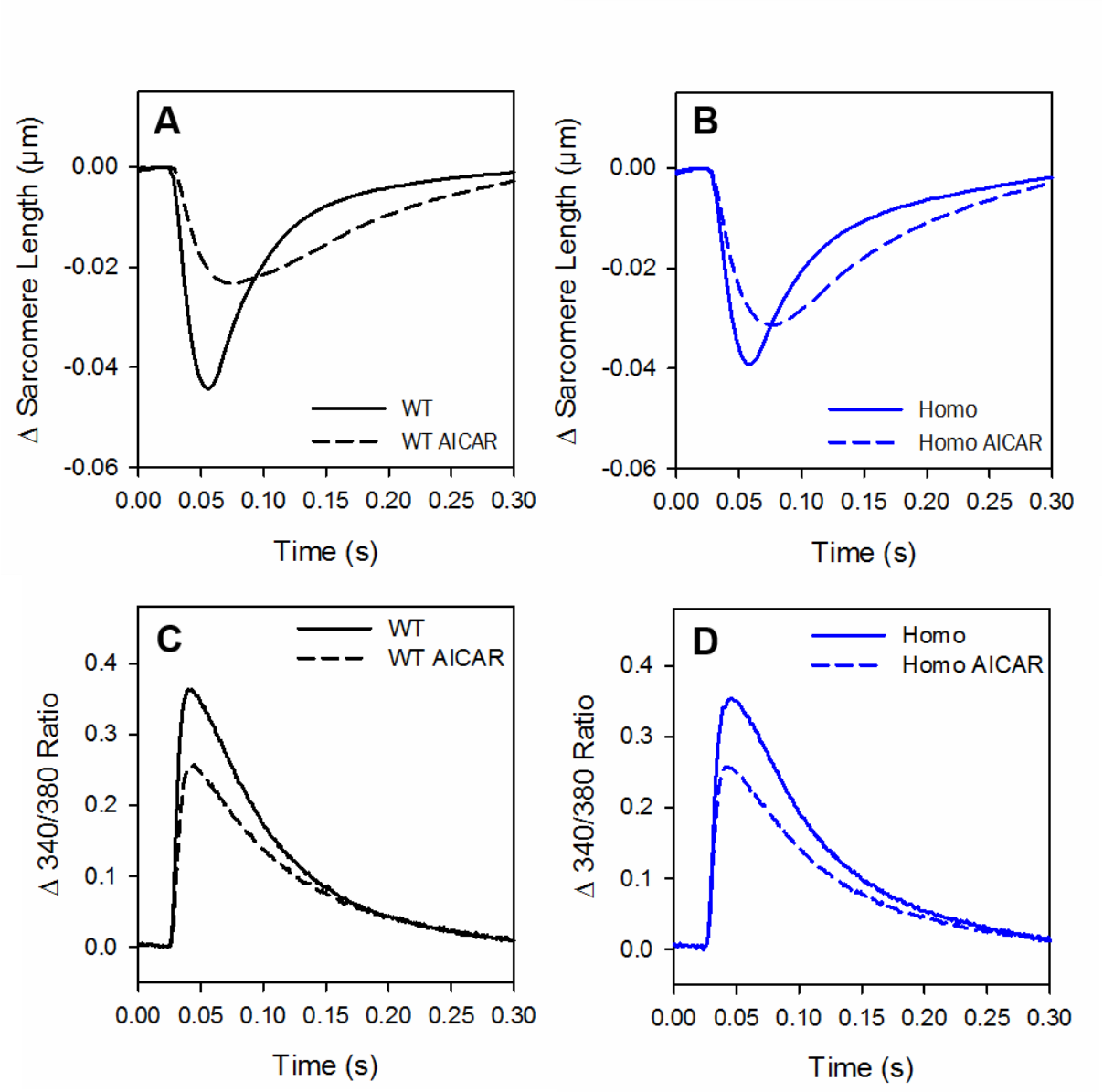


Figure 4-6 – Averaged shortening (A & B) and Ca^{2+} flux (C & D) traces at 3 Hz stimulation frequency from WT and homozygous animal cardiomyocytes with (dashed) or without (solid) a 15-minute incubation with 2 mM AICAR. This treatment significantly reduced the magnitude and rate of cardiomyocyte contractility and Ca^{2+} flux in all cells. This effect is reduced in cardiomyocytes from mutant animals. 5 animals per genotype group were assessed, 15-20 cardiomyocytes per treatment were measured.

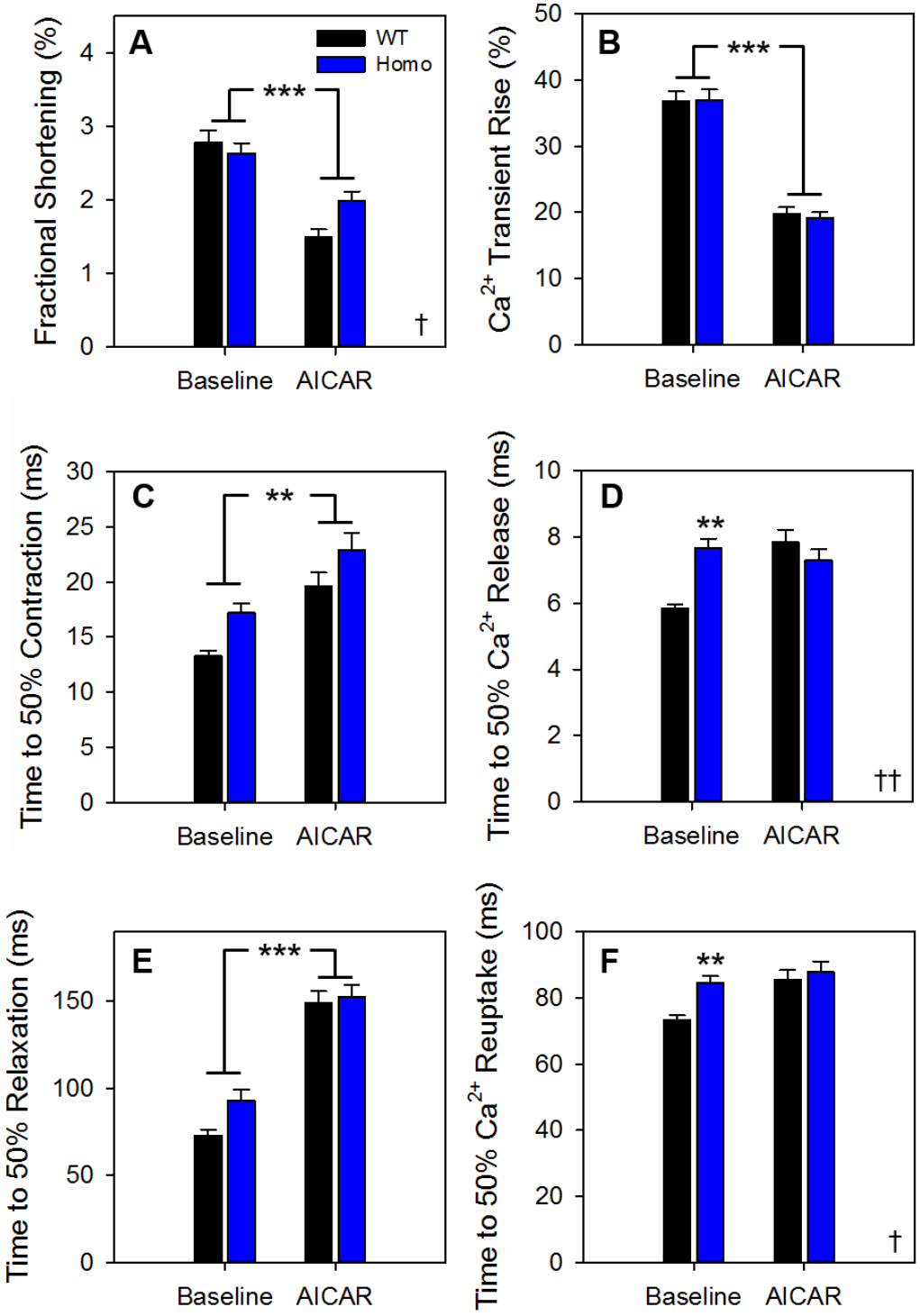


Figure 4-7 – Quantification of the effect of AICAR on cardiomyocyte fractional shortening (A), Ca^{2+} transient magnitude (B), contraction rate (C), Ca^{2+} release rate (D), relaxation rate (E), and Ca^{2+} reuptake rate (F) at 3 Hz stimulation frequency. Treatment with AICAR resulted in significantly reduced fractional shortening and Ca^{2+} transient magnitudes and significantly slowed contraction and relaxation rates. The effect of AICAR treatment was significantly different on cells from homozygous animals compared to cells from WT animals in terms of fractional shortening, Ca^{2+} release rate, and Ca^{2+} reuptake rate. Significance of differences were determined using 2-way ANOVA followed by post-hoc corrected tests.

To investigate potential differences in the relationship between contraction and Ca^{2+} release, averaged traces of the two parameters were plotted against one another (Figure 4-8, A & B). This analysis revealed reductions in sarcomere lengths and Ca^{2+} concentrations caused by AICAR treatment in both genotype groups. Normalizing the origin of contraction (Figure 4-8, C & D) demonstrated that AICAR treatment significantly reduced both contractility and Ca^{2+} release, though to a lesser extent in cardiomyocytes from Homozygous animals. Further, the contractile loop shape was altered by treatment, resulting in larger loop area. During Ca^{2+} release (bottom of absolute plots, top of normalized plots), the relationship is not significantly affected. However, during the relaxation phase (bottom of absolute plots, top of normalized plots) AICAR treatment caused a significant reduction in the slope of relaxation relative to Ca^{2+} reuptake.

To probe the effect of AICAR treatment on SR Ca^{2+} load and NCX activity, AICAR-treated cells were spritzed with caffeine and the resulting Ca^{2+} transient was recorded. Averaged Ca^{2+} release traces and quantification of release magnitude and reuptake rates are shown in Figure 4-9. AICAR treatment caused a significant reduction in SR load and increase in Ca^{2+} extrusion in cardiomyocytes from WT animals but had no significant effect on either parameter in cells from Homozygous animals.

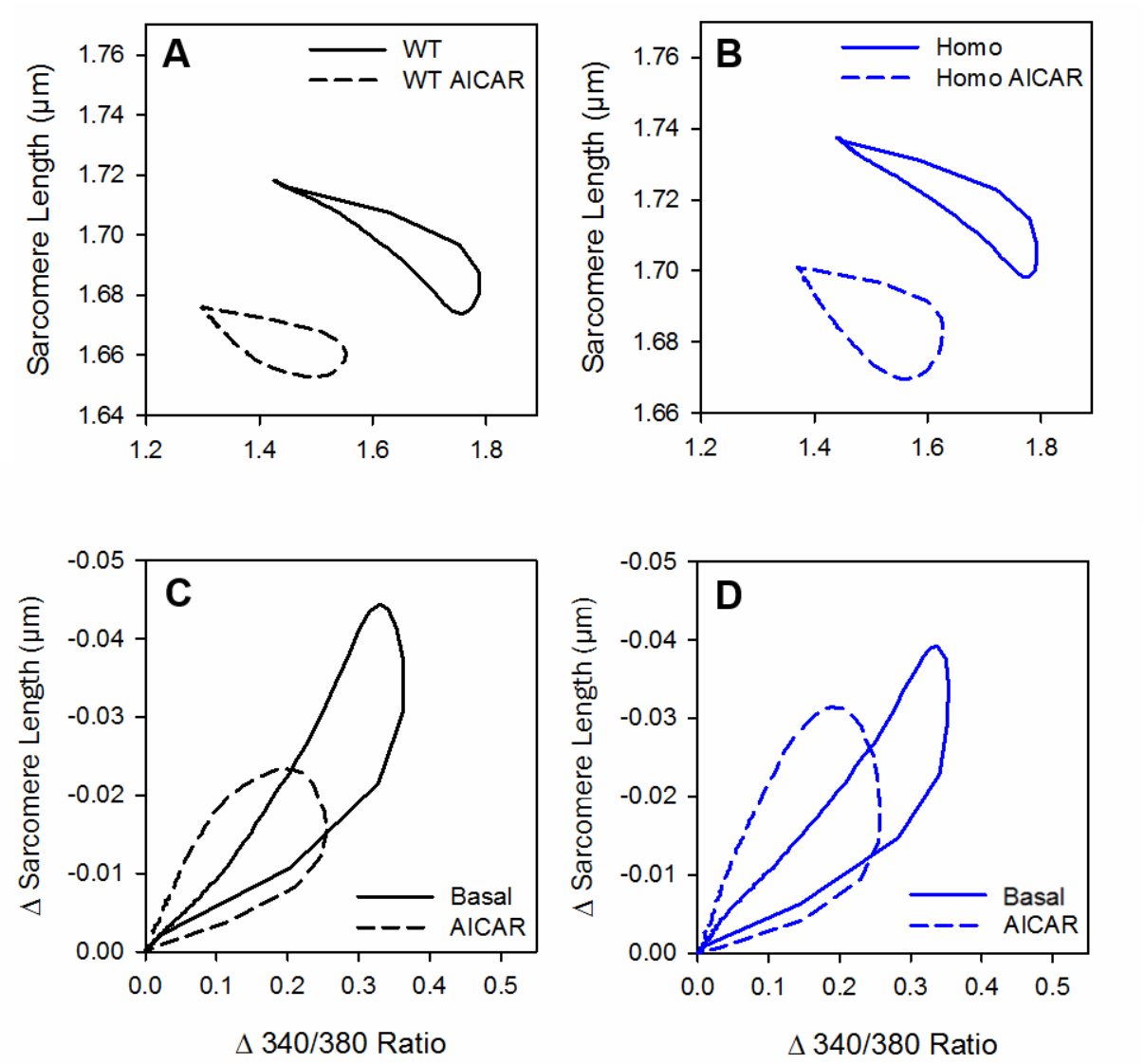


Figure 4-8 - Absolute (A & B) and normalized (C & D) shortening and Ca^{2+} transient relationships of cardiomyocytes from WT and Homozygote animals at 3 Hz stimulation. AICAR significantly reduced both shortening and Ca^{2+} transient magnitudes but also affected their relationship.

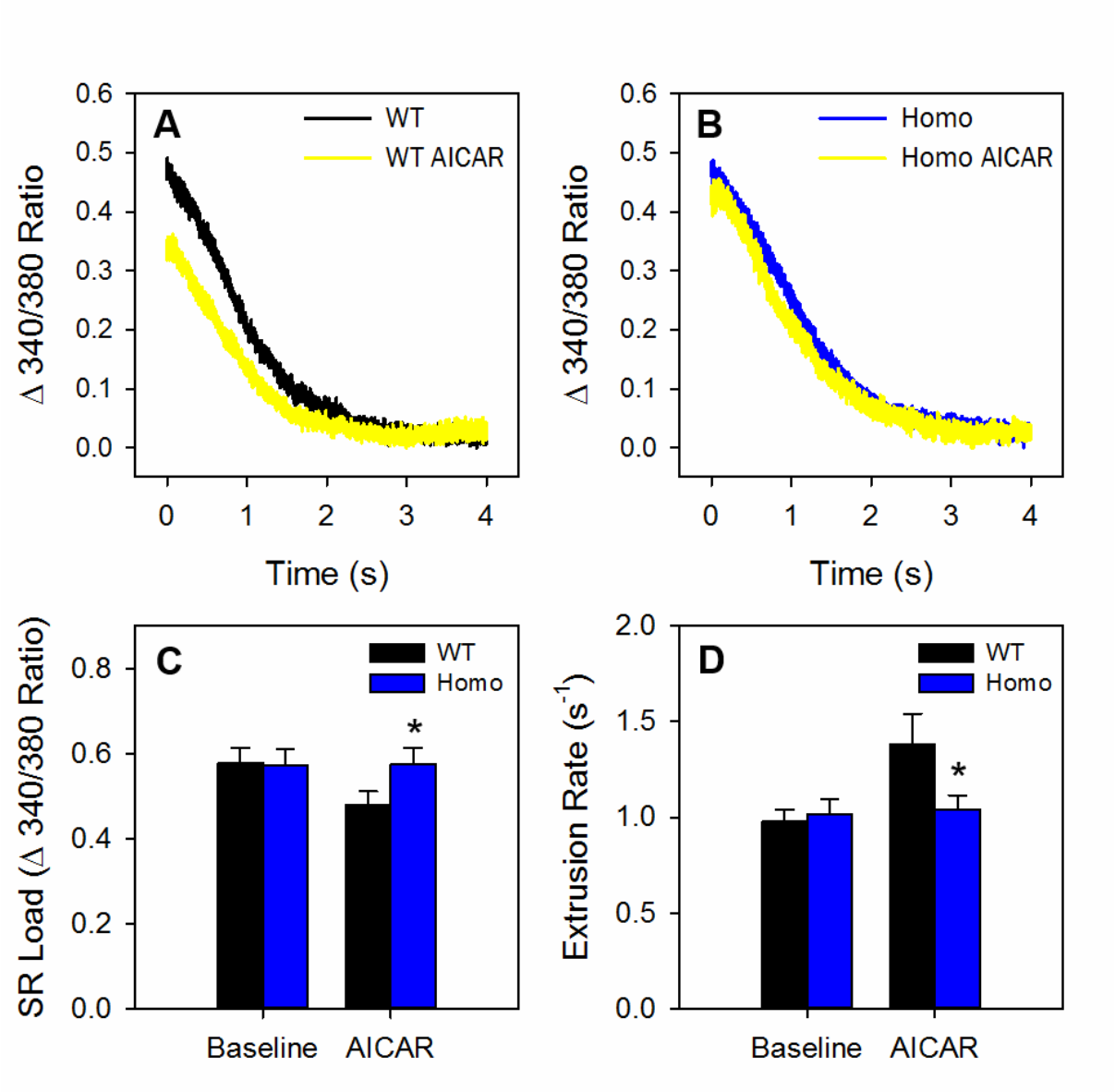


Figure 4-9 - Averaged Ca^{2+} reuptake traces following caffeine spritz of cells with (yellow) and without (blue, black) a 15-minute AICAR incubation (A, B), total sarcoplasmic reticulum load as given by the magnitude of FURA-2-AM signal rise (C), and Ca^{2+} extrusion rate following caffeine spritz (D). AICAR significantly reduced SR load and increased the rate of Ca^{2+} extrusion in cells from WT animals but had no effect on cells from homozygous animals. 5 animals per group were assessed, and 5-10 cells per heart were measured. Significance of differences was determined using post-hoc corrected tests following 2-way ANOVA.

4.5 Discussion

In this chapter, cardiomyocytes from WT and AMPK R299Q γ2 mutant mice were studied to determine if the mutation affects cellular contractility and Ca^{2+} handling. The work identified the following:

i. Magnitudes of cardiomyocyte shortening and Ca^{2+} release were not significantly different between WT and mutant cells. However, rates of contraction, relaxation, Ca^{2+} release, and Ca^{2+} reuptake were significantly slower in cells from Homozygous animals compared to WT controls.
ii. Cardiomyocytes from mutant animals exhibited altered frequency dependence of contractility. In particular, basal sarcomere length in Homozygous cells remained constant as stimulation frequency was increased. In addition, dysregulation of the shortening vs frequency relationship was observed in Homozygous cells.
iii. No differences in SR Ca^{2+} load or total Ca^{2+} extrusion rates (measured after caffeine stimulation) were detected in mutant cells. However, calculation of SERCA Ca^{2+} reuptake using these data revealed significantly reduced SERCA activity in mutant cells.
iv. The response to isoproterenol treatment was greater in mutant cells than WT controls, particularly in fractional shortening.
v. Treatment with AICAR caused a significant reduction in all aspects of contractility – shortening, Ca^{2+} release, and all kinetic measurements. This effect was smaller in mutant cells.
vi. Treatment with AICAR reduced SR Ca^{2+} load and total Ca^{2+} extrusion rate in WT cells but not in mutant cells.

Several of these findings are discussed in more detail below.

4.5.1 Slowed Ca^{2+} handling and contractility

An essential component of the *in vivo* cardiac dysfunction observed in AMPK R299Q γ2 mutant mice via invasive haemodynamics was slowed relaxation during diastole (Section 3.1). This effect was recapitulated in isolated cardiomyocytes, where cells from mutant animals exhibited reduced relaxation speeds across stimulation frequencies. These data support the hypothesis that cardiomyocyte dysfunction underlies the whole organ phenotype (as opposed to potentially abnormal glycogen or collagen distributions). The explanation for impaired cardiomyocyte relaxation could lie within the sarcomere or the Ca^{2+} handling apparatus.

Sarcomeric explanations of slowed relaxation generally rely on two metrics – Ca^{2+} sensitivity and cross-bridge cycling. With increased Ca^{2+} sensitivity of activation, sarcomeres generate more force at sub-maximal Ca^{2+} concentrations. During the Ca^{2+} transient, the Ca^{2+} rise is too rapid for sarcomeric Ca^{2+} sensitivity to have a noticeable effect on shortening speeds. However, during the slower decline of the Ca^{2+} transient, increased thin filament Ca^{2+} sensitivity would result in lengthened periods of available cross-bridge binding sites and therefore slower cardiomyocyte relaxation. Besides Ca^{2+} sensitivity, the rate of cardiomyocyte relaxation is also affected by cross-bridge cycling rates. Experiments in various muscle types have illustrated that myosin cycling rates are directly associated with relaxation speeds [Palmer and Kentish, 1998; Gordon *et al.*, 2003]. The proposed mechanism for this relationship is that slowed cross-bridge cycling delays transitions from attached, force-producing stages of the cross-bridge cycle to detached, non-force-producing positions. In Chapter 3, fibres from mutant animals were shown to exhibit increased Ca^{2+} sensitivity of activation but no significant changes in cross-bridge cycling rates.

Thus, a reasonable explanation for slowed cardiomyocyte relaxation could be enhanced Ca^{2+} sensitivity of activation. However, because rates of Ca^{2+} release and reuptake were also slowed, effect of the mutation on contractile function cannot only be accounted for by sarcomeric alterations. Instead, modification of the Ca^{2+} handling apparatus (including the LTCC, RyR, NCX, SERCA, and PLN) is also likely to contribute to the phenotype.

Evidence for the alteration of any of these Ca^{2+} handling regulators can be proposed based on observed functional changes in untreated cardiomyocytes. In mutant cells, rates of both Ca^{2+} release and Ca^{2+} reuptake were significantly slowed compared to WT cells. Rise of the Ca^{2+} transient in the cardiomyocyte is due to calcium-induced calcium-release (CICR) via the LTCC and RyR-mediated SR release. Therefore, modification of either component, or both, could contribute to the phenotype. Resolution of the mechanism causing slowed Ca^{2+} rise in these cells would require isolating the stages of CICR. One potential experiment that could accomplish this challenge would be patch-clamping of the LTCC to determine its isolated contribution.

In a similar fashion, alteration of multiple regulators could contribute to the slowed Ca^{2+} transient decay observed in the mutant cells. Of particular interest are the NCX and SERCA, which are primarily responsible for Ca^{2+} extrusion and SR Ca^{2+} reuptake, respectively. However, in this case, determination of the mechanism causing slowed Ca^{2+} transient decay in mutant cardiomyocytes could be accomplished using pharmacological means. By stimulating the cells with caffeine, SERCA activity was inhibited and activity of the NCX (and other slow mechanisms) could be measured independently [Bassani, 1995]. Subtracting these activities from the total Ca^{2+} decay rate allowed the determination that reduced SERCA activity,

and not reduced NCX activity, caused the slowed Ca^{2+} transient decay rate. As the relative contribution of SERCA Ca^{2+} reuptake vs NCX Ca^{2+} extrusion is thought to underlie the force-frequency relationship [Bers, 2000; Maier *et al.*, 2000], the altered SERCA activity in mutant cells may also contribute to the observed dysregulation of the normal force-frequency relationship.

A number of mechanisms could contribute to reduced SERCA activity in the mutant cells. First, a reduction in SERCA expression or retention would result in less functional pumping activity on the SR membrane. Second, higher levels, or reduced phosphorylation, of SERCA's inhibitory binding protein, PLN, would result in lowered SERCA activity. Finally, because SERCA's activity is ATP-dependent, a reduction in the energetic status of the cardiomyocytes could lead to reduced SERCA activity. The clarification of these potential mechanisms is described in Chapter 5.

As described previously, slowed Ca^{2+} reuptake by SERCA is implicated in a number of disease mechanisms. One key pathway involved in these hypothesized mechanisms is increased basal Ca^{2+} levels leading to increased Ca^{2+}-dependent signalling. However, in these experiments, no increase in basal Ca^{2+} was observed in mutant cardiomyocytes despite the slowed SERCA reuptake. Plausible explanations for this observation arise from the experimental conditions. Though the pacing frequencies used here (1, 3, 6 Hz) are typical, they may not be a reasonable mimic of *in vivo* activity (~10 Hz). Though SERCA activity is reduced in these cells, extended diastolic periods offered by slower stimulation frequencies allow the cells to regain normal resting Ca^{2+} concentrations. At the higher contractile frequencies experienced *in vivo*, slowed SERCA activity may result in increased diastolic Ca^{2+} concentrations. Unfortunately, pacing at 10 Hz is not possible using

these preparations so this hypothesis cannot be tested directly. An alternative, or perhaps contributing, mechanism is that increased basal Ca^{2+} concentrations only materialize after an extended period of reduced SERCA activity.

4.5.2 Increased isoproterenol response

The result of increased responsiveness to PKA treatment in skinned fibres from R299Q γ2 mutant animals led to the assumption that mutant cardiac tissue possessed a lower level of phosphorylation at PKA target sites. Potential mechanisms underlying this alteration include a reduction in levels or activity at any point in the β-adrenergic signalling cascade (sympathetic activation, G-protein couple receptors, cAMP, etc.) or an increase in phosphatase activity. The additional finding of an increased response to isoproterenol in intact cardiomyocytes possessing the R299Q γ2 mutation also suggests that mutant cells have greater adrenergic reserve. Together, these results suggest that basal phosphorylation of PKA target sites is reduced, but that the upstream β-adrenergic signalling cascade retains sensitivity to stimulation. One hypothesis that could explain these findings is that increased AMPK activity may directly reduce PKA activity or increase phosphatase activity within the cardiomyocyte. However, the global nature of the R299Q γ2 model utilised, combined with AMPK's diverse effects on neural [Xue and Kahn, 2006], sinoatrial nodal [Yavari, 2010], and metabolic [Hardie, 2011] function, ensures that upstream alteration of cardiomyocyte activity cannot be excluded. Specifically, it may be possible that systemically overactive AMPK may increase β-adrenergic receptor density and facilitate an increased response to isoproterenol treatment.

The caveat to these data interpretations is the assumption that isoproterenol treatment represents a physiological signal. If a 10 nM isoproterenol treatment is

significantly super-physiological, it could overcome a down-regulated β-adrenergic response system and still yield a major response. Due to this potential complication, confirmation of the suggested mechanism by biochemical analysis is required.

This pathway is of particular interest because the β-adrenergic system is commonly affected by cardiac disease states [Triposkiadis *et al.*, 2009]. In general, progression to heart failure is associated with hyperactivity of the sympathetic nervous system aimed at preserving cardiac output. However, this hyperactivity can ultimately become maladaptive, leading to diastolic dysfunction and increased risk of sudden death [Grassi *et al.*, 2009]. The intermediate mechanism leading to these outcomes is impaired regulation of the β-adrenergic receptor system including decreased overall density [Bristow *et al.*, 1982], altered balance of stimulatory and inhibitory G-protein couple receptors [Engelhardt *et al.*, 1996], and impaired compartmentalization of cAMP/PKA signalling due to A-kinase anchoring proteins [Dodge-Kafka *et al.*, 2005]. These mechanisms can lead to impaired balance in activity of Ca^{2+} handling proteins [Piacentino *et al.*, 2003] and promote cardiomyocyte apoptosis [Olivetti *et al.*, 1997]. In this model, however, we suspect that the pathway leading to PKA activation is retains at least some of its function. Instead, regulation directly reducing PKA activity, or increasing the activity of PKA-target phosphatases, is more likely.

4.5.3 Dramatic effect of AICAR treatment in WT cells

One of the more striking results of experiments in this chapter is the significant inhibition of contractility following AICAR incubation. The effect was marked in WT cardiomyocytes, reducing the magnitudes and rates of shortening and Ca^{2+} handling by as much as 50 %. In general, the effect of AICAR treatment caused functional changes comparable to the R299Q γ2 mutation except to a greater

extent. This observation is consistent with the finding of increased basal AMPK activity in the R299Q γ2 mutant mice.

Beginning with the changes in Ca^{2+} handling, AICAR treatment appears to alter all aspects of Ca^{2+} release and reuptake. This finding would suggest broad changes to the entire Ca^{2+} handling apparatus. Particularly, the reduction in Ca^{2+} release and reuptake speeds points to changes in activities of the primary Ca^{2+} channels and pumps. As conductance of these membrane agents is assumed to be first-order [Hodgkin *et al.*, 1952; Opie, 2003], the times to 50 % Ca^{2+} release and reuptake should not be dependent on initial concentrations. Therefore, it is very likely that AICAR treatment causes impaired calcium-induced calcium release via the L-type Ca^{2+} channel and/or RyR as well as reduced Ca^{2+} reuptake/extrusion via SERCA and/or the NCX.

The reduction in Ca^{2+} transient magnitude may be a product of these changes, but it is also likely affected by the reduction in total SR load observed via caffeine treatment. This reduction in SR load must be an acute response within the 15 minute incubation and subsequent experimental period. The most likely mechanism leading to this outcome is slowed SR Ca^{2+} reuptake during pacing, causing increased Ca^{2+} extrusion and depleted SR Ca^{2+} stores. However, rather than increased diastolic Ca^{2+} concentrations, reduced diastolic Ca^{2+} concentrations were observed. This suggests that SR Ca^{2+} stores may be depleted prior to pacing and measurement, perhaps via SR Ca^{2+} leak and subsequent extrusion.

In addition to significant alteration of Ca^{2+} handling, AICAR treatment also differentially modified shortening. The changes observed in fractional shortening, rate of contraction, and rate of relaxation are approximately explained by the

consistent changes in Ca^{2+} handling. However, relationships between the Ca^{2+} transient and shortening are clearly modified by AICAR treatment. Both baseline sarcomere length and diastolic Ca^{2+} concentration decrease upon AICAR treatment. These changes are counterintuitive given the direct relationship between contraction levels and Ca^{2+} concentrations. Simultaneous decreases in both diastolic parameters requires a significant increase in sarcomeric Ca^{2+} sensitivity, which could be explained by increased AMPK phosphorylation of TnI S150.

The effect of AICAR treatment on the energetic efficiency of cardiomyocyte function is less clear from these data. The treatment caused slowed sarcomeric response to Ca^{2+} reuptake, consistent with increased sarcomeric Ca^{2+} sensitivity, leading to extended periods of cross-bridge activity and contraction. This delayed relaxation would cause increased ATP usage by the sarcomere relative to the level of shortening achieved. As slowed cardiomyocyte relaxation is unlikely to improve cardiac output, the net effect of AICAR treatment on the energetic efficiency of contractile function is likely to be negative. However, the level of Ca^{2+} flux was significantly reduced by AICAR treatment, lessening the energetic cost associated with Ca^{2+} transport. This will mitigate the reduced sarcomeric efficiency and lead to an unclear net effect on total cardiac energetic efficiency.

The effect of AICAR treatment on WT cardiomyocytes reported in this chapter disagrees with earlier work from the laboratory [Oliveira *et al.*, 2012]. Oliveira et al observed increased contractility in cardiomyocytes following AICAR incubation, but only in cells containing FURA-2-AM. No intentional differences in methodology were applied, though a new IonOptix-µStep Myocyte Contractility System was utilized for the experiments presented here. Further, the sample size published by Oliveira et al (14 cells per group) was significantly smaller than the number of cells examined

here (70-90 cells per group). The difference between data sets is therefore due to an unknown methodological alteration or a statistical anomaly.

4.5.4 Reduced effect of AICAR treatment on mutant cardiomyocytes

In most parameters, the effect of AICAR treatment was smaller in cardiomyocytes from mutant animals. The simplest mechanism explaining this differential response is that the R299Q γ2 mutation, located in the first CBS domain associated with AMPK regulation, results in reduced responsiveness to the stimulatory signal. Data presented in Chapter 3 may further clarify this hypothesis. Specifically, γ2-specific AMPK activity was shown to be unresponsive to AMP in homozygous R299Q γ2 whole heart homogenates. However, ACC S79 phosphorylation (attributable to overall AMPK activity) was increased by AICAR treatment to comparable levels in WT and homozygous cardiomyocytes. These results suggest that γ2-containing AMPK complexes have reduced responsiveness, but the majority γ1-containing complexes are sufficient to phosphorylate ACC under severe stress. As AMPK γ2 subunits contain varying N-terminal extensions responsible for sub-cellular localization within cardiomyocytes [Pinter *et al.*, 2013], it is possible that γ2-specific effects may be responsible for the differing functional response to AICAR between WT and homozygous cardiomyocytes.

Further, an important consideration in interpreting the results of AICAR treatment on cardiomyocyte function is the potential for off-target effects of the drug, particularly at the relatively high 2 mM dose. These off-target effects have been noted in various experiments. Fundamentally, as an AMP analogue, the ZMP molecule created from AICAR stimulates glycogen phosphorylase [Longnus *et al.*, 2003] and inhibits fructose-1,6-biphosphatase [Vincent *et al.*, 1991] besides its activating effect on AMPK. These effects, or perhaps unidentified mechanisms,

result in *in vivo* impacts that cannot be attributed solely to AMPK activity. For example, in skeletal muscle cells, AICAR was shown to inhibit aspects of mitochondrial function and impair oxygen consumption [Spangenburg *et al.*, 2013] whereas genetic activation of AMPK does not [Lee-Young *et al.*, 2009]. Perhaps more relevantly, AICAR was shown to reduce the leak of Ca^{2+} from mutant RyR associated with malignant hyperthermia in a manner independent of AMPK [Lanner *et al.*, 2012]. These potential complications condition the mechanistic insight gained from AICAR treatment of cardiomyocytes reported in this chapter.

Chapter 5 – Biochemical alterations underlying cardiac contractile abnormalities in AMPK R299Q γ2 mice

5.1 Introduction

The two preceding chapters describe a range of functional alterations to contractile mechanics and Ca^{2+} handling in cardiac tissue from AMPK R299Q γ2 mutant animals. However, these experiments do not fully clarify the molecular modifications underlying the observed changes. To improve our understanding of the mechanisms leading to dysfunction in AMPK R299Q γ2 mice, a range of biochemical assessments were conducted.

The changes underlying the observed alterations to contractility and Ca^{2+} handling were of particular interest. Given that these functions are predominantly controlled by a handful of key proteins and channels (discussed in Chapter 1), it is likely that modification of these agents is responsible for dysfunction. Therefore, experiments presented in this chapter aimed to characterize the levels and post-translational modification states of the most crucial regulatory proteins involved in cardiac contraction and Ca^{2+} handling. These studies utilized samples of demembranated ventricular muscle and isolated cardiomyocytes that were snap frozen immediately following extraction/experimentation and maintained at -80 °C until analysis. Therefore, these samples closely match the tissues subjected to functional assessment. Examination of these samples involved one- and two-dimensional gel electrophoresis to separate proteins of interest by molecular weight and isoelectric point. Subsequently, phosphorylation-site-specific and total protein antibodies were used to identify precise targets and their modified states.

The contractile regulatory proteins of particular interest were TnI, MyBPC, and myosin ELC and RLC. The overall level of TnI phosphorylation was assessed using the PhosTag reagent. Subsequently, phosphorylation-site-specific antibodies to TnI pS150 and TnI pS23/S24 were utilized to determine the location of altered phosphorylation state. These sites are targeted by AMPK and PKA, respectively, and cause opposing effects on myofilament Ca^{2+} sensitivity [Layland *et al.*, 2005]. Changes to these sites may therefore underlie the increased Ca^{2+} sensitivity exhibited by demembranated fibres from mutant animals. The distribution of MyBPC and myosin light chain modification states was examined using 2D gel electrophoresis. The isoelectric distribution of myosin RLC is primarily due to phosphorylation at S13 by PKA, resulting in increased cross-bridge cycling speeds at low Ca^{2+} concentrations [Zhang *et al.*, 2002]. Alterations to ELC isoelectric position are also likely caused by phosphorylation, though the specific cause and effect of this phosphorylation is less well understood [Muthu *et al.*, 2011]. MyBPC's isoelectric position is affected by a range of post-translational modifications, resulting in a large number of potential positions [Bouley *et al.*, 2004]. To specify the nature of observed changes to MyBPC isoelectric position, phosphorylation-site-specific antibodies to MyBPC pS273, pS282, and pS302 were applied. These sites are primarily phosphorylated by PKA and PKC and may alter cross-bridge cycling kinetics and relaxation rates [Sadayappan *et al.*, 2005]. Together, changes to the phosphorylation status of MyBPC and the myosin light chains could contribute to slowed sarcomeric relaxation in mutant animals.

The overall level of PLN, as well as levels of phosphorylation at PLN S16 and T17, was assessed in cardiomyocytes isolated from R299Q γ2 mutant and WT mice. These phosphorylations, by PKA and CaM-dependent protein kinase, respectively,

cause a dissociation of PLN from SERCA and increased Ca^{2+} reuptake into the SR [Bers, 2002]. Therefore, alteration of total level or phosphorylation state of PLN may explain the slowed Ca^{2+} reuptake rate observed in cardiomyocytes from mutant animals.

The tissue type examined in each experiment is noted in the figure legends. Demembranated fibres frozen following mechanical assessment were used when possible to provide a direct comparison between functional parameters and biochemical state. However, as the majority of non-sarcomeric proteins are removed by treating the fibres with Triton X-100, isolated cardiomyocyte pellets were used for assessments of non-sarcomeric targets.

5.2 Alterations to sarcomeric regulatory proteins

Given AMPK's ability to directly phosphorylate TnI at S150, overall phosphorylation status of the thin filament regulatory protein was measured. These experiments utilized the PhosTag reagent, which was added to a traditional SDS-PAGE gel in order to retard protein species proportionally to the number of phosphorylations present. Using a total TnI antibody, this method allowed separation of TnI into un-, mono-, and bis-phosphorylated species. Confirmation of the identity of each band was accomplished using un-phosphorylated (recombinant) and bis-phosphorylated (PKA-treated recombinant) loading controls. In demembranated ventricular fibre samples from WT animals, TnI was present almost exclusively in a bis-phosphorylated state (Figure 5-1). In mutant animals, however, a dose-dependent increase in mono- and un-phosphorylated TnI was observed. Using a weighted average calculation, a reduction in total TnI phosphorylation in mutant fibres was identified.

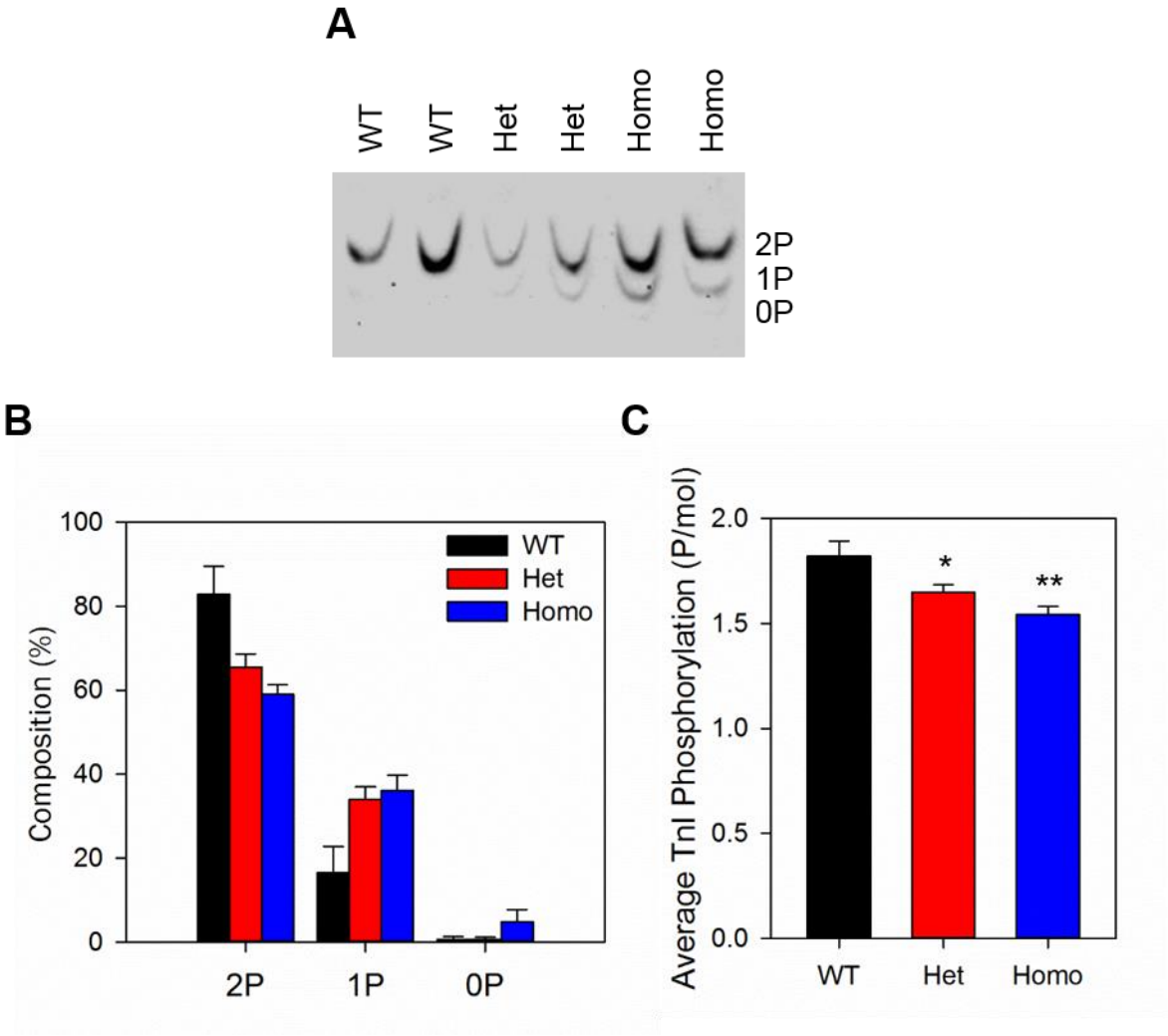


Figure 5-1 – Characteristic PhosTag Western blot using a total TnI antibody (A), quantitation of average phosphorylation species composition (B), and calculated number of phosphorylations per molecule (C). Fibres from mutant animals exhibited a shifted phosphorylation composition, resulting in a reduced number of average phosphorylations per molecule. Measurements were taken from 6-8 fibres from 4-5 mice in each group. Significance of differences compared to WT controls were determined using post-hoc corrected tests.

As phosphorylation at various sites on cTnI have differing function effects [Solaro and Kobayashi, 2011], we investigated site-specific alterations that would explain the difference in total phosphorylation. Using digested samples of demembranated ventricular muscle, sequential Western blots (alternated by membrane stripping) using antibodies specifically targeting phospho-TnI S150 (pTnI S150), phospho-TnI S23/S24 (pTnI S23/S24), and total TnI were conducted. Samples from mutant animals exhibited a dose-dependent increase in pTnI S150 phosphorylation.

Comparable decreases in pTnI S23/S24 phosphorylation were observed in heterozygous and homozygous samples.

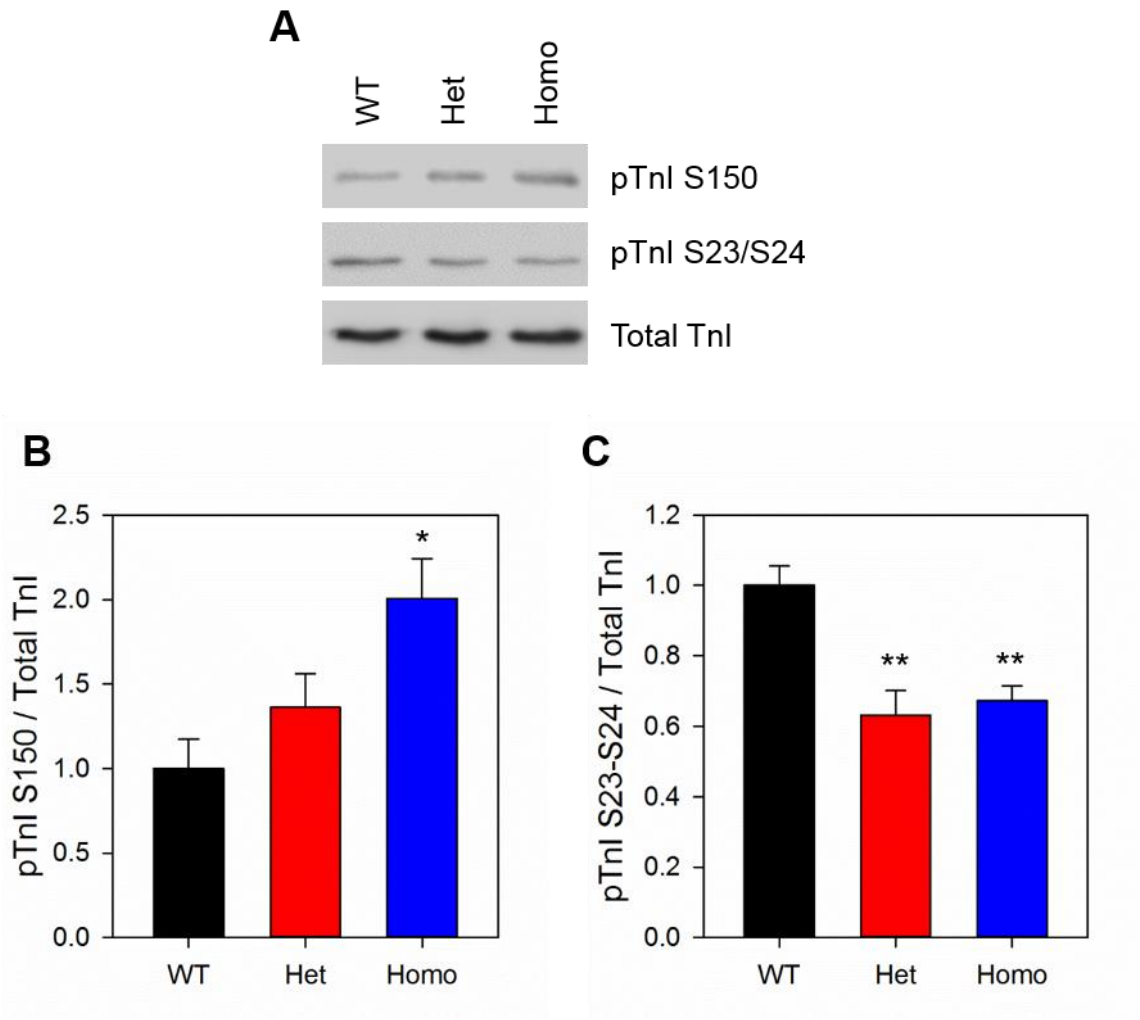


Figure 5-2 – Characteristic Western blots using phospho-TnI S150, phospho-TnI S23/S24, and total TnI antibodies (A) and normalized quantification summaries (B & C). Fibres from mutant animals exhibited increased TnI S150 phosphorylation and reduced TnI S23/S24 phosphorylation. Measurements were taken from 6-8 fibres from 4-5 mice in each group. Significance of differences compared to WT controls were determined using post-hoc corrected tests.

Next, alterations to additional targets were explored in a non-hypothesis-driven manner through 2D gel electrophoresis of digested isolated cardiomyocytes. This technique separates proteins by molecular weight and isoelectric point, allowing differentiation of distinct proteins and their potentially modified forms. A high-sensitivity fluorescent stain (Sypro Ruby) was applied to the gels, allowing identification of numerous protein spot patterns (Figure 5-3). Of particular interest

were proteins that exhibited species at differing isoelectric points, as these likely represent levels of post-translational modification, particularly phosphorylation [Berth *et al.*, 2007]. Distribution of the spots was analysed to determine the average isoelectric point using a weighted average calculation.

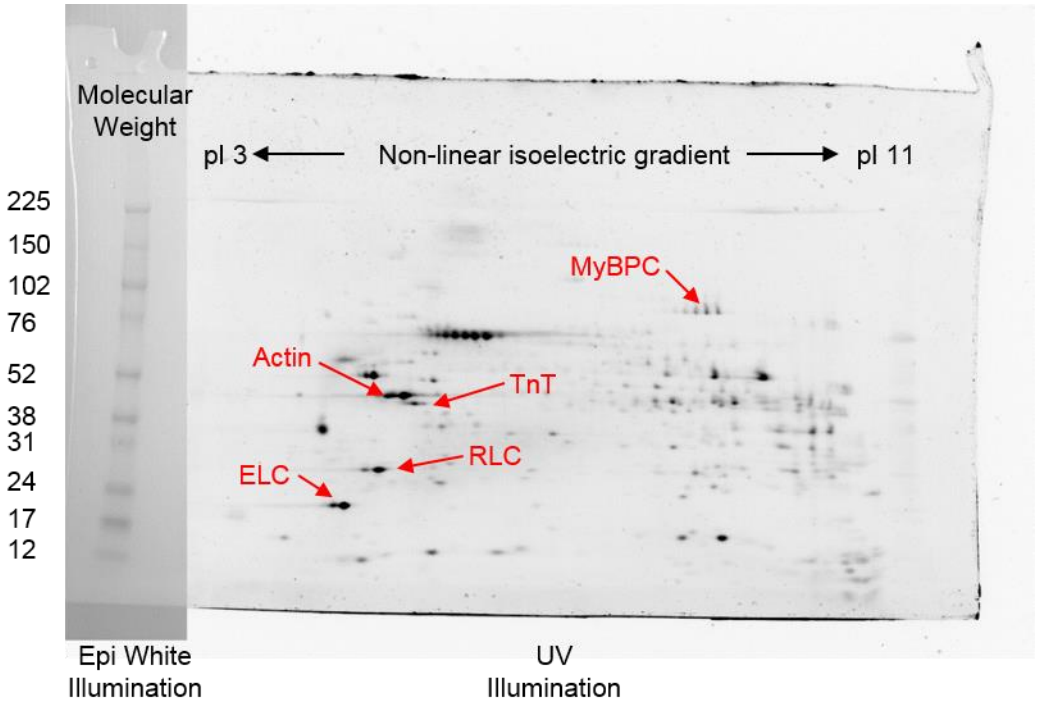


Figure 5-3 – Example 2D gel electrophoresis result. Images generated using white light (molecular weight marker) and UV (Sypro stain) illumination are merged for convenience.

The first protein assessed in this manner was MyBPC, which migrates distinctly from other abundant proteins at high molecular weight (between 100-150 kDa) and moderate isoelectric point (~pI 5-7) [Sadayappan *et al.*, 2006]. Confirmation of its identity was accomplished by blotting a 2D gel and applying a MyBPC antibody. In samples of WT cardiomyocytes, up to 14 discernible isoelectric spots were detected, usually appearing in a vertical doublet. In samples of homozygous cardiomyocytes, no more than 10 spots were detected. In all samples, the most abundant spot was isoelectric position 1 (Figure 5-4). However, the relative

distribution was significantly different between WT and homozygous samples. Specifically, compared to WT samples, the spot composition of homozygous samples was shifted towards lower isoelectric positions (more basic).

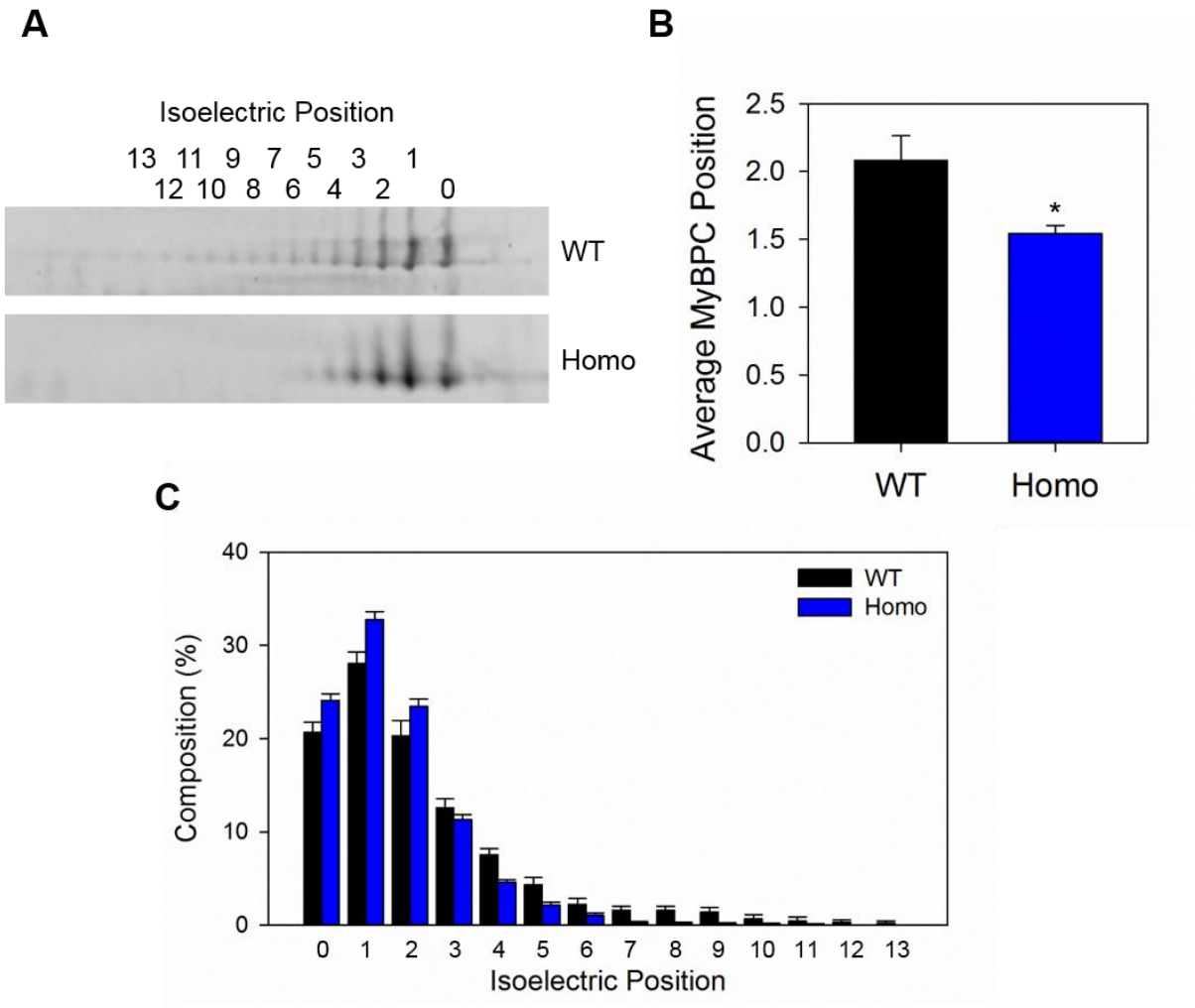


Figure 5-4 – Characteristic MyBPC isolations from 2D gel results (A) and quantification of weighted average isoelectric position (B) based on isoelectric position composition (C). Cardiomyocyte samples from homozygous animals exhibited fewer spots shifted to acidic isoelectric positions, resulting in a more basic average isoelectric position. Measurements were taken from 5 cardiomyocyte samples per group. Significance of differences were determined using t-tests.

A second readily identifiable protein was the myosin ELC, appearing at molecular weight ~20 kDa and acidic pI (predicted 17 kDa and pI 4.1 [Helper *et al.*, 1988]). In both genotypes, a maximum of three isoelectric positions was identified. The most acidic position (position 0) was most abundant, representing 60-70 % of the total

signal. Position 1 contributed 30-40 % of the total signal. In samples with a distinguishable Position 2, less than 5 % of the total signal was contributed by this position. No significant difference in the distribution or average isoelectric position was detected between WT and homozygous groups.

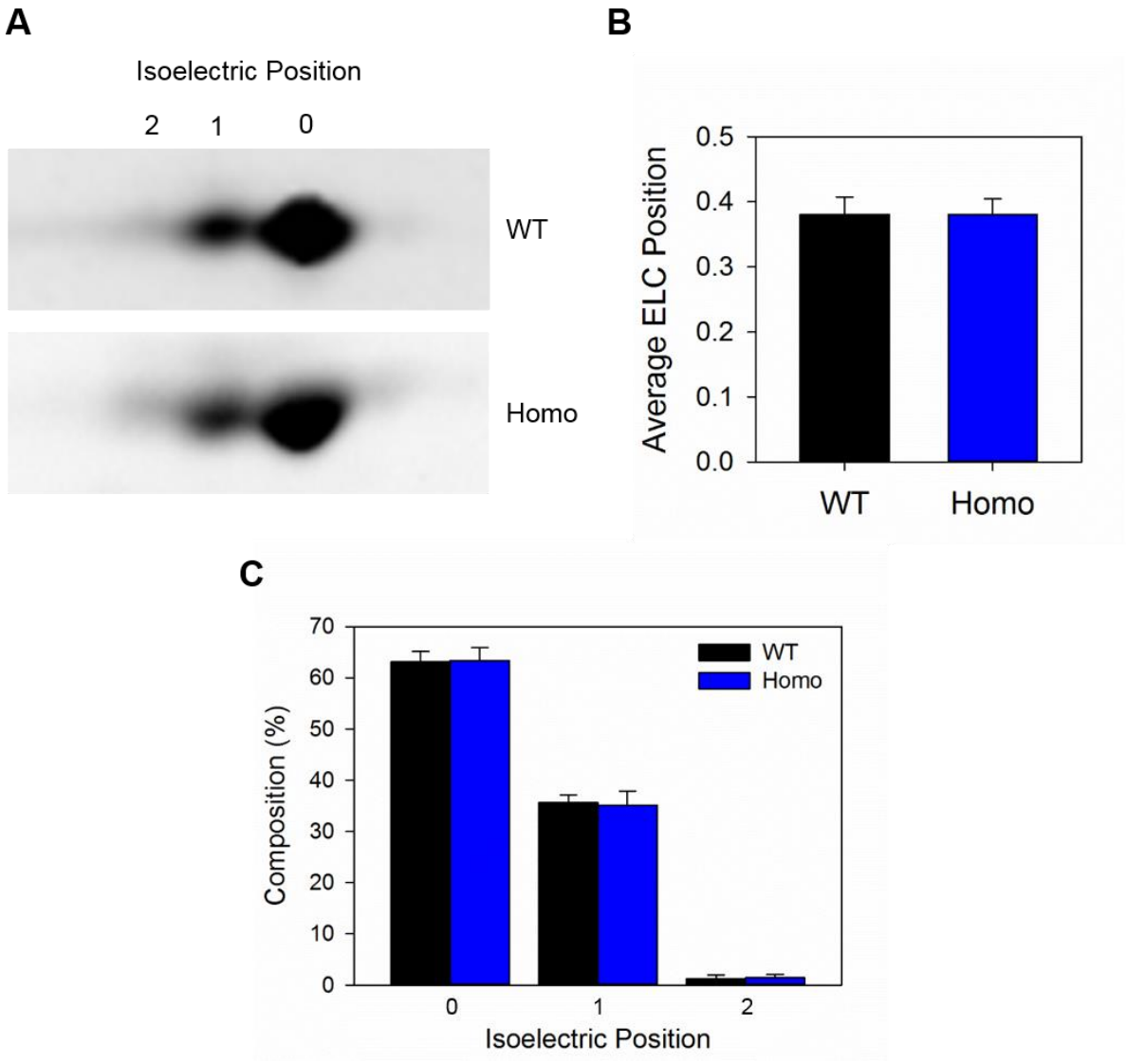


Figure 5-5 – Characteristic ELC isolations from 2D gel results (A) and quantification of weighted average isoelectric position (B) based on isoelectric position composition (C). No significant differences were observed between WT and homozygous groups. Measurements were taken from 5 cardiomyocyte samples per group. Significance of differences were determined using t-tests.

A third target identified on the fluorescently-stained 2D gels was myosin RLC, which appeared slightly heavier and more basic than ELC (predicted 20 kDa and pI 5.1

[Dokhac *et al.*, 1986]). No more than three isoelectric positions were identified in either WT or homozygous samples. In both genotypes, the Position 0 was the most abundant, followed by Position 1. Samples of cardiomyocytes from homozygous animals exhibited a higher proportion of basic RLC, resulting in a lower average isoelectric position.

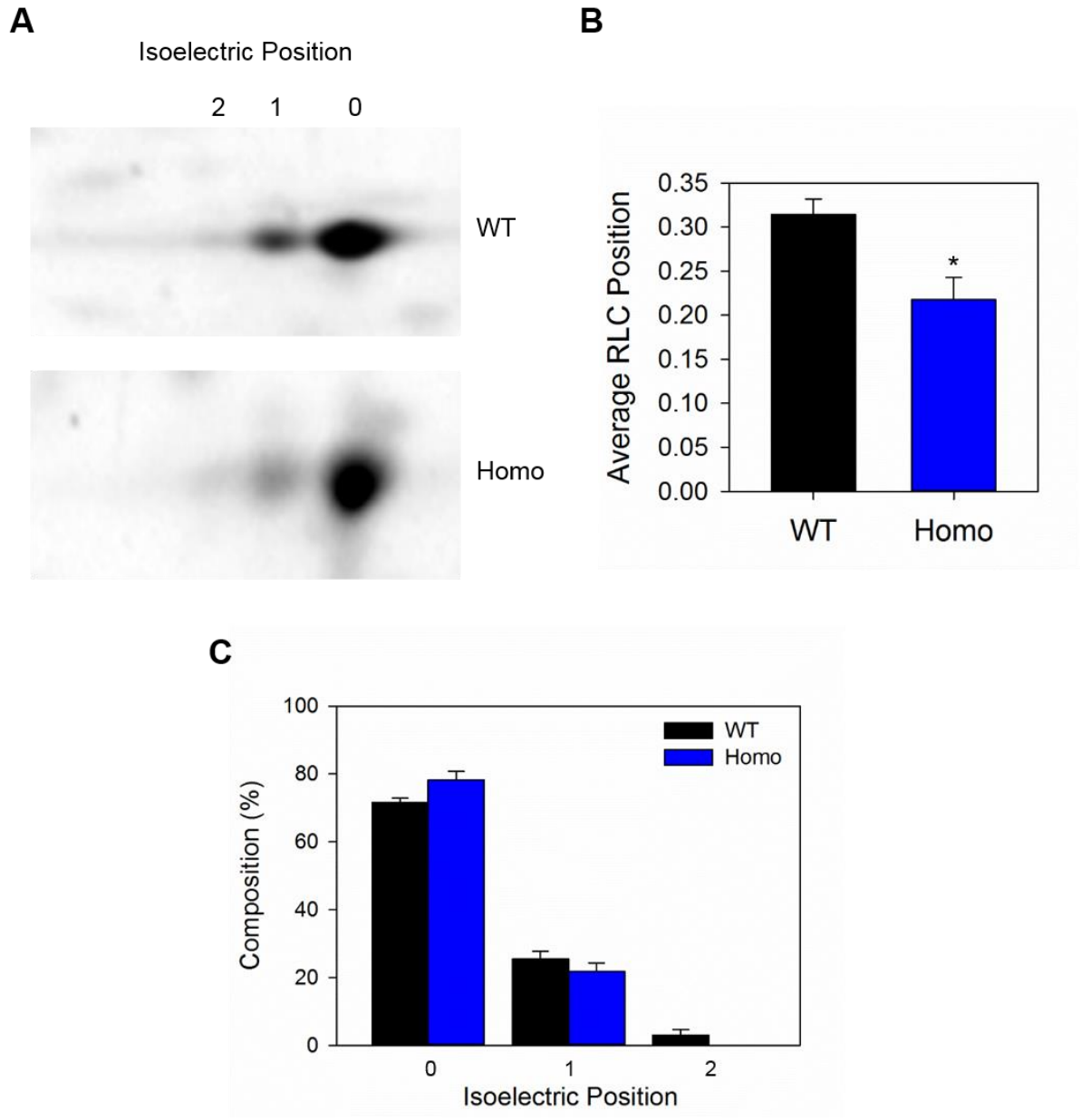


Figure 5-6 – Characteristic RLC isolations from 2D gel results (A) and quantification of weighted average isoelectric position (B) based on isoelectric position composition (C). Cardiomyocyte samples from homozygous animals exhibited fewer spots shifted to acidic isoelectric positions, resulting in a more basic average isoelectric position. Measurements were taken from 5 cardiomyocyte samples per group. Significance of differences were determined using t-tests.

Clarification of the MyBPC modifications resulting in a shifted isoelectric position in mutant cardiomyocytes was desirable because the number of observable isoelectric species was greater than the predicted number of phosphorylations [Copeland *et al.*, 2010], suggesting that other post-translational modifications contribute to the distribution. Therefore, phosphorylation-site-specific antibodies to MyBPC S273, S282, and S302 were applied to determine if changes at these sites could underlie the observed overall change. Across all three sites, a significant ($p < 0.01$) reduction in phosphorylation was observed in homozygous cardiomyocytes compared to WT controls. At each site independently, a significant reduction in phosphorylation was only detected at S282 ($p < 0.05$).

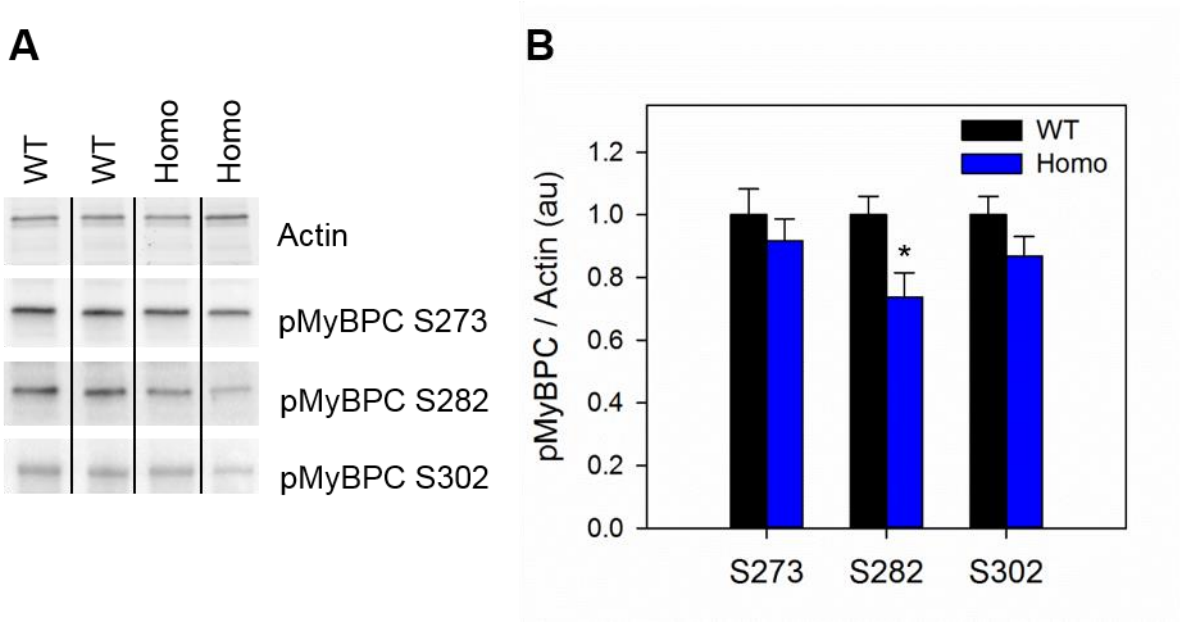


Figure 5-7 – Characteristic actin band on stain-free gel and Western blots using phospho-MyBPC S273, phospho-MyBPC S282, and phospho-MyBPC S302 antibodies (A) and associated normalized quantitation (B). Cardiomyocyte samples from homozygous animals exhibited reduced PLN phosphorylation at both S16 and T17 sites. Measurements were taken from 6 cardiomyocyte samples per group. Significance of differences were determined using t-tests.

5.3 Alterations to Ca^{2+} handling proteins

Changes observed in Ca^{2+} handling parameters in isolated cardiomyocytes encouraged biochemical investigation of the essential Ca^{2+} handling proteins with regard to level and phosphorylation state. Of particular interest was PLN because its level can be altered in various disease states and it is known to be regulated by phosphorylation [MacLennan and Kranias, 2003]. Using cardiomyocyte samples from WT and homozygous animals, levels of PLN were assessed via Western blot. Levels of PLN were normalized against actin, which was measured using stain-free gels prior to Western blot transfer. No significant difference in the PLN/actin ratio was detected by genotype groups.

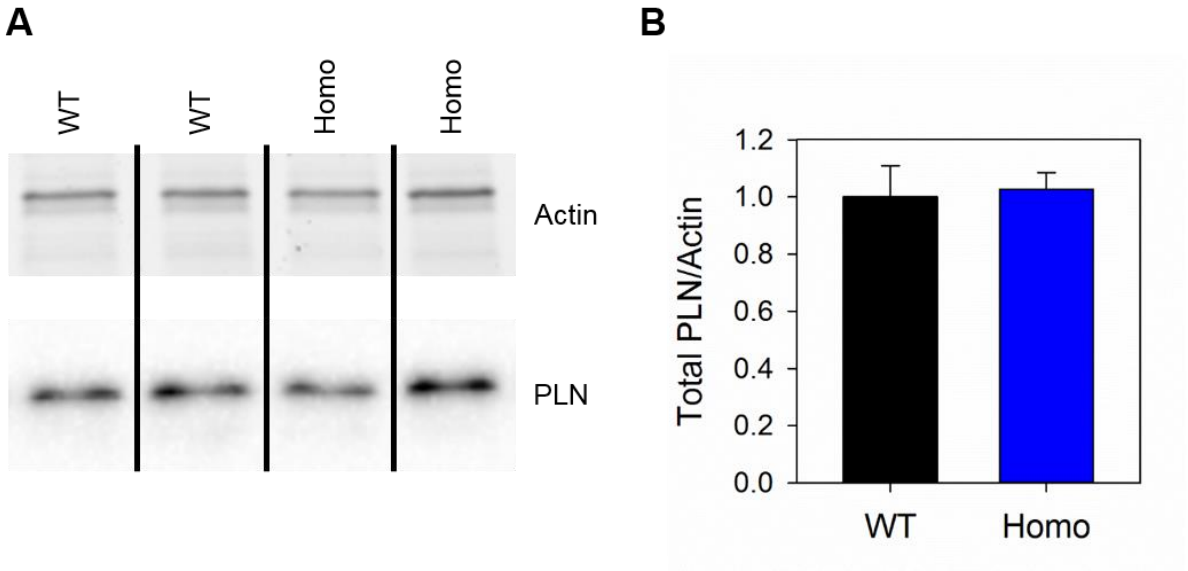


Figure 5-8 - Characteristic Western blot using total PLN antibody normalized to actin from stain-free gel image (A) and associated quantitation (B). No significant differences were observed between WT and homozygous groups. Measurements were taken from 6 cardiomyocyte samples per group. Significance of differences were determined using t-tests.

The phosphorylation of PLN was subsequently assessed using phosphorylation-site-specific antibodies for PLN S16 and PLN T17. In cardiomyocytes from homozygous animals, phosphorylation at PLN S16 and T17 was reduced by 45 % and 31 %, respectively, compared to phosphorylation in cardiomyocytes from WT animals. Both reductions were statistically significant.

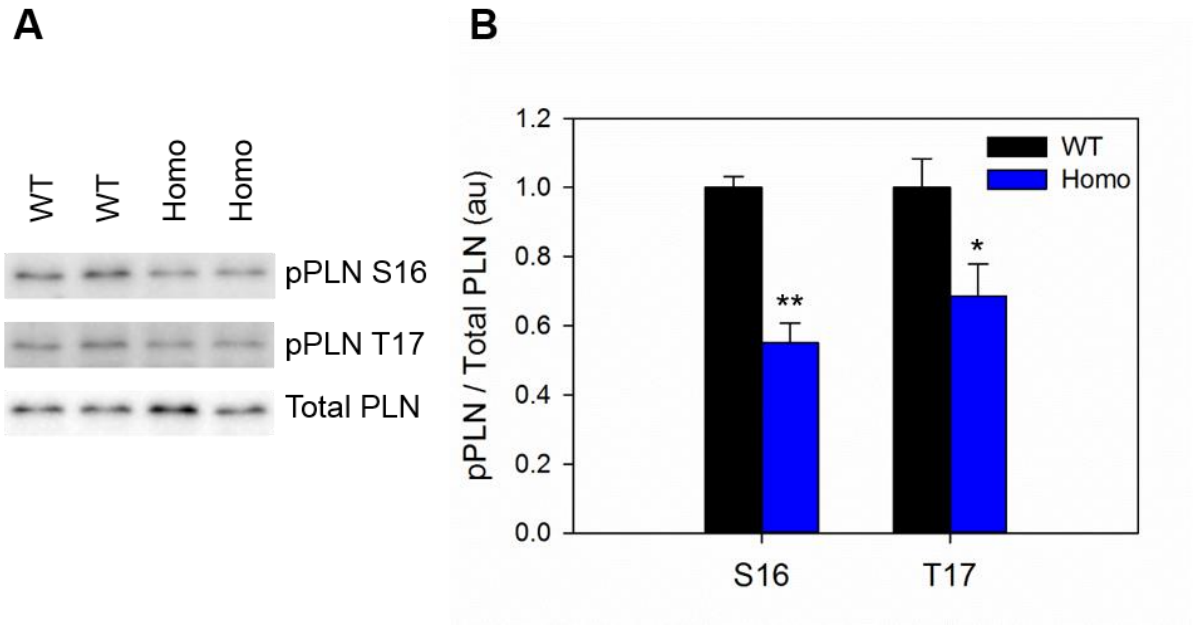


Figure 5-9 – Characteristic Western blots using phospho-PLN S16, phospho-PLN T17, and total PLN antibodies (A) and associated normalized quantitation (B). Cardiomyocyte samples from mutant animals exhibited reduced PLN phosphorylation at both S16 and T17 sites. Measurements were taken from 6 cardiomyocyte samples per group. Significance of differences were determined using t-tests.

To investigate the mechanism underlying the considerable functional changes observed following a 15-minute AICAR incubation, phosphorylation of key regulatory proteins was assessed in treated and untreated cardiomyocytes. The only appreciable difference between these cell populations and those which were examined functionally is the lack of electrical stimulation in the biochemical samples. Interestingly, no significant effect of AICAR treatment was observed on the phosphorylation of TnI S23/S24, PLN S16, PLN T17, or MyBPC S282.

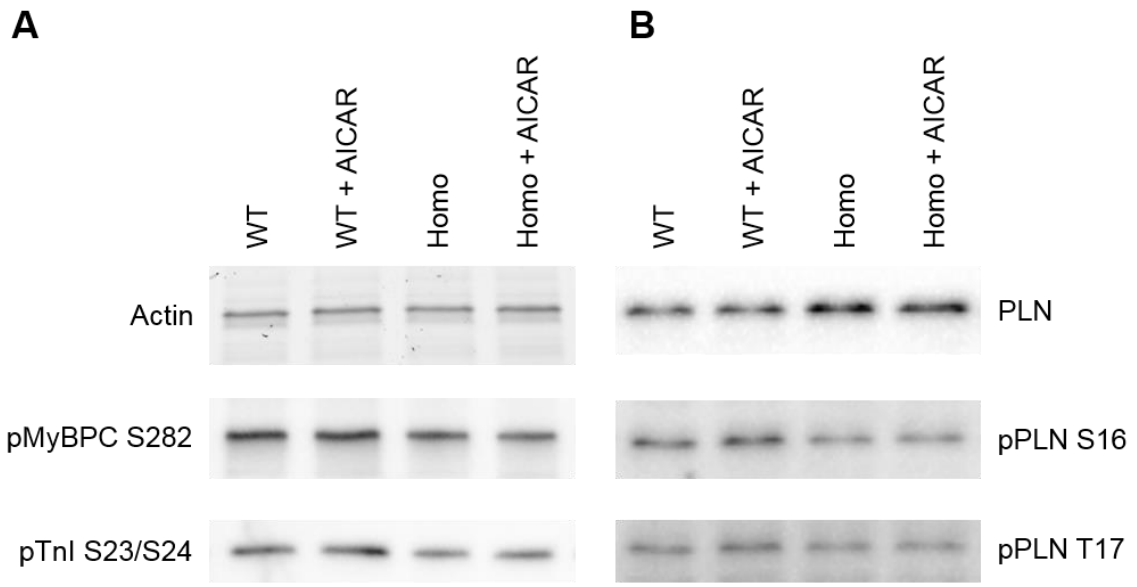


Figure 5-10 – Characteristic actin band on stain-free gel and Western blots using phospho-MyBPC S282 and TnI S23/S24 (A), and characteristic Western bltos using total PLN, phospho-PLN S16 and T17 antibodies (B). No significant effect of AICAR treatment was noted in either genotype group. Measurements were taken from 6 cardiomyocyte samples per group.

5.4 Alteration of the PKA signalling pathway

To isolate the cause of the observed differences in phosphorylation of PKA target sites in sarcomeric and Ca^{2+} handling proteins, the regulatory components of the PKA signalling pathway were examined. The level and phosphorylation state of the PKA's type II regulatory subunit (RII) was measured in isolated cardiomyocytes from WT and AMPK R299Q γ2 homozygous animals. No difference in absolute levels of the protein were detected between groups, but a significant reduction in phosphorylation of PKA RII S96 was observed in homozygous samples.

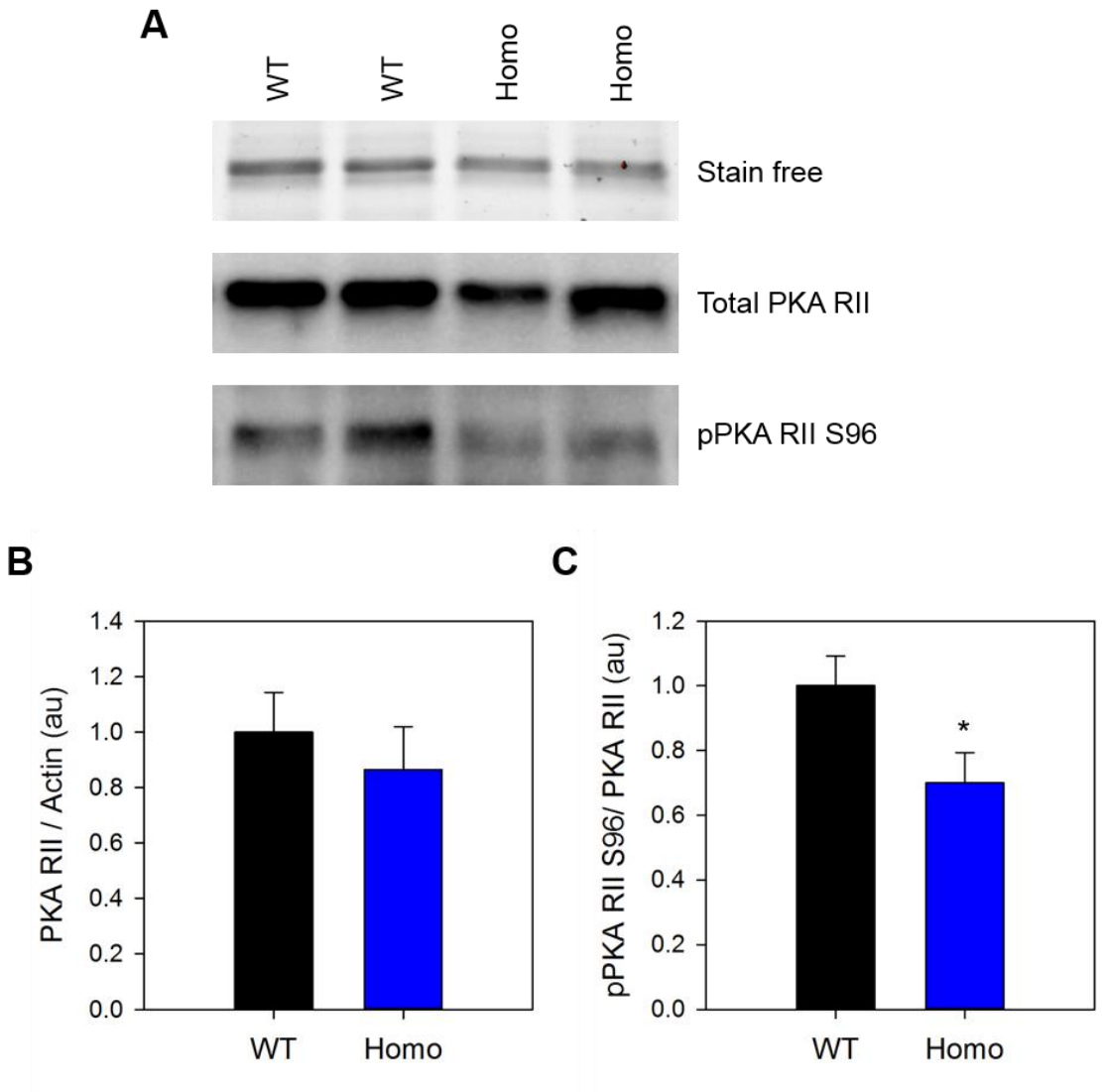


Figure 5-11 - Characteristic actin band on stain-free gel and Western blots using total PKA RII and phospho-PKA RII S96 antibodies (A), and associated ratios of PKA RII to actin (B) and pPKA RII S96 to total PKA RII (C). Samples of mutant cardiomyocytes exhibited no difference in total PKA RII levels but a reduction in phosphorylation at PKA RII S96. Measurements were taken from 6 cardiomyocyte samples per group. Significance of differences were determined using t-tests.

5.5 Discussion

This chapter describes results from various biochemical assessments of demembranated cardiac muscle fibres and isolated cardiomyocytes from WT and AMPK R299Q γ2 mutant animals. Compared to WT samples, mutant animal samples exhibited:

I. Reduced total TnI phosphorylation, increased TnI S150 phosphorylation, decreased TnI S23/S24 phosphorylation
II. Reduced average MyBPC isoelectric position, reduced MyBPC S282 phosphorylation (no significant difference in MyBPC S273 or S302 phosphorylation)
III. No difference in average ELC isoelectric position
IV. Reduced average RLC isoelectric position
V. No difference in PLN level, but reduction in phosphorylation at S16 and T17
VI. No difference in PKA RII level, but reduction in phosphorylation at S96

Relationships between these findings and the previously described functional alterations are discussed below. In addition, the improved understanding of the pathogenesis of PRKAG2 cardiomyopathy developed through these experiments is described.

5.5.1 Altered phosphorylation of sarcomeric proteins underlies myofilament dysfunction

Experiments in this chapter revealed that mutant animals exhibit altered post-translational modification of TnI, MyBPC, and myosin RLC. These changes supply plausible mechanistic explanations for observed functional modifications.

Phosphorylation-site-specific Western blots suggested increased phosphorylation of TnI at S150. Given the direct ability of AMPK to phosphorylate TnI S150, this finding is consistent with increased basal AMPK activity in mutant animals. Further, as TnI S150 phosphorylation increases sarcomeric Ca^{2+} sensitivity [Sancho Solis *et al.*, 2011; Oliveira *et al.*, 2012], these changes could explain the increased Ca^{2+} sensitivity observed in demembranated ventricular fibres from mutant animals. However, decreased phosphorylation of TnI at S23/S24 was also observed in mutant tissue samples. As this alteration also increases sarcomeric Ca^{2+} sensitivity, the specific mechanism causing Ca^{2+} sensitization is obfuscated.

Clarification of this mechanism may be accomplished by noting that an overall reduction in TnI phosphorylation was observed in mutant animals, suggesting that the magnitude of phosphorylation decrease at S23/S24 was greater than the increase observed at S150. This is consistent with an understanding that S150 phosphorylation is relatively low [Sancho Solis *et al.*, 2011], whereas S23/S24 phosphorylation is close to stoichiometric [Solaro and Kobayashi, 2011]. Thus, relative changes in S23/S24 phosphorylation have a far greater effect on total TnI phosphorylation. Further, PKA treatment of mutant fibres normalized Ca^{2+} sensitivity to WT + PKA levels, suggesting that differences in S23/S24 phosphorylation predominantly underlie the observed Ca^{2+} sensitization.

Further indication that S150 phosphorylation does not contribute significantly to total phosphorylation of cTnI was given by PhosTag Western blots using a total cTnI antibody. No more than three bands (0P, 1P, 2P) were observed and average states of 1.82, 1.65, and 1.54 P_i/mol cTnI were calculated for WT, heterozygous, and homozygous samples respectively. In comparison, samples from human heart myofibrils ranged from 1.62 P_i/mol cTnI in donor hearts to 0.29 P_i/mol cTnI in failing

hearts [Messer *et al.*, 2009]. Though levels of cTnI phosphorylation are lower in human than in mice, no phosphorylation bands above 2P were observed. Futher, using phosphorylation-site-specific antibodies, Messer et al demonstrated that S23/24 phosphorylation accounts for the majority of sites 1P and 2P and that rarer phosphorylations (e.g. T143) were only observed at higher phosphorylation levels (e.g. 4P) in *in vitro*-phosphorylated samples. As S150 phosphorylation is less than 3 % at baseline [Sancho Solis *et al.*, 2011], it likely does not contribute to the bands observed in the PhosTag Western blots presented in this chapter.

Reduced phosphorylation of MyBPC and myosin RLC may also contribute to the observed dysfunction. In general, these reductions would be expected to slow cross-bridge cycling and diastolic relaxation. Whereas slowed relaxation was observed *in vivo* and in isolated cardiomyocytes, no change in cross-bridge cycling was seen in demembranated fibres. It is unclear if this discrepancy is due to differing experimental conditions (e.g. isometric contractions in fibres vs. unloaded contractions in cardiomyocytes) or an alternative mechanism.

5.5.2 Reduced phosphorylation of Ca^{2+} handling proteins underlies Ca^{2+} transient dysfunction

Blots presented in this chapter show reduced phosphorylation of PLN at S16 and T17 in AMPK R299Q γ2 mutant mice. Either phosphorylation is sufficient to cause disassociation of PLN from SERCA, allowing significantly increased SR Ca^{2+} reuptake [Kranias and Solaro, 1982; Wegener *et al.*, 1989]. The reduction in PLN phosphorylation observed in mutant animals would therefore be a reasonable explanation for the reduced SERCA activity and Ca^{2+} reuptake rates seen in mutant cardiomyocytes.

PLN T17 is one of the few sites investigated in the chapter where reduced phosphorylation cannot be attributed to reduced PKA activity. Instead, this site is a target of Ca^{2+}/CaM-dependent protein kinase, which is activated by increased cytosolic Ca^{2+} concentrations. However, neither diastolic nor systolic Ca^{2+} concentrations were significantly altered in cardiomyocytes from mutant animals. Another possibility that could explain reduction in phosphorylation at both sites is increased activity of protein phosphatase 1, one of three main Ser/Thr phosphatases [Pathak *et al.*, 2005]. In human and experimental heart failure, activity of this phosphatase is increased [Neumann *et al.*, 1997] and is directly associated with reduced phospholamban phosphorylation [Carr *et al.*, 2002].

5.5.3 Contribution of altered contractile function to the pathogenesis of PRKAG2 cardiomyopathy

Results reported in the first three chapters of this thesis provide a plausible mechanism to explain the *in vivo* dysfunction observed in the AMPK R299Q γ2 mutant mice (Figure 5-12). Specifically, the R299Q γ2 mutation results in reduced phosphorylation of key cardiac regulatory proteins. These molecular modifications result in slowed cardiomyocyte Ca^{2+} reuptake and sarcomeric relaxation. Distinguishing these cellular mechanisms is complicated by their inherent interdependence – increased cytosolic Ca^{2+} concentrations due to slowed SR reuptake necessarily slows sarcomeric relaxation, and delayed sarcomeric Ca^{2+} release due to enhanced myofilament Ca^{2+} sensitivity impedes Ca^{2+} reuptake. Together, the cellular mechanisms provide a clear explanation for impaired diastolic relaxation observed *in vivo*. Numerous mechanisms, in particular the Frank-Starling response, could account for the transmission of impaired relaxation to systolic dysfunction. These data suggest that impaired cardiac function in our knock-in

model of PRKAG2 cardiomyopathy is not due to increased glycogen storage but instead reduced contractile capability of the myocardium itself.

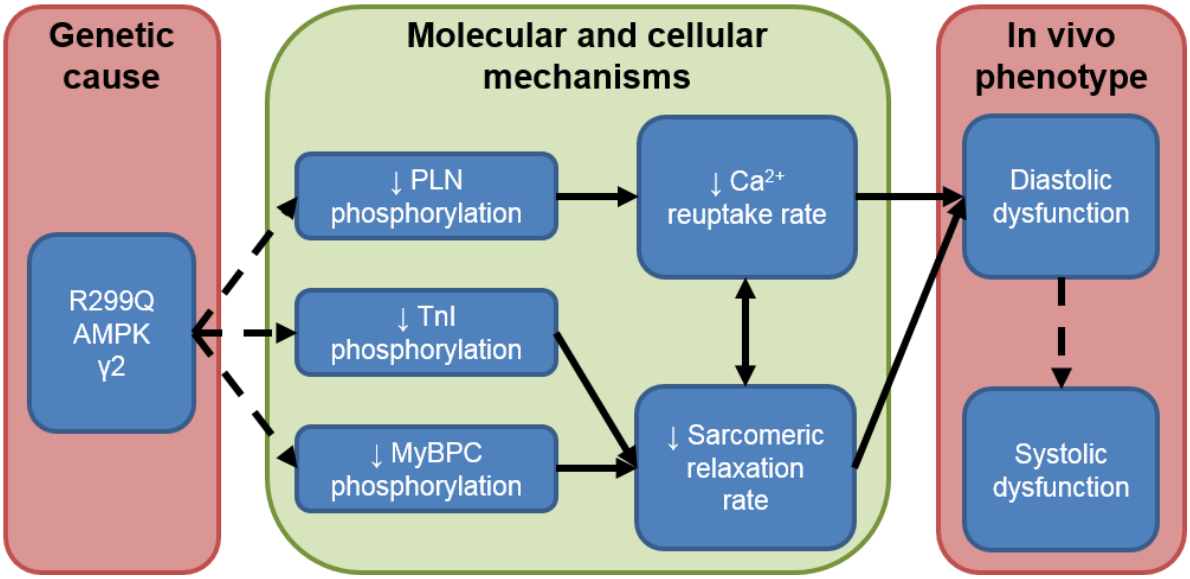


Figure 5-12 - Hypothesized mechanism leading from R299Q AMPK γ2 mutation to whole organ dysfunction. Established causal links between experimental results are shown in solid lines. Implied, or unclear, causal mechanisms are indicated with dashed lines.

The least clear link in this hypothesized mechanism of pathogenesis is the lack of an explanation for how an AMPK γ2 mutation, which causes increased basal AMPK activity, reduces phosphorylation of a variety of regulatory proteins. The simplest pathway linking these established results would be a reduction in activity of PKA, which has been shown to phosphorylate each of the targets. Unfortunately, the promiscuity and nuanced activities of the AMPK and PKA pathways make direct identification of interactions difficult. During glucose starvation, in which AMPK is activated, PKA activity is reduced [Zaman *et al.*, 2009]. In the reverse fashion, PKA has been shown to directly inhibit AMPK by phosphorylating the α subunit at S173 [Djouder *et al.*, 2010]. A negative feedback pathway between AMPK and PKA in the cardiac system is therefore not inconsistent with their known roles. AMPK is

activated by energetic stress and acts to increase ATP levels [Hardie, 2007], while PKA is activated by sympathetic regulation and results in increased ATP usage [Lindemann *et al.*, 1983]. With these opposing activities in mind, an AMPK-activating mutation could plausibly be expected to reduce PKA activity. However, the specific component of the PKA activation pathway that is altered by AMPK signalling is not inherently clear.

A number of potential alterations to the PKA signalling pathway (Figure 5-13) could lead to reduced phosphorylation of target sites. On the PKA-promoting side, down-regulation or inhibition of β-adrenergic receptors, adenylate cyclase, PKA itself, or the A-kinase anchoring proteins (AKAPs) could underlie the effect. In the reverse fashion, up-regulation or activation of phosphodiesterases or phosphatases would cause a reduction in PKA activity. Further, cGMP has also been shown to modify the cAMP response to catecholamines [Stangherlin and Zaccolo, 2012], increasing the number of potential alterations that could explain PKA dysfunction in the AMPK R299Q γ2 mice.

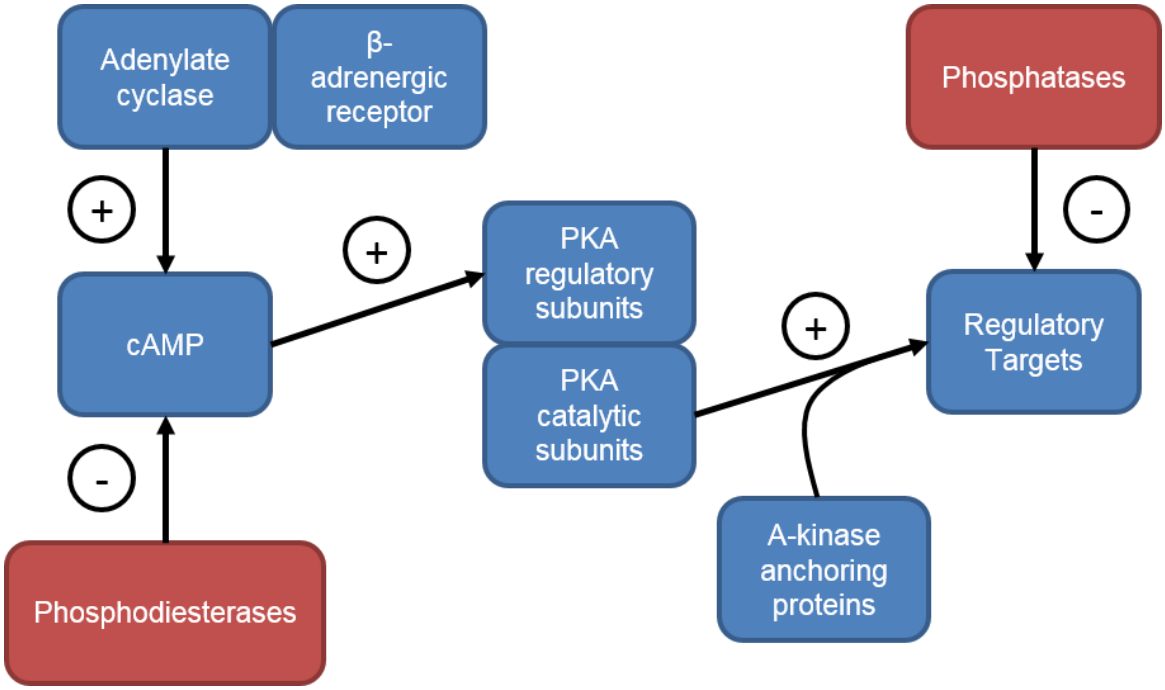


Figure 5-13 - Schematic illustration of the PKA signalling pathway. Activities leading to phosphorylation of PKA target sites are indicated by + symbols whereas - symbols indicate opposing actions.

An indication of the dysfunction in AMPK R299Q γ2 animals was given by the reduction in phosphorylation PKA RII S96. This regulatory subunit binds to and inhibits PKA's catalytic subunit. Binding of cAMP to the regulatory subunit causes detachment from the catalytic subunit and activity of the kinase. Autophosphorylation of PKA RII at S96 reduces its affinity for the catalytic subunit and therefore promotes PKA activity [Rangel-Aldao and Rosen, 1977]. Further, PKA RII S96 phosphorylation strengthens binding to A-kinase anchoring proteins and controls the targeting of PKA activity to essential targets [Zakhary *et al.*, 2000; Manni *et al.*, 2008]. Given that PKA RII S96 is autophosphorylated, the finding of reduced phosphorylation at this site in mutant animals confirms an upstream reduction in PKA activity. Further, reduced PKA RII S96 phosphorylation may contribute to the lower levels of phosphorylation in sarcomeric and Ca^{2+} proteins due to RII-inhibition of PKA activity and impaired AKAP-targeting.

However, regardless of the specific mechanism by which AMPK activation reduces phosphorylation of PKA targets, this pathogenesis mechanism provides a valuable supplement to the glycogen accumulation pathway shown to underlie aspects of the PRKAG2 cardiomyopathy phenotype [Gollob, 2003]. Specifically, though glycogen accumulation may account for electrophysiological components of the phenotype, and contribute to cardiac hypertrophy, aspects of PRKAG2 cardiomyopathy are likely independent of increased glycogen storage [Kim *et al.*, 2014]. Data presented here suggest that *PRKAG2* mutations cause fundamental contractile abnormalities via interaction between the AMPK and PKA pathways. These modifications could underlie the contractile dysfunction observed clinically.

Chapter 6 – Dilated cardiomyopathy-associated mutations in αB-crystallin alter its regulation of cardiac muscle passive stiffness

6.1 Introduction

Passive stiffness of cardiac muscle is primarily controlled by the giant sarcomeric protein titin and the extra-cellular matrix protein collagen. The proteins can be modified in various disease states, resulting in altered ventricular compliance and contributing to diastolic dysfunction [Zile and Brutsaert, 2002]. These alterations are of particular importance in DCM, in which myocardial fibrosis and LV dilatation are canonical features of the clinical phenotype [Watkins *et al.*, 2011]. Mutations known to cause DCM predominantly affect genes encoding sarcomeric and cytoskeletal proteins involved in cardiac muscle stretch sensing [Jefferies and Towbin, 2010], further confirming the importance of ventricular stiffness in disease pathogenesis.

A missense mutation causing a single amino acid substitution (R157H) in the gene encoding the small heat shock protein, αB-crystallin, was found in a population of Japanese DCM patients [Inagaki *et al.*, 2006], but not in control chromosomes. Yet despite αB-crystallin's high cardiac prevalence (3-5 % of total soluble protein [Bhat and Nagineni, 1989]), a complete understanding of its role has yet to be developed. Recent work has suggested that αB-crystallin binds spring-like titin Ig domains and alters their unfolding [Bullard *et al.*, 2004]. With this activity in mind, the DCM-associated R157H mutation may alter overall cardiac muscle stiffness and initiate disease pathogenesis. To better understand interactions between αB-crystallin, titin, and overall cardiac muscle stiffness, a collaboration with the Department of Theoretical and Physical Chemistry at the University of Oxford was established. The

primary goal of our collaborators was to specify the binding interaction of αB-crystallin and titin using mass spectrometry (MS) and nuclear magnetic resonance (NMR).

6.2 Characterization of the titin:αB-crystallin interaction

A solution containing the titin Ig domain I26 and αB-crystallin in a 2:1 ratio was assessed using MS. The mass/charge ratio of generated species ranged from < 7,000 to > 15,000, with definable peaks only in the central (~9,000-11,000) region (Figure 6-1, A). To resolve these peaks and determine their molecular identity, a technique called collision-induced dissociation (CID) was applied. This method involves colliding charged MS fragmentation ions with neutral gas molecules, resulting in further fragmentation of the charged ions [Wells and McLuckey, 2005]. This fragmentation is asymmetric, with fragmented monomers retaining a larger proportion of charge than the stripped oligomers [Benesch *et al.*, 2006]. Stripped oligomers are therefore of a much lower charge state than their parent ions, resulting in a larger separation in mass/charge ratios and improved species identification [Aquilina *et al.*, 2003]. CID spectra generated from the central mass/charge peak of the total I26:αB-crystallin MS spectrum could be represented by the sum of spectra of αB-crystallin and titin I26 (Figure 6-1, B & C). The species identified in the CID spectrum ranged from 21-27 αB-crystallin monomers paired with < 1 titin I26 domain. These species represent oligomers that lost 2 subunits during CID.

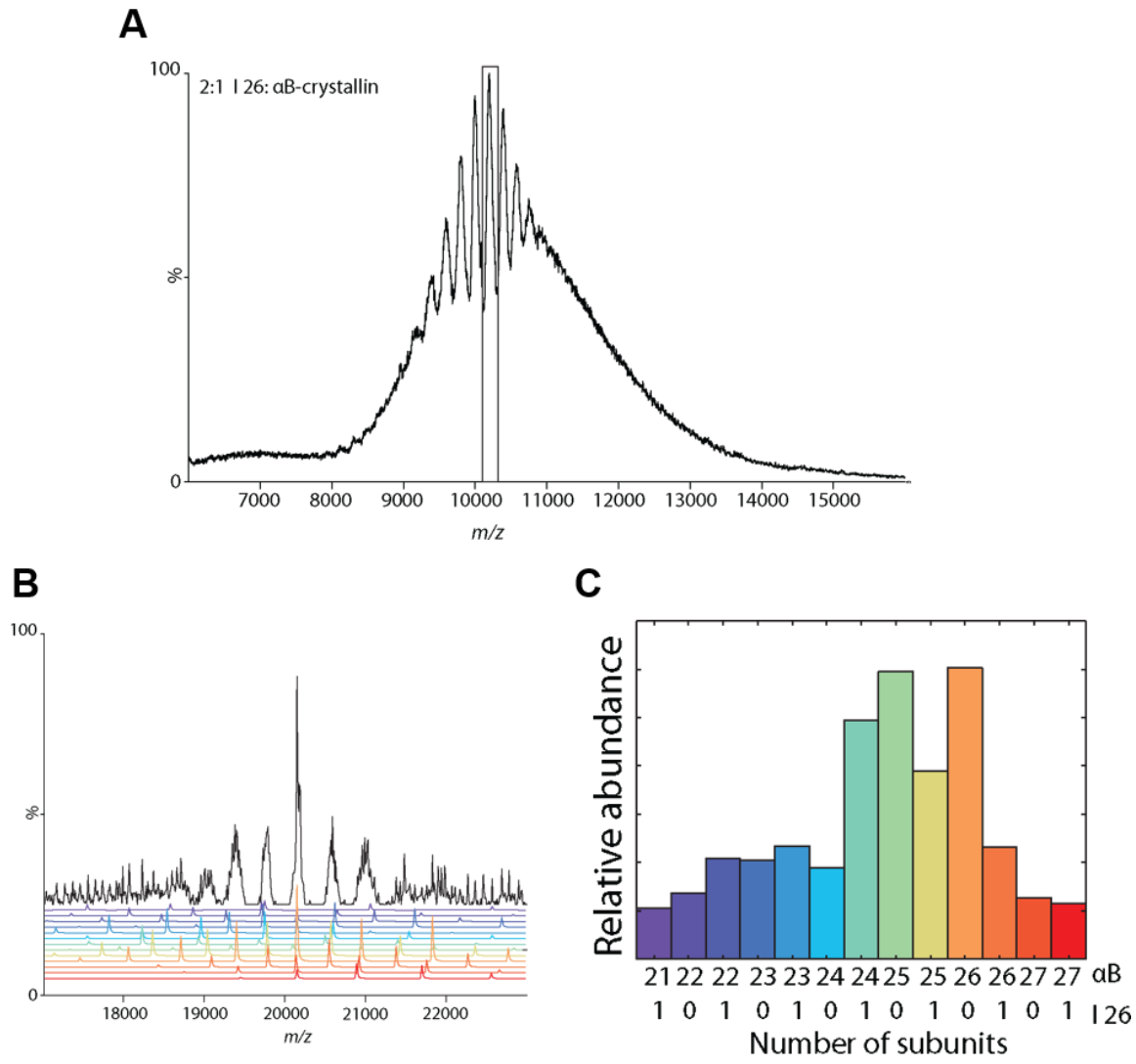


Figure 6-1 – Native mass spectrum (A) and high energy collision-induced dissociation (CID) (B) of a 2:1 titin I26:αB-crystallin ratio, and relative abundance of contributing species (C). Native mass spectroscopy yields overlapping, non-resolvable m/z peaks. Dissolution of the central m/z peak (boxed) via CID [Benesch *et al.*, 2006] results in greater separation of charge states, allowing resolution of peaks. Contributing species were determined to be oligomers of 20+ αB-crystallin monomers and 0-1 titin I26 domains.

To further clarify the interaction between αB-crystallin and titin I26, NMR measurements were made of the proteins in isolation and together. Comparisons between individual and combined spectra revealed no significant shifts in spot position (Figure 6-2). However, numerous spots associated with both αB-crystallin and titin I26 exhibited dramatically differing intensity when both proteins were

analysed simultaneously. Some spots observed in the individual spectra were completely absent in the combined spectrum. These results suggest binding between the two proteins. Further, as the only portion of αB-crystallin visible in its NMR spectrum is its highly flexible, polar C-terminal region [Treweek *et al.*, 2010], these results suggest that titin binding is accomplished via this domain.

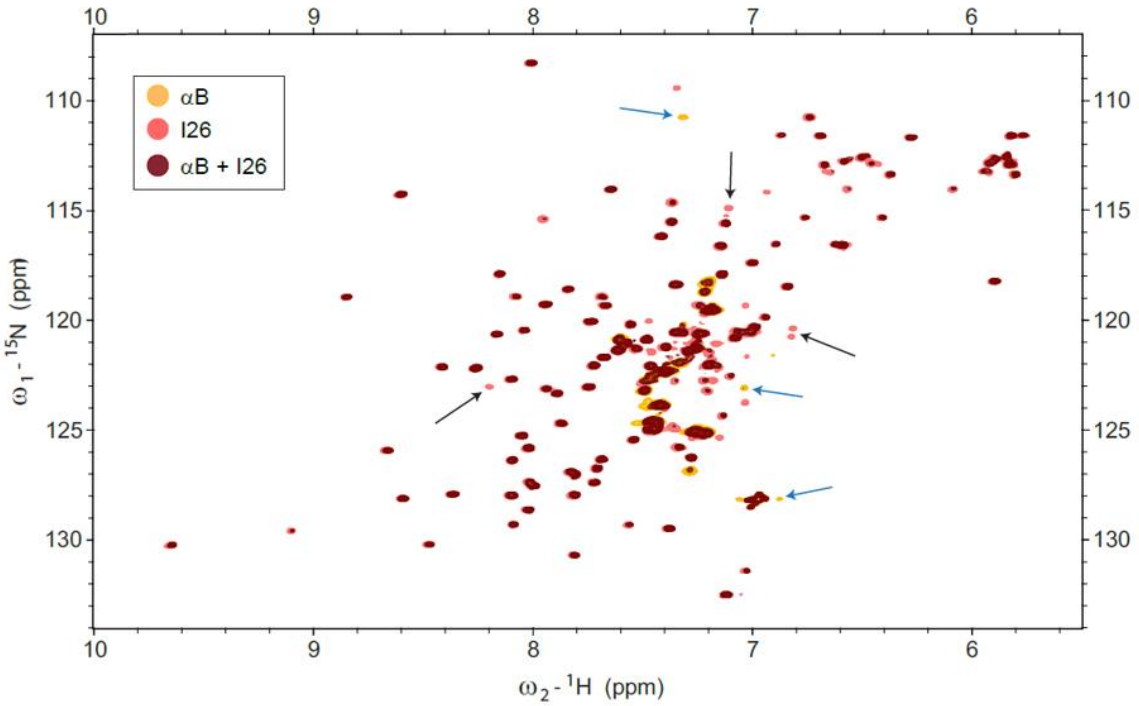


Figure 6-2 – Nuclear magnetic resonance spectra of αB-crystallin (yellow), titin (pink), and a mixture of the two (red). Neither titin nor αB-crystallin independent peaks shift position dramatically in the mixed spectra. However, intensity of spots does vary considerably, with some titin and αB-crystallin peaks disappearing entirely in the mixed spectra (black and blue arrows, respectively).

In αB-crystallin oligomers, the flexible C-terminal region is proposed to bind to the core region of adjacent molecules. The structural similarity of this core domain and titin Ig-domains (Figure 6-3) suggests that this C-terminal region could also bind titin, as suggested by the NMR results. Specifically, a 9-AA palindromic peptide (ERTIPITRE) from αB-crystallin's C-terminus, including the 157 residue, fits the binding groove of both αB-crystallin's core domain and the titin Ig domain.

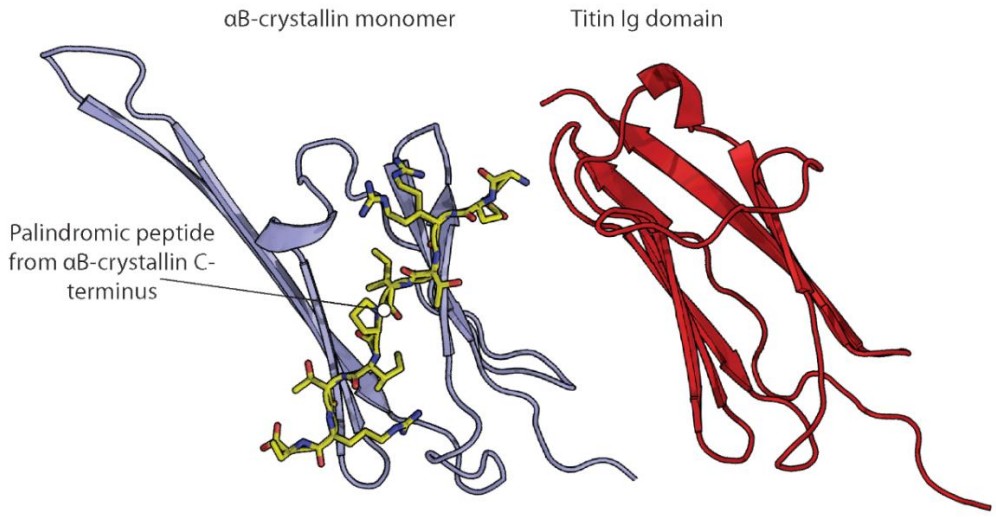


Figure 6-3 – Ribbon structures of αB-crystallin monomer, titin Ig domain, and αB-crystallin C-terminal binding peptide. A 9-AA peptide from αB-crystallin's C-terminus is hypothesized to bind to a groove within adjacent αB-crystallin monomers and facilitate formation of large oligomers. Structural similarity between the αB-crystallin groove and titin Ig domains suggests that the C-terminal peptide may also be responsible for binding titin.

To determine if this hypothesized interaction occurs *in vitro*, a 1:50 mixture of tandem titin Ig domains (26/27) and the αB-crystallin C-terminal peptide was measured using mass spectrometry. The resulting spectrum revealed large peaks matching the expected titin tandem domain mass/charge values as well as smaller peaks suggesting the binding of 1 or 2 peptides (Figure 6-4). Given large molar excess of peptide, this result suggests weak or transient binding of the peptide to up to two positions within the tandem titin domain.

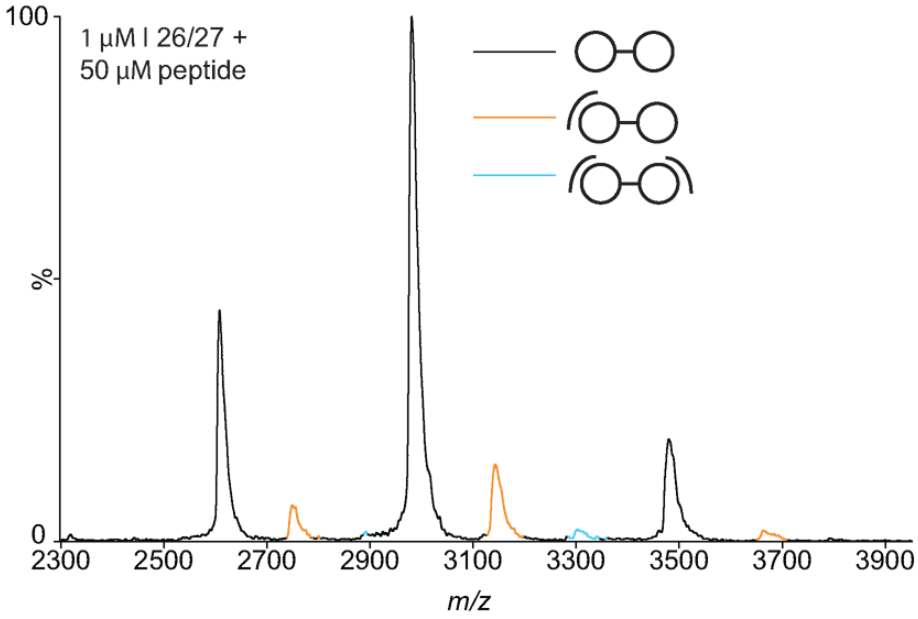


Figure 6-4 - Native mass spectrum of 1 µM titin I26/27 + 50 µM αB-crystallin C-terminal binding peptide. Black peaks represent tandem titin Ig domains without bound peptide, orange peaks represent the binding of 1 peptide per tandem titin domain, and blue peaks the binding of 2 peptides per tandem titin domain.

6.3 Specific aims

The work of our collaborators demonstrated that αB-crystallin forms large oligomers (20+ monomers) and binds to titin Ig domains. This interaction is likely facilitated by its highly flexible, polar C-terminal region. Further, a 9-AA peptide from αB-crystallin's C-terminus was shown to bind directly to titin Ig domains in isolation. To understand the physiological significance of these interactions, measurements using demembranated mouse ventricular muscles were undertaken. The specific aims of this work were the following:

I. Develop a methodology to quantify cardiac muscle passive stiffness
II. Using this method, assess cardiac muscle stiffness with and without αB-crystallin

III. Determine the effect of the DCM-associated R157 mutation on αB-crystallin's activity

IV. Investigate the stiffening potential of a peptide engineered based on the hypothesized titin-binding domain of αB-crystallin

6.4 Development of a measure of cardiac stiffness

Characterizations of cardiac muscle stiffness are often limited to a basic relationship between SL and passive (i.e. Ca^{2+} independent) force. However, the viscoelastic nature of biological materials results in time- and history-dependent passive forces. Therefore, to thoroughly and reproducibly assess cardiac muscle stiffness it is necessary to apply an automated series of length changes during force recording. Here, mouse left ventricular muscle fibres were sequentially stretched from a short physiological length (SL = 2.0 μm) to a super-physiological length (SL = 2.6 μm) at 0.1 μm increments. Upon application of this strain and hold procedure, corresponding stresses induced in the fibre decreased over time (Figure 2-3). This property is termed "stress relaxation" and is characteristic of all viscoelastic materials [Fung, 1993].

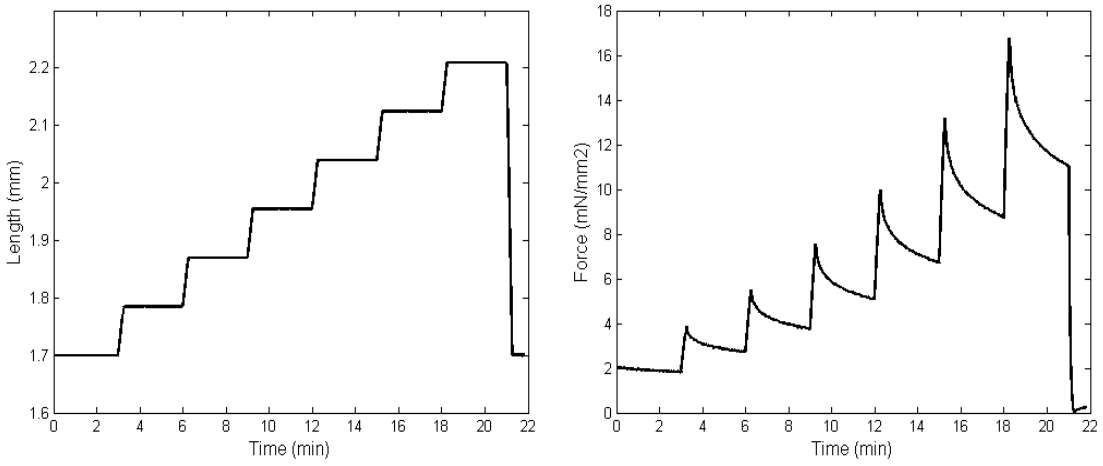


Figure 6-5 - Characteristic stress relaxation curves of cardiac muscle fibres stretched from sarcomere length 2.0 μm to 2.6 μm by increments of 0.1 μm.

To quantify these stress relaxation curves and determine physical properties of the fibres it is desirable to fit the raw data with an appropriate equation. Prior publications assessing stress relaxation behaviour have applied first-, second-, or third-order exponential decay functions to fit the data [Minajeva *et al.*, 2001]. However, no rationale for the use of these fits was provided, and fit coefficients were not given any physiological relevance. Therefore, to fully understand the importance of the stress relaxation fits, a viscoelastic model of the behaviour was developed from first principles. In general, these models are comprised of Hookean springs and Newtonian dashpots (Figure 6-6) [Roylance, 2001].



Figure 6-6 - Illustration of Hookean spring (A) and Newtonian dashpot (B). Figures adapted from Wikipedia - Viscoelasticity.

The physical properties of these theoretical elements are uniquely defined. For Hookean springs, the relationship between stress (σ) and strain (ϵ) is given by

$$\sigma = k\epsilon$$

where the spring constant *k* has units of N/m^2. Springs therefore exhibit instantaneous deformation relative to an applied stress. In addition, their action is completely reversible, modelling the storage of mechanical energy as strain energy. In Newtonian dashpots, the relation between stress and strain rate is given by

$$\sigma = \eta \frac{d\epsilon}{dt}$$

where the viscosity constant η has units of N-s/m^2. Dashpots therefore model time-dependent relaxation and a loss of mechanical energy to entropy. Springs and dashpots can be combined, either linearly or in parallel, to form models with properties similar to viscoelastic materials. The most commonly used viscoelastic models to fit stress relaxation data are the Maxwell and Standard Linear Solid (SLS) models (Figure 6-7).

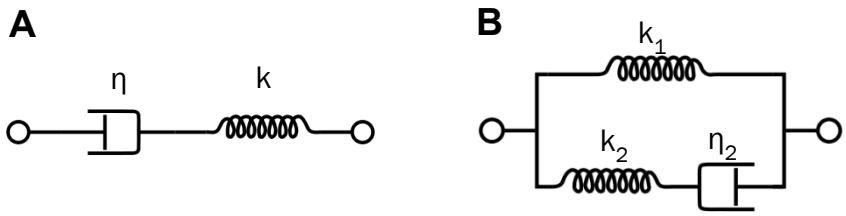


Figure 6-7 - Illustration of Maxwell (A) Standard Linear Solid (B) viscoelastic models.

To derive equations governing the behaviour of these models, properties of each element must be combined. If elements are added in series, the stress on each element is equal to the total stress while the total strain is equal to the sum of the strain in each element. If elements are combined in parallel, the strain on each element is equal to the total strain while the total stress is equal to the sum of the stress in each arm. These properties, combined with the equations governing springs and dashpots, allow derivation of general stress-strain and stress relaxation

equations for the models. For the Maxwell model, stress and strain relationships are given by

$$\sigma = \sigma_s = \sigma_d$$

$$\epsilon = \epsilon_s + \epsilon_d$$

where the subscripts *s* and *d* represent the spring and dashpot, respectively. Differentiating the strain equation allows substitution of the characteristic spring and dashpot equations, yielding a single stress-strain relationship for the Maxwell model:

$$\frac{d\epsilon}{dt} = \frac{d\epsilon_s}{dt} + \frac{d\epsilon_d}{dt}$$

$$\frac{d\epsilon}{dt} = \frac{1}{k} * \frac{d\sigma}{dt} + \frac{\sigma}{\eta}$$

During stress relaxation, strain is constant ($d\epsilon/dt = 0$) and the first order differential equation for stress can be solved to yield:

$$\sigma(t) = \sigma_0 e^{\frac{-k}{\eta} * t}$$

where σ_0 is the initial stress and *t* is time after stretch. In this model, as time goes to infinity, stress decays to zero. However, in cardiac muscle fibres, stress relaxation curves decay to a non-zero value. Therefore, a simple Maxwell model will not accurately fit stress relaxation curves from cardiac muscle fibres.

The SLS model represents a reasonable second estimation because its parallel spring and Maxwell elements will yield both decaying and constant forces during stress relaxation. Solving for the stress-stain relationship of the entire model using a similar methodology yields

$$\frac{d\epsilon}{dt} = \frac{\frac{k_2}{\eta_2}\left(\frac{\eta_2}{k_2} * \frac{d\sigma}{dt} + \sigma - k_1\epsilon\right)}{k_1 + k_2}$$

Again, during stress relaxation, strain is constant (dϵ/dt = 0) and the differential equation above can be solved to yield:

$$\sigma(t) = k_1 + k_2 e^{\frac{-k_2}{\eta_2} * t}$$

As can be seen from the equation, this model implies a stress relaxation response that decays (t → ∞) to a non-zero value determined by the stiffness of the independent spring. However, fitting this model to experimental data yields unsatisfactory results (Figure 6-8).

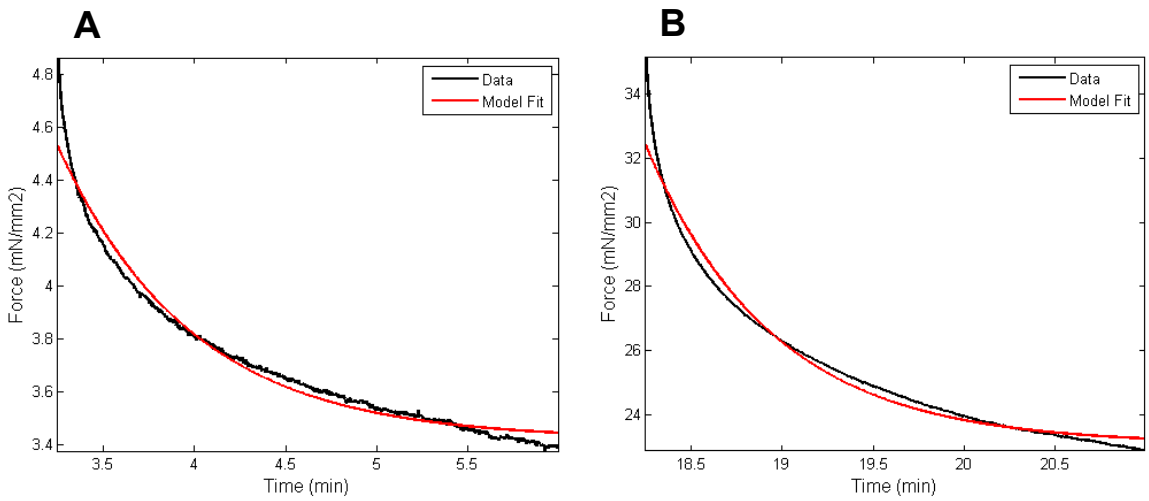


Figure 6-8 - Characteristic fits of cardiac muscle fibre stress relaxation data using a Standard Linear Model at sarcomere lengths 2.1µm (A) and 2.6µm (B).

The cause of this poor fit is that the SLS model assumes a single decay time whereas real biological tissues exhibit multiple relaxation times due to complex composition of materials. To account for this complexity, the mechanical model must be expanded to include additional Maxwell elements in parallel. This extension

is termed the Maxwell–Wiechert Model and can include as many Maxwell elements as necessary to accurately simulate the system response. In the case of cardiac muscle fibres, two Maxwell elements were found to be sufficient to fit the data (Figure 6-9).

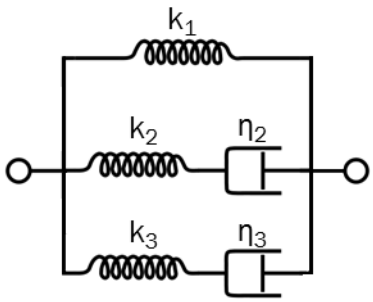


Figure 6-9 - Illustration of viscoelastic model used for fitting cardiac fibre stress relaxation data.

Solving for the stress-strain relationship of this model is simplified using the Laplace transform whereby

$$\mathcal{L}\left(\frac{d\epsilon}{dt}\right) = s\bar{\epsilon}$$

$$\mathcal{L}\left(\frac{d\sigma}{dt}\right) = s\bar{\sigma}$$

and the stress-strain relationship for this model is given by:

$$\bar{\sigma} = \bar{\sigma}_1 + \left(k_1 + \frac{k_2 s}{\left(s + \frac{k_2}{\eta_2}\right)} + \frac{k_3 s}{\left(s + \frac{k_3}{\eta_3}\right)}\right)\bar{\epsilon}$$

During stress relaxation (dϵ/dt = 0), the above equation is solved to yield:

$$\sigma(t) = k_1 + k_2 e^{\frac{-k_2}{\eta_2} * t} + k_3 e^{\frac{-k_3}{\eta_3} * t}$$

The substitution $\tau = \eta/k$ further simplifies the equation and improves fitting performance, yielding a final model:

$$\sigma(t) = k_1 + k_2 e^{\frac{-t}{\tau_2}} + k_3 e^{\frac{-t}{\tau_3}}$$

The second and third terms are differentiated by selection of initial fit conditions – a small τ_2 and large τ_3. This model accurately fits cardiac muscle fibre stress relaxation data, allowing quantification of the viscoelastic parameters of the muscle at multiple lengths (Figure 6-10). These data permit comparisons within individual fibres (Figure 6-11) as well as among fibres.

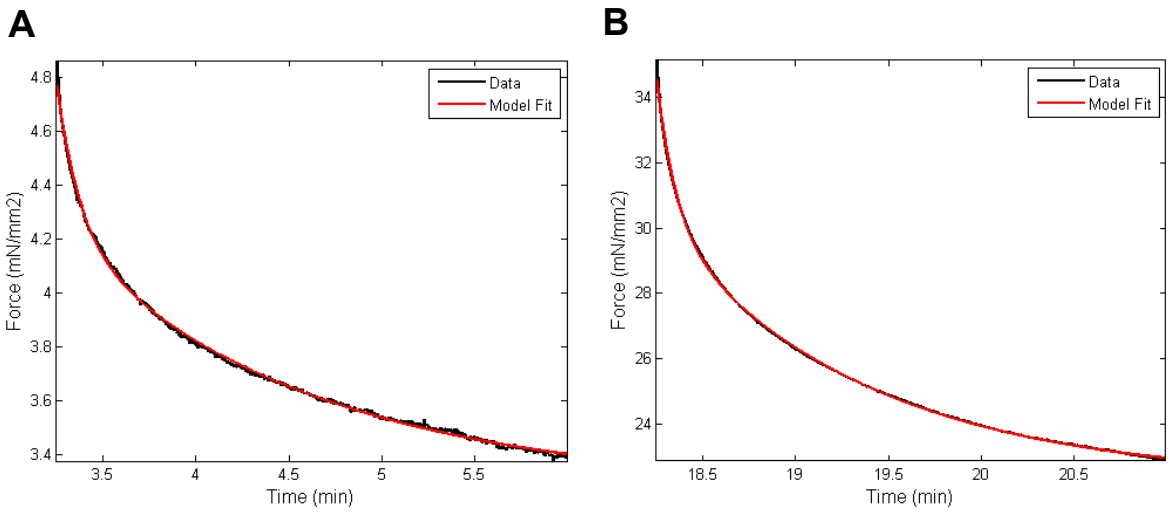


Figure 6-10 - Characteristic fits of cardiac muscle fibre stress relaxation data using a Maxwell–Wiechert model at sarcomere lengths 2.1µm (A) and 2.6µm (B).

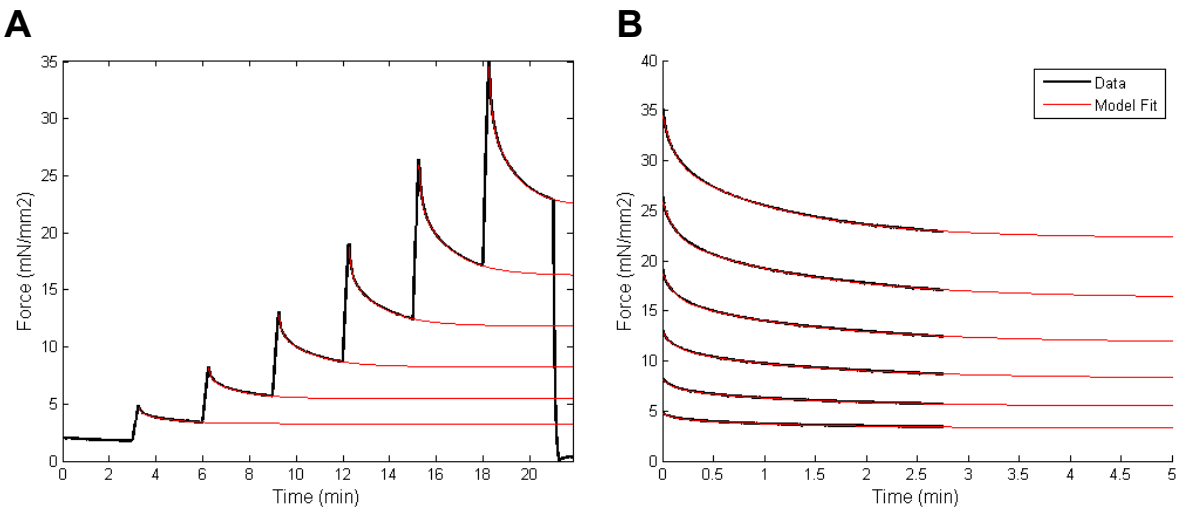


Figure 6-11 - Illustration of model fits to stress relaxation data at sarcomere lengths between 2.0μm and 2.6μm over the course of a single experiment (A) as well as on isolated stress relaxation curves (B).

Physiologically, the fit coefficients represent:

Table 2 - Physiological significance of viscoelastic fit parameters.

Fit parameter	Significance
k_1	Residual stiffness
k_2	Rapidly decaying stiffness
k_3	Slowly decaying stiffness
τ_2	Rate of rapid stiffness decay
τ_3	Rate of slow stiffness decay

An obvious question derived from this decomposition is whether each fit parameter also corresponds to a particular cellular material (e.g. titin or collagen). This consideration is clarified by experiments in which titin-based stiffness was eliminated by de-polymerizing the thick and thin filaments using 0.6 M KCl and 1.0 M KI solutions [Wu *et al.*, 2000], which revealed that both KCl/KI-sensitive (~titin) and KCl/KI-insensitive (~collagen) forces exhibit viscoelastic behaviour. Further, collagen alone is known to exhibit stress relaxation curves characterized by multiple

exponential decay constants [Purslow *et al.*, 1998]. These results suggest that the stress relaxation behaviour of cardiac muscle cannot be mathematically decomposed into contributions by each material. Instead, the total behaviour of the fibres represents the sum of contributions from all elements of the preparation, each possessing distinct viscoelastic activity.

The sum of the stiffness coefficients (k_1, k_2, k_3) represents total stiffness of the fibre at each length (prior to any stress relaxation decay). The ratio of each individual stiffness term over this total stiffness value represents the contribution of that type of stiffness to the total. Comparisons between each of these values over the range of SLs yield significant information regarding the passive stiffness behaviour of the tissue. Of particular interest is the relationship between total stress and strain, which exhibits second order increases over the experimental range (Figure 6-12, A). The elastic stiffness constant (E) was also calculated for each fibre by plotting elastic stiffness (dσ/dϵ) against stress and applying a linear fit [Mirsky, 1976]:

$$\frac{d\sigma}{d\epsilon} = E * \sigma + c$$

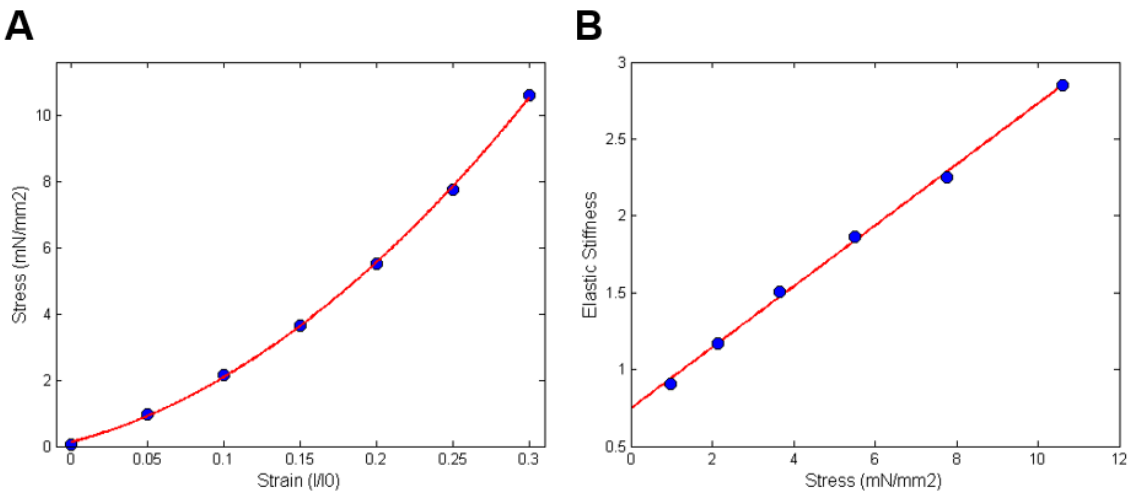


Figure 6-12 - Relationship between stiffness and sarcomere length. All measures of stiffness (total, residual, rapidly decaying, slowly decaying) were plotted against strain (A) and the curves

were fit with a second order polynomial. The elastic stiffness ($d\sigma/d\epsilon$) was also plotted against stress to determine the elastic stiffness constant of each fibre (B).

It was occasionally convenient to represent the stiffness of each fibre as a single value. Young's Modulus, the slope of a linear fit to the stress-strain relationship, was used as a basic approximation.

6.4 Effect of WT and DCM-associated αB-crystallin mutant on cardiac muscle stiffness

The effect of αB-crystallin on force development in cardiac muscle was measured in murine left ventricular trabeculae. Fibres were treated overnight in a solution containing 1 % Triton X-100, which is a detergent that permeabilizes eukaryotic membranes [Koley and Bard, 2010]. This treatment was hypothesized to remove endogenous αB-crystallin due to its predominantly cytosolic localization [van de Klundert *et al.*, 1998]. Fibres were then incubated in a relaxing solution containing human αB-crystallin for 1 hour and subsequently mechanically assessed in solutions containing the same αB-crystallin concentration. The removal of endogenous αB-crystallin and replacement with recombinant αB-crystallin was confirmed via Western blot. Intact (unskinned) fibres contained detectable levels of endogenous αB-crystallin whereas BSA-incubated demembranated fibres had little to no remaining αB-crystallin. Unwashed skinned fibres incubated with recombinant αB-crystallin exhibited greater levels of αB-crystallin than intact fibres (Figure 6-13).

Fibres incubated with αB-crystallin exhibited significantly increased stiffness compared to BSA-incubated controls (Figure 6-14) at all sarcomere lengths. Fibres incubated with the mutant R157H αB-crystallin also exhibited increased stiffness, but the effect was significantly smaller. Fitting the stress-strain curves with a line revealed that the average linear Young's Moduli of WT and R157H αB-crystallin-

incubated fibres were 136 % and 74 % greater than the average linear Young's Modulus of BSA-incubated fibres, respectively. However, no difference in Ca^{2+}-dependent active force development was observed in αB-crystallin-incubated fibres.

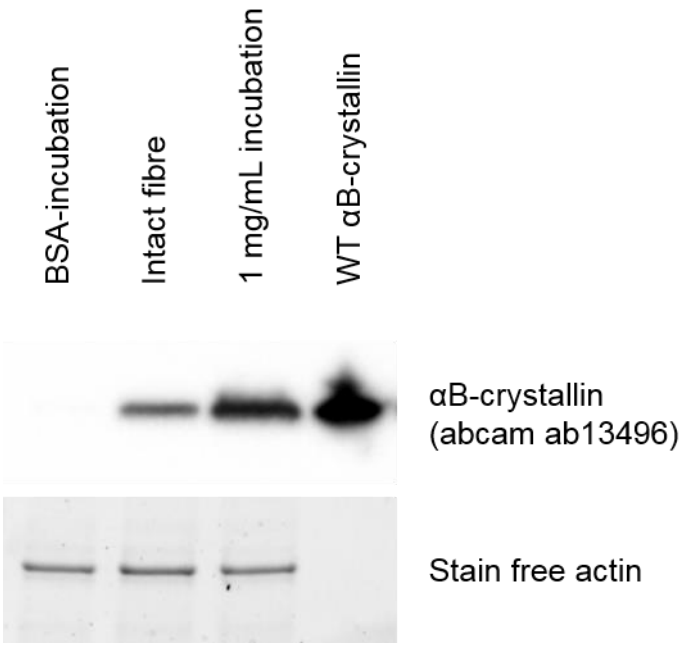


Figure 6-13 – Characteristic Western blot using an antibody targeting αB-crystallin and stain-free gel as a loading control. Skinned fibres incubated with BSA exhibited little to no endogenous αB-crystallin whereas fibres incubated with αB-crystallin yielded a positive result. Intact (unskinned) fibres expressed an intermediate level of αB-crystallin.

The relative stiffness of αB-crystallin-incubated fibres compared to BSA-incubated controls was relatively consistent across sarcomere lengths (Table 3). However, both WT and R157H αB-crystallin caused the greatest stiffening at the physiological maximum sarcomere length of 2.3 μm.

The viscoelastic model used to fit stress relaxation curves allowed the decomposition of total stiffness into residual, rapidly decaying, and slowly decaying stiffness at each sarcomere length (Figure 6-15). Relative contribution of these parameters to total stiffness was approximately 70 %, 20 %, and 10 %, respectively. Further, as sarcomere length increases, contribution of residual stiffness decreases whereas contribution of both decaying stiffnesses increases.

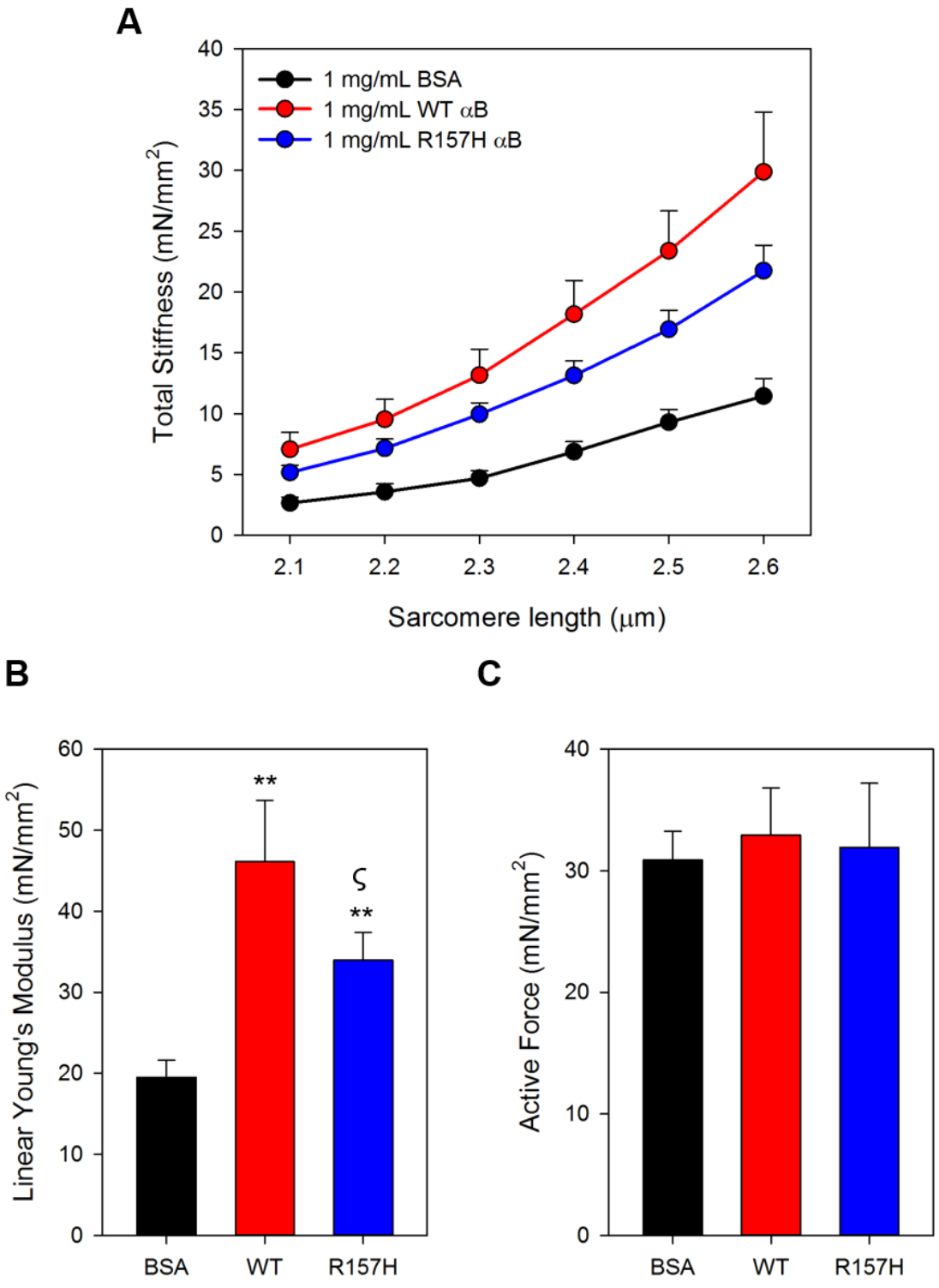


Figure 6-14 – Effect of full length WT and R157H αB-crystallin on total cardiac stiffness and active force. The total stiffness at each sarcomere length (A) was significantly increased in fibres incubated with WT or R157 αB-crystallin compared to BSA-incubated controls. Overall stiffness, as measured by a linear Young's modulus (B), was increased in both αB-crystallin groups compared to controls, though to a lesser extent with R157H αB-crystallin. No significant differences in active force production at SL = 2.0 μm (C) was observed between groups. ** indicates a $p < 0.01$ difference compared to control, ς indicates a $p < 0.05$ difference between WT- and R157H-incubated groups using post-hoc corrected tests. 15-20 fibres were measured per group.

Table 3 – Relative stiffness of WT and R157H αB-crystallin-incubated fibres compared to BSA-incubated controls.

SL (μm)	WT αB-crystallin	R157H αB-crystallin
2.1	2.66	1.94
2.2	2.66	2.00
2.3	2.80	2.12
2.4	2.64	1.91
2.5	2.51	1.82
2.6	2.61	1.90

To determine if observed changes in stiffness composition were significantly different, linear fits were made to each plot and coefficients of the fits compiled (Figure 6-16). The negative slope of residual stiffness and positive slope of rapidly decaying stiffness was significant across all three groups. The negative slope of slowly decaying stiffness was only significant for R157H αB-crystallin-incubated fibres. The average intercept of the residual stiffness fits for WT αB-crystallin-incubated fibres was significantly lower than both other groups. The average intercept of the rapidly decaying stiffness fits was significantly higher in WT αB-crystallin-incubated fibres than BSA-incubated controls.

The rates of force decay following each fibre lengthening were measured via two exponential coefficients in the fitting equation. Mean values for each parameter were plotted against sarcomere length (Figure 6-17). No significant differences in either decay rate were observed over the range of sarcomere lengths or between groups.

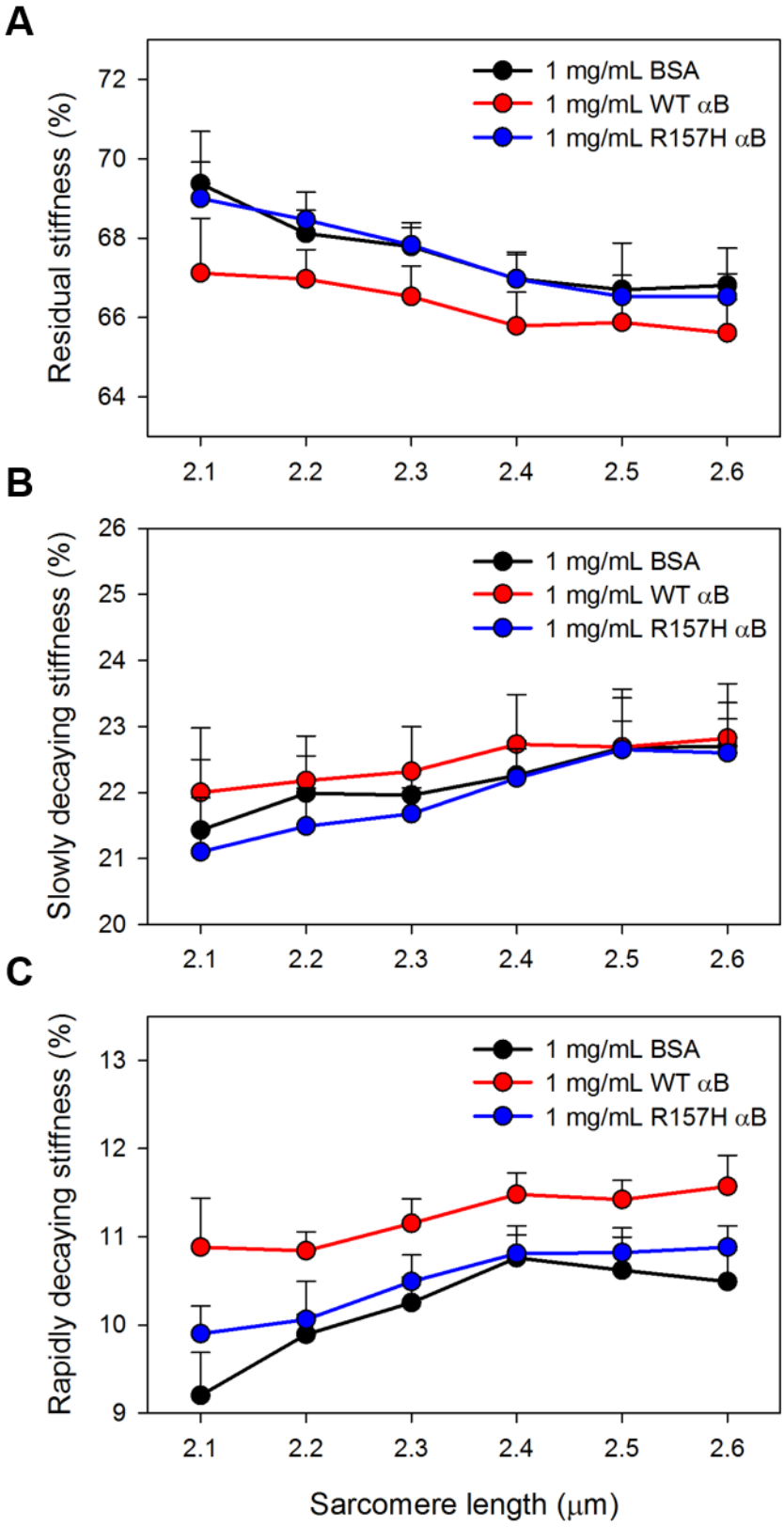


Figure 6-15 – Contribution of residual (A), slowly decaying (B), and rapidly decaying (C) stiffness as a percentage of total stiffness at each sarcomere length. Fibres incubated with WT αB-crystallin exhibited a mild shift of stiffness contribution from residual to rapidly decaying across all lengths.

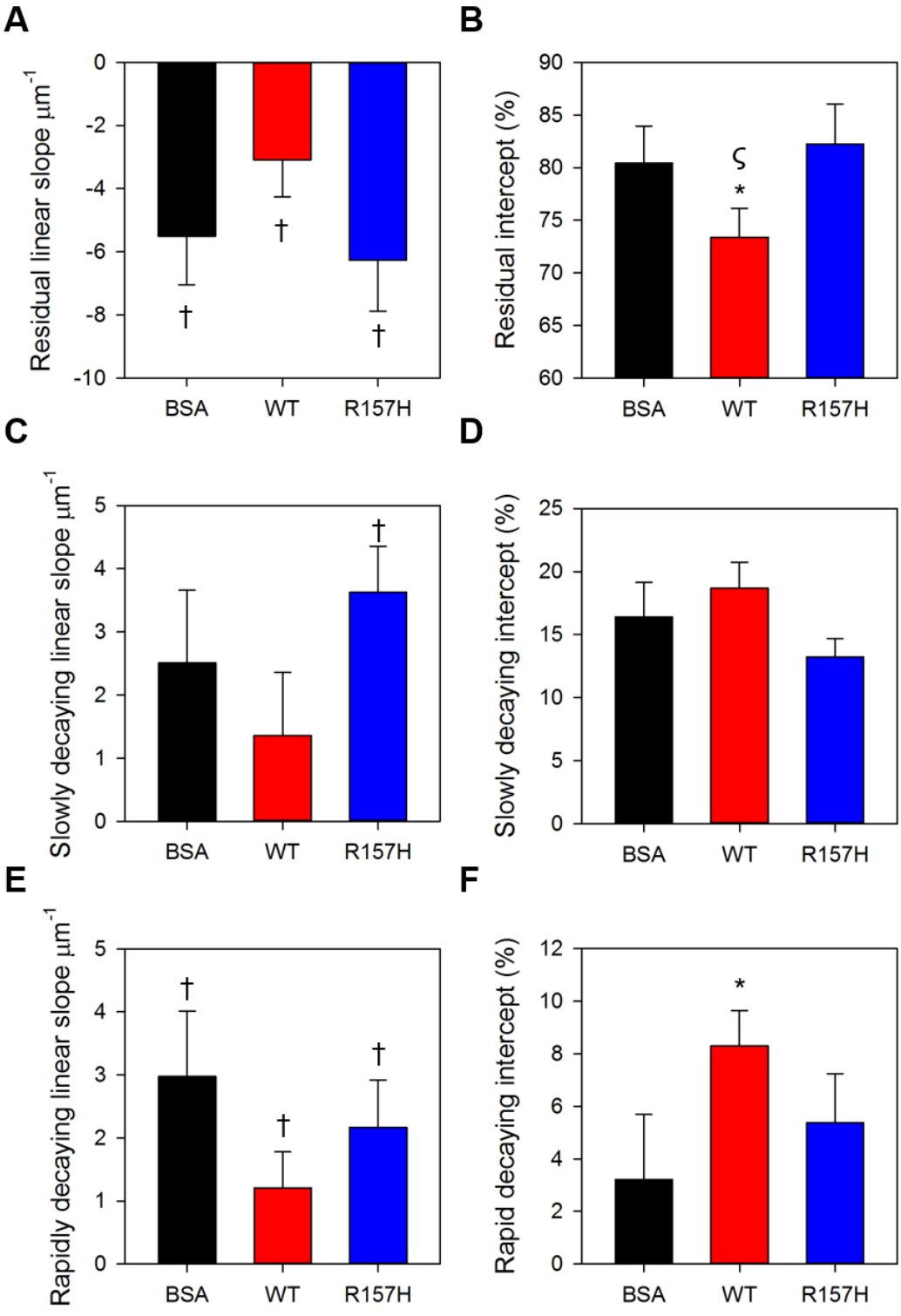


Figure 6-16 – Mean +/- SEM coefficients of best linear fit of residual (A & B), slowly decaying (C & D), and rapidly decaying (E & F) stiffness vs sarcomere length. Fibres incubated with WT αB-crystallin exhibited a reduced average residual stiffness intercept compared to control and R157H αB-crystallin-incubated fibres and an increased average rapidly decaying stiffness intercept compared to control. * indicates $p < 0.05$ compared to BSA and ς indicates $p < 0.05$ compared to R157H by post-hoc corrected test. † indicates a significantly ($p < 0.05$) non-zero slope by one-sample t-test.

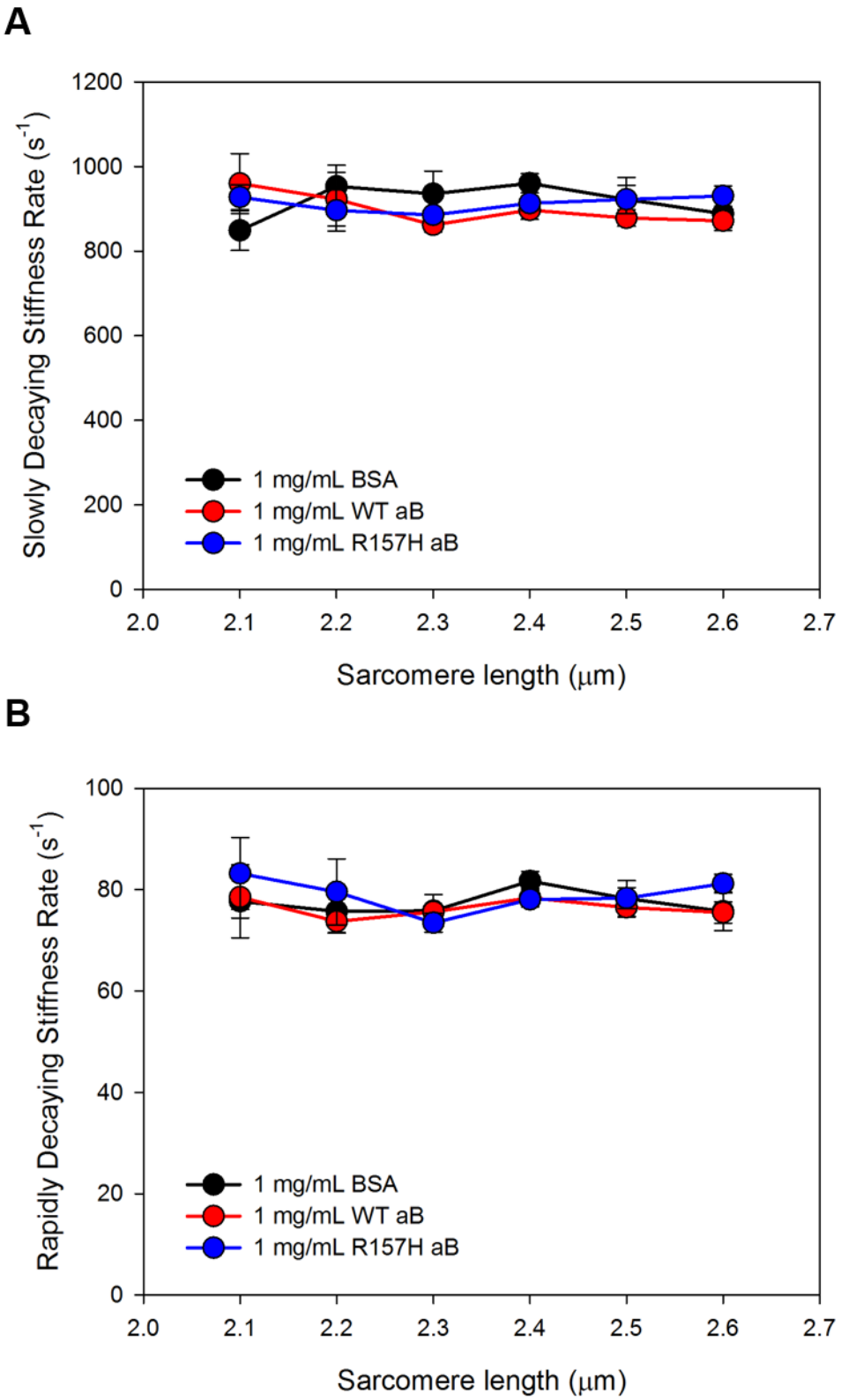


Figure 6-17 – Mean +/- SEM slow (A) and rapid (B) stiffness decay rates vs sarcomere length. No significant differences in decay rates were observed between genotype groups or across sarcomere lengths.

6.5 Effect of 9-AA peptide on cardiac muscle stiffness

A 9-AA peptide from αB-crystallin's C-terminus was shown to bind to titin Ig domains in mass spectrometry experiments. To determine if this peptide is sufficient to alter overall cardiac muscle stiffness, demembranated fibres were incubated and stretched in a solution containing the WT peptide (ERTIPITRE) or its R157H analogue (EHTIPITRE). The peptide concentration in these solutions matched the molar equivalent of full length αB-crystallin (1 mg/ml full length αB-crystallin = 50 μM = 0.055 mg/ml peptide). Control fibres were incubated in a solution containing equivalent concentrations of a peptide with identical amino acids in a random order (TIERPREIT). Fibres incubated with the titin-binding peptides exhibited increased stiffness compared to control fibres (Figure 6-18) with the WT peptide showing a greater effect than the R157H peptide.

To assess the concentration dependence of stiffening, fibres were incubated in full length WT and R157H αB-crystallin at 0.5, 1.0, and 5.0 mg/ml concentrations. These experiments were repeated using peptides at equivalent molar concentrations. The stiffening effect of full-length WT αB-crystallin exhibited a significant concentration dependence (Figure 6-19). All other treatments caused comparable levels of stiffening at all three incubation concentrations.

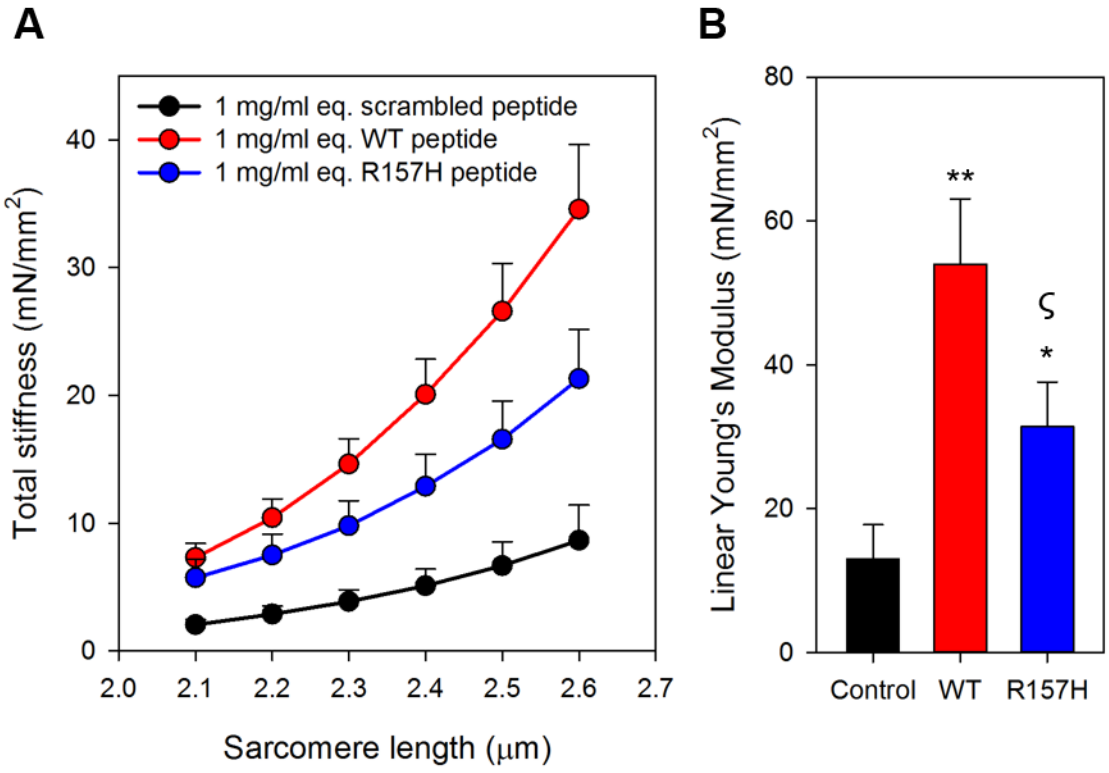


Figure 6-18 – Effect of WT and R157H mutant 9-AA titin-binding peptide on cardiac muscle stiffness. The total stiffness at each sarcomere length (A) was significantly increased in fibres incubated with WT or R157H peptides compared to scrambled peptide-incubated controls. Overall stiffness, as measured by a linear Young's modulus (B), was increased in both αB-crystallin peptide groups compared to controls, though to a lesser extent with the R157H peptide. */** indicates a $p < 0.05/0.01$ difference compared to control, ς indicates a $p < 0.05$ difference between WT- and R157H-incubated groups using post-hoc corrected tests. 15-20 fibres were measured per group.

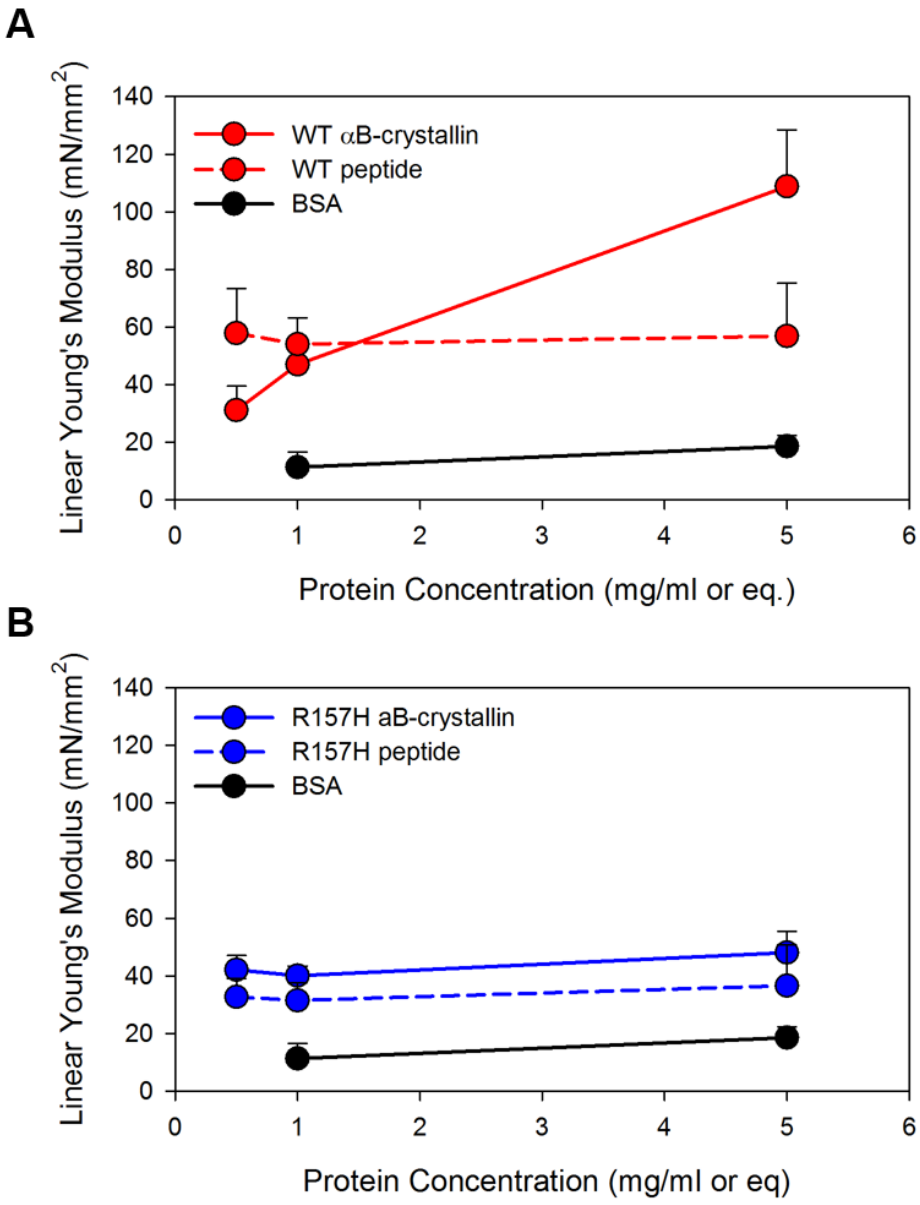


Figure 6-19 – Concentration dependence of fibre stiffness following incubation with full length WT αB-crystallin and titin-binding WT peptide (A) and full length R157H αB-crystallin and titin-binding R157H peptide (B). A concentration dependence of fibre stiffening was observed following incubation with full length WT αB-crystallin, but not any other treatment.

6.6 Discussion

In this chapter, the role of αB-crystallin in regulating cardiac muscle stiffness was assessed. First, a method for assessing cardiac muscle stiffness was developed from first principles. This method was utilized to measure the effect of αB-crystallin on total ventricular muscle stiffness. The differing effect of the DCM-associated R157H αB-crystallin was also probed. Finally, the titin-binding and cardiac-stiffening effect of a 9-AA peptide from the C-terminus of αB-crystallin was measured. The major results of these experiments were:

I. The development of a three-stage viscoelastic model representing residual, rapidly decaying, and slowly decaying stiffness accurately fits stress relaxation in demembranated cardiac muscle fibres.
II. Incubation with αB-crystallin increased the stiffness of demembranated cardiac muscle and increased the contribution of rapidly decaying stiffness to total stiffness, but did not affect active force production. Mutant R157H αB-crystallin caused a smaller stiffening effect.
III. A 9-AA titin-binding peptide that includes the 157 residue, shown to bind titin *in vitro*, caused a milder level of stiffening compared to full-length αB-crystallin.

6.6.1 Novel insight into the αB-crystallin:titin interaction

The binding of αB-crystallin to titin was initially established by fractioning a sample of porcine myocardium and noting the presence of αB-crystallin within the titin fraction (Figure 6-20) [Golenhofen *et al.*, 2002]. This interaction was further specified by comparing the location of αB-crystallin-binding antibodies to antibodies binding known regions of titin in stretched rabbit myofibrils [Bullard *et al.*, 2004]. These experiments suggested that αB-crystallin binds to titin within the extensible

N2B region. However, the specifics of this interaction, in particular the binding domains of each partner, had not been established.

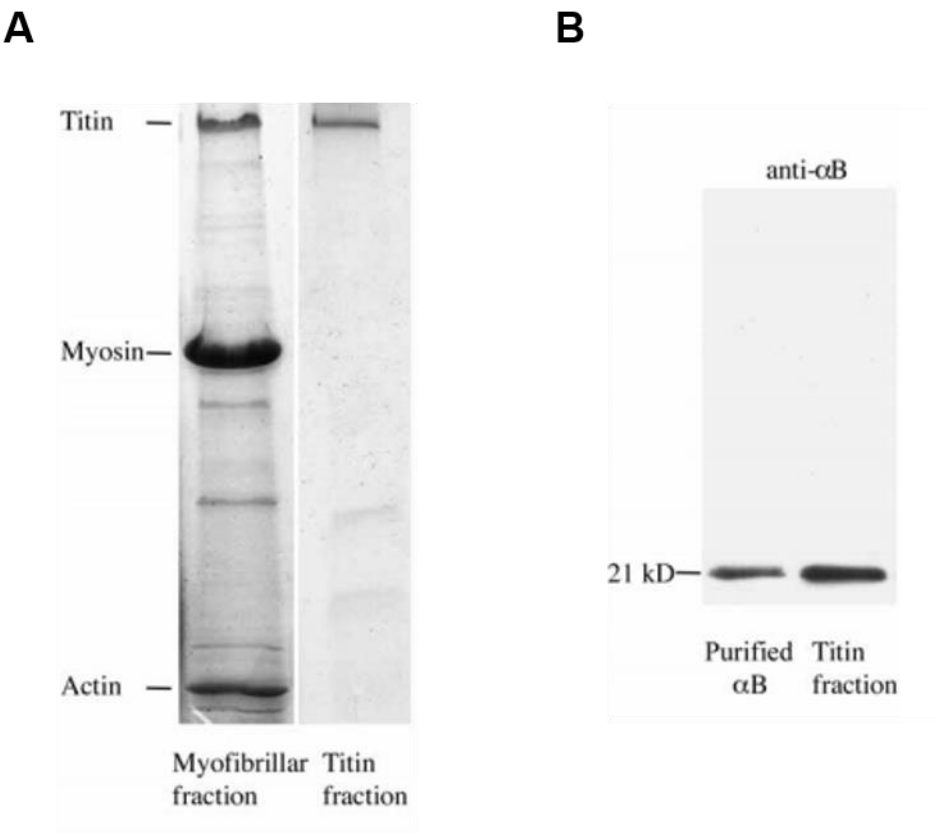


Figure 6-20 – Characteristic Coomassie-Blue stained SDS-PAGE gels of total myofibrillar and titin fractions of ischemic porcine myocardium (A) and Western blot with antibody to αB-crystallin (B). A significant αB-crystallin signal was detected in the titin fraction, indicating association or binding of the proteins. Figure adapted from Golenhofen, N et al [Golenhofen *et al.*, 2002] Figure 4.

Results presented in this chapter significantly improve resolution of the αB-crystallin:titin interaction. Specifically, the MS data reveal that αB-crystallin forms large oligomers (20+ subunits) and binds to titin Ig domains, which comprise a considerable proportion of the titin molecule within the I-band region [Bullard *et al.*, 2004]. As tandem Ig domains are the first regions of titin to extend during stretching of cardiac myofibrils [Linke *et al.*, 1999], αB-crystallin stabilization could restrict unfolding and directly confer stiffness to fibre at physiological stretch levels.

The MS data also provide an approximate indication of the αB-crystallin:titin interaction stoichiometry, with 21-27 αB-crystallin subunits bound to 0-1 titin I26 domains in the CID spectra. Given that the experiment is conducted with a 2:1 molar ratio of I26:αB-crystallin, this stoichiometry suggests a preference for αB-crystallin to bind to itself rather than titin. This suggests that the majority of αB-crystallin subunits bind to oligomers and only transiently interact with titin. In this manner, large oligomers of αB-crystallin may buffer the large concentration of the protein within the cytosol and limit its effective concentration. The preference of αB-crystallin binding to itself versus targets such as titin may also be controlled by cellular status. For example, ischemic conditions, known to cause a translocation of αB-crystallin from the cytosol to the sarcomere [Martin *et al.*, 1997], may increase the propensity of binding to titin. Upon return to normal cellular conditions, αB-crystallin may detach from titin and reform larger oligomers in the cytosol.

A caveat to this analysis arises due to the CID technique used to resolve the MS spectra. Specifically, the CID method caused the dissociation of 2 unidentifiable subunits from each complex. It is therefore possible that a second titin domain, and/or additional αB-crystallin subunits, participate in binding *in vivo*. This is of particular interest because the cross-linking of nearby titin Ig domains by αB-crystallin oligomers would be expected to confer significantly more stiffness than the binding to a single Ig domain.

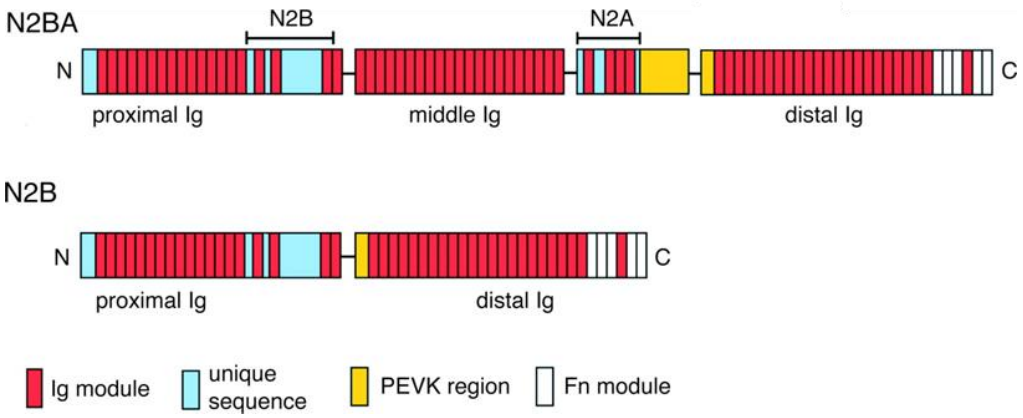


Figure 6-21 – Primary structure of I-band region of long (N2BA) and short (N2B) isoforms of cardiac titin. Both isoforms express a large proportion of extensible Ig domains to which αB-crystallin may bind and stiffen. Figure adapted from [Bullard *et al.*, 2004] Figure 1.

The NMR data presented in this chapter confirmed the binding of αB-crystallin to titin Ig domains and also indicated that the likely binding location on αB-crystallin resides within its C-terminus. The specific location was confirmed by demonstrating that a palindromic 9-AA peptide from αB-crystallin's C-terminus binds to tandem titin Ig domains using MS. This peptide is also thought to bind to the core domain of other αB-crystallin subunits. More recent data suggest that αB-crystallin oligomers may simultaneously bind two or more titin Ig domains, supporting the hypothesis that cross-linking of adjacent molecules may contribute to the stiffening effect observed in fibres.

Further clarification of αB-crystallin:titin interaction will be accomplished by solving the crystal structure of the bound pair. Recent efforts have yielded diffractable crystals, but no structure has yet been determined.

6.6.2 Regulation of cardiac muscle stiffness by αB-crystallin

The stiffness of cardiac muscle is predominantly controlled by titin and collagen. In most muscle types, the two proteins contribute to tension equally near the maximal physiological sarcomere length [Wu *et al.*, 2000]. At shorter lengths, titin contributes more significantly to stiffness. The molecular basis of titin's stiffness is attributed to three primary mechanisms – entropic worm-like-chain elasticity, Ig domain unfolding, and minor structural changes within the PEVK domain [Minajeva *et al.*, 2001]. It is therefore plausible that the αB-crystallin:titin Ig domain interaction described in the previous section underlies the stiffening observed in demembranated cardiac muscle fibres due to αB-crystallin incubation.

Specifically, we hypothesize that the C-terminal domain of αB-crystallin binds to titin Ig domains and stabilizes their folded state. As titin Ig domains unfold during early stages of ventricular stretching [Linke *et al.*, 1999; Wu *et al.*, 2000], stabilization of these domains likely contributes to overall cardiac stiffness at physiological sarcomere lengths. This hypothesized mechanism is supported by atomic force microscopy measurements in which series of titin Ig domains (I91-I98) were stretched with, or without, αB-crystallin [Bullard *et al.*, 2004]. Force measurements during the stretching procedure exhibit a sawtooth pattern corresponding to sequential unfolding of six of the eight Ig domains followed by detachment of the molecule from the apparatus (Figure 6-22). The peak force required for Ig domain unfolding was increased by 30-40 pN in the presence of αB-crystallin, approximately 50 % greater than without αB-crystallin [Bullard *et al.*, 2004]. Thus, αB-crystallin binding to titin Ig domains significantly increases the force required to cause unfolding and may underlie stiffening of the overall fibre.

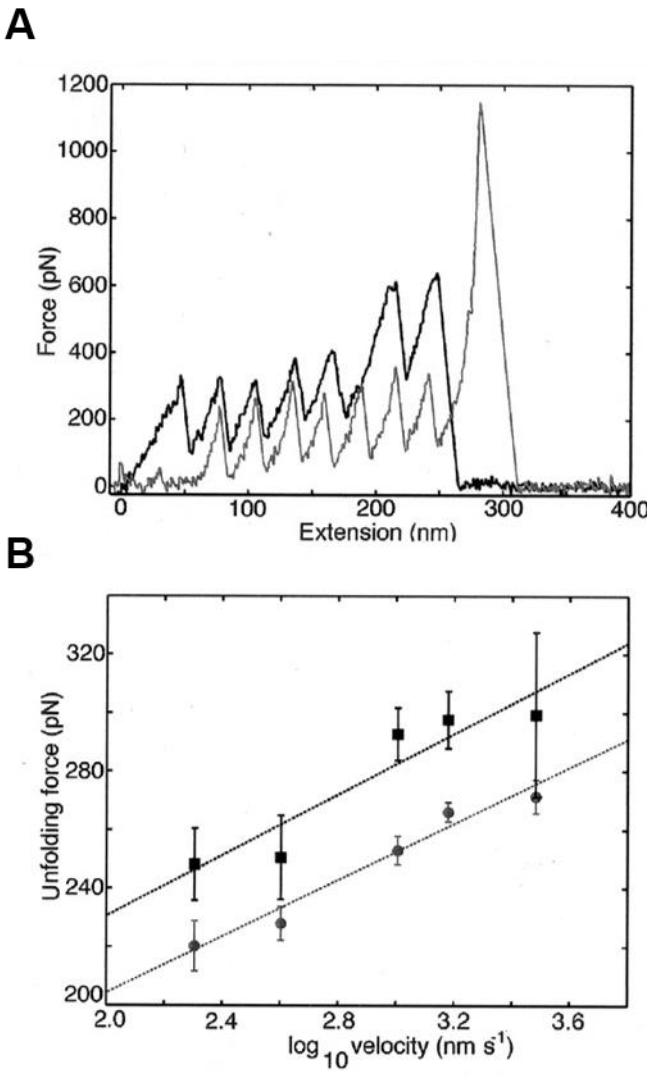


Figure 6-22 – Typical atomic force extension traces of titin Ig domains I91-I98 in the presence (black) and absence (grey) of αB-crystallin (A) and average unfolding forces as a function of log of stretch rate in the presence (squares) and absence (circles) of αB-crystallin (B). The presence of αB-crystallin increased the force required to unfold titin Ig domains. Figure adapted from Bullard, B. et al [Bullard *et al.*, 2004] Figure 8.

Despite this straightforward mechanism, it remains unclear whether stabilization of titin Ig domains is sufficient to yield the magnitude of stiffening observed in whole fibres. Incubation with WT αB-crystallin or the WT peptide increased linear stiffness of fibres by over 2-fold, far more than the 50 % increase in titin Ig domain unfolding force observed in atomic force measurements. These results suggest that the effect of αB-crystallin on titin stiffness may be modulated by the presence of additional sarcomeric proteins.

Further, the stiffening effect of full length WT αB-crystallin was shown to be concentration dependent. At 0.5 mg/ml (or equivalent), full length WT αB-crystallin caused less stiffening than the titin-binding peptide alone. A reasonable explanation for this finding is that full length WT αB-crystallin is expected to form large oligomers, reducing the availability of titin-binding domains. However, at 5.0 mg/ml (or equivalent), full length WT αB-crystallin caused significantly greater stiffening than the peptide. This finding suggests that high concentrations of αB-crystallin may stiffen cardiac muscle by mechanisms besides Ig domain stabilization. One plausible mechanism is that αB-crystallin oligomers cross-link titin and other proteins. These hypothesized cross-links increase the number of potential αB-crystallin binding sites and could explain the large increase in stiffness. The R157H mutation appears to mitigate these cross-linking activities, as incubation with high concentrations of the mutant protein did not yield stiffness gains comparable to those seen with high concentrations of WT αB-crystallin.

Sarcomeric cross-linking by αB-crystallin is also supported by measurements of cardiac stiffness in the presence of the titin-binding αB-crystallin peptide. These experiments suggested that low concentrations of the peptide were sufficient to stiffen the muscle, but high concentrations had no additional effect. As the peptides retain titin-binding activity, the overall stiffening effect can be explained by stabilization of titin Ig domains. However, because the peptides are unable to form oligomers, they cannot cross-link titin Ig domains with other sarcomeric proteins, explaining the lack of further stiffness increases at higher concentrations.

The contribution of αB-crystallin cross-linking to physiological cardiac stiffness is difficult to estimate because the effective protein concentration is unknown. As in the vertebrate lens, αB-crystallin is expected to bind to many unfolding proteins

within cardiomyocytes. Further, the quaternary structure of αB-crystallin (subunits per oligomer, etc.) is likely to depend on cellular status. Both of these factors will affect the availability of αB-crystallin binding domains. Though experimental buffers aim to mimic physiological ion concentrations, they are highly simplified compared to the cytosol and also lack non-sarcomeric proteins, which may be αB-crystallin binding partners. Therefore, experimental αB-crystallin concentrations may be considerably different than the effective *in vivo* concentration.

6.6.3 Conclusions

The results presented in this chapter demonstrate that αB-crystallin binds to titin Ig domains via a small peptide within its C-terminus. The incubation of demembranated fibres with αB-crystallin causes a significant stiffening of the total fibre, presumably due to stabilization of titin Ig domains and additional cross-linking interactions. The hypothesized titin-binding 9-AA peptide from αB-crystallin's C-terminus was also shown to stiffen cardiac muscle, though to a smaller extent than full-length αB-crystallin. In both full-length αB-crystallin and the isolated titin-binding peptides, the DCM-associated R157H mutation was shown to moderately reduce the stiffening effect. These results suggest that a reduction of cardiac stiffness may contribute to the pathogenesis of DCM.

Chapter 7 – Discussion

7.1 Altered contractile mechanics contribute to the pathogenesis of non-sarcomeric cardiomyopathies

7.1.1 Contractile abnormalities underlie PRKAG2 cardiomyopathy pathogenesis

Mutations in the AMPK γ2 subunit cause a cardiomyopathy characterized by left ventricular hypertrophy, systolic and/or diastolic impairment, cardiac glycogen accumulation, ventricular pre-excitation, and sudden death [Blair *et al.*, 2001; Gollob *et al.*, 2001]. Clinical reports and phenotypes of mice overexpressing mutant AMPK γ2 subunits have led to the characterization of PRKAG2 cardiomyopathy as a glycogen storage disease [Arad *et al.*, 2002; Arad *et al.*, 2003]. However, recent clinical reports demonstrate the existence of symptomatic, genotype-positive PRKAG2 cardiomyopathy patients without any glycogen accumulation [Tan *et al.*, 2008; Kelly *et al.*, 2009], suggesting that other mechanisms may contribute to pathogenesis of the disease.

Recent results from Rong Tian's laboratory help clarify the contribution of glycogen storage to the overall PRKAG2 phenotype [Kim *et al.*, 2014]. Mice overexpressing PRKAG2 cardiomyopathy-causing N488I AMPK γ2 exhibited cardiac hypertrophy, impaired ejection fraction, glycogen accumulation, and ventricular pre-excitation. Crossing the mice with a line that lacked glycogen synthase activity rescued the glycogen accumulation and ventricular pre-excitation phenotypes, but did not fully rescue cardiac hypertrophy or ejection fraction. Inhibiting mammalian target of rapamycin (mTOR), a cellular growth mediator affected by both AMPK and PKA [Miller *et al.*, 2007; Mihaylova and Shaw, 2011], by rapamycin in AMPK mutant mice lacking glycogen synthase was shown to prevent hypertrophy. The authors

conclude that glycogen accumulation predominantly accounts for the electro-physiological aspects of PRKAG2 cardiomyopathy, but not hypertrophy or contractile dysfunction.

Results presented in this thesis support, and help explain, the finding that aspects of PRKAG2 cardiomyopathy phenotype are independent of glycogen accumulation. Our novel knock-in mouse model of PRKAG2 cardiomyopathy exhibits impaired LV function evidenced by reduced EF and slowed relaxation at a young age, without glycogen accumulation. Cardiomyocytes from these animals recapitulated the impaired relaxation phenotype, suggesting that dysfunction begins at the cellular level and cannot be accounted for by systemic alterations. Specifically, slowed relaxation was found to be caused by reduced SERCA activity and enhanced myofilament Ca^{2+} sensitivity. These functional modifications resulted from reduced phosphorylation of PKA target sites on PLN, TnI, and MyBPC. These data reveal that alterations to the contractile and Ca^{2+} handling apparatuses contribute to development of PRKAG2 cardiomyopathy independent of glycogen accumulation.

7.1.2 Biomechanical abnormalities due to DCM-associated αB-crystallin mutation

A search for αB-crystallin mutations in a population of Japanese DCM patients revealed a missense mutation resulting in a R157H substitution [Inagaki *et al.*, 2006]. The mutation was located with a conserved region of αB-crystallin and was not found in 400 control chromosomes. One patient exhibited a mild cardiomyopathy that developed only after the fourth decade. Two of her six siblings were also affected with DCM and sudden death. Mutant R157H αB-crystallin exhibited reduced titin binding in mammalian-two-hybrid assays but no difference in cellular distribution.

Experiments presented in Chapter 6 further these investigations by clarifying the interaction between αB-crystallin and titin, the effect of αB-crystallin on overall cardiac stiffness, and the impact of the R157H mutation on these activities. The most important finding was that the R157H αB-crystallin mutant causes reduced muscular stiffening compared to WT αB-crystallin. Given that αB-crystallin had previously been shown to bind titin and increase the force required to unfold its Ig domains [Bullard *et al.*, 2004], the R157H mutation was hypothesized to alter this binding and therefore affect overall titin-based cardiac stiffness. The finding that the R157H mutation lies within the 9-AA titin-binding region within αB-crystallin's C-terminus supports this hypothesis. Further, the mutant R157H peptide was shown to increase stiffness to a lesser extent than the WT peptide. Together, these data suggest that the R157H αB-crystallin mutation causes DCM by reducing the contribution of titin to total cardiac stiffness.

7.2 Implications of novel pathogenesis mechanisms in broader disease

Barring traditional caveats associated with animal models of human disease, the pathogenesis mechanisms described in the previous sections are of direct relevance to patients with cardiomyopathies resulting from mutations in *PRKAG2* and *CRYAB*. However, mutations in these genes are very rare, potentially limiting the clinical impact of the mechanisms described. Nevertheless, similarities between PRKAG2- and CRYAB-associated cardiomyopathies and the broader families of HCM and DCM suggest that shared mechanisms of disease progression may exist. If these associations are correct, treatments targeting mechanisms that underlie PRKAG2 cardiomyopathy and CRYAB-associated cardiomyopathy may be effective for HCM and DCM and have broader implications for acquired cardiac conditions.

7.2.1 Shared consequences of contractile and Ca^{2+} handling dysfunction in PRKAG2 cardiomyopathy and HCM

The phenotypic parallels between HCM caused by sarcomeric mutations and PRKAG2 cardiomyopathy are well-established. In fact, early reports of AMPK γ2 mutations discussed their role as a cause of HCM [Blair *et al.*, 2001]. Though distinctive levels of glycogen accumulation and conductance abnormalities, particularly in overexpressing murine models, have led to a separate classification of the PRKAG2 cardiac syndrome [Gollob *et al.*, 2002], similarities between aspects of the phenotypes suggests shared mechanisms of pathogenesis. Of particular interest is that the increased sarcomeric Ca^{2+} sensitivity observed in our model is also characteristic of HCM-causing mutations, in particular those in thin filament proteins [Redwood *et al.*, 1999]. Sarcomeric Ca^{2+} sensitization has been implicated in many downstream features of HCM, including propensity for arrhythmias, increased ATP utilization leading to energy deprivation, and progression towards cardiac hypertrophy.

The relationship between sarcomeric Ca^{2+} sensitization and arrhythmias was described in Section 3.5.1. Briefly, in transgenic models of HCM caused by TnT mutations, the propensity for arrhythmia was found to be directly proportional to the level of Ca^{2+} sensitization [Baudenbacher *et al.*, 2008; Schober *et al.*, 2012]. Arrhythmogenicity was recapitulated using the Ca^{2+} sensitizing molecule EMD 57033 and obviated using the Ca^{2+} desensitizing molecule blebbistatin, supporting a causal relationship between sarcomeric Ca^{2+} sensitivity and arrhythmogenesis in HCM.

In addition to causing arrhythmias, sarcomeric Ca^{2+} sensitization is proposed to cause excess ATP utilization without corresponding increases in cardiac output

[Ashrafian *et al.*, 2003; Ashrafian and Watkins, 2007]. As the Ca^{2+} transient rises and falls, increased thin filament sensitivity would result in more rapid activation and delayed relaxation. Increased cross-bridge cycling required for this hypercontractility causes excess ATP usage. As the healthy heart ejects the majority of its contents during systole, the hypercontractility conferred by Ca^{2+} sensitization would not be expected to significantly increase cardiac output [Ashrafian *et al.*, 2003]. A variety of disease models have exhibited a phenotype consistent with this hypothesis. In mouse and rat models of HCM caused by Ca^{2+}-sensitizing TnT mutations (and by Ca^{2+} sensitizer EMD 57033), Ca^{2+} sensitivity was directly associated with focal energy deprivation [Luedde *et al.*, 2009; Huke *et al.*, 2013]. Human patients with HCM-causing TnT mutations, as well as other common sarcomeric mutations, also exhibited an impaired energetic state, even before overt development of hypertrophy [Crilley *et al.*, 2003].

The link between Ca^{2+} sensitivity and hypertrophic signalling implicates similar mechanisms. Increased buffering of Ca^{2+} by the thin filament leads to prolonged Ca^{2+} transients (reported in Chapter 4 and elsewhere [Baudenbacher *et al.*, 2008; Schober *et al.*, 2012]) and increases cytosolic Ca^{2+} concentrations. Further, because SERCA is highly sensitive to ATP concentrations as it requires a high ΔG of ATP hydrolysis [Spindler *et al.*, 1998], an impaired energetic state resulting from increased Ca^{2+} sensitivity would cause reduced SERCA activity and further Ca^{2+} accumulation in the cytosol [Ashrafian *et al.*, 2003]. Once cytosolic Ca^{2+} concentrations are increased, a range of transcriptional processes are activated to induce cardiac hypertrophy [Frey *et al.*, 2000; Frey and Olson, 2003]. This signalling pathway is initiated by stimulation of the Ca^{2+}-calmodulin-activated protein phosphatase calcineurin, which is a serine/threonine phosphatase uniquely

activated by increased intracellular calcium concentrations [Crabtree, 1999]. When triggered, calcineurin directly dephosphorylates members of the nuclear factor of activated T-cells (NFAT) transcription factor family [Molkentin, 2004]. Dephosphorylated NFATs translocate to the nucleus and participate in the induction of various genes, dependent on the cell type [Hogan *et al.*, 2003]. In cardiomyocytes, calcineurin-activated NFAT stimulates b-type natriuretic factor, a canonical hypertrophic marker, via the cardiac zinc finger transcription factor GATA4 [Molkentin *et al.*, 1998].

Despite the clear effect of NFAT signalling in initiation of cardiac hypertrophy via transcriptional effects, this pathway must act in concert with other effectors to control the range of protein synthesis and degradation processes involved in the hypertrophic response. The mitogen-activated protein kinase (MAPK) family has been implicated as one key contributor to this coordination [Molkentin, 2004]. The MAPK pathway consists of p38 kinases, c-Jun N-terminal kinases (JNKs), and extracellular signal-regulated kinases (ERKs) [Garrington and Johnson, 1999]. The p38 kinases and JNKs are primarily activated by stress signals whereas the ERK pathway is triggered by growth factor stimulation [Garrington and Johnson, 1999]. In neonatal cardiomyocytes, stimulation of each MAPK pathway has been shown to cause hypertrophy [Liang and Molkentin, 2003]. Further, all three pathways have been shown to modulate the calcineurin/NFAT signalling pathway [Molkentin, 2004]. The ERK pathway has been shown to be able to either activate [Genot *et al.*, 1996] or inhibit [Porter *et al.*, 2000] calcineurin/NFAT signalling depending on cell type and stimulation. The p38 kinases and JNKs can directly phosphorylate NFAT transcription factors in their N-terminal regulatory domains, opposing the calcineurin-dependent dephosphorylation and resulting in reduced NFAT nuclear

translocation [Chow *et al.*, 1997; Gomez del Arco *et al.*, 2000; Porter *et al.*, 2000; Yang *et al.*, 2002]. Thus, the MAPK pathways are pivotal regulators of the calcineurin-NFAT pathway leading to cardiac hypertrophy.

Beyond the NFAT/MAPK pathway, increased cytosolic Ca^{2+} concentrations caused by increased sarcomeric Ca^{2+} sensitivity also activates the calcium/calmodulin-dependent protein kinase (CaMK) family [Frey *et al.*, 2000]. These kinases play major roles in cardiac contractility and calcium handling, but are also likely involved in control of hypertrophy. CaMK has been shown to phosphorylate the transcription factor MEF2, causing increased transcriptional activity [Blaeser *et al.*, 2000]. Further, CaMK phosphorylates a family of transcriptional repressors, histone deacetylases, to cause their release from MEF2 [Lu *et al.*, 2000]. These activities result in CaMK being a potent contributor to the development of cardiac hypertrophy. Evidence for this importance is given in studies that find increased CaMK activity in hypertrophied myocardium from patients and animal models [Anderson *et al.*, 2011], overexpression of CaMK causing hypertrophy in cultured cardiomyocytes and mouse models [Passier *et al.*, 2000], and reduced or inhibited development of hypertrophy using a variety of methods that inhibit CaMK [Zhu *et al.*, 2000; Backs *et al.*, 2009; Ling *et al.*, 2009; Anderson *et al.*, 2011].

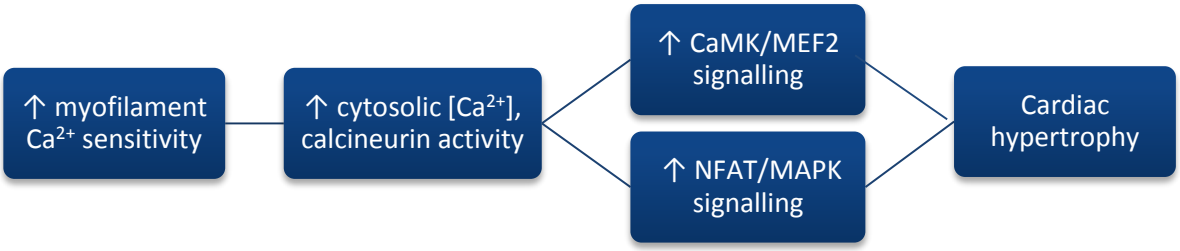


Figure 7-1 - Schematic illustration of hypothesized mechanism linking increased myofilament Ca^{2+} sensitivity to cardiac hypertrophy.

The fundamental cause of increased myofilament Ca^{2+} sensitivity may also be shared between PRKAG2 cardiomyopathy and sarcomeric HCM. We initially hypothesized that increased Ca^{2+} sensitivity in the R299Q γ2 mice would be caused by greater phosphorylation of TnI S150 by AMPK. However, both functional assessments of demembranated cardiac muscle before and after PKA treatment and biochemical measurements of site-specific phosphorylation status of TnI suggested that the role of TnI S150 phosphorylation by AMPK was minimal. Instead, reduced phosphorylation of TnI at S23/S24 is likely to underlie the observed increase in Ca^{2+} sensitivity. This result suggests that cross-talk between AMPK and β-adrenergic signalling pathways is responsible for sarcomeric dysfunction in this model of PRKAG2 cardiomyopathy.

In sarcomeric HCM, *in vitro* studies of mutant regulatory proteins revealed that Ca^{2+} sensitization can be directly caused by the various mutations [Robinson *et al.*, 2002; Robinson *et al.*, 2007]. However, in samples of cardiac tissue from end-stage HCM patients with MyBPC mutations, increased myofilament Ca^{2+} sensitivity was shown to be caused by reduced PKA phosphorylation [van Dijk *et al.*, 2009; van Dijk *et al.*, 2012]. More recently, samples of tissue from human HCM patients bearing mutations in *MYH7*, *MYBPC3*, *TNNT2*, *TNNI3*, and *TPM1* revealed that treatment with activated PKA normalized Ca^{2+} sensitivity to donor levels [Sequeira *et al.*, 2013]. These results suggest that increased myofilament Ca^{2+} sensitivity in HCM may also be due to altered β-adrenergic signalling. An important difference between these observations of PKA-dependent alteration to Ca^{2+} sensitivity is the disease stage. In our mouse model of PRKAG2 cardiomyopathy, the effect was seen at a young age, suggesting a direct or early role of the alteration to disease

development. Conversely, human samples are necessarily taken from end-stage patients, obfuscating whether the changes are disease-causing or compensatory.

A link between sarcomeric HCM, PRKAG2 cardiomyopathy, and reduced phosphorylation centres on energetic compromise (Figure 7-2). In traditional HCM, incorporation of mutant sarcomeric proteins and subsequent contractile inefficiency generates an impaired energetic state [Ashrafian *et al.*, 2003]. Molecularly, this impaired state manifests as a reduction in ATP concentrations [Ingwall and Weiss, 2004] and would be expected to activate AMPK via its regulatory γ subunits. In the opposite fashion, PRKAG2 cardiomyopathy-causing mutations inappropriately activate AMPK and cause dysfunctional regulation of cardiac energetics [Ahmad *et al.*, 2005; Banerjee *et al.*, 2007]. My data demonstrate that an AMPK complex with increased basal activity causes impaired contractile mechanics and Ca^{2+} handling. Further, activating AMPK directly with AICAR resulted in significantly impaired cardiomyocyte contractility. These results suggest that increased AMPK activity may involve feedback that negatively affects contractile function in both PRKAG2 cardiomyopathy and HCM. Biochemical assessments of dysfunctional tissues suggested that reduced phosphorylation of key regulatory proteins may underlie the reduced performance. This suggests that activated AMPK may inhibit activity of regulatory protein kinases such as PKA or increase activity of phosphatases in both PRKAG2 cardiomyopathy and HCM.

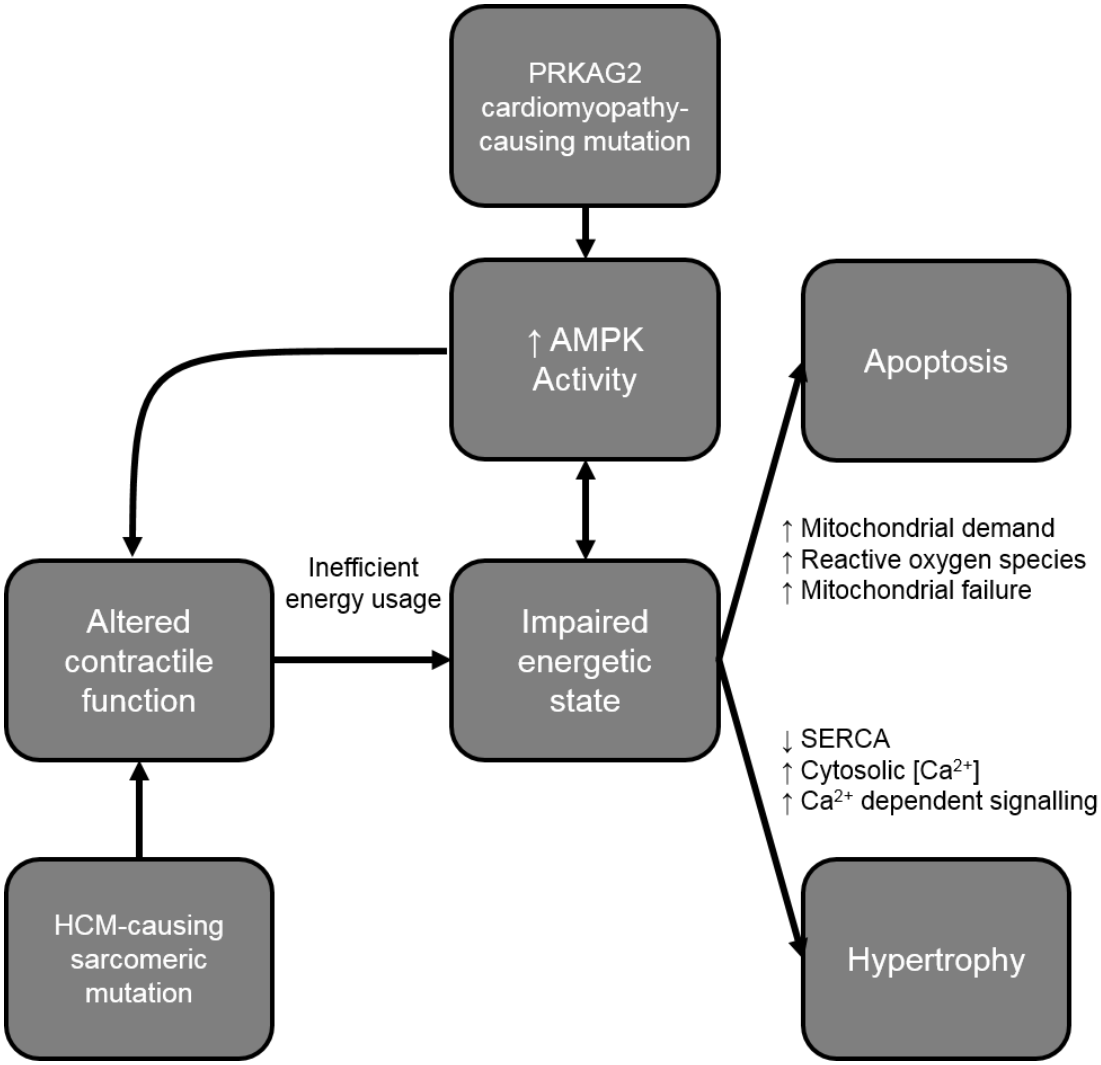


Figure 7-2 – Hypothesized pathogenesis mechanism shared between PRKAG2 cardiomyopathy and HCM.

Broadly, it is likely that energetic compromise contributes to the pathogenesis of many cardiac diseases beyond PRKAG2 and HCM. In failing human hearts, ATP concentrations are reduced by 25-30 % compared to controls [Nascimben *et al.*, 1996; Starling *et al.*, 1998]. Activation of AMPK by reduced ATP/ADP ratios early in this progression [Shen *et al.*, 1999; Ingwall and Weiss, 2004] may seek to preserve the energetic state of cardiomyocytes by inhibiting contractility. In particular, results presented in this thesis suggest that AMPK inhibits cardiomyocyte function by reducing the phosphorylation of key β-adrenergic response targets. In heart failure,

the β-adrenergic pathway is over-stimulated in an attempt to improve function. However, the β_1 receptors (responsible for cardiac stimulation [Lands *et al.*, 1967]) are down-regulated to levels that correlate with disease severity [Engelhardt *et al.*, 1996] and the remaining receptors are desensitized [Lohse *et al.*, 2003]. The ultimate outcome of these changes is a reduction in phosphorylation of most β-adrenergic targets [Lohse *et al.*, 2003] (with RyR being the notable exception [Marx *et al.*, 2000]). It is possible that increased AMPK activity in end-stage heart failure contributes to this phenotype by inhibiting PKA activity or increasing phosphatase activity [Neumann, 2002].

7.2.2 Altered ventricular stiffness can lead to DCM

The phenotype associated with DCM includes LV dilatation, systolic dysfunction, myocyte death, and myocardial fibrosis [Watkins *et al.*, 2011]. This end stage phenotype can result from numerous potential injuries or can be caused by a variety of inherited mutations (30-48 % of cases [Towbin and Bowles, 2002]). Mutations known to cause DCM occur in over 40 genes that encode predominantly cytoskeletal and sarcomeric proteins [Jefferies and Towbin, 2010]. Non-inherited forms of DCM can occur due to infection, drug use, or autoimmune activity [Jefferies and Towbin, 2010].

Of particular relevance to results presented in this thesis is the association of altered cardiac compliance with DCM. A conserved feature of the disease is remodelling of the LV involving modification of the cytoskeleton and extracellular matrix [Hein *et al.*, 2000]. Generally, these changes result in a reduction in overall cardiac stiffness. Multiple researchers have suggested that this change is primarily caused by a shift in titin isoform expression from the stiffer N2B isoform towards the more compliant N2BA isoform [Makarenko *et al.*, 2004; Nagueh *et al.*, 2004]. However, the ratio of

rigid type I collagen to more compliant type III collagen has been shown to be increased in DCM [Marijianowski *et al.*, 1995]. Together, these changes result in a reduction of the titin-based contribution to overall cardiac stiffness in DCM [Makarenko *et al.*, 2004]. The importance of reduced titin-based cardiac stiffness in the pathogenesis of DCM is reinforced by the finding of missense mutations in region of the titin gene encoding its Z-disk [Itoh-Satoh *et al.*, 2002] and elastic I-band regions [Gerull *et al.*, 2002], as well as truncating mutations within the A-band [Roberts *et al.*, 2015].

The R157H αB-crystallin mutation investigated in this thesis supports this proposed DCM pathogenesis mechanism. As αB-crystallin binds to titin and directly regulates its stiffness, and this mutation was shown to cause a reduced stiffening effect, a reduced overall contribution of titin to cardiac muscle stiffness would be expected in patients harbouring the R157H mutation. The downstream implications of reduced titin stiffness were previously investigated in DCM patients exhibiting a range of N2BA:N2B ratios [Nagueh *et al.*, 2004]. A positive correlation between N2BA:N2B ratio and *in vivo* EDV/EDP ratio was observed, consistent with greater filling in a more compliant ventricle. Though increased diastolic filling is often regarded as a functional improvement, EF was negatively correlated with N2BA:N2B ratio in this same experiment, indicating reduced cardiac output.

The relationship between diastolic filling and cardiac output balances the contributions of the Frank-Starling and Laplace Laws of the Heart. Specifically, LDA results in greater force production by the myofilament at longer diastolic lengths. In contrast, Laplace's Law of the Heart requires that the contractile force generated by the myocardium be directly proportional to its radius to achieve a given level of pressure. Therefore, the ability of the heart to maintain EF with greater diastolic

filling depends on LDA to yield proportionally greater forces. Interestingly, increased titin-based stiffness has been shown to reduce lattice spacing, increase myofilament Ca^{2+} sensitivity, and increase LDA [Fukuda *et al.*, 2003]. In the opposite fashion, reduced titin stiffness leading to increased diastolic filling in DCM may simultaneously impair LDA and prevent maintenance of EF.

7.3 Therapeutic implications

The ultimate value of understanding cellular and molecular mechanisms of disease pathogenesis is to permit development of novel therapeutics that might improve patient outcomes. This thesis has utilized a range of functional and biochemical assessments to characterize the underlying disease pathways associated with rare mutations in genes encoding AMPK γ2 and αB-crystallin. Fortunately, key similarities between these genetic disorders and the more common diseases of HCM and DCM allow conclusions from these studies to be more broadly applied. These novel, or clarified, mechanisms therefore provide opportunities for disease prevention/reversion.

7.3.1 Novel treatment opportunities in hypertrophic cardiomyopathy

Current treatment options for HCM are extended pharmaceutical regimens, implantable devices, and surgical interventions [Elliott *et al.*, 2014]. These treatments aim to reduce symptoms (such as chest pain and shortness of breath) and complications (such as LV outflow tract obstruction and arrhythmia) but may not affect the underlying disease progression. To create therapies that prevent development of HCM, targeting the fundamental mechanisms of disease pathogenesis is essential. In particular, the results presented in this thesis highlight the importance of increased myofilament Ca^{2+} sensitivity, altered Ca^{2+} handling and signalling, and energetic compromise in the progression of disease.

Increased myofilament Ca^{2+} sensitivity is common in many cases of HCM and has been associated with much of the eventual clinical phenotype. Therefore, reducing myofilament Ca^{2+} sensitivity may be a rational therapeutic goal. Unfortunately, no clinically viable pharmaceutical myofilament desensitizers are currently available. A potential alternative option is to deliver an engineered regulatory variant to compensate for the observed sensitization. This strategy has been successfully employed in both *in vitro* experiments and animal models of HCM. Davis and Metzger demonstrated the combinatorial effect of multiple regulatory variants in isolated cardiomyocytes and cardiac muscle fibres [Davis and Metzger, 2010]. Specifically, their results showed that delivery of two sarcomeric sensitizing mutations leads to greater Ca^{2+} sensitivity than either independently. Further, combining a sensitizing TnI variant (R193H) with a desensitizing TnC variant (G159D) resulted in intermediate myofilament sensitivity. Jagatheesan et al. employed a comparable methodology to manipulate Ca^{2+} sensitivity [Jagatheesan *et al.*, 2007]. The authors generated a mouse model with a HCM-associated Tm mutation (E180G) causing increased Ca^{2+} sensitivity, severe cardiac hypertrophy and dysfunction, and reduced life expectancy. Crossing the Tm E180G animals with animals expressing chimeric α-/β- Tm (α-TM amino acids 1–257 and β-TM amino acids 258–284), which was shown to cause decreased myofilament Ca^{2+} sensitivity [Jagatheesan *et al.*, 2003], resulted in double-transgenic animals with normal myofilament Ca^{2+} sensitivity and rescued cardiac function. Application of this theory in human patients could also restore normal myofilament sensitivity and prevent the progression of HCM. However, a pressing concern with this strategy is ensuring precision in the adjustment of Ca^{2+} sensitivity. As DCM is associated with

desensitized myofilaments, over-correction of sensitivity in HCM could result in a conversion of pathology rather than regression.

Altered sarcomeric Ca^{2+} sensitivity also contributes to impaired Ca^{2+} handling in HCM models due to the potent Ca^{2+} buffering capacity of myofilaments (100:1 bound:free Ca^{2+} [Bers, 2008]). These changes, combined with secondary alterations to the Ca^{2+} handling apparatus itself (described in Chapter 4 and elsewhere [Fatkin *et al.*, 2000; Somura *et al.*, 2001]), increased diastolic Ca^{2+} levels and enhanced downstream Ca^{2+} signalling, thereby leading to hypertrophy and arrhythmias [Frey *et al.*, 2000; Baudenbacher *et al.*, 2008]. Therefore, modifying cardiac Ca^{2+} handling is a rational opportunity to prevent HCM progression. One method with demonstrated success in animal models of HCM is the inhibition of L-type Ca^{2+} channels using diltiazem [Semsarian *et al.*, 2002]. This treatment restored levels of Ca^{2+} handling proteins within cardiomyocytes bearing a myosin heavy chain mutation and prevented disease development. In another study, increasing SR Ca^{2+} reuptake by delivering SERCA2a via adenovirus prevented hypertrophy and improved cardiac function in a mouse model of HCM caused by a Tm mutation [Pena *et al.*, 2010]. Thus, though prominent HCM-causing mutations do not directly alter the cardiac Ca^{2+} handling apparatus, targeting these regulatory mechanisms may be an effective therapeutic strategy.

Energetic compromise is a well-established component of the HCM phenotype. Sarcomeric mutations have been shown to cause an increased ATP cost of force production (“tension cost”) [Frey *et al.*, 2006]. This cost results in an impaired energetic state that precedes overt HCM phenotypes in both animal models [Luedde *et al.*, 2009] and human patients [Crilley *et al.*, 2003]. This dysfunctional metabolic state would be expected to activate energetic sensors such as AMPK. As

shown in this thesis, activating AMPK can itself result in impaired contractile function. Therefore, improving the efficiency of cardiac metabolism or energy usage could abrogate development of the disease.

The efficiency of cardiac metabolism is initially modulated by utilization of free fatty acids (FFA) or carbohydrates as the initial substrate. The oxygen cost of ATP production is theoretically only 13 % lower using FFA than carbohydrates [Ashrafian *et al.*, 2011]. However, various “oxygen wasting” mechanisms associated with FFA metabolism result in a ~35 % reduction in efficiency compared to carbohydrate metabolism [Vik-Mo and Mjos, 1981]. This reduction may contribute to energetic compromise in both HCM and congestive heart failure, where the metabolic substrate is shifted towards FFA [Paolisso *et al.*, 1994; Tuunanen *et al.*, 2007]. Therefore, to improve cardiac energetic efficiency in disease states, it may be beneficial to shift metabolism back to carbohydrate substrates. One pharmaceutical agent capable of driving this adjustment is the piperazine-derived racemate perhexiline. Perhexiline was originally developed in the 1970’s to treat angina, though its mechanism of action has only been clarified recently [Ashrafian *et al.*, 2007]. Perhexiline inhibits carnitine palmitoyltransferase, an enzyme responsible for uptake of long-chain fatty acids into mitochondria. Inhibition of this enzyme therefore reduces FFA utilization and improves cardiac energetic efficiency (explaining its anti-anginal effect). In a randomized trial in symptomatic HCM patients, perhexiline treatment resulted in improved cardiac energetics, reduced cardiac dysfunction, and greater exercise capacity compared to placebo-treated controls [Abozguia *et al.*, 2010]. This success supports the causative role of impaired energetics in the pathogenesis of HCM and also suggests that metabolic modification may represent a reasonable therapeutic option.

7.3.2 Novel treatment opportunities in dilated cardiomyopathy

The results presented in Chapter 6 and elsewhere suggest a causative role of reduced myocardial stiffness in the pathogenesis of DCM. In inherited forms of the disease, particularly those caused by mutations to structural proteins such as titin, the link to stiffness is clear. In contrast, acquired forms of DCM caused by toxicity or malnutrition may cause changes to ventricular compliance due to secondary remodelling. Increasing titin-based cardiac stiffness, therefore, may represent a novel therapeutic strategy to prevent progression of the disease.

Structural work described in Chapter 6 also identified a suitable target for affecting cardiac stiffness – titin Ig domains. Further, the finding that a 9-AA peptide was sufficient to induce muscular stiffening provides a viable therapeutic design. The small size of this peptide would permit its transport to the heart via viral gene delivery. Alternatively, binding of αB-crystallin to titin could be mimicked, or inhibited, by small molecules. Design of these therapeutics will be significantly promoted by further clarification of the αB-crystallin:titin interaction, particularly solving of the crystal structure. These strategies could allow restoration of titin-based force in heart failure or DCM conditions and prevent this contribution to disease development. However, care must be taken to prevent over-compensation of cardiac stiffness, which could rapidly lead to impaired ventricular filling. Even worse, inhibition of titin-based stiffening could increase the risk of myocardial rupture following an adverse event.

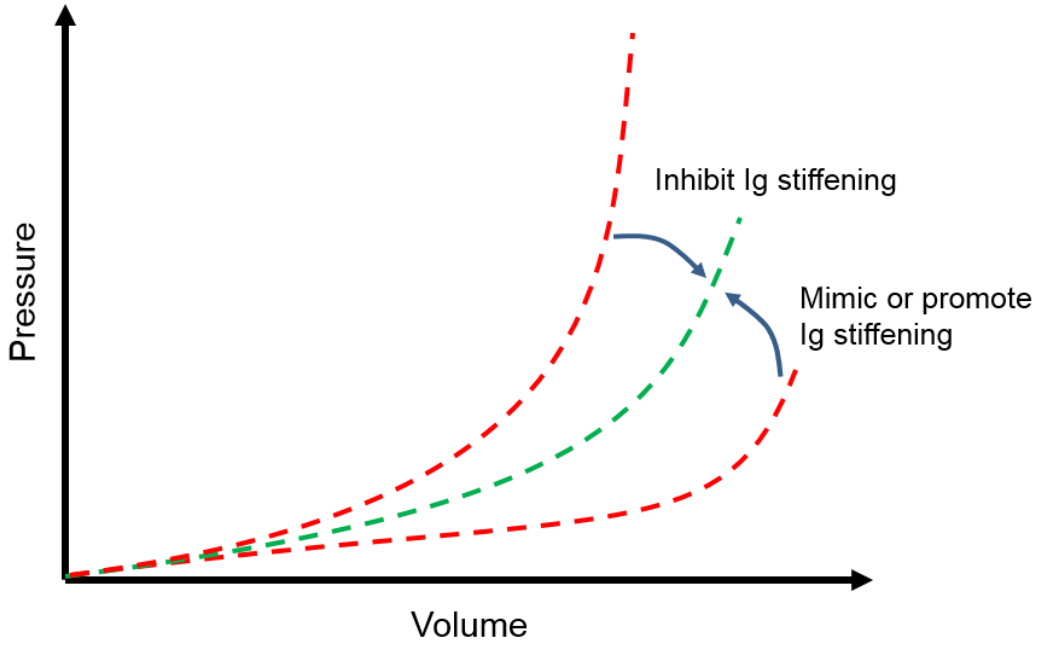


Figure 7-3 - Modification of ventricular stiffness by mimicking or inhibiting titin Ig domain stiffness could restore normal ventricular compliance.

Alternative methods for improving cardiac output in DCM rely on enhancing contractile function to compensate for ventricular dilatation. Enhancing Ca^{2+} sensitivity of force production or myosin activity using pharmaceuticals such as levosimendan or omecamtiv mecarbil, respectively, may be viable strategies [Shen *et al.*, 2010]. Another option with demonstrable success relies on enhancing myosin cross-bridge cycling using ATP analogues. Specifically, Regnier et al showed that 2-deoxy-ATP (dATP) causes faster myosin binding and cycling speeds *in vitro* compared to ATP [Regnier *et al.*, 1998]. When utilized as the contractile substrate in isolated cardiac muscles, dATP causes increased force production, force redevelopment rates, and NTPase at all Ca^{2+} levels [Adhikari *et al.*, 2004]. Delivery of dATP to living cardiomyocytes was accomplished by upregulating ribonucleotide reductase, the enzyme responsible for the rate-limiting step of dATP synthesis. This resulted in the dATP increasing from ~0.1 % to ~1.5 % of adenine nucleotide pool,

increasing the magnitude and rate of cardiomyocyte shortening without affecting Ca^{2+} concentrations [Korte *et al.*, 2011]. Transgenic overexpression of ribonucleotide reductase in a mouse model resulted in enhanced left ventricular function without hypertrophy or altered diastolic function [Nowakowski *et al.*, 2013]. Finally, demembranated cardiac muscle from end-stage heart failure patients exhibited increased force production, Ca^{2+} sensitivity, and force redevelopment rates when utilizing dATP [Moussavi-Harami *et al.*, 2015]. These results suggest that switching the cardiac contractile substrate may be sufficient to enhance systolic dysfunction and ameliorate diminished cardiac output in DCM and/or heart failure.

7.4 Future directions

7.4.1 Hypertrophic cardiomyopathy, energy compromise, and PRKAG2 cardiomyopathy

The results presented in this thesis suggest that increased AMPK activity impairs cardiac contractile function by reducing the phosphorylation of PKA target sites. Although the two kinases have generally opposing regulatory effects (discussed in Section 5.5.4), a direct causative link between AMPK and PKA has not been established. Given the wide array of known interactors for both kinases, numerous potential mechanisms could underlie the cross-talk between pathways. For example, genetically inactivating AMPK in yeast resulted in reduced phosphorylation of adenylyl cyclase and the PKA regulatory subunit, both of which directly regulate PKA activity [Braun *et al.*, 2014]. Measuring the levels, phosphorylation status, and activity of enzymes upstream of PKA, may therefore clarify the interaction between the pathways. Further, clarification of the localization of PKA activity by cAMP, A-kinase anchoring proteins, and phosphodiesterases

[Zaccolo and Pozzan, 2002] may reveal differing effects. Further, downstream effectors of PKA phosphorylation, notably protein phosphatases, could also be affected by the AMPK signalling pathway. Elucidation of the interaction between AMPK and PKA via these agents could provide more specific targets for pharmaceutical intervention. However, the interactome of AMPK is complex (Figure 7-4). Therefore, though assessing individual proteins hypothesized to link the AMPK and PKA pathways may provide positive indications, exclusion of the remaining viable targets necessarily biases the investigation. Instead, a non-hypothesis-driven study would more faithfully identify interactions between AMPK and PKA.

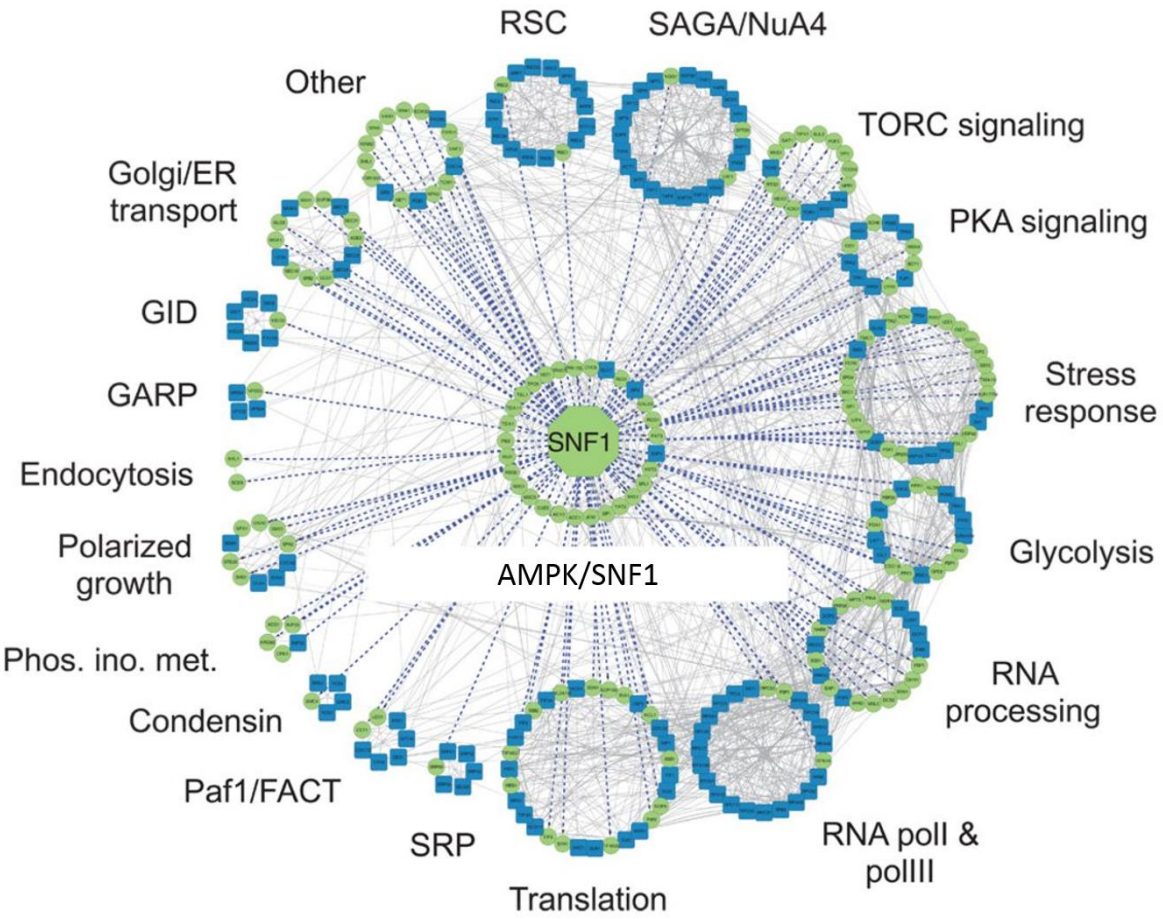


Figure 7-4 - Network of interactions between AMPK/Snf1 and various cellular pathways. Proteins with AMPK-dependent phosphorylation are shown in green and known AMPK-interacting proteins in blue. Adapted from Braun et al [Braun *et al.*, 2014] figure 1.

A comparable study was undertaken using mass spectrometry in *Saccharomyces cerevisiae* [Braun *et al.*, 2014]. The work identified 145 proteins that were differentially phosphorylated upon genetic inactivation of AMPK. However, the AMPK interactome may be considerably different in yeast than human cardiomyocytes. Therefore, an analysis of the phosphoproteome of cardiomyocytes from R299Q AMPK γ2 mice could highlight novel interactions that underlie observed molecular and functional modifications. A blunter approach could also be to assess the phosphoproteome of cardiomyocytes treated with an AMPK-activator such as AICAR, A-769662 [Sanders *et al.*, 2007], or compound 911 [Xiao *et al.*, 2013]. These investigations would reveal the range of modifications caused by altered AMPK activity in mammalian cardiomyocytes and provide valuable information regarding PRKAG2 cardiomyopathy as well as other cardiac conditions to which energetic compromise contributes.

7.4.2 Regulation of cardiac stiffness by αB-crystallin

Ongoing work in the lab of our collaborators in the Department of Physical and Theoretical Chemistry aims to crystallize the structure of the complex of titin Ig domains and αB-crystallin. This work will precisely identify the target region within titin as well as the portion of αB-crystallin responsible for binding. A successful result will therefore further educate the development of small molecules capable of mimicking or inhibiting the stiffening of titin Ig domains.

Besides this ongoing structural work, the role of αB-crystallin in regulating overall cardiac function may be probed further. Though the direct effect of the protein on titin Ig domain [Bullard *et al.*, 2004] and demembranated cardiac muscle (Chapter 6) stiffness has already been described, the *in vivo* effect has yet to be fully elucidated. An efficient method for determining the *in vivo* role of αB-crystallin would

be to produce mouse models with varying levels of αB-crystallin functionality. A knock-in model possessing the DCM-associated R157H αB-crystallin mutant would yield valuable insight into its contribution to disease pathogenesis. This animal could also be a suitable model to test the efficacy of αB-crystallin peptide or small molecule delivery mechanisms to alter overall cardiac stiffness. Together, these studies would represent significant progress in understanding the importance of αB-crystallin in cardiac health and disease.

7.5 Concluding remarks

This thesis investigated the contribution of altered cardiac biomechanics and Ca^{2+} handling to the pathogenesis of cardiomyopathy. In a mouse model of PRKAG2 cardiomyopathy, enhanced myofilament Ca^{2+} sensitivity and slowed cardiomyocyte relaxation were observed. These changes were explained by reduced phosphorylation of PKA target sites within the sarcomere and Ca^{2+} handling apparatus, suggesting novel interplay between AMPK and PKA pathways. This finding provides insight into the pathogenesis of PRKAG2 cardiomyopathy, which previously was characterized solely as a glycogen storage disease. The lack of glycogen accumulation in these animals, combined with abnormal contractile and Ca^{2+} handling properties, reveals a more nuanced mechanism of PRKAG2 cardiomyopathy development. Further, the identified interaction between energy- (AMPK) and stress- (PKA) signalling networks is likely to be involved in numerous additional disease pathways.

Investigations into the association of αB-crystallin mutations with DCM pathology elucidated the protein's role in regulating cardiac muscle biomechanics. αB-crystallin was shown to bind to titin Ig domains via a small region within its C-terminus and increase the overall stiffness of cardiac muscle. The DCM-associated

R157H mutant caused a smaller stiffening effect, suggesting that modification of cardiac muscle stiffness may contribute to the development of DCM. Further, the hypothesized titin-binding region (9-AA peptide) of αB-crystallin was shown to stiffen cardiac muscle alone. These results provide detail into the role of αB-crystallin in cardiac muscle function/dysfunction and suggest methods to regulate overall cardiac muscle stiffness.

References

Abozguia, K., P. Elliott, W. McKenna, T. T. Phan, G. Nallur-Shivu, I. Ahmed, A. R. Maher, K. Kaur, J. Taylor, A. Henning, H. Ashrafian, H. Watkins and M. Frenneaux (2010). "Metabolic modulator perhexiline corrects energy deficiency and improves exercise capacity in symptomatic hypertrophic cardiomyopathy." Circulation **122**(16): 1562-1569.

Adhikari, B. B., M. Regnier, A. J. Rivera, K. L. Kreutziger and D. A. Martyn (2004). "Cardiac length dependence of force and force redevelopment kinetics with altered cross-bridge cycling." Biophys J **87**(3): 1784-1794.

Ahmad, F., M. Arad, N. Musi, H. He, C. Wolf, D. Branco, A. R. Perez-Atayde, D. Stapleton, D. Bali, Y. Xing, R. Tian, L. J. Goodyear, C. I. Berul, J. S. Ingwall, C. E. Seidman and J. G. Seidman (2005). "Increased alpha2 subunit-associated AMPK activity and PRKAG2 cardiomyopathy." Circulation **112**(20): 3140-3148.

Akman, H. O., J. N. Sampayo, F. A. Ross, J. W. Scott, G. Wilson, L. Benson, C. Bruno, S. Shanske, D. G. Hardie and S. Dimauro (2007). "Fatal infantile cardiac glycogenosis with phosphorylase kinase deficiency and a mutation in the gamma2-subunit of AMP-activated protein kinase." Pediatr Res **62**(4): 499-504.

Amodeo, G. A., M. J. Rudolph and L. Tong (2007). "Crystal structure of the heterotrimer core of Saccharomyces cerevisiae AMPK homologue SNF1." Nature **449**(7161): 492-495.

Anderson, M. E., J. H. Brown and D. M. Bers (2011). "CaMKII in myocardial hypertrophy and heart failure." J Mol Cell Cardiol **51**(4): 468-473.

Aquilina, J. A., J. L. Benesch, O. A. Bateman, C. Slingsby and C. V. Robinson (2003). "Polydispersity of a mammalian chaperone: mass spectrometry reveals the population of oligomers in alphaB-crystallin." Proc Natl Acad Sci U S A **100**(19): 10611-10616.

Arad, M., D. W. Benson, A. R. Perez-Atayde, W. J. McKenna, E. A. Sparks, R. J. Kanter, K. McGarry, J. G. Seidman and C. E. Seidman (2002). "Constitutively active AMP kinase mutations cause glycogen storage disease mimicking hypertrophic cardiomyopathy." J Clin Invest **109**(3): 357-362.

Arad, M., I. P. Moskowitz, V. V. Patel, F. Ahmad, A. R. Perez-Atayde, D. B. Sawyer, M. Walter, G. H. Li, P. G. Burgon, C. T. Maguire, D. Stapleton, J. P. Schmitt, X. X. Guo, A. Pizard, S. Kupershmidt, D. M. Roden, C. I. Berul, C. E. Seidman and J. G. Seidman (2003). "Transgenic mice overexpressing mutant PRKAG2 define the cause of Wolff-Parkinson-White syndrome in glycogen storage cardiomyopathy." Circulation **107**(22): 2850-2856.

Arad, M., C. E. Seidman and J. G. Seidman (2007). "AMP-activated protein kinase in the heart: role during health and disease." Circ Res **100**(4): 474-488.

Arai, M., N. R. Alpert, D. H. MacLennan, P. Barton and M. Periasamy (1993). "Alterations in sarcoplasmic reticulum gene expression in human heart failure. A possible mechanism for alterations in systolic and diastolic properties of the failing myocardium." Circ Res **72**(2): 463-469.

Arai, M., H. Matsui and M. Periasamy (1994). "Sarcoplasmic reticulum gene expression in cardiac hypertrophy and heart failure." Circ Res **74**(4): 555-564.

Arrell, D. K., I. Neverova, H. Fraser, E. Marban and J. E. Van Eyk (2001). "Proteomic analysis of pharmacologically preconditioned cardiomyocytes reveals novel phosphorylation of myosin light chain 1." Circ Res **89**(6): 480-487.

Ashrafian, H., J. D. Horowitz and M. P. Frenneaux (2007). "Perhexiline." Cardiovasc Drug Rev **25**(1): 76-97.

Ashrafian, H., W. J. McKenna and H. Watkins (2011). "Disease pathways and novel therapeutic targets in hypertrophic cardiomyopathy." Circ Res **109**(1): 86-96.

Ashrafian, H., C. Redwood, E. Blair and H. Watkins (2003). "Hypertrophic cardiomyopathy:a paradigm for myocardial energy depletion." Trends Genet **19**(5): 263-268.

Ashrafian, H. and H. Watkins (2007). "Reviews of translational medicine and genomics in cardiovascular disease: new disease taxonomy and therapeutic implications

cardiomyopathies: therapeutics based on molecular phenotype." J Am Coll Cardiol **49**(12): 1251-1264.
Avraham, R. (2000). The Circulatory System. Philadelphia, PA, Chelsea House Publishers.
Backs, J., T. Backs, S. Neef, M. M. Kreusser, L. H. Lehmann, D. M. Patrick, C. E. Grueter, X. Qi, J. A. Richardson, J. A. Hill, H. A. Katus, R. Bassel-Duby, L. S. Maier and E. N. Olson (2009). "The delta isoform of CaM kinase II is required for pathological cardiac hypertrophy and remodeling after pressure overload." Proc Natl Acad Sci U S A **106**(7): 2342-2347.
Banerjee, S. K., K. R. McGaffin, X. N. Huang and F. Ahmad (2010). "Activation of cardiac hypertrophic signaling pathways in a transgenic mouse with the human PRKAG2 Thr400Asn mutation." Biochim Biophys Acta **1802**(2): 284-291.
Banerjee, S. K., R. Ramani, S. Saba, J. Rager, R. Tian, M. A. Mathier and F. Ahmad (2007). "A PRKAG2 mutation causes biphasic changes in myocardial AMPK activity and does not protect against ischemia." Biochem Biophys Res Commun **360**(2): 381-387.
Bassani, R. A. B., J.W.M.; Bers, D. M. (1995). "Relaxation in ferret ventricular myocytes: role of the sarcolemmal Ca ATPase." Pflügers Archiv **430**(4): 573-578.
Bateman, A. (1997). "The structure of a domain common to archaebacteria and the homocystinuria disease protein." Trends Biochem Sci **22**(1): 12-13.
Baudenbacher, F., T. Schober, J. R. Pinto, V. Y. Sidorov, F. Hilliard, R. J. Solaro, J. D. Potter and B. C. Knollmann (2008). "Myofilament Ca2+ sensitization causes susceptibility to cardiac arrhythmia in mice." J Clin Invest **118**(12): 3893-3903.
Belus, A., N. Piroddi, B. Scellini, C. Tesi, G. D'Amati, F. Girolami, M. Yacoub, F. Cecchi, I. Olivotto and C. Poggesi (2008). "The familial hypertrophic cardiomyopathy-associated myosin mutation R403Q accelerates tension generation and relaxation of human cardiac myofibrils." J Physiol **586**(Pt 15): 3639-3644.
Benesch, J. L., J. A. Aquilina, B. T. Ruotolo, F. Sobott and C. V. Robinson (2006). "Tandem mass spectrometry reveals the quaternary organization of macromolecular assemblies." Chem Biol **13**(6): 597-605.
Berne, R. L., M; Koeppen, B; Stanton, B (2004). Physiology, Elsevier Mosby.
Bers, D. (2001). Excitation-Contraction Coupling and Cardiac Contractile Force, Springer.
Bers, D. M. (2000). "Calcium fluxes involved in control of cardiac myocyte contraction." Circ Res **87**(4): 275-281.
Bers, D. M. (2002). "Cardiac excitation-contraction coupling." Nature **415**(6868): 198-205.
Bers, D. M. (2006). "Cardiac ryanodine receptor phosphorylation: target sites and functional consequences." Biochem J **396**(1): e1-3.
Bers, D. M. (2008). "Calcium cycling and signaling in cardiac myocytes." Annu Rev Physiol **70**: 23-49.
Bers, D. M. and T. Guo (2005). "Calcium signaling in cardiac ventricular myocytes." Ann N Y Acad Sci **1047**: 86-98.
Berth, M., F. M. Moser, M. Kolbe and J. Bernhardt (2007). "The state of the art in the analysis of two-dimensional gel electrophoresis images." Appl Microbiol Biotechnol **76**(6): 1223-1243.
Beuckelmann, D. J., M. Nabauer and E. Erdmann (1992). "Intracellular calcium handling in isolated ventricular myocytes from patients with terminal heart failure." Circulation **85**(3): 1046-1055.
Bhat, S. P. and C. N. Nagineni (1989). "alpha B subunit of lens-specific protein alpha-crystallin is present in other ocular and non-ocular tissues." Biochem Biophys Res Commun **158**(1): 319-325.
Blaeser, F., N. Ho, R. Prywes and T. A. Chatila (2000). "Ca(2+)-dependent gene expression mediated by MEF2 transcription factors." J Biol Chem **275**(1): 197-209.
Blair, E., C. Redwood, H. Ashrafian, M. Oliveira, J. Broxholme, B. Kerr, A. Salmon, I. Ostman-Smith and H. Watkins (2001). "Mutations in the gamma(2) subunit of AMP-activated protein kinase cause familial hypertrophic cardiomyopathy: evidence for the central role of energy compromise in disease pathogenesis." Hum Mol Genet **10**(11): 1215-1220.

Bouley, J., C. Chambon and B. Picard (2004). "Mapping of bovine skeletal muscle proteins using two-dimensional gel electrophoresis and mass spectrometry." Proteomics **4**(6): 1811-1824.

Braun, K. A., S. Vaga, K. M. Dombek, F. Fang, S. Palmisano, R. Aebersold and E. T. Young (2014). "Phosphoproteomic analysis identifies proteins involved in transcription-coupled mRNA decay as targets of Snf1 signaling." Sci Signal **7**(333): ra64.

Bristow, M. R., R. Ginsburg, W. Minobe, R. S. Cubicciotti, W. S. Sageman, K. Lurie, M. E. Billingham, D. C. Harrison and E. B. Stinson (1982). "Decreased catecholamine sensitivity and beta-adrenergic-receptor density in failing human hearts." N Engl J Med **307**(4): 205-211.

Bullard, B., C. Ferguson, A. Minajeva, M. C. Leake, M. Gautel, D. Labeit, L. Ding, S. Labeit, J. Horwitz, K. R. Leonard and W. A. Linke (2004). "Association of the chaperone alphaB-crystallin with titin in heart muscle." J Biol Chem **279**(9): 7917-7924.

Burkart, E. M., M. P. Sumandea, T. Kobayashi, M. Nili, A. F. Martin, E. Homsher and R. J. Solaro (2003). "Phosphorylation or glutamic acid substitution at protein kinase C sites on cardiac troponin I differentially depress myofilament tension and shortening velocity." J Biol Chem **278**(13): 11265-11272.

Burwinkel, B., J. W. Scott, C. Buhrer, F. K. van Landeghem, G. F. Cox, C. J. Wilson, D. Grahame Hardie and M. W. Kilimann (2005). "Fatal congenital heart glycogenosis caused by a recurrent activating R531Q mutation in the gamma 2-subunit of AMP-activated protein kinase (PRKAG2), not by phosphorylase kinase deficiency." Am J Hum Genet **76**(6): 1034-1049.

Buscemi, N., D. B. Foster, I. Neverova and J. E. Van Eyk (2002). "p21-activated kinase increases the calcium sensitivity of rat triton-skinned cardiac muscle fiber bundles via a mechanism potentially involving novel phosphorylation of troponin I." Circ Res **91**(6): 509-516.

Cabral-Lilly, D., L. S. Tobacman, J. P. Mehegan and C. Cohen (1997). "Molecular polarity in tropomyosin-troponin T co-crystals." Biophys J **73**(4): 1763-1770.

Cannell, M. B., H. Cheng and W. J. Lederer (1994). "Spatial non-uniformities in [Ca2+]i during excitation-contraction coupling in cardiac myocytes." Biophys J **67**(5): 1942-1956.

Carling, D., F. V. Mayer, M. J. Sanders and S. J. Gamblin (2011). "AMP-activated protein kinase: nature's energy sensor." Nat Chem Biol **7**(8): 512-518.

Carling, D., M. J. Sanders and A. Woods (2008). "The regulation of AMP-activated protein kinase by upstream kinases." Int J Obes (Lond) **32 Suppl 4**: S55-59.

Carling, D., C. Thornton, A. Woods and M. J. Sanders (2012). "AMP-activated protein kinase: new regulation, new roles?" Biochem J **445**(1): 11-27.

Carr, A. N., A. G. Schmidt, Y. Suzuki, F. del Monte, Y. Sato, C. Lanner, K. Breeden, S. L. Jing, P. B. Allen, P. Greengard, A. Yatani, B. D. Hoit, I. L. Grupp, R. J. Hajjar, A. A. DePaoli-Roach and E. G. Kranias (2002). "Type 1 phosphatase, a negative regulator of cardiac function." Mol Cell Biol **22**(12): 4124-4135.

Catterall, W. A. (1995). "Structure and function of voltage-gated ion channels." Annu Rev Biochem **64**: 493-531.

Cazorla, O., Y. Wu, T. C. Irving and H. Granzier (2001). "Titin-based modulation of calcium sensitivity of active tension in mouse skinned cardiac myocytes." Circ Res **88**(10): 1028-1035.

Cheney, R. E., M. A. Riley and M. S. Mooseker (1993). "Phylogenetic analysis of the myosin superfamily." Cell Motil Cytoskeleton **24**(4): 215-223.

Cheng, H., W. J. Lederer and M. B. Cannell (1993). "Calcium sparks: elementary events underlying excitation-contraction coupling in heart muscle." Science **262**(5134): 740-744.

Cheung, P. C., I. P. Salt, S. P. Davies, D. G. Hardie and D. Carling (2000). "Characterization of AMP-activated protein kinase gamma-subunit isoforms and their role in AMP binding." Biochem J **346 Pt 3**: 659-669.

Chow, C. W., M. Rincon, J. Cavanagh, M. Dickens and R. J. Davis (1997). "Nuclear accumulation of NFAT4 opposed by the JNK signal transduction pathway." Science **278**(5343): 1638-1641.

Chu, G., J. W. Lester, K. B. Young, W. Luo, J. Zhai and E. G. Kranias (2000). "A single site (Ser16) phosphorylation in phospholamban is sufficient in mediating its maximal cardiac responses to beta -agonists." J Biol Chem **275**(49): 38938-38943.

Cooke, R. (1986). "The mechanism of muscle contraction." CRC Crit Rev Biochem **21**(1): 53-118.

Cooke, R. (1997). "Actomyosin interaction in striated muscle." Physiol Rev **77**(3): 671-697.

Copeland, O., S. Sadayappan, A. E. Messer, G. J. Steinen, J. van der Velden and S. B. Marston (2010). "Analysis of cardiac myosin binding protein-C phosphorylation in human heart muscle." J Mol Cell Cardiol **49**(6): 1003-1011.

Coven, D. L., X. Hu, L. Cong, R. Bergeron, G. I. Shulman, D. G. Hardie and L. H. Young (2003). "Physiological role of AMP-activated protein kinase in the heart: graded activation during exercise." Am J Physiol Endocrinol Metab **285**(3): E629-636.

Crabtree, G. R. (1999). "Generic signals and specific outcomes: signaling through Ca2+, calcineurin, and NF-AT." Cell **96**(5): 611-614.

Crilley, J. G., E. A. Boehm, E. Blair, B. Rajagopalan, A. M. Blamire, P. Styles, W. J. McKenna, I. Ostman-Smith, K. Clarke and H. Watkins (2003). "Hypertrophic cardiomyopathy due to sarcomeric gene mutations is characterized by impaired energy metabolism irrespective of the degree of hypertrophy." J Am Coll Cardiol **41**(10): 1776-1782.

Cuello, F., S. C. Bardswell, R. S. Haworth, E. Ehler, S. Sadayappan, J. C. Kentish and M. Avkiran (2011). "Novel role for p90 ribosomal S6 kinase in the regulation of cardiac myofilament phosphorylation." J Biol Chem **286**(7): 5300-5310.

Curtis, B. M. and W. A. Catterall (1984). "Purification of the calcium antagonist receptor of the voltage-sensitive calcium channel from skeletal muscle transverse tubules." Biochemistry **23**(10): 2113-2118.

Curtis, B. M. and W. A. Catterall (1985). "Phosphorylation of the calcium antagonist receptor of the voltage-sensitive calcium channel by cAMP-dependent protein kinase." Proc Natl Acad Sci U S A **82**(8): 2528-2532.

Daniel, T. and D. Carling (2002). "Functional analysis of mutations in the gamma 2 subunit of AMP-activated protein kinase associated with cardiac hypertrophy and Wolff-Parkinson-White syndrome." J Biol Chem **277**(52): 51017-51024.

Davies, J. K., D. J. Wells, K. Liu, H. R. Whitrow, T. D. Daniel, R. Grignani, C. A. Lygate, J. E. Schneider, G. Noel, H. Watkins and D. Carling (2006). "Characterization of the role of gamma2 R531G mutation in AMP-activated protein kinase in cardiac hypertrophy and Wolff-Parkinson-White syndrome." Am J Physiol Heart Circ Physiol **290**(5): H1942-1951.

Davies, S. P., D. Carling and D. G. Hardie (1989). "Tissue distribution of the AMP-activated protein kinase, and lack of activation by cyclic-AMP-dependent protein kinase, studied using a specific and sensitive peptide assay." Eur J Biochem **186**(1-2): 123-128.

Davis, J. and J. M. Metzger (2010). "Combinatorial effects of double cardiomyopathy mutant alleles in rodent myocytes: a predictive cellular model of myofilament dysregulation in disease." PLoS One **5**(2): e9140.

Davis, J. S., S. Hassanzadeh, S. Winitsky, H. Lin, C. Satorius, R. Vemuri, A. H. Aletras, H. Wen and N. D. Epstein (2001). "The overall pattern of cardiac contraction depends on a spatial gradient of myosin regulatory light chain phosphorylation." Cell **107**(5): 631-641.

de Tombe, P. P., R. D. Mateja, K. Tachampa, Y. Ait Mou, G. P. Farman and T. C. Irving (2010). "Myofilament length dependent activation." J Mol Cell Cardiol **48**(5): 851-858.

del Monte, F., S. E. Harding, U. Schmidt, T. Matsui, Z. B. Kang, G. W. Dec, J. K. Gwathmey, A. Rosenzweig and R. J. Hajjar (1999). "Restoration of contractile function in isolated cardiomyocytes from failing human hearts by gene transfer of SERCA2a." Circulation **100**(23): 2308-2311.

Dellefave, L. and E. M. McNally (2010). "The genetics of dilated cardiomyopathy." Curr Opin Cardiol **25**(3): 198-204.
Ding, P., J. Huang, P. K. Battiprolu, J. A. Hill, K. E. Kamm and J. T. Stull (2010). "Cardiac myosin light chain kinase is necessary for myosin regulatory light chain phosphorylation and cardiac performance in vivo." J Biol Chem **285**(52): 40819-40829.
DiPolo, R. and L. Beauge (2006). "Sodium/calcium exchanger: influence of metabolic regulation on ion carrier interactions." Physiol Rev **86**(1): 155-203.
Djouder, N., R. D. Tuerk, M. Suter, P. Salvioni, R. F. Thali, R. Scholz, K. Vaahtomeri, Y. Auchli, H. Rechsteiner, R. A. Brunisholz, B. Viollet, T. P. Makela, T. Wallimann, D. Neumann and W. Krek (2010). "PKA phosphorylates and inactivates AMPKalpha to promote efficient lipolysis." EMBO J **29**(2): 469-481.
Dodge-Kafka, K. L., J. Soughayer, G. C. Pare, J. J. Carlisle Michel, L. K. Langeberg, M. S. Kapiloff and J. D. Scott (2005). "The protein kinase A anchoring protein mAKAP coordinates two integrated cAMP effector pathways." Nature **437**(7058): 574-578.
Dokhac, L., A. D'Albis, C. Janmot and S. Harbon (1986). "Myosin light chain phosphorylation in intact rat uterine smooth muscle. Role of calcium and cyclic AMP." J Muscle Res Cell Motil **7**(3): 259-268.
Elliott, P., B. Andersson, E. Arbustini, Z. Bilinska, F. Cecchi, P. Charron, O. Dubourg, U. Kuhl, B. Maisch, W. J. McKenna, L. Monserrat, S. Pankuweit, C. Rapezzi, P. Seferovic, L. Tavazzi and A. Keren (2008). "Classification of the cardiomyopathies: a position statement from the European Society Of Cardiology Working Group on Myocardial and Pericardial Diseases." Eur Heart J **29**(2): 270-276.
Elliott, P. M., A. Anastasakis, M. A. Borger, M. Borggrefe, F. Cecchi, P. Charron, A. A. Hagege, A. Lafont, G. Limongelli, H. Mahrholdt, W. J. McKenna, J. Mogensen, P. Nihoyannopoulos, S. Nistri, P. G. Pieper, B. Pieske, C. Rapezzi, F. H. Rutten, C. Tillmanns and H. Watkins (2014). "2014 ESC Guidelines on diagnosis and management of hypertrophic cardiomyopathy: the Task Force for the Diagnosis and Management of Hypertrophic Cardiomyopathy of the European Society of Cardiology (ESC)." Eur Heart J **35**(39): 2733-2779.
Ellis, S. B., M. E. Williams, N. R. Ways, R. Brenner, A. H. Sharp, A. T. Leung, K. P. Campbell, E. McKenna, W. J. Koch, A. Hui and et al. (1988). "Sequence and expression of mRNAs encoding the alpha 1 and alpha 2 subunits of a DHP-sensitive calcium channel." Science **241**(4873): 1661-1664.
Engelhardt, S., M. Bohm, E. Erdmann and M. J. Lohse (1996). "Analysis of beta-adrenergic receptor mRNA levels in human ventricular biopsy specimens by quantitative polymerase chain reactions: progressive reduction of beta 1-adrenergic receptor mRNA in heart failure." J Am Coll Cardiol **27**(1): 146-154.
Fabiato, A. (1982). "Fluorescence and differential light absorption recordings with calcium probes and potential-sensitive dyes in skinned cardiac cells." Can J Physiol Pharmacol **60**(4): 556-567.
Fabiato, A. (1983). "Calcium-induced release of calcium from the cardiac sarcoplasmic reticulum." Am J Physiol **245**(1): C1-14.
Fabiato, A. and F. Fabiato (1975). "Contractions induced by a calcium-triggered release of calcium from the sarcoplasmic reticulum of single skinned cardiac cells." J Physiol **249**(3): 469-495.
Fabiato, A. and F. Fabiato (1977). "Calcium release from the sarcoplasmic reticulum." Circ Res **40**(2): 119-129.
Fabiato, A. and F. Fabiato (1978). "Calcium-induced release of calcium from the sarcoplasmic reticulum of skinned cells from adult human, dog, cat, rabbit, rat, and frog hearts and from fetal and new-born rat ventricles." Ann N Y Acad Sci **307**: 491-522.
Fabiato, A. and F. Fabiato (1979). "Calcium and cardiac excitation-contraction coupling." Annu Rev Physiol **41**: 473-484.

Farah, C. S., C. A. Miyamoto, C. H. Ramos, A. C. da Silva, R. B. Quaggio, K. Fujimori, L. B. Smillie and F. C. Reinach (1994). "Structural and regulatory functions of the NH2- and COOH-terminal regions of skeletal muscle troponin I." J Biol Chem **269**(7): 5230-5240.

Farah, C. S. and F. C. Reinach (1995). "The troponin complex and regulation of muscle contraction." FASEB J **9**(9): 755-767.

Fatkin, D., B. K. McConnell, J. O. Mudd, C. Semsarian, I. G. Moskowitz, F. J. Schoen, M. Giewat, C. E. Seidman and J. G. Seidman (2000). "An abnormal Ca(2+) response in mutant sarcomere protein-mediated familial hypertrophic cardiomyopathy." J Clin Invest **106**(11): 1351-1359.

Flashman, E., C. Redwood, J. Moolman-Smook and H. Watkins (2004). "Cardiac myosin binding protein C: its role in physiology and disease." Circ Res **94**(10): 1279-1289.

Fleischer, S., E. M. Ogunbunmi, M. C. Dixon and E. A. Fleer (1985). "Localization of Ca2+ release channels with ryanodine in junctional terminal cisternae of sarcoplasmic reticulum of fast skeletal muscle." Proc Natl Acad Sci U S A **82**(21): 7256-7259.

Fox, A. P., M. C. Nowycky and R. W. Tsien (1987). "Kinetic and pharmacological properties distinguishing three types of calcium currents in chick sensory neurones." J Physiol **394**: 149-172.

Fox, A. P., M. C. Nowycky and R. W. Tsien (1987). "Single-channel recordings of three types of calcium channels in chick sensory neurones." J Physiol **394**: 173-200.

Frank, K., C. Tilgmann, T. R. Shannon, D. M. Bers and E. G. Kranias (2000). "Regulatory role of phospholamban in the efficiency of cardiac sarcoplasmic reticulum Ca2+ transport." Biochemistry **39**(46): 14176-14182.

Freiburg, A. and M. Gautel (1996). "A molecular map of the interactions between titin and myosin-binding protein C. Implications for sarcomeric assembly in familial hypertrophic cardiomyopathy." Eur J Biochem **235**(1-2): 317-323.

Frey, N., K. Brixius, R. H. Schwinger, T. Benis, A. Karpowski, H. P. Lorenzen, M. Luedde, H. A. Katus and W. M. Franz (2006). "Alterations of tension-dependent ATP utilization in a transgenic rat model of hypertrophic cardiomyopathy." J Biol Chem **281**(40): 29575-29582.

Frey, N., M. Luedde and H. A. Katus (2012). "Mechanisms of disease: hypertrophic cardiomyopathy." Nat Rev Cardiol **9**(2): 91-100.

Frey, N., T. A. McKinsey and E. N. Olson (2000). "Decoding calcium signals involved in cardiac growth and function." Nat Med **6**(11): 1221-1227.

Frey, N. and E. N. Olson (2003). "Cardiac hypertrophy: the good, the bad, and the ugly." Annu Rev Physiol **65**: 45-79.

Fuchs, F. and S. H. Smith (2001). "Calcium, cross-bridges, and the Frank-Starling relationship." News Physiol Sci **16**: 5-10.

Fukuda, N., Y. Wu, G. Farman, T. C. Irving and H. Granzier (2003). "Titin isoform variance and length dependence of activation in skinned bovine cardiac muscle." J Physiol **553**(Pt 1): 147-154.

Fung, Y. C. (1993). Biomechanics : mechanical properties of living tissues. New York, Springer-Verlag.

Garrington, T. P. and G. L. Johnson (1999). "Organization and regulation of mitogen-activated protein kinase signaling pathways." Curr Opin Cell Biol **11**(2): 211-218.

Geeves, M. A. and K. C. Holmes (2005). "The molecular mechanism of muscle contraction." Adv Protein Chem **71**: 161-193.

Geier, C., A. Perrot, C. Ozcelik, P. Binner, D. Counsell, K. Hoffmann, B. Pilz, Y. Martiniak, K. Gehmlich, P. F. van der Ven, D. O. Furst, A. Vornwald, E. von Hodenberg, P. Nurnberg, T. Scheffold, R. Dietz and K. J. Osterziel (2003). "Mutations in the human muscle LIM protein gene in families with hypertrophic cardiomyopathy." Circulation **107**(10): 1390-1395.

Geisterfer-Lowrance, A. A., S. Kass, G. Tanigawa, H. P. Vosberg, W. McKenna, C. E. Seidman and J. G. Seidman (1990). "A molecular basis for familial hypertrophic cardiomyopathy: a beta cardiac myosin heavy chain gene missense mutation." Cell **62**(5): 999-1006.

Genot, E., S. Cleverley, S. Henning and D. Cantrell (1996). "Multiple p21ras effector pathways regulate nuclear factor of activated T cells." EMBO J **15**(15): 3923-3933.
Gerull, B., M. Gramlich, J. Atherton, M. McNabb, K. Trombitas, S. Sasse-Klaassen, J. G. Seidman, C. Seidman, H. Granzier, S. Labeit, M. Frenneaux and L. Thierfelder (2002). "Mutations of TTN, encoding the giant muscle filament titin, cause familial dilated cardiomyopathy." Nat Genet **30**(2): 201-204.
Ghosh, A. and M. E. Greenberg (1995). "Calcium signaling in neurons: molecular mechanisms and cellular consequences." Science **268**(5208): 239-247.
Goldman, D. E. (1943). "Potential, Impedance, and Rectification in Membranes." J Gen Physiol **27**(1): 37-60.
Golenhofen, N., A. Arbeiter, R. Koob and D. Drenckhahn (2002). "Ischemia-induced association of the stress protein alpha B-crystallin with I-band portion of cardiac titin." J Mol Cell Cardiol **34**(3): 309-319.
Gollob, M. H. (2003). "Glycogen storage disease as a unifying mechanism of disease in the PRKAG2 cardiac syndrome." Biochem Soc Trans **31**(Pt 1): 228-231.
Gollob, M. H., M. S. Green, A. S. Tang, T. Gollob, A. Karibe, A. S. Ali Hassan, F. Ahmad, R. Lozado, G. Shah, L. Fananapazir, L. L. Bachinski and R. Roberts (2001). "Identification of a gene responsible for familial Wolff-Parkinson-White syndrome." N Engl J Med **344**(24): 1823-1831.
Gollob, M. H., M. S. Green, A. S. Tang and R. Roberts (2002). "PRKAG2 cardiac syndrome: familial ventricular preexcitation, conduction system disease, and cardiac hypertrophy." Curr Opin Cardiol **17**(3): 229-234.
Gomez del Arco, P., S. Martinez-Martinez, J. L. Maldonado, I. Ortega-Perez and J. M. Redondo (2000). "A role for the p38 MAP kinase pathway in the nuclear shuttling of NFATp." J Biol Chem **275**(18): 13872-13878.
Gordon, A. M., E. Homsher and M. Regnier (2000). "Regulation of contraction in striated muscle." Physiol Rev **80**(2): 853-924.
Gordon, A. M., M. Regnier and E. Homsher (2001). "Skeletal and cardiac muscle contractile activation: tropomyosin "rocks and rolls"." News Physiol Sci **16**: 49-55.
Gordon, A. M., A. J. Rivera, C. K. Wang and M. Regnier (2003). "Cooperative activation of skeletal and cardiac muscle." Adv Exp Med Biol **538**: 371-378; discussion 378-379.
Grassi, G., G. Seravalle, F. Quarti-Trevano, R. Dell'Oro, F. Arenare, D. Spaziani and G. Mancia (2009). "Sympathetic and baroreflex cardiovascular control in hypertension-related left ventricular dysfunction." Hypertension **53**(2): 205-209.
Griffith, L. M., S. M. Downs and J. A. Spudich (1987). "Myosin light chain kinase and myosin light chain phosphatase from Dictyostelium: effects of reversible phosphorylation on myosin structure and function." J Cell Biol **104**(5): 1309-1323.
Gruen, M. and M. Gautel (1999). "Mutations in beta-myosin S2 that cause familial hypertrophic cardiomyopathy (FHC) abolish the interaction with the regulatory domain of myosin-binding protein-C." J Mol Biol **286**(3): 933-949.
Grynkiewicz, G., M. Poenie and R. Y. Tsien (1985). "A new generation of Ca2+ indicators with greatly improved fluorescence properties." J Biol Chem **260**(6): 3440-3450.
Guo, W., S. J. Bharmal, K. Esbona and M. L. Greaser (2010). "Titin diversity--alternative splicing gone wild." J Biomed Biotechnol **2010**: 753675.
Halliburton, W. D. (1887). "On Muscle-Plasma." J Physiol **8**(3-4): 133-202.
Hardie, D. G. (2007). "AMP-activated protein kinase as a drug target." Annu Rev Pharmacol Toxicol **47**: 185-210.
Hardie, D. G. (2007). "AMP-activated/SNF1 protein kinases: conserved guardians of cellular energy." Nat Rev Mol Cell Biol **8**(10): 774-785.
Hardie, D. G. (2011). "AMP-activated protein kinase: an energy sensor that regulates all aspects of cell function." Genes Dev **25**(18): 1895-1908.
Hardie, D. G. (2011). "Signal transduction: How cells sense energy." Nature **472**(7342): 176-177.

Hardie, D. G. (2014). "AMPK-Sensing Energy while Talking to Other Signaling Pathways." Cell Metab **20**(6): 939-952.
Hardie, D. G., D. Carling and M. Carlson (1998). "The AMP-activated/SNF1 protein kinase subfamily: metabolic sensors of the eukaryotic cell?" Annu Rev Biochem **67**: 821-855.
Hardie, D. G., F. A. Ross and S. A. Hawley (2012). "AMPK: a nutrient and energy sensor that maintains energy homeostasis." Nat Rev Mol Cell Biol **13**(4): 251-262.
Harris, S. P., C. R. Bartley, T. A. Hacker, K. S. McDonald, P. S. Douglas, M. L. Greaser, P. A. Powers and R. L. Moss (2002). "Hypertrophic cardiomyopathy in cardiac myosin binding protein-C knockout mice." Circ Res **90**(5): 594-601.
Harris, S. P., E. Rostkova, M. Gautel and R. L. Moss (2004). "Binding of myosin binding protein-C to myosin subfragment S2 affects contractility independent of a tether mechanism." Circ Res **95**(9): 930-936.
Hasenfuss, G., H. Reinecke, R. Studer, M. Meyer, B. Pieske, J. Holtz, C. Holubarsch, H. Posival, H. Just and H. Drexler (1994). "Relation between myocardial function and expression of sarcoplasmic reticulum Ca(2+)-ATPase in failing and nonfailing human myocardium." Circ Res **75**(3): 434-442.
Hawley, S. A., J. Boudeau, J. L. Reid, K. J. Mustard, L. Udd, T. P. Makela, D. R. Alessi and D. G. Hardie (2003). "Complexes between the LKB1 tumor suppressor, STRAD alpha/beta and MO25 alpha/beta are upstream kinases in the AMP-activated protein kinase cascade." J Biol **2**(4): 28.
Hawley, S. A., D. A. Pan, K. J. Mustard, L. Ross, J. Bain, A. M. Edelman, B. G. Frenguelli and D. G. Hardie (2005). "Calmodulin-dependent protein kinase kinase-beta is an alternative upstream kinase for AMP-activated protein kinase." Cell Metab **2**(1): 9-19.
Hein, S., S. Kostin, A. Heling, Y. Maeno and J. Schaper (2000). "The role of the cytoskeleton in heart failure." Cardiovasc Res **45**(2): 273-278.
Helper, D. J., J. A. Lash and D. R. Hathaway (1988). "Distribution of isoelectric variants of the 17,000-dalton myosin light chain in mammalian smooth muscle." J Biol Chem **263**(30): 15748-15753.
Hernandez, O. M., M. Jones, G. Guzman and D. Szczesna-Cordary (2007). "Myosin essential light chain in health and disease." Am J Physiol Heart Circ Physiol **292**(4): H1643-1654.
Herrmann-Frank, A., H. C. Luttgau and D. G. Stephenson (1999). "Caffeine and excitation-contraction coupling in skeletal muscle: a stimulating story." J Muscle Res Cell Motil **20**(2): 223-237.
Herron, T. J., E. Rostkova, G. Kunst, R. Chaturvedi, M. Gautel and J. C. Kentish (2006). "Activation of myocardial contraction by the N-terminal domains of myosin binding protein-C." Circ Res **98**(10): 1290-1298.
Hodgkin, A. L., A. F. Huxley and B. Katz (1952). "Measurement of current-voltage relations in the membrane of the giant axon of Loligo." J Physiol **116**(4): 424-448.
Hogan, P. G., L. Chen, J. Nardone and A. Rao (2003). "Transcriptional regulation by calcium, calcineurin, and NFAT." Genes Dev **17**(18): 2205-2232.
Holmes, K. C. (1996). "Muscle proteins--their actions and interactions." Curr Opin Struct Biol **6**(6): 781-789.
Holmes, K. C. (2008). Myosins: A Superfamily of Molecular Motors, Springer.
Holmes, K. C., D. Popp, W. Gebhard and W. Kabsch (1990). "Atomic model of the actin filament." Nature **347**(6288): 44-49.
Horwitz, J. (1992). "Alpha-crystallin can function as a molecular chaperone." Proc Natl Acad Sci U S A **89**(21): 10449-10453.
Horwitz, J. (2000). "The function of alpha-crystallin in vision." Semin Cell Dev Biol **11**(1): 53-60.
Houdusse, A., M. L. Love, R. Dominguez, Z. Grabarek and C. Cohen (1997). "Structures of four Ca2+-bound troponin C at 2.0 A resolution: further insights into the Ca2+-switch in the calmodulin superfamily." Structure **5**(12): 1695-1711.

Huke, S., R. Venkataraman, M. Faggioni, S. Bennuri, H. S. Hwang, F. Baudenbacher and B. C. Knollmann (2013). "Focal energy deprivation underlies arrhythmia susceptibility in mice with calcium-sensitized myofilaments." Circ Res **112**(10): 1334-1344.

Hurley, R. L., K. A. Anderson, J. M. Franzone, B. E. Kemp, A. R. Means and L. A. Witters (2005). "The Ca2+/calmodulin-dependent protein kinase kinases are AMP-activated protein kinase kinases." J Biol Chem **280**(32): 29060-29066.

Huxley, A. F. and R. M. Simmons (1971). "Proposed mechanism of force generation in striated muscle." Nature **233**(5321): 533-538.

Inagaki, N., T. Hayashi, T. Arimura, Y. Koga, M. Takahashi, H. Shibata, K. Teraoka, T. Chikamori, A. Yamashina and A. Kimura (2006). "Alpha B-crystallin mutation in dilated cardiomyopathy." Biochem Biophys Res Commun **342**(2): 379-386.

Ingwall, J. S. and R. G. Weiss (2004). "Is the failing heart energy starved? On using chemical energy to support cardiac function." Circ Res **95**(2): 135-145.

Inui, M., A. Saito and S. Fleischer (1987). "Isolation of the ryanodine receptor from cardiac sarcoplasmic reticulum and identity with the feet structures." J Biol Chem **262**(32): 15637-15642.

Itoh-Satoh, M., T. Hayashi, H. Nishi, Y. Koga, T. Arimura, T. Koyanagi, M. Takahashi, S. Hohda, K. Ueda, T. Nouchi, M. Hiroe, F. Marumo, T. Imaizumi, M. Yasunami and A. Kimura (2002). "Titin mutations as the molecular basis for dilated cardiomyopathy." Biochem Biophys Res Commun **291**(2): 385-393.

Iwamoto, T., Y. Pan, S. Wakabayashi, T. Imagawa, H. I. Yamanaka and M. Shigekawa (1996). "Phosphorylation-dependent regulation of cardiac Na+/Ca2+ exchanger via protein kinase C." J Biol Chem **271**(23): 13609-13615.

Jaenicke, R. and C. Slingsby (2001). "Lens crystallins and their microbial homologs: structure, stability, and function." Crit Rev Biochem Mol Biol **36**(5): 435-499.

Jagatheesan, G., S. Rajan, N. Petrashevskaya, A. Schwartz, G. Boivin, G. M. Arteaga, R. J. Solaro, S. B. Liggett and D. F. Wieczorek (2007). "Rescue of tropomyosin-induced familial hypertrophic cardiomyopathy mice by transgenesis." Am J Physiol Heart Circ Physiol **293**(2): H949-958.

Jagatheesan, G., S. Rajan, N. Petrashevskaya, A. Schwartz, G. Boivin, S. Vahebi, P. DeTombe, R. J. Solaro, E. Labitzke, G. Hilliard and D. F. Wieczorek (2003). "Functional importance of the carboxyl-terminal region of striated muscle tropomyosin." J Biol Chem **278**(25): 23204-23211.

Jay, S. D., S. B. Ellis, A. F. McCue, M. E. Williams, T. S. Vedvick, M. M. Harpold and K. P. Campbell (1990). "Primary structure of the gamma subunit of the DHP-sensitive calcium channel from skeletal muscle." Science **248**(4954): 490-492.

Jefferies, J. L. and J. A. Towbin (2010). "Dilated cardiomyopathy." Lancet **375**(9716): 752-762.

Jiang, D., R. Wang, B. Xiao, H. Kong, D. J. Hunt, P. Choi, L. Zhang and S. R. Chen (2005). "Enhanced store overload-induced Ca2+ release and channel sensitivity to luminal Ca2+ activation are common defects of RyR2 mutations linked to ventricular tachycardia and sudden death." Circ Res **97**(11): 1173-1181.

Kabsch, W., H. G. Mannherz, D. Suck, E. F. Pai and K. C. Holmes (1990). "Atomic structure of the actin:DNase I complex." Nature **347**(6288): 37-44.

Kamisago, M., S. D. Sharma, S. R. DePalma, S. Solomon, P. Sharma, B. McDonough, L. Smoot, M. P. Mullen, P. K. Woolf, E. D. Wigle, J. G. Seidman and C. E. Seidman (2000). "Mutations in sarcomere protein genes as a cause of dilated cardiomyopathy." N Engl J Med **343**(23): 1688-1696.

Kelly, B. P., M. W. Russell, J. R. Hennessy and G. J. Ensing (2009). "Severe hypertrophic cardiomyopathy in an infant with a novel PRKAG2 gene mutation: potential differences between infantile and adult onset presentation." Pediatr Cardiol **30**(8): 1176-1179.

Kentish, J. C., D. T. McCloskey, J. Layland, S. Palmer, J. M. Leiden, A. F. Martin and R. J. Solaro (2001). "Phosphorylation of troponin I by protein kinase A accelerates relaxation and crossbridge cycle kinetics in mouse ventricular muscle." Circ Res **88**(10): 1059-1065.

Kim, M., R. W. Hunter, L. Garcia-Menendez, G. Gong, Y. Y. Yang, S. C. Kolwicz, Jr., J. Xu, K. Sakamoto, W. Wang and R. Tian (2014). "Mutation in the gamma2-subunit of AMP-activated protein kinase stimulates cardiomyocyte proliferation and hypertrophy independent of glycogen storage." Circ Res **114**(6): 966-975.

Kimura, Y., K. Kurzydlowski, M. Tada and D. H. MacLennan (1997). "Phospholamban inhibitory function is activated by depolymerization." J Biol Chem **272**(24): 15061-15064.

Knollmann, B. C., P. Kirchhof, S. G. Sirenko, H. Degen, A. E. Greene, T. Schober, J. C. Mackow, L. Fabritz, J. D. Potter and M. Morad (2003). "Familial hypertrophic cardiomyopathy-linked mutant troponin T causes stress-induced ventricular tachycardia and Ca2+-dependent action potential remodeling." Circ Res **92**(4): 428-436.

Koley, D. and A. J. Bard (2010). "Triton X-100 concentration effects on membrane permeability of a single HeLa cell by scanning electrochemical microscopy (SECM)." Proc Natl Acad Sci U S A **107**(39): 16783-16787.

Konhilas, J. P., T. C. Irving and P. P. de Tombe (2002). "Frank-Starling law of the heart and the cellular mechanisms of length-dependent activation." Pflugers Arch **445**(3): 305-310.

Konhilas, J. P., T. C. Irving, B. M. Wolska, E. E. Jweied, A. F. Martin, R. J. Solaro and P. P. de Tombe (2003). "Troponin I in the murine myocardium: influence on length-dependent activation and interfilament spacing." J Physiol **547**(Pt 3): 951-961.

Kooij, V., M. Saes, K. Jaquet, R. Zaremba, D. B. Foster, A. M. Murphy, C. Dos Remedios, J. van der Velden and G. J. Stienen (2010). "Effect of troponin I Ser23/24 phosphorylation on Ca2+-sensitivity in human myocardium depends on the phosphorylation background." J Mol Cell Cardiol **48**(5): 954-963.

Korte, F. S., J. Dai, K. Buckley, E. R. Feest, N. Adamek, M. A. Geeves, C. E. Murry and M. Regnier (2011). "Upregulation of cardiomyocyte ribonucleotide reductase increases intracellular 2 deoxy-ATP, contractility, and relaxation." J Mol Cell Cardiol **51**(6): 894-901.

Kranias, E. G. and R. J. Solaro (1982). "Phosphorylation of troponin I and phospholamban during catecholamine stimulation of rabbit heart." Nature **298**(5870): 182-184.

Labeit, S. and B. Kolmerer (1995). "Titins: giant proteins in charge of muscle ultrastructure and elasticity." Science **270**(5234): 293-296.

Lai, F. A., K. Anderson, E. Rousseau, Q. Y. Liu and G. Meissner (1988). "Evidence for a Ca2+ channel within the ryanodine receptor complex from cardiac sarcoplasmic reticulum." Biochem Biophys Res Commun **151**(1): 441-449.

Lakowicz, J. R., I. Gryczynski, H. C. Cheung, C. K. Wang and M. L. Johnson (1988). "Distance distributions in native and random-coil troponin I from frequency-domain measurements of fluorescence energy transfer." Biopolymers **27**(5): 821-830.

Lands, A. M., A. Arnold, J. P. McAuliff, F. P. Luduena and T. G. Brown, Jr. (1967). "Differentiation of receptor systems activated by sympathomimetic amines." Nature **214**(5088): 597-598.

Lanner, J. T., D. K. Georgiou, A. Dagnino-Acosta, A. Ainbinder, Q. Cheng, A. D. Joshi, Z. Chen, V. Yarotskyy, J. M. Oakes, C. S. Lee, T. O. Monroe, A. Santillan, K. Dong, L. Goodyear, Ismailov, II, G. G. Rodney, R. T. Dirksen and S. L. Hamilton (2012). "AICAR prevents heat-induced sudden death in RyR1 mutant mice independent of AMPK activation." Nat Med **18**(2): 244-251.

Layland, J., R. J. Solaro and A. M. Shah (2005). "Regulation of cardiac contractile function by troponin I phosphorylation." Cardiovasc Res **66**(1): 12-21.

Lee-Young, R. S., S. R. Griffee, S. E. Lynes, D. P. Bracy, J. E. Ayala, O. P. McGuinness and D. H. Wasserman (2009). "Skeletal muscle AMP-activated protein kinase is essential for the metabolic response to exercise in vivo." J Biol Chem **284**(36): 23925-23934.

Levine, R. J., R. W. Kensler, Z. Yang, J. T. Stull and H. L. Sweeney (1996). "Myosin light chain phosphorylation affects the structure of rabbit skeletal muscle thick filaments." Biophys J **71**(2): 898-907.

Levine, R. J., Z. Yang, N. D. Epstein, L. Fananapazir, J. T. Stull and H. L. Sweeney (1998). "Structural and functional responses of mammalian thick filaments to alterations in myosin regulatory light chains." J Struct Biol **122**(1-2): 149-161.
Liang, Q. and J. D. Molkentin (2003). "Redefining the roles of p38 and JNK signaling in cardiac hypertrophy: dichotomy between cultured myocytes and animal models." J Mol Cell Cardiol **35**(12): 1385-1394.
Lindemann, J. P., L. R. Jones, D. R. Hathaway, B. G. Henry and A. M. Watanabe (1983). "beta-Adrenergic stimulation of phospholamban phosphorylation and Ca2+-ATPase activity in guinea pig ventricles." J Biol Chem **258**(1): 464-471.
Ling, H., T. Zhang, L. Pereira, C. K. Means, H. Cheng, Y. Gu, N. D. Dalton, K. L. Peterson, J. Chen, D. Bers and J. H. Brown (2009). "Requirement for Ca2+/calmodulin-dependent kinase II in the transition from pressure overload-induced cardiac hypertrophy to heart failure in mice." J Clin Invest **119**(5): 1230-1240.
Linke, W. A. (2008). "Sense and stretchability: the role of titin and titin-associated proteins in myocardial stress-sensing and mechanical dysfunction." Cardiovasc Res **77**(4): 637-648.
Linke, W. A., D. E. Rudy, T. Centner, M. Gautel, C. Witt, S. Labeit and C. C. Gregorio (1999). "I-band titin in cardiac muscle is a three-element molecular spring and is critical for maintaining thin filament structure." J Cell Biol **146**(3): 631-644.
Lohse, M. J., S. Engelhardt and T. Eschenhagen (2003). "What is the role of beta-adrenergic signaling in heart failure?" Circ Res **93**(10): 896-906.
Longnus, S. L., R. B. Wambolt, H. L. Parsons, R. W. Brownsey and M. F. Allard (2003). "5-Aminoimidazole-4-carboxamide 1-beta -D-ribofuranoside (AICAR) stimulates myocardial glycogenolysis by allosteric mechanisms." Am J Physiol Regul Integr Comp Physiol **284**(4): R936-944.
Lote, C. (2012). Principles of Renal Physiology.
Lowey, S., G. S. Waller and K. M. Trybus (1993). "Function of skeletal muscle myosin heavy and light chain isoforms by an in vitro motility assay." J Biol Chem **268**(27): 20414-20418.
Lowey, S., G. S. Waller and K. M. Trybus (1993). "Skeletal muscle myosin light chains are essential for physiological speeds of shortening." Nature **365**(6445): 454-456.
Lu, J., T. A. McKinsey, R. L. Nicol and E. N. Olson (2000). "Signal-dependent activation of the MEF2 transcription factor by dissociation from histone deacetylases." Proc Natl Acad Sci U S A **97**(8): 4070-4075.
Luedde, M., U. Flogel, M. Knorr, C. Grundt, H. J. Hippe, B. Brors, D. Frank, U. Haselmann, C. Antony, M. Voelkers, J. Schrader, P. Most, B. Lemmer, H. A. Katus and N. Frey (2009). "Decreased contractility due to energy deprivation in a transgenic rat model of hypertrophic cardiomyopathy." J Mol Med (Berl) **87**(4): 411-422.
Luo, W., G. Chu, Y. Sato, Z. Zhou, V. J. Kadambi and E. G. Kranias (1998). "Transgenic approaches to define the functional role of dual site phospholamban phosphorylation." J Biol Chem **273**(8): 4734-4739.
Lymn, R. W. and E. W. Taylor (1971). "Mechanism of adenosine triphosphate hydrolysis by actomyosin." Biochemistry **10**(25): 4617-4624.
MacLennan, D. H. (1970). "Purification and properties of an adenosine triphosphatase from sarcoplasmic reticulum." J Biol Chem **245**(17): 4508-4518.
MacLennan, D. H. and E. G. Kranias (2003). "Phospholamban: a crucial regulator of cardiac contractility." Nat Rev Mol Cell Biol **4**(7): 566-577.
MacLennan, D. H., W. J. Rice and N. M. Green (1997). "The mechanism of Ca2+ transport by sarco(endo)plasmic reticulum Ca2+-ATPases." J Biol Chem **272**(46): 28815-28818.
Maier, L. S., D. M. Bers and B. Pieske (2000). "Differences in Ca(2+)-handling and sarcoplasmic reticulum Ca(2+)-content in isolated rat and rabbit myocardium." J Mol Cell Cardiol **32**(12): 2249-2258.
Makarenko, I., C. A. Opitz, M. C. Leake, C. Neagoe, M. Kulke, J. K. Gwathmey, F. del Monte, R. J. Hajjar and W. A. Linke (2004). "Passive stiffness changes caused by upregulation of

compliant titin isoforms in human dilated cardiomyopathy hearts." Circ Res **95**(7): 708-716.
Malik, M. N. and A. Martonosi (1971). "Equilibrium and rapid kinetic studies of the effect of N-ethylmaleimide on the binding of ADP to myosin, and H-meromyosin." Arch Biochem Biophys **144**(2): 556-565.
Manni, S., J. H. Mauban, C. W. Ward and M. Bond (2008). "Phosphorylation of the cAMP-dependent protein kinase (PKA) regulatory subunit modulates PKA-AKAP interaction, substrate phosphorylation, and calcium signaling in cardiac cells." J Biol Chem **283**(35): 24145-24154.
Margossian, S. S. (1985). "Reversible dissociation of dog cardiac myosin regulatory light chain 2 and its influence on ATP hydrolysis." J Biol Chem **260**(25): 13747-13754.
Marijianowski, M. M., P. Teeling, J. Mann and A. E. Becker (1995). "Dilated cardiomyopathy is associated with an increase in the type I/type III collagen ratio: a quantitative assessment." J Am Coll Cardiol **25**(6): 1263-1272.
Maron, B. J. (1996). "Triggers for sudden cardiac death in the athlete." Cardiol Clin **14**(2): 195-210.
Maron, B. J. (2002). "Hypertrophic cardiomyopathy: a systematic review." JAMA **287**(10): 1308-1320.
Maron, B. J., J. M. Gardin, J. M. Flack, S. S. Gidding, T. T. Kurosaki and D. E. Bild (1995). "Prevalence of hypertrophic cardiomyopathy in a general population of young adults. Echocardiographic analysis of 4111 subjects in the CARDIA Study. Coronary Artery Risk Development in (Young) Adults." Circulation **92**(4): 785-789.
Maron, B. J., P. D. Thompson, J. C. Puffer, C. A. McGrew, W. B. Strong, P. S. Douglas, L. T. Clark, M. J. Mitten, M. H. Crawford, D. L. Atkins, D. J. Driscoll and A. E. Epstein (1996). "Cardiovascular preparticipation screening of competitive athletes. A statement for health professionals from the Sudden Death Committee (clinical cardiology) and Congenital Cardiac Defects Committee (cardiovascular disease in the young), American Heart Association." Circulation **94**(4): 850-856.
Marston, S., O. Copeland, A. Jacques, K. Livesey, V. Tsang, W. J. McKenna, S. Jalilzadeh, S. Carballo, C. Redwood and H. Watkins (2009). "Evidence from human myectomy samples that MYBPC3 mutations cause hypertrophic cardiomyopathy through haploinsufficiency." Circ Res **105**(3): 219-222.
Martin, J. L., R. Mestril, R. Hilal-Dandan, L. L. Brunton and W. H. Dillmann (1997). "Small heat shock proteins and protection against ischemic injury in cardiac myocytes." Circulation **96**(12): 4343-4348.
Marx, S. O., S. Reiken, Y. Hisamatsu, T. Jayaraman, D. Burkhoff, N. Rosemblit and A. R. Marks (2000). "PKA phosphorylation dissociates FKBP12.6 from the calcium release channel (ryanodine receptor): defective regulation in failing hearts." Cell **101**(4): 365-376.
Maytum, R., S. S. Lehrer and M. A. Geeves (1999). "Cooperativity and switching within the three-state model of muscle regulation." Biochemistry **38**(3): 1102-1110.
McDonald, K. S. and R. L. Moss (1995). "Osmotic compression of single cardiac myocytes eliminates the reduction in Ca2+ sensitivity of tension at short sarcomere length." Circ Res **77**(1): 199-205.
McKillop, D. F. and M. A. Geeves (1993). "Regulation of the interaction between actin and myosin subfragment 1: evidence for three states of the thin filament." Biophys J **65**(2): 693-701.
McMurray, J. J., S. Adamopoulos, S. D. Anker, A. Auricchio, M. Bohm, K. Dickstein, V. Falk, G. Filippatos, C. Fonseca, M. A. Gomez-Sanchez, T. Jaarsma, L. Kober, G. Y. Lip, A. P. Maggioni, A. Parkhomenko, B. M. Pieske, B. A. Popescu, P. K. Ronnevik, F. H. Rutten, J. Schwitter, P. Seferovic, J. Stepinska, P. T. Trindade, A. A. Voors, F. Zannad, A. Zeiher, D. Task Force for the, A. Treatment of, C. Chronic Heart Failure of the European Society of, J. J. Bax, H. Baumgartner, C. Ceconi, V. Dean, C. Deaton, R. Fagard, C. Funck-Brentano, D. Hasdai, A. Hoes, P. Kirchhof, J. Knuuti, P. Kolh, T. McDonagh, C. Moulin, B. A. Popescu, Z. Reiner, U. Sechtem, P. A. Sirnes, M. Tendera, A. Torbicki, A. Vahanian, S. Windecker,

T. McDonagh, U. Sechtem, L. A. Bonet, P. Avraamides, H. A. Ben Lamin, M. Brignole, A. Coca, P. Cowburn, H. Dargie, P. Elliott, F. A. Flachskampf, G. F. Guida, S. Hardman, B. Iung, B. Merkely, C. Mueller, J. N. Nanas, O. W. Nielsen, S. Orn, J. T. Parissis, P. Ponikowski and E. S. C. C. f. P. Guidelines (2012). "ESC guidelines for the diagnosis and treatment of acute and chronic heart failure 2012: The Task Force for the Diagnosis and Treatment of Acute and Chronic Heart Failure 2012 of the European Society of Cardiology. Developed in collaboration with the Heart Failure Association (HFA) of the ESC." Eur J Heart Fail **14**(8): 803-869.

Medugorac, I. (1982). "Characterization of intramuscular collagen in mammalian left ventricle." Basic Res Cardiol **77**(6): 589-598.

Merrill, G. F., E. J. Kurth, D. G. Hardie and W. W. Winder (1997). "AICA riboside increases AMP-activated protein kinase, fatty acid oxidation, and glucose uptake in rat muscle." Am J Physiol **273**(6 Pt 1): E1107-1112.

Messer, A. E., C. E. Gallon, W. J. McKenna, C. G. Dos Remedios and S. B. Marston (2009). "The use of phosphate-affinity SDS-PAGE to measure the cardiac troponin I phosphorylation site distribution in human heart muscle." Proteomics Clin Appl **3**(12): 1371-1382.

Metzger, J. M. and M. V. Westfall (2004). "Covalent and noncovalent modification of thin filament action: the essential role of troponin in cardiac muscle regulation." Circ Res **94**(2): 146-158.

Meyer, M., W. Schillinger, B. Pieske, C. Holubarsch, C. Heilmann, H. Posival, G. Kuwajima, K. Mikoshiba, H. Just, G. Hasenfuss and et al. (1995). "Alterations of sarcoplasmic reticulum proteins in failing human dilated cardiomyopathy." Circulation **92**(4): 778-784.

Mihaylova, M. M. and R. J. Shaw (2011). "The AMPK signalling pathway coordinates cell growth, autophagy and metabolism." Nat Cell Biol **13**(9): 1016-1023.

Mikami, A., K. Imoto, T. Tanabe, T. Niidome, Y. Mori, H. Takeshima, S. Narumiya and S. Numa (1989). "Primary structure and functional expression of the cardiac dihydropyridine-sensitive calcium channel." Nature **340**(6230): 230-233.

Miller, A. L., A. S. Garza, B. H. Johnson and E. B. Thompson (2007). "Pathway interactions between MAPKs, mTOR, PKA, and the glucocorticoid receptor in lymphoid cells." Cancer Cell Int **7**: 3.

Minajeva, A., M. Kulke, J. M. Fernandez and W. A. Linke (2001). "Unfolding of titin domains explains the viscoelastic behavior of skeletal myofibrils." Biophys J **80**(3): 1442-1451.

Mirsky, I. (1976). "Assessment of passive elastic stiffness of cardiac muscle: mathematical concepts, physiologic and clinical considerations, directions of future research." Prog Cardiovasc Dis **18**(4): 277-308.

Miyamoto, M. I., F. del Monte, U. Schmidt, T. S. DiSalvo, Z. B. Kang, T. Matsui, J. L. Guerrero, J. K. Gwathmey, A. Rosenzweig and R. J. Hajjar (2000). "Adenoviral gene transfer of SERCA2a improves left-ventricular function in aortic-banded rats in transition to heart failure." Proc Natl Acad Sci U S A **97**(2): 793-798.

Molkentin, J. D. (2004). "Calcineurin-NFAT signaling regulates the cardiac hypertrophic response in coordination with the MAPKs." Cardiovasc Res **63**(3): 467-475.

Molkentin, J. D., J. R. Lu, C. L. Antos, B. Markham, J. Richardson, J. Robbins, S. R. Grant and E. N. Olson (1998). "A calcineurin-dependent transcriptional pathway for cardiac hypertrophy." Cell **93**(2): 215-228.

Moolman, J. C., V. A. Corfield, B. Posen, K. Ngumbela, C. Seidman, P. A. Brink and H. Watkins (1997). "Sudden death due to troponin T mutations." J Am Coll Cardiol **29**(3): 549-555.

Moretti, A., H. J. Weig, T. Ott, M. Seyfarth, H. P. Holthoff, D. Grewe, A. Gillitzer, L. Bott-Flugel, A. Schomig, M. Ungerer and K. L. Laugwitz (2002). "Essential myosin light chain as a target for caspase-3 in failing myocardium." Proc Natl Acad Sci U S A **99**(18): 11860-11865.

Moss, R. L., G. G. Giulian and M. L. Greaser (1985). "The effects of partial extraction of TnC upon the tension-pCa relationship in rabbit skinned skeletal muscle fibers." J Gen Physiol **86**(4): 585-600.

Moss, R. L., M. Razumova and D. P. Fitzsimons (2004). "Myosin crossbridge activation of cardiac thin filaments: implications for myocardial function in health and disease." Circ Res **94**(10): 1290-1300.

Moussavi-Harami, F., M. V. Razumova, A. W. Racca, Y. Cheng, A. Stempien-Otero and M. Regnier (2015). "2-Deoxy adenosine triphosphate improves contraction in human end-stage heart failure." J Mol Cell Cardiol **79**: 256-263.

Movsesian, M. A., M. Karimi, K. Green and L. R. Jones (1994). "Ca(2+)-transporting ATPase, phospholamban, and calsequestrin levels in nonfailing and failing human myocardium." Circulation **90**(2): 653-657.

Mozaffarian, D., E. J. Benjamin, A. S. Go, D. K. Arnett, M. J. Blaha, M. Cushman, S. de Ferranti, J. P. Despres, H. J. Fullerton, V. J. Howard, M. D. Huffman, S. E. Judd, B. M. Kissela, D. T. Lackland, J. H. Lichtman, L. D. Lisabeth, S. Liu, R. H. Mackey, D. B. Matchar, D. K. McGuire, E. R. Mohler, 3rd, C. S. Moy, P. Muntner, M. E. Mussolino, K. Nasir, R. W. Neumar, G. Nichol, L. Palaniappan, D. K. Pandey, M. J. Reeves, C. J. Rodriguez, P. D. Sorlie, J. Stein, A. Towfighi, T. N. Turan, S. S. Virani, J. Z. Willey, D. Woo, R. W. Yeh, M. B. Turner, C. American Heart Association Statistics and S. Stroke Statistics (2015). "Heart disease and stroke statistics-2015 update: a report from the american heart association." Circulation **131**(4): e29-e322.

Muthu, P., L. Wang, C. C. Yuan, K. Kazmierczak, W. Huang, O. M. Hernandez, M. Kawai, T. C. Irving and D. Szczesna-Cordary (2011). "Structural and functional aspects of the myosin essential light chain in cardiac muscle contraction." FASEB J **25**(12): 4394-4405.

Nabauer, M., G. Callewaert, L. Cleemann and M. Morad (1989). "Regulation of calcium release is gated by calcium current, not gating charge, in cardiac myocytes." Science **244**(4906): 800-803.

Nagueh, S. F., G. Shah, Y. Wu, G. Torre-Amione, N. M. King, S. Lahmers, C. C. Witt, K. Becker, S. Labeit and H. L. Granzier (2004). "Altered titin expression, myocardial stiffness, and left ventricular function in patients with dilated cardiomyopathy." Circulation **110**(2): 155-162.

Nascimben, L., J. S. Ingwall, P. Pauletto, J. Friedrich, J. K. Gwathmey, V. Saks, A. C. Pessina and P. D. Allen (1996). "Creatine kinase system in failing and nonfailing human myocardium." Circulation **94**(8): 1894-1901.

Neumann, J. (2002). "Altered phosphatase activity in heart failure, influence on Ca2+ movement." Basic Res Cardiol **97 Suppl 1**: I91-95.

Neumann, J., T. Eschenhagen, L. R. Jones, B. Linck, W. Schmitz, H. Scholz and N. Zimmermann (1997). "Increased expression of cardiac phosphatases in patients with end-stage heart failure." J Mol Cell Cardiol **29**(1): 265-272.

Nicoll, D. A., S. Longoni and K. D. Philipson (1990). "Molecular cloning and functional expression of the cardiac sarcolemmal Na(+)-Ca2+ exchanger." Science **250**(4980): 562-565.

Nicoll, D. A., M. Ottolia, L. Lu, Y. Lu and K. D. Philipson (1999). "A new topological model of the cardiac sarcolemmal Na+-Ca2+ exchanger." J Biol Chem **274**(2): 910-917.

Niggli, E. and W. J. Lederer (1991). "Molecular operations of the sodium-calcium exchanger revealed by conformation currents." Nature **349**(6310): 621-624.

Nixon, B. R., A. Thawornkaiwong, J. Jin, E. A. Brundage, S. C. Little, J. P. Davis, R. J. Solaro and B. J. Biesiadecki (2012). "AMP-activated protein kinase phosphorylates cardiac troponin I at Ser-150 to increase myofilament calcium sensitivity and blunt PKA-dependent function." J Biol Chem **287**(23): 19136-19147.

Nowakowski, S. G., S. C. Kolwicz, F. S. Korte, Z. Luo, J. N. Robinson-Hamm, J. L. Page, F. Brozovich, R. S. Weiss, R. Tian, C. E. Murry and M. Regnier (2013). "Transgenic overexpression of ribonucleotide reductase improves cardiac performance." Proc Natl Acad Sci U S A **110**(15): 6187-6192.

Oakhill, J. S., Z. P. Chen, J. W. Scott, R. Steel, L. A. Castelli, N. Ling, S. L. Macaulay and B. E. Kemp (2010). "beta-Subunit myristoylation is the gatekeeper for initiating metabolic stress

sensing by AMP-activated protein kinase (AMPK)." Proc Natl Acad Sci U S A **107**(45): 19237-19241.
Oda, T., M. Iwasa, T. Aihara, Y. Maeda and A. Narita (2009). "The nature of the globular- to fibrous-actin transition." Nature **457**(7228): 441-445.
Odermatt, A., S. Becker, V. K. Khanna, K. Kurzydlowski, E. Leisner, D. Pette and D. H. MacLennan (1998). "Sarcolipin regulates the activity of SERCA1, the fast-twitch skeletal muscle sarcoplasmic reticulum Ca2+-ATPase." J Biol Chem **273**(20): 12360-12369.
Odermatt, A., P. E. Taschner, S. W. Scherer, B. Beatty, V. K. Khanna, D. R. Cornblath, V. Chaudhry, W. C. Yee, B. Schrank, G. Karpati, M. H. Breuning, N. Knoers and D. H. MacLennan (1997). "Characterization of the gene encoding human sarcolipin (SLN), a proteolipid associated with SERCA1: absence of structural mutations in five patients with Brody disease." Genomics **45**(3): 541-553.
Okagaki, T., F. E. Weber, D. A. Fischman, K. T. Vaughan, T. Mikawa and F. C. Reinach (1993). "The major myosin-binding domain of skeletal muscle MyBP-C (C protein) resides in the COOH-terminal, immunoglobulin C2 motif." J Cell Biol **123**(3): 619-626.
Oliveira, S. M., Y. H. Zhang, R. S. Solis, H. Isackson, M. Bellahcene, A. Yavari, K. Pinter, J. K. Davies, Y. Ge, H. Ashrafian, J. W. Walker, D. Carling, H. Watkins, B. Casadei and C. Redwood (2012). "AMP-activated protein kinase phosphorylates cardiac troponin I and alters contractility of murine ventricular myocytes." Circ Res **110**(9): 1192-1201.
Olivetti, G., R. Abbi, F. Quaini, J. Kajstura, W. Cheng, J. A. Nitahara, E. Quaini, C. Di Loreto, C. A. Beltrami, S. Krajewski, J. C. Reed and P. Anversa (1997). "Apoptosis in the failing human heart." N Engl J Med **336**(16): 1131-1141.
Opie, L. (2003). Heart Physiology: From Cell to Circulation, Lippincott Williams and Wilkins.
Otterbein, L. R., P. Graceffa and R. Dominguez (2001). "The crystal structure of uncomplexed actin in the ADP state." Science **293**(5530): 708-711.
Ouyang, Y., R. Mamidi, J. J. Jayasundar, M. Chandra and W. J. Dong (2010). "Structural and kinetic effects of PAK3 phosphorylation mimic of cTnI(S151E) on the cTnC-cTnI interaction in the cardiac thin filament." J Mol Biol **400**(5): 1036-1045.
Palmer, S. and J. C. Kentish (1998). "Roles of Ca2+ and crossbridge kinetics in determining the maximum rates of Ca2+ activation and relaxation in rat and guinea pig skinned trabeculae." Circ Res **83**(2): 179-186.
Pan, B. S. and R. J. Solaro (1987). "Calcium-binding properties of troponin C in detergent-skinned heart muscle fibers." J Biol Chem **262**(16): 7839-7849.
Paolisso, G., A. Gambardella, D. Galzerano, A. D'Amore, P. Rubino, M. Verza, P. Teasuro, M. Varricchio and F. D'Onofrio (1994). "Total-body and myocardial substrate oxidation in congestive heart failure." Metabolism **43**(2): 174-179.
Passier, R., H. Zeng, N. Frey, F. J. Naya, R. L. Nicol, T. A. McKinsey, P. Overbeek, J. A. Richardson, S. R. Grant and E. N. Olson (2000). "CaM kinase signaling induces cardiac hypertrophy and activates the MEF2 transcription factor in vivo." J Clin Invest **105**(10): 1395-1406.
Patel, V. V., M. Arad, I. P. Moskowitz, C. T. Maguire, D. Branco, J. G. Seidman, C. E. Seidman and C. I. Berul (2003). "Electrophysiologic characterization and postnatal development of ventricular pre-excitation in a mouse model of cardiac hypertrophy and Wolff-Parkinson-White syndrome." J Am Coll Cardiol **42**(5): 942-951.
Pathak, A., F. del Monte, W. Zhao, J. E. Schultz, J. N. Lorenz, I. Bodi, D. Weiser, H. Hahn, A. N. Carr, F. Syed, N. Mavila, L. Jha, J. Qian, Y. Marreez, G. Chen, D. W. McGraw, E. K. Heist, J. L. Guerrero, A. A. DePaoli-Roach, R. J. Hajjar and E. G. Kranias (2005). "Enhancement of cardiac function and suppression of heart failure progression by inhibition of protein phosphatase 1." Circ Res **96**(7): 756-766.
Pearlstone, J. R. and L. B. Smillie (1983). "Effects of troponin-I plus-C on the binding of troponin-T and its fragments to alpha-tropomyosin. Ca2+ sensitivity and cooperativity." J Biol Chem **258**(4): 2534-2542.
Pena, J. R., A. C. Szkudlarek, C. M. Warren, L. S. Heinrich, R. D. Gaffin, G. Jagatheesan, F. del Monte, R. J. Hajjar, P. H. Goldspink, R. J. Solaro, D. F. Wieczorek and B. M. Wolska (2010). "Neonatal gene transfer of Serca2a delays onset of hypertrophic remodeling and

improves function in familial hypertrophic cardiomyopathy." J Mol Cell Cardiol **49**(6): 993-1002.
Periasamy, M. and S. Huke (2001). "SERCA pump level is a critical determinant of Ca(2+)homeostasis and cardiac contractility." J Mol Cell Cardiol **33**(6): 1053-1063.
Periasamy, M. and A. Kalyanasundaram (2008). "SERCA2a gene therapy for heart failure: ready for primetime?" Mol Ther **16**(6): 1002-1004.
Perry, S. V. (1998). "Troponin T: genetics, properties and function." J Muscle Res Cell Motil **19**(6): 575-602.
Pfuhl, M. and M. Gautel (2012). "Structure, interactions and function of the N-terminus of cardiac myosin binding protein C (MyBP-C): who does what, with what, and to whom?" J Muscle Res Cell Motil **33**(1): 83-94.
Pi, Y., K. R. Kemnitz, D. Zhang, E. G. Kranias and J. W. Walker (2002). "Phosphorylation of troponin I controls cardiac twitch dynamics: evidence from phosphorylation site mutants expressed on a troponin I-null background in mice." Circ Res **90**(6): 649-656.
Piacentino, V., 3rd, C. R. Weber, X. Chen, J. Weisser-Thomas, K. B. Margulies, D. M. Bers and S. R. Houser (2003). "Cellular basis of abnormal calcium transients of failing human ventricular myocytes." Circ Res **92**(6): 651-658.
Pinter, K., R. T. Grignani, G. Czibik, H. Farza, H. Watkins and C. Redwood (2012). "Embryonic expression of AMPK gamma subunits and the identification of a novel gamma2 transcript variant in adult heart." J Mol Cell Cardiol **53**(3): 342-349.
Pinter, K., R. T. Grignani, H. Watkins and C. Redwood (2013). "Localisation of AMPK gamma subunits in cardiac and skeletal muscles." J Muscle Res Cell Motil **34**(5-6): 369-378.
Pollard, T. D. (2007). "Regulation of actin filament assembly by Arp2/3 complex and formins." Annu Rev Biophys Biomol Struct **36**: 451-477.
Porter, C. M., M. A. Havens and N. A. Clipstone (2000). "Identification of amino acid residues and protein kinases involved in the regulation of NFATc subcellular localization." J Biol Chem **275**(5): 3543-3551.
Potter, J. D. and J. Gergely (1974). "Troponin, tropomyosin, and actin interactions in the Ca2+ regulation of muscle contraction." Biochemistry **13**(13): 2697-2703.
Puglisi, J. L., P. H. Goldspink, A. V. Gomes, M. S. Utter, D. M. Bers and R. J. Solaro (2014). "Influence of a constitutive increase in myofilament Ca(2+)-sensitivity on Ca(2+)-fluxes and contraction of mouse heart ventricular myocytes." Arch Biochem Biophys **552-553**: 50-59.
Purslow, P. P., T. J. Wess and D. W. Hukins (1998). "Collagen orientation and molecular spacing during creep and stress-relaxation in soft connective tissues." J Exp Biol **201**(Pt 1): 135-142.
Qintar, M., A. Morad, H. Alhawasli, K. Shorbaji, B. Firwana, A. Essali and W. Kadro (2012). "Pacing for drug-refractory or drug-intolerant hypertrophic cardiomyopathy." Cochrane Database Syst Rev **5**: CD008523.
Quinones, M. A., W. H. Gaasch and J. K. Alexander (1976). "Influence of acute changes in preload, afterload, contractile state and heart rate on ejection and isovolumic indices of myocardial contractility in man." Circulation **53**(2): 293-302.
Rangel-Aldao, R. and O. M. Rosen (1977). "Effect of cAMP and ATP on the reassociation of phosphorylated and nonphosphorylated subunits of the cAMP-dependent protein kinase from bovine cardiac muscle." J Biol Chem **252**(20): 7140-7145.
Rayment, I., H. M. Holden, M. Whittaker, C. B. Yohn, M. Lorenz, K. C. Holmes and R. A. Milligan (1993). "Structure of the actin-myosin complex and its implications for muscle contraction." Science **261**(5117): 58-65.
Rayment, I., W. R. Rypniewski, K. Schmidt-Base, R. Smith, D. R. Tomchick, M. M. Benning, D. A. Winkelmann, G. Wesenberg and H. M. Holden (1993). "Three-dimensional structure of myosin subfragment-1: a molecular motor." Science **261**(5117): 50-58.
Razumova, M. V., J. F. Shaffer, A. Y. Tu, G. V. Flint, M. Regnier and S. P. Harris (2006). "Effects of the N-terminal domains of myosin binding protein-C in an in vitro motility assay: Evidence for long-lived cross-bridges." J Biol Chem **281**(47): 35846-35854.

Redwood, C. S., J. C. Moolman-Smook and H. Watkins (1999). "Properties of mutant contractile proteins that cause hypertrophic cardiomyopathy." Cardiovasc Res **44**(1): 20-36.
Regnier, M., D. M. Lee and E. Homsher (1998). "ATP analogs and muscle contraction: mechanics and kinetics of nucleoside triphosphate binding and hydrolysis." Biophys J **74**(6): 3044-3058.
Reisler, E. (1993). "Actin molecular structure and function." Curr Opin Cell Biol **5**(1): 41-47.
Ren, X. and K. D. Philipson (2013). "The topology of the cardiac Na(+)/Ca(2)(+) exchanger, NCX1." J Mol Cell Cardiol **57**: 68-71.
Reuter, H. (1983). "Calcium channel modulation by neurotransmitters, enzymes and drugs." Nature **301**(5901): 569-574.
Reuter, H. and N. Seitz (1968). "The dependence of calcium efflux from cardiac muscle on temperature and external ion composition." J Physiol **195**(2): 451-470.
Richard, P., P. Charron, L. Carrier, C. Ledeuil, T. Cheav, C. Pichereau, A. Benaiche, R. Isnard, O. Dubourg, M. Burban, J. P. Gueffet, A. Millaire, M. Desnos, K. Schwartz, B. Hainque, M. Komajda and E. H. F. Project (2003). "Hypertrophic cardiomyopathy: distribution of disease genes, spectrum of mutations, and implications for a molecular diagnosis strategy." Circulation **107**(17): 2227-2232.
Rios, E. and G. Brum (1987). "Involvement of dihydropyridine receptors in excitation-contraction coupling in skeletal muscle." Nature **325**(6106): 717-720.
Rios, E. and G. Pizarro (1991). "Voltage sensor of excitation-contraction coupling in skeletal muscle." Physiol Rev **71**(3): 849-908.
Roberts, A. M., J. S. Ware, D. S. Herman, S. Schafer, J. Baksi, A. G. Bick, R. J. Buchan, R. Walsh, S. John, S. Wilkinson, F. Mazzarotto, L. E. Felkin, S. Gong, J. A. MacArthur, F. Cunningham, J. Flannick, S. B. Gabriel, D. M. Altshuler, P. S. Macdonald, M. Heinig, A. M. Keogh, C. S. Hayward, N. R. Banner, D. J. Pennell, D. P. O'Regan, T. R. San, A. de Marvao, T. J. Dawes, A. Gulati, E. J. Birks, M. H. Yacoub, M. Radke, M. Gotthardt, J. G. Wilson, C. J. O'Donnell, S. K. Prasad, P. J. Barton, D. Fatkin, N. Hubner, J. G. Seidman, C. E. Seidman and S. A. Cook (2015). "Integrated allelic, transcriptional, and phenomic dissection of the cardiac effects of titin truncations in health and disease." Sci Transl Med **7**(270): 270ra276.
Robertson, S. P., J. D. Johnson, M. J. Holroyde, E. G. Kranias, J. D. Potter and R. J. Solaro (1982). "The effect of troponin I phosphorylation on the Ca2+-binding properties of the Ca2+-regulatory site of bovine cardiac troponin." J Biol Chem **257**(1): 260-263.
Robinson, P., P. J. Griffiths, H. Watkins and C. S. Redwood (2007). "Dilated and hypertrophic cardiomyopathy mutations in troponin and alpha-tropomyosin have opposing effects on the calcium affinity of cardiac thin filaments." Circ Res **101**(12): 1266-1273.
Robinson, P., M. Mirza, A. Knott, H. Abdulrazzak, R. Willott, S. Marston, H. Watkins and C. Redwood (2002). "Alterations in thin filament regulation induced by a human cardiac troponin T mutant that causes dilated cardiomyopathy are distinct from those induced by troponin T mutants that cause hypertrophic cardiomyopathy." J Biol Chem **277**(43): 40710-40716.
Rousseau, E., J. Ladine, Q. Y. Liu and G. Meissner (1988). "Activation of the Ca2+ release channel of skeletal muscle sarcoplasmic reticulum by caffeine and related compounds." Arch Biochem Biophys **267**(1): 75-86.
Roylance, D. (2001) "Engineering Viscoelasticity." Materials Science and Engineering.
Ruth, P., A. Rohrkasten, M. Biel, E. Bosse, S. Regulla, H. E. Meyer, V. Flockerzi and F. Hofmann (1989). "Primary structure of the beta subunit of the DHP-sensitive calcium channel from skeletal muscle." Science **245**(4922): 1115-1118.
Sadayappan, S., J. Gulick, H. Osinska, L. A. Martin, H. S. Hahn, G. W. Dorn, 2nd, R. Klevitsky, C. E. Seidman, J. G. Seidman and J. Robbins (2005). "Cardiac myosin-binding protein-C phosphorylation and cardiac function." Circ Res **97**(11): 1156-1163.
Sadayappan, S., H. Osinska, R. Klevitsky, J. N. Lorenz, M. Sargent, J. D. Molkentin, C. E. Seidman, J. G. Seidman and J. Robbins (2006). "Cardiac myosin binding protein C phosphorylation is cardioprotective." Proc Natl Acad Sci U S A **103**(45): 16918-16923.

Sancho Solis, R., Y. Ge and J. W. Walker (2011). "A preferred AMPK phosphorylation site adjacent to the inhibitory loop of cardiac and skeletal troponin I." Protein Sci **20**(5): 894-907.

Sanders, M. J., Z. S. Ali, B. D. Hegarty, R. Heath, M. A. Snowden and D. Carling (2007). "Defining the mechanism of activation of AMP-activated protein kinase by the small molecule A-769662, a member of the thienopyridone family." J Biol Chem **282**(45): 32539-32548.

Schaertl, S., S. S. Lehrer and M. A. Geeves (1995). "Separation and characterization of the two functional regions of troponin involved in muscle thin filament regulation." Biochemistry **34**(49): 15890-15894.

Schaub, M. C., S. V. Perry and W. Hacker (1972). "The regulatory proteins of the myofibril. Characterization and biological activity of the calcium-sensitizing factor (troponin A)." Biochem J **126**(1): 237-249.

Schober, T., S. Huke, R. Venkataraman, O. Gryshchenko, D. Kryshtal, H. S. Hwang, F. J. Baudenbacher and B. C. Knollmann (2012). "Myofilament Ca sensitization increases cytosolic Ca binding affinity, alters intracellular Ca homeostasis, and causes pause-dependent Ca-triggered arrhythmia." Circ Res **111**(2): 170-179.

Schwinger, R. H., M. Bohm, U. Schmidt, P. Karczewski, U. Bavendiek, M. Flesch, E. G. Krause and E. Erdmann (1995). "Unchanged protein levels of SERCA II and phospholamban but reduced Ca2+ uptake and Ca(2+)-ATPase activity of cardiac sarcoplasmic reticulum from dilated cardiomyopathy patients compared with patients with nonfailing hearts." Circulation **92**(11): 3220-3228.

Schwinger, R. H., G. Munch, B. Bolck, P. Karczewski, E. G. Krause and E. Erdmann (1999). "Reduced Ca(2+)-sensitivity of SERCA 2a in failing human myocardium due to reduced serin-16 phospholamban phosphorylation." J Mol Cell Cardiol **31**(3): 479-491.

Scott, J. W., S. A. Hawley, K. A. Green, M. Anis, G. Stewart, G. A. Scullion, D. G. Norman and D. G. Hardie (2004). "CBS domains form energy-sensing modules whose binding of adenosine ligands is disrupted by disease mutations." J Clin Invest **113**(2): 274-284.

Seidman, J. G. and C. Seidman (2001). "The genetic basis for cardiomyopathy: from mutation identification to mechanistic paradigms." Cell **104**(4): 557-567.

Selcen, D. and A. G. Engel (2003). "Myofibrillar myopathy caused by novel dominant negative alpha B-crystallin mutations." Ann Neurol **54**(6): 804-810.

Semsarian, C., I. Ahmad, M. Giewat, D. Georgakopoulos, J. P. Schmitt, B. K. McConnell, S. Reiken, U. Mende, A. R. Marks, D. A. Kass, C. E. Seidman and J. G. Seidman (2002). "The L-type calcium channel inhibitor diltiazem prevents cardiomyopathy in a mouse model." J Clin Invest **109**(8): 1013-1020.

Sequeira, V., P. J. Wijnker, L. L. Nijenkamp, D. W. Kuster, A. Najafi, E. R. Witjas-Paalberends, J. A. Regan, N. Boontje, F. J. Ten Cate, T. Germans, L. Carrier, S. Sadayappan, M. A. van Slegtenhorst, R. Zaremba, D. B. Foster, A. M. Murphy, C. Poggesi, C. Dos Remedios, G. J. Stienen, C. Y. Ho, M. Michels and J. van der Velden (2013). "Perturbed length-dependent activation in human hypertrophic cardiomyopathy with missense sarcomeric gene mutations." Circ Res **112**(11): 1491-1505.

Shen, W., K. Asai, M. Uechi, M. A. Mathier, R. P. Shannon, S. F. Vatner and J. S. Ingwall (1999). "Progressive loss of myocardial ATP due to a loss of total purines during the development of heart failure in dogs: a compensatory role for the parallel loss of creatine." Circulation **100**(20): 2113-2118.

Shen, Y. T., F. I. Malik, X. Zhao, C. Depre, S. K. Dhar, P. Abarzua, D. J. Morgans and S. F. Vatner (2010). "Improvement of cardiac function by a cardiac Myosin activator in conscious dogs with systolic heart failure." Circ Heart Fail **3**(4): 522-527.

Shigekawa, M. and T. Iwamoto (2001). "Cardiac Na(+)-Ca(2+) exchange: molecular and pharmacological aspects." Circ Res **88**(9): 864-876.

Sidhu, J. S., Y. S. Rajawat, T. G. Rami, M. H. Gollob, Z. Wang, R. Yuan, A. J. Marian, F. J. DeMayo, D. Weilbacher, G. E. Taffet, J. K. Davies, D. Carling, D. S. Khoury and R. Roberts (2005). "Transgenic mouse model of ventricular preexcitation and atrioventricular reentrant

tachycardia induced by an AMP-activated protein kinase loss-of-function mutation responsible for Wolff-Parkinson-White syndrome." Circulation **111**(1): 21-29.
Silver, P. J., L. M. Buja and J. T. Stull (1986). "Frequency-dependent myosin light chain phosphorylation in isolated myocardium." J Mol Cell Cardiol **18**(1): 31-37.
Smith, C. A. and I. Rayment (1996). "Active site comparisons highlight structural similarities between myosin and other P-loop proteins." Biophys J **70**(4): 1590-1602.
Solaro, R. J. (2007). "Mechanisms of the Frank-Starling law of the heart: the beat goes on." Biophys J **93**(12): 4095-4096.
Solaro, R. J. and T. Kobayashi (2011). "Protein phosphorylation and signal transduction in cardiac thin filaments." J Biol Chem **286**(12): 9935-9940.
Solaro, R. J. and H. M. Rarick (1998). "Troponin and tropomyosin: proteins that switch on and tune in the activity of cardiac myofilaments." Circ Res **83**(5): 471-480.
Somura, F., H. Izawa, M. Iwase, Y. Takeichi, R. Ishiki, T. Nishizawa, A. Noda, K. Nagata, Y. Yamada and M. Yokota (2001). "Reduced myocardial sarcoplasmic reticulum Ca(2+)-ATPase mRNA expression and biphasic force-frequency relations in patients with hypertrophic cardiomyopathy." Circulation **104**(6): 658-663.
Spangenburg, E. E., K. C. Jackson and R. A. Schuh (2013). "AICAR inhibits oxygen consumption by intact skeletal muscle cells in culture." J Physiol Biochem **69**(4): 909-917.
Spindler, M., K. W. Saupe, M. E. Christe, H. L. Sweeney, C. E. Seidman, J. G. Seidman and J. S. Ingwall (1998). "Diastolic dysfunction and altered energetics in the alphaMHC403/+ mouse model of familial hypertrophic cardiomyopathy." J Clin Invest **101**(8): 1775-1783.
Spirito, P., P. Bellone, K. M. Harris, P. Bernabo, P. Bruzzi and B. J. Maron (2000). "Magnitude of left ventricular hypertrophy and risk of sudden death in hypertrophic cardiomyopathy." N Engl J Med **342**(24): 1778-1785.
Spyracopoulos, L., M. X. Li, S. K. Sia, S. M. Gagne, M. Chandra, R. J. Solaro and B. D. Sykes (1997). "Calcium-induced structural transition in the regulatory domain of human cardiac troponin C." Biochemistry **36**(40): 12138-12146.
Squire, J. M., A. L.-K. HA, J. J. Harford, L. Hudson, T. C. Irving, C. Knupp, N. S. Mok and M. K. Reedy (2003). "Myosin filament structure and myosin crossbridge dynamics in fish and insect muscles." Adv Exp Med Biol **538**: 251-266; discussion 266.
Stangherlin, A. and M. Zaccolo (2012). "cGMP-cAMP interplay in cardiac myocytes: a local affair with far-reaching consequences for heart function." Biochem Soc Trans **40**(1): 11-14.
Starling, R. C., D. F. Hammer and R. A. Altschuld (1998). "Human myocardial ATP content and in vivo contractile function." Mol Cell Biochem **180**(1-2): 171-177.
Stelzer, J. E., J. R. Patel, J. W. Walker and R. L. Moss (2007). "Differential roles of cardiac myosin-binding protein C and cardiac troponin I in the myofibrillar force responses to protein kinase A phosphorylation." Circ Res **101**(5): 503-511.
Stewart, P. S. and D. H. MacLennan (1974). "Surface particles of sarcoplasmic reticulum membranes. Structural features of the adenosine triphosphatase." J Biol Chem **249**(3): 985-993.
Straub, F. B. (1942). Studies Int med Chem Univ Szeged **2**: 3-15.
Sundaralingam, M., R. Bergstrom, G. Strasburg, S. T. Rao, P. Roychowdhury, M. Greaser and B. C. Wang (1985). "Molecular structure of troponin C from chicken skeletal muscle at 3-angstrom resolution." Science **227**(4689): 945-948.
Sweeney, H. L., Z. Yang, G. Zhi, J. T. Stull and K. M. Trybus (1994). "Charge replacement near the phosphorylatable serine of the myosin regulatory light chain mimics aspects of phosphorylation." Proc Natl Acad Sci U S A **91**(4): 1490-1494.
Sykes, B. D. (2003). "Pulling the calcium trigger." Nat Struct Biol **10**(8): 588-589.
Szczesna, D., J. Zhao, M. Jones, G. Zhi, J. Stull and J. D. Potter (2002). "Phosphorylation of the regulatory light chains of myosin affects Ca2+ sensitivity of skeletal muscle contraction." J Appl Physiol (1985) **92**(4): 1661-1670.

Tada, M., M. A. Kirchberger and A. M. Katz (1975). "Phosphorylation of a 22,000-dalton component of the cardiac sarcoplasmic reticulum by adenosine 3':5'-monophosphate-dependent protein kinase." J Biol Chem **250**(7): 2640-2647.
Takahashi, M., M. J. Seagar, J. F. Jones, B. F. Reber and W. A. Catterall (1987). "Subunit structure of dihydropyridine-sensitive calcium channels from skeletal muscle." Proc Natl Acad Sci U S A **84**(15): 5478-5482.
Takasago, T., T. Imagawa, K. Furukawa, T. Ogurusu and M. Shigekawa (1991). "Regulation of the cardiac ryanodine receptor by protein kinase-dependent phosphorylation." J Biochem **109**(1): 163-170.
Takeda, S., A. Yamashita, K. Maeda and Y. Maeda (2003). "Structure of the core domain of human cardiac troponin in the Ca(2+)-saturated form." Nature **424**(6944): 35-41.
Tan, H. L., A. C. van der Wal, M. E. Campian, H. H. Kruyswijk, B. ten Hove Jansen, D. J. van Doorn, H. J. Oskam, A. E. Becker and A. A. Wilde (2008). "Nodoventricular accessory pathways in PRKAG2-dependent familial preexcitation syndrome reveal a disorder in cardiac development." Circ Arrhythm Electrophysiol **1**(4): 276-281.
Tanabe, T., H. Takeshima, A. Mikami, V. Flockerzi, H. Takahashi, K. Kangawa, M. Kojima, H. Matsuo, T. Hirose and S. Numa (1987). "Primary structure of the receptor for calcium channel blockers from skeletal muscle." Nature **328**(6128): 313-318.
Tanigawa, G., J. A. Jarcho, S. Kass, S. D. Solomon, H. P. Vosberg, J. G. Seidman and C. E. Seidman (1990). "A molecular basis for familial hypertrophic cardiomyopathy: an alpha/beta cardiac myosin heavy chain hybrid gene." Cell **62**(5): 991-998.
Thierfelder, L., H. Watkins, C. MacRae, R. Lamas, W. McKenna, H. P. Vosberg, J. G. Seidman and C. E. Seidman (1994). "Alpha-tropomyosin and cardiac troponin T mutations cause familial hypertrophic cardiomyopathy: a disease of the sarcomere." Cell **77**(5): 701-712.
Timson, D. J. (2003). "Fine tuning the myosin motor: the role of the essential light chain in striated muscle myosin." Biochimie **85**(7): 639-645.
Tobacman, L. S. (1996). "Thin filament-mediated regulation of cardiac contraction." Annu Rev Physiol **58**: 447-481.
Towbin, J. A. and N. E. Bowles (2002). "The failing heart." Nature **415**(6868): 227-233.
Townley, R. and L. Shapiro (2007). "Crystal structures of the adenylate sensor from fission yeast AMP-activated protein kinase." Science **315**(5819): 1726-1729.
Toyoshima, C., M. Nakasako, H. Nomura and H. Ogawa (2000). "Crystal structure of the calcium pump of sarcoplasmic reticulum at 2.6 A resolution." Nature **405**(6787): 647-655.
Treweek, T. M., A. Rekas, M. J. Walker and J. A. Carver (2010). "A quantitative NMR spectroscopic examination of the flexibility of the C-terminal extensions of the molecular chaperones, alphaA- and alphaB-crystallin." Exp Eye Res **91**(5): 691-699.
Trinick, J., P. Knight and A. Whiting (1984). "Purification and properties of native titin." J Mol Biol **180**(2): 331-356.
Tripet, B., J. E. Van Eyk and R. S. Hodges (1997). "Mapping of a second actin-tropomyosin and a second troponin C binding site within the C terminus of troponin I, and their importance in the Ca2+-dependent regulation of muscle contraction." J Mol Biol **271**(5): 728-750.
Triposkiadis, F., G. Karayannis, G. Giamouzis, J. Skoularigis, G. Louridas and J. Butler (2009). "The sympathetic nervous system in heart failure physiology, pathophysiology, and clinical implications." J Am Coll Cardiol **54**(19): 1747-1762.
Trybus, K. M. (1994). "Role of myosin light chains." J Muscle Res Cell Motil **15**(6): 587-594.
Tskhovrebova, L. and J. Trinick (2003). "Titin: properties and family relationships." Nat Rev Mol Cell Biol **4**(9): 679-689.
Tuunanen, H., J. Kuusisto, J. Toikka, P. Jaaskelainen, P. Marjamaki, K. Peuhkurinen, T. Viljanen, P. Sipola, K. Q. Stolen, J. Hannukainen, P. Nuutila, M. Laakso and J. Knuuti (2007). "Myocardial perfusion, oxidative metabolism, and free fatty acid uptake in patients with hypertrophic cardiomyopathy attributable to the Asp175Asn mutation in the

alpha-tropomyosin gene: a positron emission tomography study." J Nucl Cardiol **14**(3): 354-365.
Uyeda, T. Q., P. D. Abramson and J. A. Spudich (1996). "The neck region of the myosin motor domain acts as a lever arm to generate movement." Proc Natl Acad Sci U S A **93**(9): 4459-4464.
Uys, G. M., A. Ramburan, B. Loos, C. J. Kinnear, L. J. Korkie, J. Mouton, J. Riedemann and J. C. Moolman-Smook (2011). "Myomegalin is a novel A-kinase anchoring protein involved in the phosphorylation of cardiac myosin binding protein C." BMC Cell Biol **12**: 18.
van de Klundert, F. A., M. L. Gijsen, I. P. R. van den, L. H. Snoeckx and W. W. de Jong (1998). "alpha B-crystallin and hsp25 in neonatal cardiac cells--differences in cellular localization under stress conditions." Eur J Cell Biol **75**(1): 38-45.
van den Heuvel, R., W. Hendriks, W. Quax and H. Bloemendal (1985). "Complete structure of the hamster alpha A crystallin gene. Reflection of an evolutionary history by means of exon shuffling." J Mol Biol **185**(2): 273-284.
Van Der Ouderaa, F. J., W. W. De Jong, A. Hilderink and H. Bloemendal (1974). "The amino-acids sequence of the alphaB2 chain of bovine alpha-crystallin." Eur J Biochem **49**(1): 157-168.
van der Velden, J., Z. Papp, R. Zaremba, N. M. Boontje, J. W. de Jong, V. J. Owen, P. B. Burton, P. Goldmann, K. Jaquet and G. J. Stienen (2003). "Increased Ca2+-sensitivity of the contractile apparatus in end-stage human heart failure results from altered phosphorylation of contractile proteins." Cardiovasc Res **57**(1): 37-47.
van der Ven, P. F., J. W. Bartsch, M. Gautel, H. Jockusch and D. O. Furst (2000). "A functional knock-out of titin results in defective myofibril assembly." J Cell Sci **113 (Pt 8)**: 1405-1414.
van Dijk, S. J., D. Dooijes, C. dos Remedios, M. Michels, J. M. Lamers, S. Winegrad, S. Schlossarek, L. Carrier, F. J. ten Cate, G. J. Stienen and J. van der Velden (2009). "Cardiac myosin-binding protein C mutations and hypertrophic cardiomyopathy: haploinsufficiency, deranged phosphorylation, and cardiomyocyte dysfunction." Circulation **119**(11): 1473-1483.
van Dijk, S. J., E. R. Paalberends, A. Najafi, M. Michels, S. Sadayappan, L. Carrier, N. M. Boontje, D. W. Kuster, M. van Slegtenhorst, D. Dooijes, C. dos Remedios, F. J. ten Cate, G. J. Stienen and J. van der Velden (2012). "Contractile dysfunction irrespective of the mutant protein in human hypertrophic cardiomyopathy with normal systolic function." Circ Heart Fail **5**(1): 36-46.
van Eerd, J. P. and K. Takahshi (1976). "Determination of the complete amino acid sequence of bovine cardiac troponin C." Biochemistry **15**(5): 1171-1180.
VanBuren, P., G. S. Waller, D. E. Harris, K. M. Trybus, D. M. Warshaw and S. Lowey (1994). "The essential light chain is required for full force production by skeletal muscle myosin." Proc Natl Acad Sci U S A **91**(26): 12403-12407.
Vicart, P., A. Caron, P. Guicheney, Z. Li, M. C. Prevost, A. Faure, D. Chateau, F. Chapon, F. Tome, J. M. Dupret, D. Paulin and M. Fardeau (1998). "A missense mutation in the alphaB-crystallin chaperone gene causes a desmin-related myopathy." Nat Genet **20**(1): 92-95.
Vik-Mo, H. and O. D. Mjos (1981). "Influence of free fatty acids on myocardial oxygen consumption and ischemic injury." Am J Cardiol **48**(2): 361-365.
Vincent, M. F., P. J. Marangos, H. E. Gruber and G. Van den Berghe (1991). "Inhibition by AICA riboside of gluconeogenesis in isolated rat hepatocytes." Diabetes **40**(10): 1259-1266.
Vittone, L., C. Mundina-Weilenmann, M. Said, P. Ferrero and A. Mattiazzi (2002). "Time course and mechanisms of phosphorylation of phospholamban residues in ischemia-reperfused rat hearts. Dissociation of phospholamban phosphorylation pathways." J Mol Cell Cardiol **34**(1): 39-50.
Wagenknecht, T., R. Grassucci, J. Frank, A. Saito, M. Inui and S. Fleischer (1989). "Three-dimensional architecture of the calcium channel/foot structure of sarcoplasmic reticulum." Nature **338**(6211): 167-170.

Wang, C. K. and H. C. Cheung (1986). "Proximity relationship in the binary complex formed between troponin I and troponin C." J Mol Biol **191**(3): 509-521.
Watkins, H., H. Ashrafian and C. Redwood (2011). "Inherited cardiomyopathies." N Engl J Med **364**(17): 1643-1656.
Weber, K. T. (1989). "Cardiac interstitium in health and disease: the fibrillar collagen network." J Am Coll Cardiol **13**(7): 1637-1652.
Wegener, A. D., H. K. Simmerman, J. P. Lindemann and L. R. Jones (1989). "Phospholamban phosphorylation in intact ventricles. Phosphorylation of serine 16 and threonine 17 in response to beta-adrenergic stimulation." J Biol Chem **264**(19): 11468-11474.
Wegner, A. (1976). "Head to tail polymerization of actin." J Mol Biol **108**(1): 139-150.
Weisberg, A. and S. Winegrad (1996). "Alteration of myosin cross bridges by phosphorylation of myosin-binding protein C in cardiac muscle." Proc Natl Acad Sci U S A **93**(17): 8999-9003.
Wells, J. M. and S. A. McLuckey (2005). "Collision-induced dissociation (CID) of peptides and proteins." Methods Enzymol **402**: 148-185.
Wendt, I. R. and C. L. Gibbs (1974). "Energy production of mammalian fast- and slow-twitch muscles during development." Am J Physiol **226**(3): 642-647.
White, S. P., C. Cohen and G. N. Phillips, Jr. (1987). "Structure of co-crystals of tropomyosin and troponin." Nature **325**(6107): 826-828.
Whitten, A. E., C. M. Jeffries, S. P. Harris and J. Trewhella (2008). "Cardiac myosin-binding protein C decorates F-actin: implications for cardiac function." Proc Natl Acad Sci U S A **105**(47): 18360-18365.
WHO (2014). Global status report on noncommunicable diseases 2014.
Woods, A., K. Dickerson, R. Heath, S. P. Hong, M. Momcilovic, S. R. Johnstone, M. Carlson and D. Carling (2005). "Ca2+/calmodulin-dependent protein kinase kinase-beta acts upstream of AMP-activated protein kinase in mammalian cells." Cell Metab **2**(1): 21-33.
Wu, Y., O. Cazorla, D. Labeit, S. Labeit and H. Granzier (2000). "Changes in titin and collagen underlie diastolic stiffness diversity of cardiac muscle." J Mol Cell Cardiol **32**(12): 2151-2162.
Xiao, B., M. J. Sanders, D. Carmena, N. J. Bright, L. F. Haire, E. Underwood, B. R. Patel, R. B. Heath, P. A. Walker, S. Hallen, F. Giordanetto, S. R. Martin, D. Carling and S. J. Gamblin (2013). "Structural basis of AMPK regulation by small molecule activators." Nat Commun **4**: 3017.
Xiao, B., M. J. Sanders, E. Underwood, R. Heath, F. V. Mayer, D. Carmena, C. Jing, P. A. Walker, J. F. Eccleston, L. F. Haire, P. Saiu, S. A. Howell, R. Aasland, S. R. Martin, D. Carling and S. J. Gamblin (2011). "Structure of mammalian AMPK and its regulation by ADP." Nature **472**(7342): 230-233.
Xiao, B., G. Zhong, M. Obayashi, D. Yang, K. Chen, M. P. Walsh, Y. Shimoni, H. Cheng, H. Ter Keurs and S. R. Chen (2006). "Ser-2030, but not Ser-2808, is the major phosphorylation site in cardiac ryanodine receptors responding to protein kinase A activation upon beta-adrenergic stimulation in normal and failing hearts." Biochem J **396**(1): 7-16.
Xu, C., R. Craig, L. Tobacman, R. Horowitz and W. Lehman (1999). "Tropomyosin positions in regulated thin filaments revealed by cryoelectron microscopy." Biophys J **77**(2): 985-992.
Xue, B. and B. B. Kahn (2006). "AMPK integrates nutrient and hormonal signals to regulate food intake and energy balance through effects in the hypothalamus and peripheral tissues." J Physiol **574**(Pt 1): 73-83.
Yamakage, M. and A. Namiki (2002). "Calcium channels--basic aspects of their structure, function and gene encoding; anesthetic action on the channels--a review." Can J Anaesth **49**(2): 151-164.
Yang, T. T., Q. Xiong, H. Enslen, R. J. Davis and C. W. Chow (2002). "Phosphorylation of NFATc4 by p38 mitogen-activated protein kinases." Mol Cell Biol **22**(11): 3892-3904.

Yavari, A. (2010). Characterisation of a Novel Gene-Targeted Model for PRKAG2 Disease. DPhil, University of Oxford.

Zaccolo, M. and T. Pozzan (2002). "Discrete microdomains with high concentration of cAMP in stimulated rat neonatal cardiac myocytes." Science **295**(5560): 1711-1715.

Zakhary, D. R., C. S. Moravec and M. Bond (2000). "Regulation of PKA binding to AKAPs in the heart: alterations in human heart failure." Circulation **101**(12): 1459-1464.

Zakhary, D. R., C. S. Moravec, R. W. Stewart and M. Bond (1999). "Protein kinase A (PKA)-dependent troponin-I phosphorylation and PKA regulatory subunits are decreased in human dilated cardiomyopathy." Circulation **99**(4): 505-510.

Zaman, S., S. I. Lippman, L. Schneper, N. Slonim and J. R. Broach (2009). "Glucose regulates transcription in yeast through a network of signaling pathways." Mol Syst Biol **5**: 245.

Zarain-Herzberg, A., D. H. MacLennan and M. Periasamy (1990). "Characterization of rabbit cardiac sarco(endo)plasmic reticulum Ca2(+)-ATPase gene." J Biol Chem **265**(8): 4670-4677.

Zhang, H., D. Wessels, P. Fey, K. Daniels, R. L. Chisholm and D. R. Soll (2002). "Phosphorylation of the myosin regulatory light chain plays a role in motility and polarity during Dictyostelium chemotaxis." J Cell Sci **115**(Pt 8): 1733-1747.

Zhu, W., Y. Zou, I. Shiojima, S. Kudoh, R. Aikawa, D. Hayashi, M. Mizukami, H. Toko, F. Shibasaki, Y. Yazaki, R. Nagai and I. Komuro (2000). "Ca2+/calmodulin-dependent kinase II and calcineurin play critical roles in endothelin-1-induced cardiomyocyte hypertrophy." J Biol Chem **275**(20): 15239-15245.

Zile, M. R. and D. L. Brutsaert (2002). "New concepts in diastolic dysfunction and diastolic heart failure: Part II: causal mechanisms and treatment." Circulation **105**(12): 1503-1508.

Zolk, O., P. Caroni and M. Bohm (2000). "Decreased expression of the cardiac LIM domain protein MLP in chronic human heart failure." Circulation **101**(23): 2674-2677.

Zot, H. G. and J. D. Potter (1982). "A structural role for the Ca2+-Mg2+ sites on troponin C in the regulation of muscle contraction. Preparation and properties of troponin C depleted myofibrils." J Biol Chem **257**(13): 7678-7683.

Zucchi, R. and S. Ronca-Testoni (1997). "The sarcoplasmic reticulum Ca2+ channel/ryanodine receptor: modulation by endogenous effectors, drugs and disease states." Pharmacol Rev **49**(1): 1-51.